

# Metabolism of NHP and SA

Dissertation

for the award of the degree

*“Doctor rerum naturalium”*

of the Georg-August-Universität Göttingen

within the doctoral program

“Plant Response To Eliminate Critical Threats”

of the Georg-August-University School of Science (GAUSS)

submitted by

Lennart Mohnike

from Gehrden, Germany

Göttingen 2022

### Thesis Committee

Prof. Dr. Ivo Feussner, Department for Plant Biochemistry, Albrecht-von-Haller-Institute for Plant Sciences, University of Goettingen

Prof. Dr. Christiane Gatz, Department of Plant Molecular Biology and Physiology, Albrecht-von-Haller-Institute for Plant Sciences, University of Goettingen

Prof. Dr. Yuelin Zhang, Department of Botany, University of British Columbia, Vancouver, Canada

### Members of the Examination Board

Referee: Prof. Dr. Ivo Feussner, Department for Plant Biochemistry, Albrecht-von-Haller-Institute for Plant Sciences, University of Goettingen

2<sup>nd</sup> Referee: Prof. Dr. Christiane Gatz, Department of Plant Molecular Biology and Physiology, Albrecht-von-Haller-Institute for Plant Sciences, University of Goettingen

### Further members of the Examination Board

Prof. Dr. Yuelin Zhang, Department of Botany, University of British Columbia, Vancouver, Canada

Prof. Dr. Andrea Polle, Department for Forest Botany and Tree Physiology, Buesgen-Institute, University of Goettingen

Prof. Dr. Gerhard Braus, Department of Molecular Microbiology and Genetics, Institute for Microbiology and Genetics, University of Goettingen

Prof. Dr. Till Ischebeck, Institute for Plant Biology and Biotechnology, University of Muenster

**Date of oral examination: 17.08.2022**

# Table of Contents

1. Abstract.....	1
2. Introduction .....	3
2.1 Initiation of plant immunity .....	4
2.2 The molecular landscape of plant hormones in defense responses .....	7
2.2.1 SA biosynthesis and perception .....	8
2.2.2 NHP biosynthesis .....	10
2.2.3 Modes of turnover for active compounds of the plant immunity.....	11
2.2.3.1 Glycosylation.....	12
2.2.3.2 Methylation.....	14
2.2.3.3 Hydroxylation .....	15
2.2.3.4 Amino acid conjugation .....	16
2.2.4 SA turnover .....	16
2.2.5 NHP turnover.....	17
2.3 Systemic acquired resistance .....	18
2.4 Metabolomics in plant science .....	19
2.5 Aims of the study .....	22
3. Chapter I. - The glycosyltransferase UGT76B1 modulates <i>N</i> -hydroxy pipecolic acid homeostasis and plant immunity .....	23
4. Chapter II. - <i>N</i> -hydroxy pipecolic acid methyl ester is involved in <i>Arabidopsis</i> immunity .....	48
5. Chapter III. – Further analysis of missing links in SA- and NHP-biosynthesis and metabolism .....	94
6. Discussion.....	99
6.1 UGT76B1 is the central hub of NHP and SA inactivation .....	101
6.1.1 <i>In vivo</i> annotation of UGT76B1 to NHP-OGlc synthesis.....	102
6.1.2 Heterologous expression and <i>in vitro</i> data support UGT76B1 function .....	103
6.1.3 Functional <i>FMO1</i> is required for <i>ugt76b1</i> phenotypic characteristics .....	103
6.1.4 Outlook to NHP, UGT76B1 and NHP-glucosides influences on plant health... ..	104
6.2 Novel NHP-metabolites as candidates for plant priming, storage or degradation? .....	106
6.3 The exporter of Pip from the chloroplast remains unknown .....	111
6.4 Future perspectives in plant immunity .....	112
6.5 Concluding remarks.....	115

7. References.....	116
8. Supplemental materials.....	131
9. Acknowledgments.....	134

## 1. Abstract

When mobile organisms face a threat, they have the options of a fight or flight as reaction. The sessile nature of plants narrows their response option down to defend themselves against the threat. Therefore, plants developed a strong innate immune system in an evolutionary context, redundant of specialized immune cells as found in animals. Besides, they are able to prime non-infected distal tissue towards a stronger immune response after pathogen attack, a phenomenon that is termed systemic acquired resistance (SAR) (Fu and Dong, 2013).

Salicylic acid (SA) and *N*-hydroxy pipelicolic acid (NHP) are small molecules and constitute two major hormones in the plant immune response. They are key molecules in basal resistance as well as to induce SAR (Delaney et al., 1994; Wildermuth et al., 2001; Chen et al., 2018; Hartmann et al., 2018; Rekhter et al., 2019b). The biosynthesis and function of SA has been intensively studied over the last decades (Wildermuth et al., 2001; Nawrath et al., 2002; Rekhter et al., 2019b; Torrens-Spence et al., 2019). In addition, the biosynthesis of NHP was unraveled recently (Chen et al., 2018; Hartmann et al., 2018). Both compounds are known to be present in a glycosylated state likely to be inactivated or stored. This is now shifting the focus towards the enzymes catalyzing the glycosylation reactions. For SA glycosylation, three UDP-dependent glycosyltransferases (UGTs) have been described: UGT74F1, UGT74F2 and UGT76B1 (Song, 2006; Dean and Delaney, 2008; von Saint Paul et al., 2011; Noutoshi et al., 2012; George Thompson et al., 2017). In terms of NHP, the NHP-*O*-glucoside (NHP-OGlc) was a known metabolite, without the description of a functional UGT enzyme that was able to catalyze the synthesis, prior to this thesis (Chen et al., 2018; Hartmann and Zeier, 2018). Lately, independent research groups were able to describe one of the proposed SA UGTs, UGT76B1, to be the major enzyme in the formation of NHP-OGlc in *Arabidopsis thaliana* (Bauer et al., 2021; Cai et al., 2021; Holmes et al., 2021; Mohnike et al., 2021).

In this work, the identification and functional characterization of UGT76B1 as NHP-OGlc forming enzyme is laid-out as published earlier in *The Plant Cell* within Mohnike et al. 2021 (Mohnike et al., 2021). The metabolite levels of NHP, SA and their respective glucosides are therein described in response to *Pseudomonas syringae* pv. *maculicola* ES4326 (*P.s.m.*) infection. The metabolic fate of NHP and SA in the *ugt76b1* mutant was underlined by additional UV-stress experiments. In addition, we provide data about the infection phenotype against *P.s.m.* and *Hyaloperonospora arabidopsidis* Noco 2 (*H.a. Noco 2*), of which we deduce an enhanced resistance phenotype of the mutant. Analyzing double mutant lines of the FLAVIN-DEPENDENT MONOOXYGENASE 1 (FMO1) with *ugt76b1*, *fmo1 ugt76b1*, we show

that enhanced resistance and growth deficiency are FMO1-dependent, therefore, NHP-dependent. Lastly, we argue against the need of NHP-O-glucosylation for successful mobility during SAR (Chapter I). Furthermore, we used our metabolome analysis platform to search for novel, so far undescribed metabolites of NHP. A novel metabolite, which is synthesized in an infection-dependent manner, is described to be a NHP-methyl-ester (MeNHP). Its biosynthesis is shown to be *AGD2-LIKE DEFENSE RESPONSE PROTEIN 1 (ALD1)*- and *FMO1*-dependent. In addition, its retention time and tandem-mass spectrometric properties were underlined via a chemically synthesized authentic standard of MeNHP. The novel compound is synthesized *in vitro* by the annotated methyl transferase *At4G22530 (NHPMT1)*. However, T-DNA insertion lines of *NHPMT1*, *nhpmt1-1* and *nhpmt1-2* are not impaired in biosynthesis of MeNHP (Chapter II). Additionally, we present a NHP and D<sub>9</sub>-labeled NHP co-infiltration experiment to identify additional *in planta* NHP-derivatives. Moreover, we layout results about successful repetition of earlier published work and investigated genes that remained inconclusive towards their influence and function in plant pathogen interaction mediated defense response of *A. thaliana*. We were able to confirm the role of *ENHANCED PSEUDOMONAS SUSCEPTIBILITY1 (EPS1)* on the biosynthesis of SA by the accumulation of its substrate isochlorogenic acid-9-glutamate (IC-9-Glu) in metabolite analysis of *eps1* mutant plants (Torrens-Spence et al., 2019). Furthermore, we show that the amino acid transporter *LYSINE/HISTIDINE 7 (LHT7)* is not solely required for NHP biosynthesis. Similarly, *ABERRANT LATERAL ROOT FORMATION 5 (ALF5)*, *ENHANCED DISEASE SUSCEPTIBILITY 5 (EDS5)* and *EDS5-homolog (EDS5H)* are not solely required as transporters in NHP biosynthesis (Chapter III).

## 2. Introduction

From the beginning of land-plant evolution, over 500 million years ago, photosynthetic organisms need to cope with a plethora of environmental stressors (de Vries and Archibald, 2018; Resemann et al., 2021). On the one hand, abiotic stress that includes temperature, UV-radiation, varying water, salt or nutrient contents of the substrate they are growing on (Waadt et al., 2022; Zhang et al., 2022). On the other hand, biotic stressors including organisms like heterotrophic bacteria and fungi that take advantage of plants as carbon source and host (Atkinson and Urwin, 2012; Suzuki et al., 2014). As postulated by Charles Darwin, challenges to an organism sometimes develop into a selective pressure, letting those traits be successful and survive that are of high benefit to the organism. Therefore, plants have developed strategies that enable them to cope with a multitude of threats on the molecular level, including generalized defense barriers (Vanholme et al., 2010). In addition, they developed fine-tuned molecular responses, to mediate a very precise and specific answer to individual challenges (Glazebrook, 2005; Zhang et al., 2022). Plants still face constantly changing environments, as due to global warming, vital parameters are at stake. Especially limited water resources and instable temperatures are a challenge (Dai, 2013). In Europe, for example, the soil-humidity is predicted to decrease (Samaniego et al., 2018). Furthermore, co-evolution of plants and pathogens is a driving force for plants to develop novel strategies to defend against invading pathogens (Burdon and Thrall, 2009).

In the 19<sup>th</sup> century the oomycete pathogen *Phytophthora infestans* that causes potato blight was the reason for one of the most severe hunger periods in Europe (Haas et al., 2009). In addition, a constantly growing population on earth demands for stable food supply chains and securities. Crop plants, therefore, are highly influenced by anthropogenic interests, breeding them towards desired traits, which may be high yield, and high resistance against biotic and abiotic threats (Dresselhaus and Hückelhoven, 2018). The economic importance of crop plants, such as soy, corn, grain, rapeseed, grapevine or potato and tomato is a driving force on plant basic research and the transition of knowledge into crop plant systems (Atkinson and Urwin, 2012; Holmes et al., 2019; Pirrello et al., 2022).

Basic molecular research on plant immunity started with studies about several plant species and their compatible pathogens to study infection and resistance phenomena (Holmes, 1938). Compatible plant pathogen interactions describe a relationship of successful plant colonization with induction of disease symptoms by a pathogen (Glazebrook, 2005). The interaction between the tobacco mosaic virus (TMV) and tobacco is a classic example. Importantly, the phenomenon of induced resistance in untreated plant tissue as result of infecting another was

observed (Ross, 1961). This phenomenon was termed systemic acquired resistance (SAR) and its mechanisms of elucidation and signaling came into research focus and laid-out the basis of our understanding of plant immunology (Fu and Dong, 2013; Klessig et al., 2018; Zeier, 2021). Research on small molecules in plant-pathogen interaction began to intensify with the finding that salicylic acid (SA) is able to induce plant immunity (Malamy and Klessig, 1992). SA has been found in plants since the end of nineteenth hundreds to early 20<sup>th</sup> century (Griffiths, 1889; Traphagen and Burke, 1903; Grimaldi, 1905). However, already Neanderthals made use of SA containing plants to self-medicate (Weyrich et al., 2017). Hermann Kolbe described the chemical structure of SA in the 1860<sup>th</sup> and was able to synthesize the hydroxy benzoate chemically (Kolbe, 1860; Kohl, 1999). However, SAs potential to induce plant immunity was described almost a hundred years after its discovery in plants (Mettraux et al., 1990; Rasmussen et al., 1991; Malamy and Klessig, 1992; Delaney et al., 1994).

Today additional molecules have been identified to play a role in the defense towards several pathogens. Recently, pipecolic acid (Pip) and its *N*-hydroxylated metabolite, *N*-hydroxy pipecolic acid (NHP) were functionally connected with immunity in *Arabidopsis thaliana*. Pipecolic acid was first isolated and described from *Phaseolus vulgaris* and its biosynthesis in beans from *L*-lysine via different intermediates was proposed (Schütte and Seelig, 1967). Meanwhile infection data show the potential of Pip and NHP to induce plant immunity in several plant species outside the Brassicaceae (Holmes et al., 2019; Schnake et al., 2020).

## 2.1 Initiation of plant immunity

The first barrier for a pathogen to overcome is the physical barrier on the plant surface, the cuticle (Lewandowska et al., 2020). A compatible fungus is able to produce an apressorium to penetrate the plant surface of the host plant. Later it produces a haustorium inside the penetrated tissue to facilitate nutrient uptake (Mendgen and Hahn, 2002). The penetration itself and preceding reactions cause damage to the plants cellular integrity resulting in molecular fragments the damage associated molecular patterns (DAMPs). For example, cell wall derived pectin fragments the oligogalacturonides, and xyloglucans were shown to induce immune responses in *Vitis vinifera* and *A. thaliana* (Aziz et al., 2004; Ferrari et al., 2007; Ferrari et al., 2013; Claverie et al., 2018). In addition, microbial molecules, such as flagellin and chitin, which are common structural molecules to bacterial flagella or fungal cell walls, are called microbe associated molecular patterns (MAMPs) (Boller and Felix, 2009). Together DAMPs and MAMPs are classified as pathogen associated molecular patters (PAMPs). Recognition of PAMPs by plants induces PAMP-triggered immunity (PTI). PTI results in a robust response of the plant that is able to halt further colonization (Jones and Dangl, 2006; Boller and Felix,



2009). PAMPs are recognized by pattern recognition receptors (PRRs) that include receptor-like kinases (RLKs) and receptor-like proteins (RLPs) (Figure 1) (Boller and Felix, 2009). A well-studied interaction is the detection of flagellin protein by the PRR FLAGELLIN-SENSING2, through its leucine rich repeat (LRR) domains (Zipfel et al., 2004). PRR co-receptors and RLCKs assist the detection and signal propagation by RLKs and RLPs. PTI is triggered either directly or via their interaction partners and receptor-like cytoplasmic kinases (RLCKs). It is transduced via mitogen-activated protein kinase (MAPK) cascades, calcium fluxes and the NADPH oxidase to result in activation of transcription factors that are responsible for transcriptional reprogramming in the infected tissue, and processes like the generation of reactive oxygen species (ROS) and callose deposition at the site of infection (Ma et al., 2013; Ngou et al., 2022).

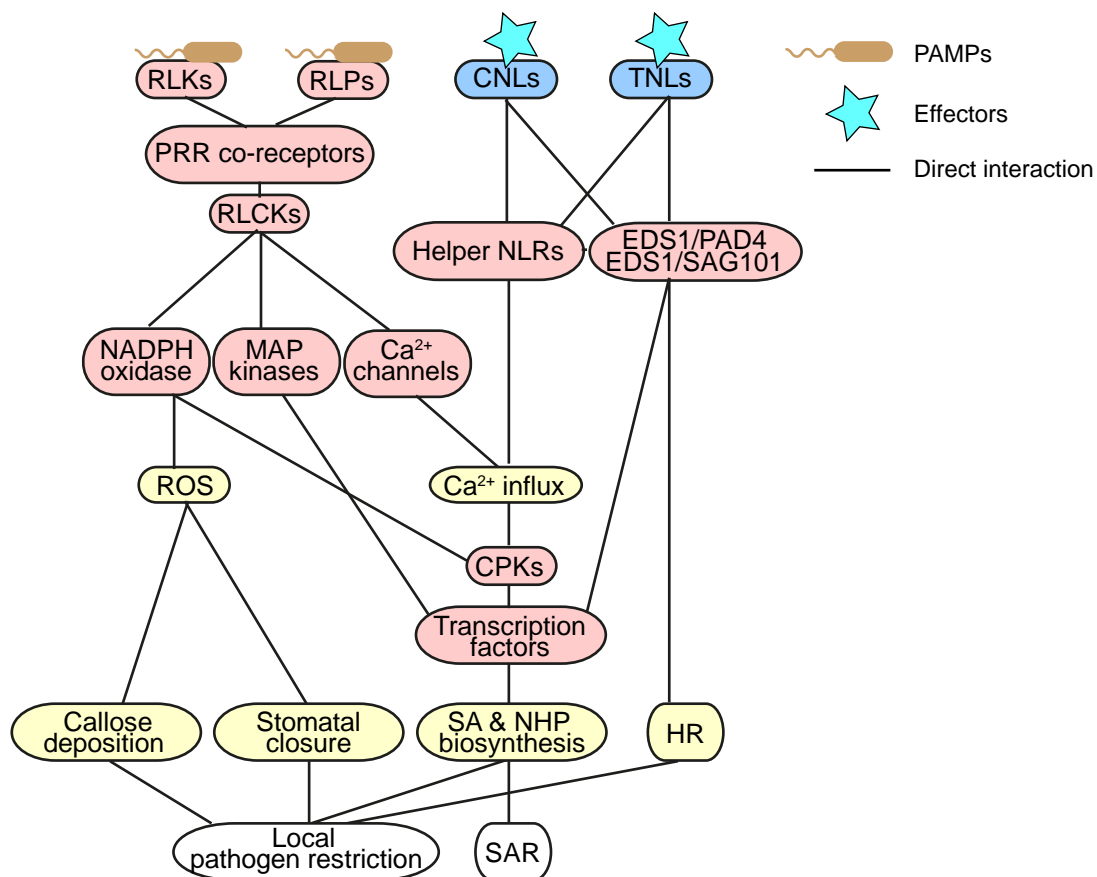


Figure 1: **The plant defense network from detection to restriction.** Receptor like kinases (RLKs), Receptor like proteins (RLPs), coiled-coil-nucleotide-binding-leucine rich repeat proteins (CNLs) and toll/interleukin-1 receptor like-nucleotide binding leucine rich repeat proteins (TNLs) recognize pathogen via molecular pattern and effector proteins. Pattern-recognition receptors (PRR) co-receptors assist in signal propagation via receptor like kinases (RLCKs). Similarly, helper nucleotide binding leucine rich repeats proteins (NLRs) and EP-domain containing (EP) proteins mediate signal proliferation. RLCKs activate the NADPH oxidases, mitogen-activated-phosphate (MAP) kinases and calcium (Ca<sup>2+</sup>) channels. Altogether these responses generate reactive oxygen species (ROS), Ca<sup>2+</sup>-influx, activation of Ca<sup>2+</sup>-dependent protein kinases (CPKs) and HR. In addition to HR, callose deposition, stomatal closure, ethylene, SA and NHP biosynthesis is triggered to restrict pathogen growth and propagate systemic acquired resistance (SAR). Only direct interactions are shown for simplicity. Figure redrawn and modified from (Ngou et al., 2022).

In addition, pathogen recognition is based-on microbial effector-molecules that are transmitted inside the plant to hijack immune responses, the effector triggered immunity (ETI). A recent example provides insight into the effector protein, ROS BURST INTERFERING PROTEIN 1 from *Ustilago maydis* that has ROS-suppressing activity. Additionally, it has the ability to delocalize the LIPOXYGENASE 3 enzyme from *Zea mays* into the nucleus, which causes suppression of a ROS burst response, too (Saado et al., 2022). On the other side, plants have developed receptor molecules to detect microbial effectors. These molecules are the resistance (R)-proteins. R-proteins may consist of a coiled-coil-domain (CC) or toll/interleukin-1 receptor (TIR)-domain linked to a core of nucleotide binding leucine rich repeat domains (NB-LRR), forming the two major groups, CC-NB-LRR (CNL) and TIR-NB-LRR (TNL) proteins. CNLs and TNLs have the ability to form multi domain complexes that fulfill distinct functions in resistance signaling, the resistosomes (Martin et al., 2020; Bi et al., 2021; Lapin et al., 2022). CNL-resistosomes were shown to form membrane pores that act as a calcium channel (Bi et al., 2021). TNL resistosomes fulfill nicotinamide dinucleotide (NAD)ase activity producing nicotinamide (NAM), cyclic ADP-ribose (cADPR) and adenosine diphosphate ribose (ADPR) from NAD<sup>+</sup> (Horsefield et al., 2019; Wan et al., 2019a). Additionally, their function as 2',3'-cyclic adenosine monophosphate and 2',3'-cyclic guanosine monophosphate synthetases were described (Yu et al., 2021a). As a result, the CNL and TNL receptors are able to induce ETI (Bi et al., 2021; Parker et al., 2022). Helper nucleotide binding leucine rich repeat proteins (helper NLRs) and lipase-like heterodimer proteins ENHANCED DISEASE SUSCEPTIBILITY 1/PHYTOALEXIN DEFICIENT 4 (EDS1/PAD4) and EDS1/SENESCENCE ASSOCIATED GENE 101 (SAG101) mediate signal proliferation concerted by CNLs and TNLs (Lapin et al., 2019; Pruitt et al., 2021). The activated response combines the generation of ROS, Ca<sup>2+</sup>-influx, activation of Ca<sup>2+</sup>-dependent protein kinases (CPKs) and hypersensitive response (HR). In addition to HR, callose deposition, stomatal closure, the biosynthesis of SA and NHP is triggered to restrict pathogen growth and to induce SAR (Ngou et al., 2022).

The sequential induction of PTI and ETI lead to the classical “Zig Zag” model of plant immunity (Figure 2A). It describes PTI and ETI as individual layers of immunity equally resulting in robust defense response (Jones and Dangl, 2006). PAMPs elicit PTI and pathogen effectors hamper the PTI response, here effector triggered susceptibility (ETS). R-proteins recognize these effectors, which causes ETI. However, recently, both PTI and ETI were shown to be equally important and depending on one and other for successful immune responses against pathogens by the threatened plant (Figure 2B) (Ngou et al., 2021; Yuan et al., 2021). The invading pathogen is connected with both PAMPs and secreted effectors. PAMPs cause PTI, leading to resistance, which the effectors on the one hand are trying to block. On the other hand the effectors are recognized by the plant R-proteins, causing ETI. In consequence, ETI potentiates PTI induced resistance (Ngou et al., 2021; Tian et al., 2021; Yuan et al., 2021).

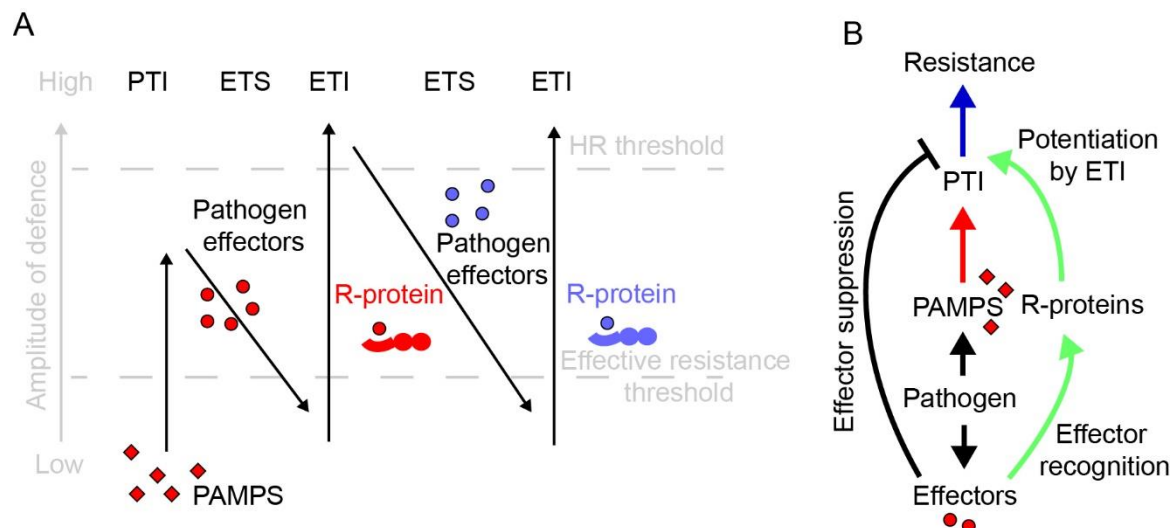


Figure 2: **Insight into PTI and ETI mediated resistance.** The classical model of defense induction “Zig-Zag” describing PTI and ETI as individual layers of immunity (A) was overruled by the recent model in which PTI and ETI are part of the same response (B). Model (A) describes the amplitude of plant defense during infection. Pathogen associated molecular pattern (PAMPS) elicit PAMP triggered immunity (PTI) over the threshold for effective resistance. Pathogen effectors work to sabotage the successful response, so called effector triggered susceptibility (ETS). However, these effector molecules are recognized by resistance proteins (R-proteins) that trigger effector triggered immunity (ETI). ETI results in an immune threshold sufficient to induce a hypersensitive response (HR). Another round of ETS and ETI may occur in a similar matter. Model (B) shows that both modes of recognition, PTI and ETI, enhance each other and thereby potentiate the resistance, to overcome suppression by the effector molecules. Figure redrawn and modified from (Jones and Dangl, 2006; Ngou et al., 2021).

## 2.2 The molecular landscape of plant hormones in defense responses

Successful detection of an external thread results in the accumulation of plant hormones, phytohormones (Delaney et al., 1994; Vernooij et al., 1994; Koo and Howe, 2009; Chen et al., 2018). They are considered as bioactive signaling molecules and are involved in developmental processes, as well as, adaption to abiotic and biotic stresses. Abscisic acid for example has the ability to mediate stomata closure and therefore bacterial entry into the leaf tissue as well as water loss. In addition, abscisic acid mediates seed dormancy during maturation (Nakashima and Yamaguchi-Shinozaki, 2013; Lim et al., 2015; Ha et al., 2016). A subset of plant hormones mediates a transcriptional and metabolic remodeling of the basal/unstressed state of the plant towards a defense response, which is connected to a pathogenic stressor (Felton and Korth, 2000; Feys and Parker, 2000; Gruner et al., 2013). Classically, the line is drawn between biotrophic pathogens that are dependent on living host tissue and necrotrophic pathogens that require necrotic host tissue to successfully develop (Glazebrook, 2005; Fu and Dong, 2013). Special receptor molecules and their associated transcription factor targets are a key to discriminate between these different threads. Thus, detection of biotrophic pathogens results in the accumulation of SA and NHP (Wildermuth et

al., 2001; Chen et al., 2018; Hartmann et al., 2018). Upon necrotrophic stressors, feeding by insects or physical harm to the plants, jasmonic acid (JA) and its bioactive form jasmonoyl isoleucine (JA-Ile) are synthesized and mediate defense signaling (Farmer et al., 2003; Devoto and Turner, 2005; Suza and Staswick, 2008; Fonseca et al., 2009; Haroth et al., 2019).

### 2.2.1 SA biosynthesis and perception

SA is a phytohormone orchestrating plant immunity towards viruses, bacteria and fungi (Delaney et al., 1994). The interaction of a biotrophic pathogen and a plant leads to the accumulation of SA in the plant tissue, as shown for *Nicotiana tabacum* with TMV and *Cucumis sativus* with *Colletotrichum lagenarium* (Ross, 1961; Malamy et al., 1990; Metraux et al., 1990). SA has been shown to induce a local immune response and to be required for successful establishment of SAR (Gaffney et al., 1993; Delaney et al., 1994).

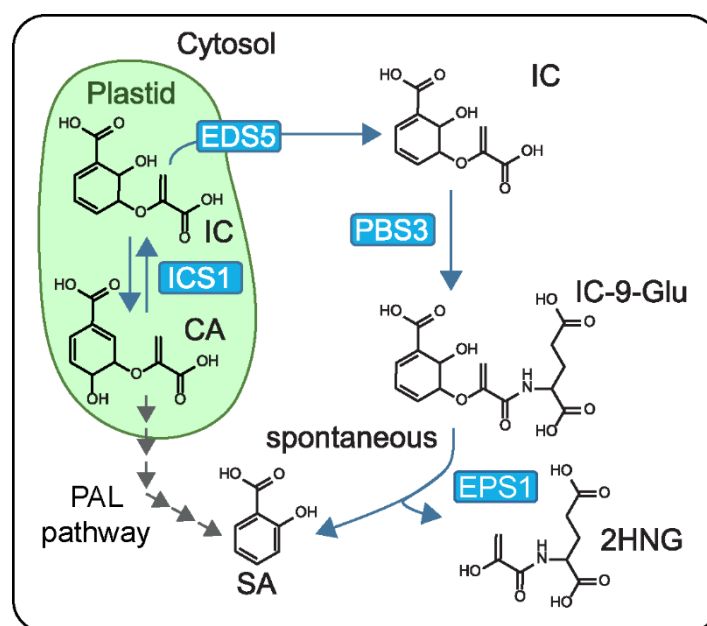


Figure 3: **Biosynthetic routes of SA.** Two routes of salicylic acid (SA) biosynthesis are proposed. On the one hand SA is synthesized via the ISOCHORISMATE SYNTHASE 1 (ICS1) dependent pathway from chorismate (CA). CA is converted by ICS1 to isochorismate (IC). ENHANCED DISEASE SUSCEPTIBILITY 5 (EDS5) is required for its plastidial export. In the cytosol, AvrPphB SUSCEPTIBLE 3 (PBS3) conjugates IC to glutamate, resulting in isochorismate-9-glutamate (IC-9-Glu). IC-9-Glu spontaneously decomposes into SA and enolpyruvyl-*N*-glutamate (2HNG). This decomposition was shown to be increased by ENHANCED PSEUDOMONAS SUSCEPTIBILITY 1 (EPS1). Another biosynthetic route is to proceed via the PHENYLALANINE AMMONIA-LYASE (PAL) pathway, which has not been fully unraveled. Figure modified from (Rekhter et al., 2019b).

In *A. thaliana*, SA derives from chorismic acid. Initially, ISOCHORISMATE SYNTHASE 1 (ICS1) isomerizes chorismic acid to isochorismic acid in the plastid (Figure 3). At least 90 % of the synthesized SA is derived from this ICS1-dependent pathway (Wildermuth et al., 2001).

The multidrug and toxic compound extrusion (MATE) protein ENHANCED DISEASE SUSCEPTIBILITY 5 (EDS5), a plastidial envelope localized transporter, is essential for isochlorogenic acid export from the plastid (Nawrath et al., 2002; Serrano et al., 2013; Rekhter et al., 2019b). In the cytosol, AvrPphB SUSCEPTIBLE 3 (PBS3), a member of the GH3-enzyme family, conjugates isochlorogenic acid to glutamic acid resulting in the intermediate isochlorogenic acid-9-glutamic acid (IC-9-Glu). (Rekhter et al., 2019b). The BAHD-acyltransferase ENHANCED PSEUDOMONAS SUSCEPTIBILITY 1 (EPS1) has an IC-9-Glu lyase activity and enhances the spontaneous decomposition into SA and enolpyruvyl-*N*-glutamate (2HNG) (Rekhter et al., 2019b; Torrens-Spence et al., 2019).

ICS1-independent SA may be synthesized via the PHENYLALANINE AMMONIA-LYASE (PAL)-pathway (Mauch-Mani and Slusarenko 1996). PAL converts phenylalanine to *trans*-cinnamic acid, which is converted into benzoic acid (Wildermuth et al., 2001). Benzoic acid is proposed to result in SA via a putative benzoic acid-2-hydroxylase reaction (Wildermuth et al., 2001). *Trans*-cinnamic acid was also proposed to be converted to *ortho*-coumaric acid, which then feeds into the SA pool (Yalpani et al., 1993).

Direct binding to the protein receptor complex NONEXPRESSER OF PR GENES 1 (NPR1) transmits the SA signal in response to a pathogen. Mutant *npr1* plants have been described as nonresponsive to inducers of SAR (Cao et al., 1994). NPR1 is suggested to be an oligomer complex directly interacting with SA via a bound copper ion (Tada et al., 2008; Wu et al., 2012). Due to changes in the redox state of the cell, reduction of disulfuric acid bonds, and in consequence monomerization of the subunits occur (Mou et al., 2003; Tada et al., 2008). The monomerization is associated with nuclear accumulation of NPR1, likely due to translocation (Mou et al., 2003; Tada et al., 2008). NPR1 is required inside the nucleus to interact with TGA-transcription factors, which transcriptionally induce expression of pathogenesis related (PR) genes (Zhang et al., 1999; Kinkema et al., 2000; Fan and Dong, 2002). The group of upregulated genes includes marker genes for plant infection *PR1*, *PR2* and *PR5* but does also include master transcription factors *SAR-DEFICIENT 1 (SARD1)* and *CALMODULIN-BINDING PROTEIN 60g (CBP60g)*. These transcription factors interact with a broad range of promoter regions, facilitating plant immunity (Sun et al., 2015). In a feed forward amplification, SA and NHP biosynthesis is enhanced, leading to accumulation of the two defense molecules (Sun et al., 2018). Recently, NPR1 was shown to facilitate repression of gene expression induced by the bacterial JA-Ile mimic the phytotoxin coronatine by direct interaction with MYC2 transcription factors (Nomoto et al., 2021). *Pseudomonas syringae* bacteria secrete coronatine to suppress and mislead the molecular response of the host plant in the direction of a JA-mediated defense (Geng et al., 2012; Nomoto et al., 2021). The importance in translating the SA-signal to facilitate a broad cellular response makes NPR1 a favorable target for bacterial

effectors (Chen et al., 2017). An additional mechanism to translate increased SA-concentration into transcriptional reprogramming are the transcriptional repressor proteins NPR3 and NPR4, of which both were shown to interact with SA (Fu et al., 2012; Ding et al., 2018). The proteins are described to retain PR gene expression in the non-infected (basal) state of the cell (Ding et al., 2018). Under pathogen stress, the proteins sense the increasing SA-concentration in the infected cell and release from the promotor regions of the PR-genes. This again results in transcription of the required defensive genes, and in consequence leads to a signal amplification (Ding et al., 2018).

### 2.2.2 NHP biosynthesis

Pip and especially NHP are of increasing interest to researchers, due to their potential of amplifying the immune response of plants under attack (Bernsdorff et al., 2016; Guerra et al., 2020). They have been suggested to mediate a fast response in infected tissue and together with SA amplifying the immune response mechanisms. Additionally, NHP is discussed to be a mediator of systemic acquired resistance into the distal non-infected tissue of a plant (Chen et al., 2018; Hartmann et al., 2018; Guerra et al., 2020).

In *A. thaliana*'s response to pathogen, NHP derives from *L*-lysine, which is subject to deamination via the enzyme AGD2-LIKE DEFENSE RESPONSE PROTEIN 1 (ALD1) (Figure 4) (Navarova et al., 2012). The ALD1 enzyme uses pyridoxal phosphate to catalyze a transamination of the  $\alpha$ -amine of *L*-lysine to pyruvate, resulting in  $\epsilon$ -amino- $\alpha$ -ketocaproic acid and alanine (Ding et al., 2016). Mutant *ald1* plants exhibit impaired local and systemic immune response (Navarova et al., 2012; Bernsdorff et al., 2016). Spontaneous cyclization under water loss of  $\epsilon$ -amino- $\alpha$ -ketocaproic acid results in the generation of  $\Delta^1$ -piperidine-2-carboxylic acid (P2C). The ketimine reductase SAR-DEFICIENT 4 (SARD4) reduces P2C into Pip using NAD(P)H as cofactor (Ding et al., 2016). However, *sard4-5* mutant plants are still able to synthesize Pip in local but not in systemic tissue (Ding et al., 2016). Via FLAVIN-DEPENDENT MONOOXYGENASE 1 (FMO1), catalyzing *N*-hydroxylation on Pip with FAD<sup>+</sup> bound to the enzyme and NAD(P)H as mobile electron donor the biologically active molecule NHP is formed (Chen et al., 2018; Hartmann et al., 2018). In addition, heterologous expression of the NHP synthesis genes *ALD1* and *FMO1* in tomato resulted in NHP synthesis without the need to express *SARD4* (Holmes et al., 2019). Hartmann and Zeier discuss a possible alternative route of *L*-lysine catabolism resulting in Pip (Hartmann and Zeier, 2018). Via the enzyme LYSINE-KETOGLUTARATE REDUCTASE/SACCHAROPINE DEHYDROGENASE (LKR/SDH), *L*-lysine is converted into saccharopine, by conjugation to  $\alpha$ -ketoglutarate. The following hydrolysis catalyzed by LKR/SDH results in glutamate and  $\alpha$ -amino adipic acid semialdehyde (AAS). AAS cyclizes into 1,6-dehydropipecolic acid (1,6-DP) under water loss. The compound

is suggested to be converted into Pip by an unknown mechanism, whereas the reaction from Pip into 1,6-DP is catalyzed by SARCOSINE OXIDASE/Pip OXIDASE (SOX/PipOX) (Hartmann and Zeier, 2018).

The receptor and mechanism to translate the NHP signal into a defense response, including transcriptional reprogramming remains elusive (Nair et al., 2021).

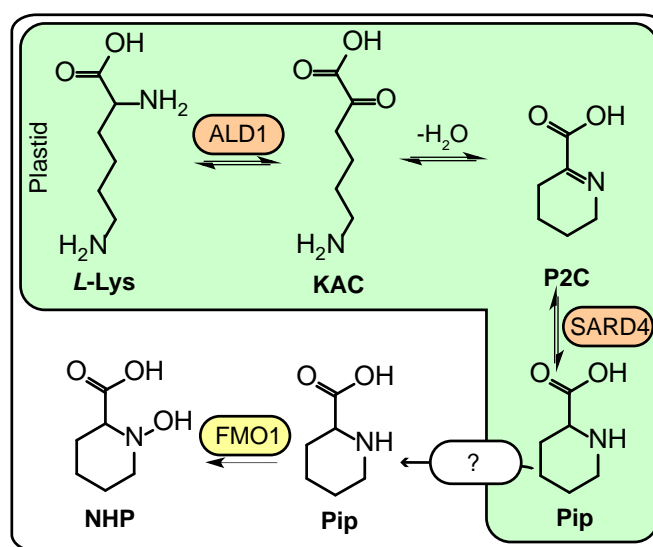


Figure 4: **Biosynthesis of NHP.** *N*-hydroxy pipecolic acid (NHP) in *Arabidopsis* derives from *L*-lysine (*L*-Lys). In the plastid *L*-Lys is subject to transamination by AGD2-LIKE DEFENSE RESPONSE PROTEIN 1 (ALD1) resulting in the formation of ε-amino-α-ketocaproic acid (KAC) (Navarova et al., 2012; Bernsdorff et al., 2016). KAC spontaneously cyclizes to Δ<sup>1</sup>-piperidine-2-carboxylic acid (P2C) under water loss. P2C is substrate of the ketimine reductase SAR-DEFICIENT 4 (SARD4) giving rise to pipecolic acid (Pip) (Ding et al., 2016). Pipecolic acid exits the plastid via a yet unknown transporter and gets subject to *N*-hydroxylation by FLAVIN-DEPENDENT MONOOXYGENASE 1 (FMO1). The FMO1 reaction with Pip results in the active hormone NHP (Chen et al., 2018; Hartmann et al., 2018).

### 2.2.3 Modes of turnover for active compounds of the plant immunity

As mentioned earlier plants are able to adapt to distinct situations in their life by orchestrating their responses with the help of hormones. Via these active molecules, they are able to elicit distinct mechanism of cellular adaptation to cope with stress factors. Nevertheless, a constitutive activation of a response may cause disadvantages to the organism like dwarfism (Zhang et al., 2010; Zhang et al., 2017). Therefore, enzymatic turnover of active molecules developed to be a successful route to balance their activity. These reactions are glycosylation, methylation, hydroxylation, amino acid conjugation or simply degradation.

### 2.2.3.1 Glycosylation

In the *Arabidopsis* genome, approximately 120 *UDP-dependent glycosyltransferase (UGT)* genes are present. The UGTs group into 12 to 14 evolutionary groups by phylogenetic analysis (Li et al., 2001; Ross et al., 2001; Lim et al., 2003). They are classified into the UGT superfamily by a UGT-defining consensus sequence of 42-44 amino acids (Mackenzie et al., 1997; Li et al., 2001; Ross et al., 2001). Further, UGTs group into a family, of which plant UGTs are given a number within 71 to 100. The characteristics of a protein family is a sequence homology of 40 % or higher. The subfamily is indicated by a letter and shows a sequence homology with 60 % or higher. Last UGTs are assigned down to an individual gene, classified by an individual number (Ross et al., 2001)

Glycosyltransferases (GTs) in general, are able to glycosylate functional groups such as: -hydroxy, -carboxy, -amine, -thiol and single bonds between carbon atoms (Bowles et al., 2006). There are different structural domains described for GTs: GT-A, GT-B or GT-C. UGTs using the nucleotide sugar diphosphate, uridine diphosphate (UDP), either belong to GT-A or GT-B topology groups, which consist of two  $\beta/\alpha/\beta$ -Rossmann-fold domains (Breton et al., 2012; Albesa-Jové and Guerin, 2016). The major difference between the GT-A and GT-B topology is a large cleft between the two Rossmann-fold domains in GT-Bs. In comparison, GT-As N-terminal domain recognizes the nucleotide sugar, whereas the C-terminal domain is required in GT-Bs (Lairson et al., 2008; Breton et al., 2012). GT-C enzymes use a lipid-phospho-sugar donor for sugar transfer to the acceptor molecule. The sugar transfer follows two different reaction mechanisms (Figure 5A) (Albesa-Jové and Guerin, 2016). The “inverting” mechanism with an enzyme-substrate complex of GT and aglycon interacting with the activated sugar via an oxocarbenium ion-like transition state (Albesa-Jové and Guerin, 2016). In addition, the vague described “retaining” mechanism via a covalent glycosyl-enzyme species or alternatively short-lived oxocarbenium ion-like species (Albesa-Jové and Guerin, 2016).

UGTs share a common reaction scheme transferring a sugar-moiety from an activated UDP-sugar cofactor to a receiver molecule. The reaction results in the product sugar conjugate, UDP and water. Two distinct products are known for *O*-glycosyltransferases, an ester and a glycoside conjugate (Lim et al., 2003). George-Thompson and colleagues proposed the mechanistic differences in glycoside or glycoside-ester formation for SA (George Thompson et al., 2017). Both mechanisms depend on His18 and Asp111 to facilitate coordination of the SA anion in the active site and orient the respective site of glycosylation towards the UDP-glucose molecule. In the salicylate glucose ester (SGE) forming mechanism, Thr15 additionally coordinates the oxygen atom of the carboxy group, opening the anionic oxygen atom for glycosylation via a nucleophilic attack (Figure 5B). The salicylic acid glucoside (SAG) forming



mechanism is supported by Thr365, which coordinates the anionic oxygen atom by a hydrogen bridge, forcing the 2-hydroxy group to face the UDP-glucose molecule (Figure 5C).

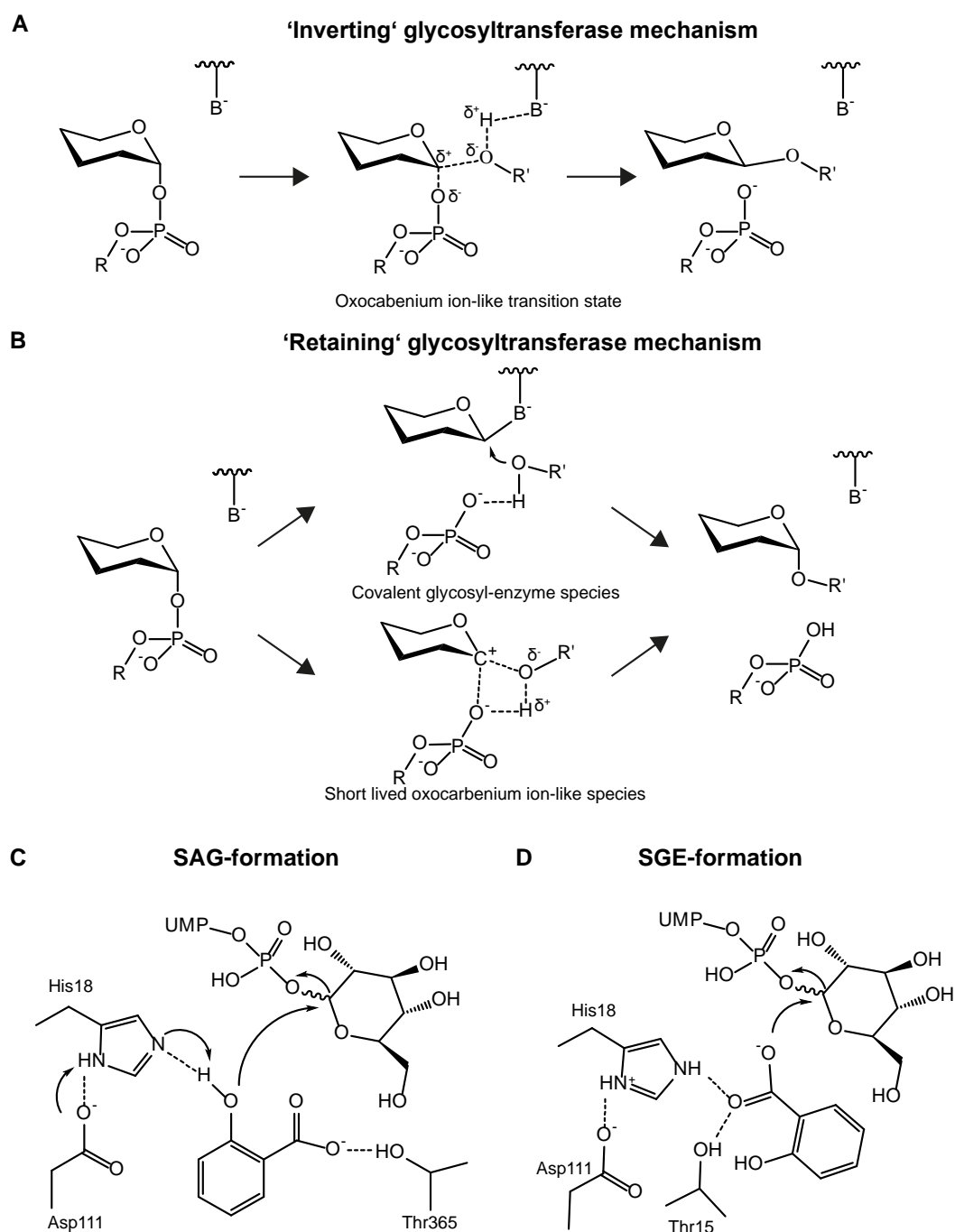


**Figure 5: General mechanism of uridine-diphosphate-glucose-dependent O-glycosyltransferases.** The aglycon substrate is conjugated to glucose from uridine-diphosphate (UDP)-glucose. The reaction products are a glycon, UDP and water. Two reaction mechanisms have been discussed, "Inverting" (A) and "Retaining" (B). The "Inverting" mechanism relies on an enzyme-substrate complex with the aglycon. The "Retaining" mechanism includes either a covalent glycosyl-enzyme species or an oxocarbenium ion-like species. The latter mechanism has not been fully understood. (C) and (D) show the amino acids of the active center of UGT74F2 being able to form both SAG and SGE. His18, Asp111 and Thr365 catalyze SAG-formation (C). The 2-OH-group of SA performs an  $S_N2$ -like reaction at the chiral carbon atom of the activated glucose of the UDP-Glc cofactor. His18, Asp111 and Thr15 catalyze SGE-formation (D). Their dual coordination of oxygen leads to the ability of the oxo-anion to perform the  $S_N2$ -like reaction at the chiral carbon atom of the activated glucose of the UDP-Glc cofactor. Figure redrawn after (Albesa-Jové and Guerin, 2016; George Thompson et al., 2017).

Glycosylation regulates physiochemical properties of metabolites, which influence: bioactivity, solubility and transport (Ross et al., 2001). These different molecular fates already imply that UGTs may play a role in plant pathogen interactions, by modulating the activity of compounds being involved as signals or phytoalexins. The regulation of bioactivity is important to balance basal metabolism with defense (Zhang et al., 2017). In context of SAR increased solubility for storage and transport may play a role in signal propagation and immune memory (Zeier, 2021). Transcripts of several UGTs are increased upon bacterial pathogen or signaling molecule treatment. However, *UGT76B1* (AT3G11340) is a highly induced transcript in RNAseq analysis and publically available co-expression data with for example *FMO1* (ATTED-II, ver. 11.0, (Yildiz et al., 2021; Obayashi et al., 2022)). Prior to this thesis *UGT76B1* was shown to use SA, isoleucic acid (ILA) and leucic acid as aglycon substrates (von Saint Paul et al., 2011; Noutoshi et al., 2012; Maksym et al., 2018). Furthermore, *UGT76B1*'s role in the crosstalk between SA and JA via ILA raised (von Saint Paul et al., 2011; Maksym et al., 2018). It is annotated as enzyme with a GT-B three-dimensional structure status that exhibits an “inverting” reaction mechanism (<https://www.uniprot.org/uniprot/Q9C768>, <http://www.cazy.org/GT1.html>, both accessed 03.05.2022).

### 2.2.3.2 Methylation

Methyl transferases (MTs) are key enzymes for epigenetic modification of DNA and histones but are also able to metabolize small molecules, like plant hormones (Zubieta et al., 2003; Lee et al., 2016; Zhang et al., 2018). MTs are able to methylate functional groups containing oxygen, nitrogen and carbon (Zubieta et al., 2001). The transition of a carboxy group into methyl-ester results in increased metabolite stability associated with increased volatility (Zubieta et al., 2003). Most commonly, MTs use *S*-adenosyl-*L*-methionine (SAM) as cofactor (Ward et al., 2021). SAM is generated from adenosine triphosphate (ATP) and methionine by SAM-synthetases (Markham et al., 1980). A common group of MTs are members of the SA:Benzoat:Theobromine (SABATH) family, exclusively found in the plant kingdom with 24 members found in *Arabidopsis* (D'Auria et al., 2003). Some SABATH family MTs were shown to transfer the methyl group to oxygen rather than nitrogen (D'Auria et al., 2003). A methylated phytohormone, for instance, is methyl JA (MeJA) and its MT has already been described (Seo et al., 2001). Another example is MeSA, which is synthesized by an SAM-dependent MT as well (Shulaev et al., 1997; Chen et al., 2003).

The active center required for substrate recognition was determined from a crystal structure of a *Clarkia breweri* SA-MT (Zubieta et al., 2003). The structure shows a binding pocket for SAM or the product of the reaction *S*-adenosyl-*L*-homocystein (SAH) and a SA binding pocket positioning the carboxylic acid group of SA in close proximity to the methyl donor site (Zubieta

et al., 2003). A conserved hydrogen-bonding motif for SAM binding of SAM-dependent MTs was characterized (Djordjevic and Stock, 1997). The general reaction mechanism of SAM-dependent MTs is a nucleophilic substitution (Figure 6). The MT substrate harbors a nucleophile that attacks the S-methyl auf SAM. The reaction results in a methylated acceptor molecule, SAH and a proton (Zubieta et al., 2003; Struck et al., 2012). Another group of MTs alternatively uses *N*<sup>5</sup>-methyltetrahydrofolate as methyl donor instead of SAM (Laduron, 1972; Banerjee and Snyder, 1973).

Turnover by methylation can result in inactivation but may also raise the opportunity of signal distribution and storage. The activity of methyl esterase (MES) enzymes has the potential to result in a mode of reactivation during immune memory or in naïve systemic tissue (Park et al., 2007). For instance, in tobacco, potato and Arabidopsis MESs capable to hydrolyze MeSA to SA were identified (Forouhar et al., 2005; Vlot et al., 2008; Manosalva et al., 2010; Shah and Zeier, 2013).

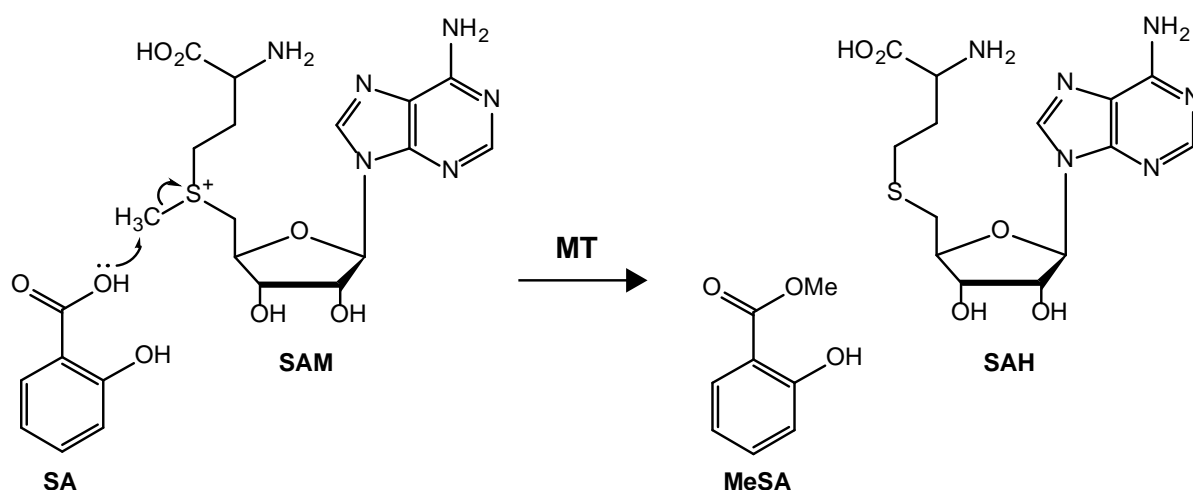


Figure 6: **Reaction mechanism of SAM-dependent methyl transferases with SA.** SA represents the nucleophilic substrate of the methyltransferase (MT). The nucleophilic group, represented by the free electron pair of the oxygen in the carboxy group of SA, attacks the partial positively charged carbon in the methyl group of the S-adenosyl-L-methionin (SAM) cofactor. Via a nucleophilic substitution mechanism, the proton is going into solution and the methyl group is added to the nucleophilic substrate. The products of the reaction are the methylated substrate, MeSA and S-adenosyl-L-homocysteine (SAH). Adapted from (Struck et al., 2012).

### 2.2.3.3 Hydroxylation

Hydroxylases are valuable enzymes to modify hormones by the addition of a hydroxyl group. Benzoic acids, for example, are subject of turnover to di-hydroxy benzoic acids (DHBAs) by hydroxylases in Arabidopsis (Zhang et al., 2013; Zhang et al., 2017). Hydroxy groups result in additional modification sites for MT or GTs. In addition to DHBAs, JA and JA-Ile were found to be hydroxylated at carbon atom 12. The JA-oxidase (JOX) converts JA to 12-hydroxy JA (12-OHJA), which itself is target for glycosylation and sulfatation resulting in 12-OGlc-JA and

12-HSO<sub>4</sub>-JA (Wasternack and Hause, 2013). Sequential hydroxylation as shown for JA-Ile by cytochrome P450 enzymes (CYP) CYP94B3 and CYP94C1 might as well result in the formation of a carboxy group (Wasternack and Hause, 2013).

### 2.2.3.4 Amino acid conjugation

Gretchen Hagen 3 (GH3) enzymes are acyl acid amido synthetases able to catalyze amino acid conjugations to small molecules (Westfall et al., 2010). The GH3 enzyme family is a very diverse group of proteins that fulfills several functions in phytohormone metabolism ranging from biosynthesis, and activation to inactivation (Westfall et al., 2010; Rekhter et al., 2019b). As already mentioned the GH3 enzyme PBS3 was shown to play a crucial role in hormone biosynthesis, conjugating IC to glutamate following a decomposition of the precursor IC-9-Glu to the active hormone SA (Rekhter et al., 2019b). Other GH3 enzymes are shown to play a role in metabolite activation such as JAR1 and GH3.10, which conjugate JA to isoleucine forming JA-Ile (Staswick and Tiryaki, 2004; Delfin et al., 2022). Inactivation of the active compound is proposed as third mechanism of GH3 enzymes. GH3.5 conjugates SA to aspartic acid leading to SA-inactivation (Mackelprang et al., 2017). Westfall and colleagues demonstrated that over expression of GH3.5 leads to increased levels of SA-Asp (Westfall et al., 2016). Additionally, GH3.5 was shown to catalyze the conjugation of indole acetic acid to aspartic acid leading as well to inactivation and degradation of auxin (Westfall et al., 2010; Mackelprang et al., 2017). The largest group, the group two GH3 enzymes: GH3.1, 2, 3, 4, 6, 9 and 17 are responsible for indole acetic acid turnover (Casanova-Sáez et al., 2022).

### 2.2.4 SA turnover

A way to terminate the SA signal is its metabolic turnover (Song et al., 2008). On the one hand, SA has a carboxy and a hydroxy group that can reversibly be chemically modified. On the other hand, the aromatic benzene backbone harboring a delocalized pi-electron system may be accessible for irreversible modifications as well. Until now, a number of enzymatic SA modifications have been described (Figure 7). At least three UGTs were shown to glycosylate SA UGT74F1, UGT74F2 and UGT76B1 (Song et al., 2008; Noutoshi et al., 2012). They can glycosylate SA at both the carboxy and the hydroxy group (von Saint Paul et al., 2011; Noutoshi et al., 2012). Song and colleagues described UGT74F2 as being early responsive to disease in Arabidopsis (Song, 2006). Later they were able to show that UGT74F2 glucosylates SA-methyl ester (MeSA) to MeSAGlc *in vitro* (Song et al., 2008). In addition, MeSAGlc formation by UGT71C3 was recently suggested *in vitro* and *in vivo*, thus influencing defense and SAR (Chen et al., 2019). BENZOIC ACID/SALICYLIC ACID METHYLTRANSFERASE1 (BSMT1) synthesizes MeSA in an SAM-dependent manner (Chen et al., 2003). Two

hydroxylases SA-3-HYDROXYLASE (S3H) and SA-5-HYDROXYLASE (S5H) are known to use SA as substrate, forming 2,3-DHBA and 2,5-DHBA (Zhang et al., 2013; Zhang et al., 2017). In addition, SA metabolites can be further targets of turnover by glycosylation (Li et al., 2014; Huang et al., 2018; Chen et al., 2019).

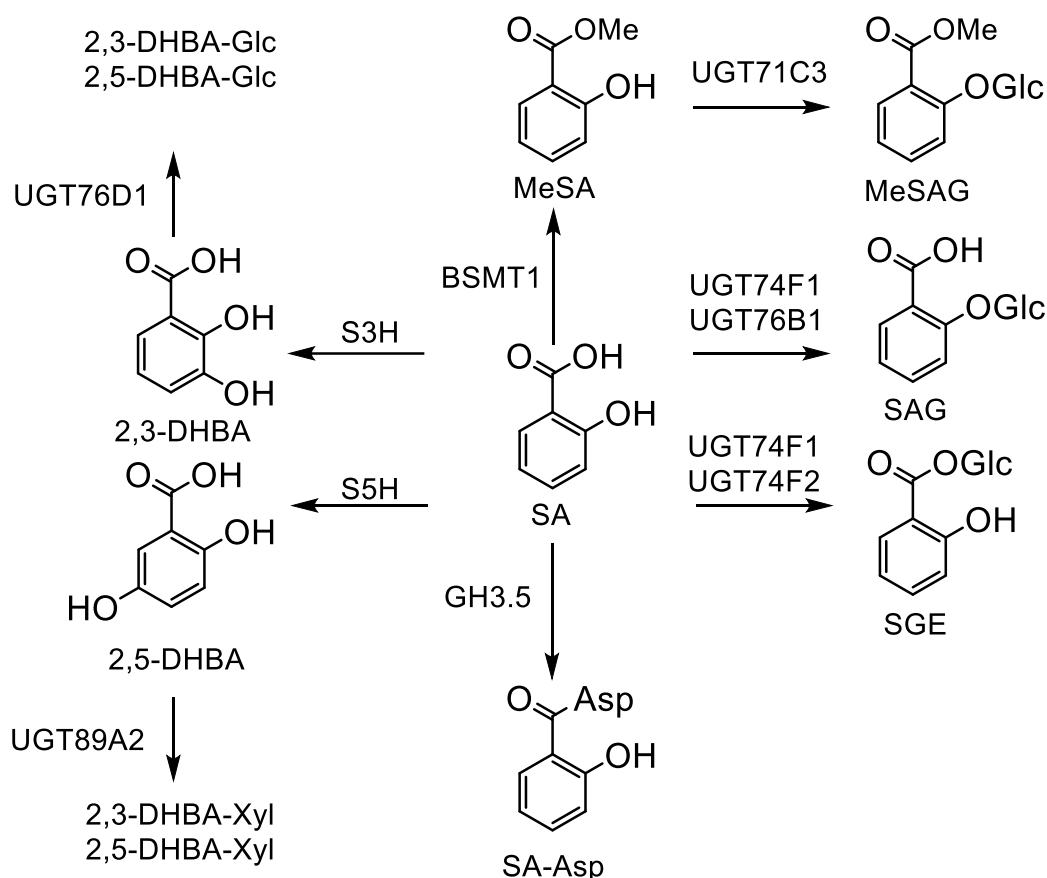


Figure 7: **Metabolic network of SA.** SA is a common defense molecule of plants (Mettraux et al., 1990). SA is metabolized into several compounds. SA glycosylation by UGT76B1 and UGT74F1 results in the SA-O-glycoside (SAG) (von Saint Paul et al., 2011; George Thompson et al., 2017). SA glycosylation reaction by UGT74F2 mainly results in SA-glycoside-ester (SGE) (Song, 2006; Song et al., 2008). SA-methyl ester (MeSA) is synthesized by BSMT1 (Chen et al., 2003). MeSA is glycosylated by UGT71C3 resulting in MeSA-O-glycoside (MeSAG) (Chen et al., 2019). SA can also be turned over via hydroxylation by the enzymes SA-3-HYDROXYLASE (S3H) and SA-5-HYDROXYLASE (S5H) forming 2,3-di-hydroxy-benzoic acid (2,3-DHBA) and 2,5-di-hydroxybenzoic acid (2,5-DHBA), respectively (Zhang et al., 2013; Zhang et al., 2017). The two DHBAs themselves can be glycosylated by UGT76D1 or xylosylated by UGT89A2 (Li et al., 2014; Huang et al., 2018). The amino acid conjugate SA-aspartate (SA-Asp) is synthesized by Gretchen Hagen 3 enzyme 5 (GH3.5) (Zhang et al., 2007; Chen et al., 2013).

## 2.2.5 NHP turnover

With respect to NHP metabolism so far a single molecular modification has been described, the glycosylation (Figure 8). Convincing evidence were laid out about the presence of the NHP-O-glycoside (NHP-OGlc) (Chen et al., 2018). In addition, a second glycoside, NHP-glycoside ester was detected (Hartmann and Zeier, 2018; Bauer et al., 2021). Nevertheless, besides the description of the glycosylated-NHP molecules neither an enzyme being able to catalyze their

synthesis nor the molecular function of NHP-glycosylation were identified. Similarly, it is unclear, whether NHP can be converted into Pip and if other NHP-metabolites are synthesized in the response to pathogen, as for example NHP-conjugates or methylated NHP molecules. None of the other mentioned enzymatic activities being able to turnover metabolites: methylation, hydroxylation, or amino acid conjugation were described for NHP prior to this thesis.

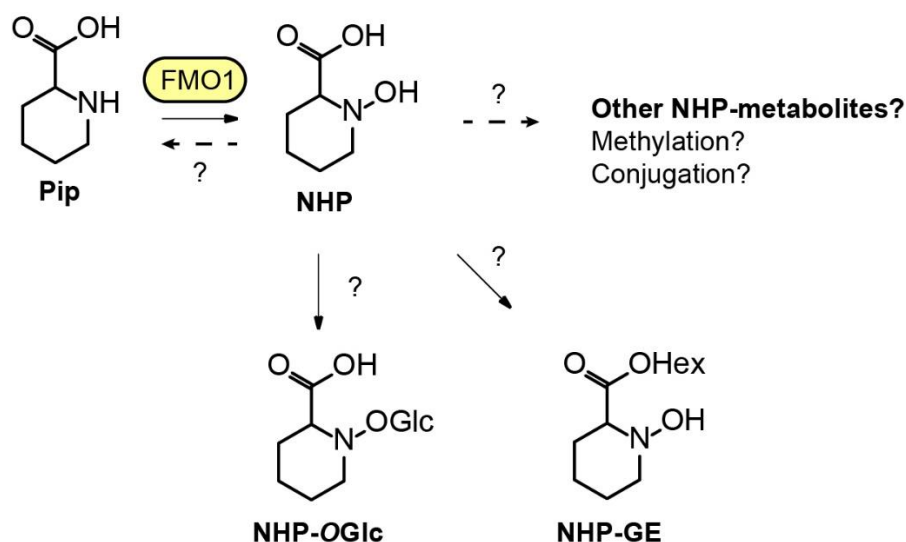


Figure 8: **NHP metabolite network.** As described above NHP is synthesized from Pip via FMO1, however further metabolic routes remain elusive. NHP was shown to be present as two glycosidic forms NHP-O-glycoside (NHP-OGlc) and NHP-glycoside-ester (NHPGE), however, no enzymes able to catalyze the biosynthesis were described prior to this thesis (Chen et al., 2018; Hartmann and Zeier, 2018; Bauer et al., 2021). If other NHP-metabolites are present in plants and if NHP can be converted to Pip remains unknown.

## 2.3 Systemic acquired resistance

In addition to a local immune response at the site of infection, plants show the ability to alert uninfected systemic tissue for a robust defense response in the event of a secondary infection (Ross, 1961). Several molecules are discussed as mobile signals promoting the primary defense response during SAR (Figure 9) (Dempsey and Klessig, 2012; Fu and Dong, 2013). MeSA, glycerol-3-phosphate, azelaic acid, JA, dehydroabietinal and Pip were functionally connected with SAR (Shulaev et al., 1997; Park et al., 2007; Truman et al., 2007; Jung et al., 2009; Chanda et al., 2011; Fu and Dong, 2013; Bernsdorff et al., 2016). However, most of the proposed molecules have not been unambiguously assigned to be a SAR mobile signal. The amount of SAR related signals is vast so that the community of plant scientists sent an “SOS” (Dempsey and Klessig, 2012). The *FMO1* gene has a critical role for successful SAR establishment (Mishina and Zeier, 2006). Together with *FMO1* functional annotation to synthesize NHP from Pip, NHP came into focus to be critical for SAR and to be the mobile

signal to the distal tissue (Chen et al., 2018; Hartmann et al., 2018). Schnake and colleagues provided further evidence about the detection of NHP in petiole exudates from local and systemic leaves of *Cucumis sativus* in an infection dependent manner (Schnake et al., 2020). During the propagation of SAR triggered by insect eggs, NHP and SA are suggested to play a key role, as *ics1*, *ald1* and *fmo1* mutants cannot trigger a SAR response (Alfonso et al., 2021). Alfonso and colleagues showed that the oviposition does trigger both a systemic immune response against the necrotrophic fungus *Botrytis cinerea* and against the oomycete pathogen *Hyaloperonospora arabidopsidis* Noco 2 (*H.a.* Noco 2) (Alfonso et al., 2021).

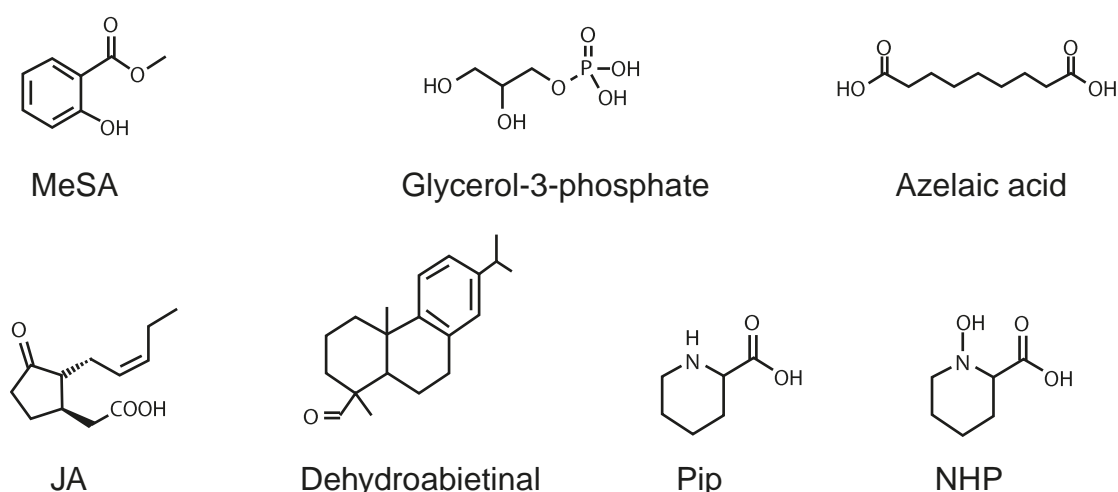


Figure 9: **Compounds suggested to be mobile signals in SAR.** MeSA, Glycerol-3-phosphate-derivatives, azelaic acid, JA, dehydroabietinal, Pip and NHP are suggest to be required as mobile signals during SAR. Modified from (Dempsey and Klessig, 2012).

## 2.4 Metabolomics in plant science

To unravel the metabolic composition within a plant tissue, metabolomics is an emerging discipline in biochemistry and molecular biology. Over the recent years, the number of publications per year applying metabolomics is steadily increasing (Letertre et al., 2020). Whereas genomics and transcriptomics deal with the whole complement of genes or transcripts and proteomics cover the level of proteins, metabolomics is the method to investigate cellular responses at the level of small molecules. Metabolites can be subdivided in central and, especially important for this work, specialized metabolism (Patti et al., 2012; Feussner and Polle, 2015). The metabolome of a developing plant undergoes dramatic changes, when the plant is challenged (Bennett and Wallsgrave, 1994). External threads like, wounding, high energetic light or bacterial and fungal pests result in a widespread response of the metabolome (König et al., 2014; Haroth et al., 2019; Gao et al., 2020). The estimated number of metabolites in the plant kingdom ranges from  $1 \times 10^5$  to  $1 \times 10^6$  compounds (Alseekh and Fernie, 2018). Taking the enormous structural diversity of small molecules in living

organisms into account, a comprehensive analysis of the metabolome, which represents the entire content of all small molecular weight molecules, is until now not possible. Nevertheless, there are different strategies available to cover a large number of compounds. Within the discipline of metabolomics, on the one hand, we aim to detect, visualize and draw conclusions out of these changes, to develop hypotheses about the mechanistically response of the analyzed plant (Kaefer et al., 2009; Kaefer et al., 2013; Kaefer et al., 2015; Chong et al., 2019; Feussner and Feussner, 2019). With non-targeted approaches, like ultra-high performance liquid chromatography coupled to electrospray ionization high resolution mass spectrometry (UHPLC-ESI-HRMS)-based metabolome analysis, the challenge to identify infection and defense marker, which are built after the attack of a pathogen, can be taken. In addition, non-targeted metabolome analysis allow to overview the metabolic changes within a threatened organism and can help to describe defense adaptation processes on a more global scale. On the other hand, targeted metabolomics profiling analyses are a way to challenge hypothesis, for example a functional gene-molecule relationship when the metabolites involved are known. Additionally, targeted quantitative metabolomics enable quantification of molecules from biological tissue, when certain prerequisites like authentic standard availability and MS calibration are matched (Herrfurth and Feussner, 2020). Approximately, 14 thousand metabolites are quantifiable within the plant kingdom (Alseekh et al., 2021). In the medical field metabolomics emerge to become a powerful tool for clinical diagnostics (Pang et al., 2019).

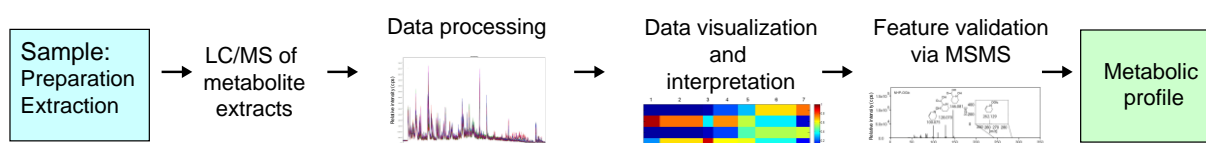
A powerful tool is the combination of UHPLC-ESI-HRMS, here referred to as non-targeted metabolome analysis (Feussner and Feussner, 2019). As the terminology suggests, the analysis of the metabolome does not only include an aim for defined compounds, but is designed to detect small molecules at a global scale within a metabolite extract in an unbiased manner (Figure 10A) (Patti et al., 2012). An UHPLC-ESI-HRMS-based method is designed to adequately separate complex metabolite extracts by the chemical properties of the constituents, via the interaction to the chromatographic column on the LC-unit. Throughout the analysis, each component retains at the column at a LC-specific retention time. In a next step, the eluting molecules are ionized via ESI, an efficient and soft ionization method. ESI represents the perfect ionization method to combine LC with mass spectrometry (Banerjee and Mazumdar, 2012). In the charged state, mainly as  $[M+H]^+$  in positive ESI or as  $[M-H]^-$  in negative ESI, the molecule ions may travel via a quadrupole of the mass spectrometer, and may be detected via their time-of-flight (TOF) in the flight tube. The detector is able to gain high mass accuracy information about each individual molecule, given as mass-to-charge ratio ( $m/z$ ). If several molecule ions of the same identity are detected, the signal intensity could increase. The intensity information hereby is classified as relative signal intensity in counts per seconds (cps), also because the ionization efficiency for each compound depends on its chemical structure and differs therefore for the metabolites. Each signal with a unique accurate



mass information given as  $m/z$  in combination with its specific retention time and its relative intensity over all the samples of one sample batch is considered as metabolite feature. The sum of these features provide a general overview about the molecular state of the tissue and allow comparison between different conditions, for instance biotic or abiotic stress treatments. However, each of the molecular features of interest requires an unequivocal identification and confirmation of its chemical structure based on accurate mass information, tandem mass spectrometry (MSMS)-experiments and/or by co-elution with an authentic standard (Patti et al., 2012). Together with compound databases like KEGG and Biocyc for the search of tentative identities by accurate mass comparison and METLIN or MassBank for unequivocal structure confirmation, the verification of the chemical structure of a metabolite markers is driven (Zhu et al., 2013). Complete annotation of a dataset is a desirable goal, however, to date no complete metabolome of any organism was described (Viant et al., 2017). In addition, the uncertainty about each molecules ionization efficiency and the influence of ion suppression by co-eluting molecules is limiting the method, to only relative information. Non-targeted metabolome datasets can be stored in public repositories like MetaboLights enabling access to the scientific community (Haug et al., 2020).

To achieve quantitative data about molecules in plant tissue, information on the specific retention time, ionization efficiency, fragmentation behavior of the analyte is mandatory. In addition, stably labeled authentic standards for each analyte that are going to be quantified need to be added to the sample before extraction. This allows to monitor the recovery rate during extraction to obtain, in combination with the knowledge about the detector calibration, absolute amounts for a compound in a complex extract (Figure 10B) (Herrfurth and Feussner, 2020). Within the quantitative metabolomics workflow, we can use a specific, very fast and sensitive mode for data acquisition, the so-called single, respectively, multiple reaction monitoring (SRM or MRM). In this mode for each compound under analysis, one or more specific transitions are defined, which contain the information about the  $m/z$  of the complete molecular ion and one or several respective fragment ions. The pieces of information can be compared and calculated back to the amount of tissue extracted, to quantitatively describe, the molecular abundance in the sample (Herrfurth and Feussner, 2020). The quantified metabolites can be compared between sample groups or even different experiments based on absolute amounts (Patti et al., 2012).

## A Non-targeted metabolome analysis



## B Quantitative metabolomics

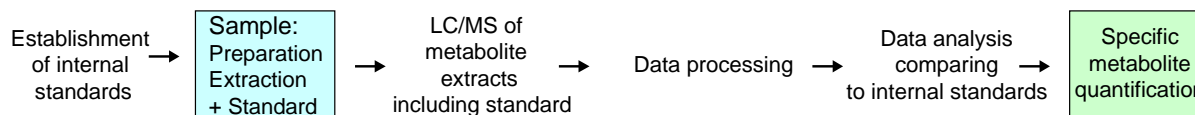


Figure 10: **Non-targeted metabolome and quantitative metabolomics analysis workflows.** Non-targeted metabolome analysis (A) require sample preparation in an experimental setup and metabolite extraction. The metabolite extract is processed via LC/MS. Derived data has to be processed and visualized for interpretation. Identified metabolic features are validated via MSMS-fragmentation. The outcome of non-targeted metabolome analysis is a metabolic profile of the analyzed sample. Quantitative metabolomics (B) require established workflows with standard metabolites for quantification. Sample preparation is followed by metabolite extraction, which includes the addition of standard metabolites. The metabolite extract is processed via LC/MS. The derived data is processed comparing native signals and standards and analyzed to allow quantitative comparisons. The outcome of a quantitative metabolomics analysis can be specific metabolite quantification. Figure modified from (Patti et al., 2012).

## 2.5 Aims of the study

The aim of the study was to unravel the metabolic network of NHP and SA, including the investigation of enzymes fulfilling essential function in either biosynthesis or metabolic turnover of these hormones mediating plant immunity. In detail, we aim to describe the function of UGT76B1 in the plant immune network and to investigate the cause of reduced growth in the *ugt76b1-1* mutant plant. We wanted to investigate the role of NHP-OGlc in the onset of SAR, and test if it was required to successful SAR establishment. Furthermore, we aim to characterize the NHP metabolome in an unbiased non-targeted metabolomics approach. Therefore, we developed a dual-infiltration approach that tracks molecule transition of infiltrated labeled and unlabeled NHP *in vivo*. Additionally, we characterize novel metabolites of NHP including NHP-OGlc-hexose (NHP-OGlc-Hex), NHP-OGlc-malonic acid (NHP-OGlcMal), NHP-methyl ester (MeNHP) and NHP-methyl ester-O-glucoside (MeNHP-OGlc). Investigations into methylated NHP towards its structural and functional features are described.

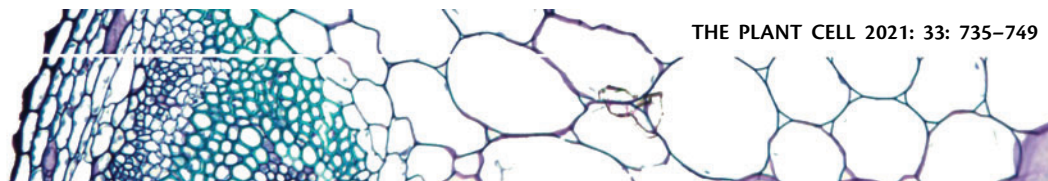
### 3. Chapter I. - The glycosyltransferase UGT76B1 modulates *N*-hydroxy pipecolic acid homeostasis and plant immunity

This article was published online in *The Plant Cell* in January 2021. The supplementary materials are attached to the main part. The full article can be found online:

<https://doi.org/10.1093/plcell/koaa045>

#### **Author contribution:**

Lennart Mohnike planned and performed the *Pseudomonas* infection underlying the non-targeted metabolome analysis by UHPLC-ESI-HRMS. Additionally, he performed *Pseudomonas* infection and UV-stress experiments for metabolite quantification. Furthermore, he amplified, cloned, expressed and established the purification of AtUGT76B1. The purified enzyme he used to conduct *in vitro* enzyme activity tests. Additionally, he performed gene expression analysis and conducted the labeled D<sub>9</sub>-NHP tracking experiment. He analyzed and processed the data from these experiments. Furthermore, he displayed and discussed the presented data and wrote the first draft of the manuscript.



# The glycosyltransferase UGT76B1 modulates *N*-hydroxy-pipecolic acid homeostasis and plant immunity

Lennart Mohnike <sup>1,†</sup>, Dmitrij Rekhter <sup>1,†</sup>, Weijie Huang <sup>2,†</sup>, Kirstin Feussner <sup>1,3</sup>,  
 Hainan Tian <sup>2</sup>, Cornelia Herrfurth <sup>1,3</sup>, Yuelin Zhang <sup>2,\*,\*†</sup> and Ivo Feussner <sup>1,3,4,\*,\*†</sup>

- 1 Department of Plant Biochemistry, Albrecht-von-Haller-Institute for Plant Sciences, University of Goettingen, D-37077 Goettingen, Germany
- 2 Department of Botany, University of British Columbia, Vancouver, BC V6T 1Z4, Canada
- 3 Service Unit for Metabolomics and Lipidomics, Goettingen center for Molecular Biosciences (GZMB), University of Goettingen, D-37077 Goettingen, Germany
- 4 Department of Plant Biochemistry, Goettingen Center for Molecular Biosciences (GZMB), University of Goettingen, D-37077 Goettingen, Germany

\*Author for correspondence: ifeussn@uni-goettingen.de (I.F.) and yuelin.zhang@ubc.ca (Y.Z)

<sup>†</sup>These authors contributed equally to this work.

<sup>\*</sup>Senior authors.

Y.Z. and I.F. designed and supervised the study. Experimental research was conducted by L.M., D.R., W.H., K.F., and H.T., and C.H. L.M., D.R., W.H., K.F., C.H., Y.Z., and I.F. analyzed the data and wrote the manuscript.

The authors responsible for distribution of materials integral to the findings presented in this article in accordance with the policy described in the Instructions for Authors (<https://academic.oup.com/plcell/pages/General-Instructions>) are: Yuelin Zhang (yuelin.zhang@ubc.ca) and Ivo Feussner (ifeussn@uni-goettingen.de).

## Abstract

The tradeoff between growth and defense is a critical aspect of plant immunity. Therefore, the plant immune response needs to be tightly regulated. Salicylic acid (SA) is an important plant hormone regulating defense against biotrophic pathogens. Recently, *N*-hydroxy-pipecolic acid (NHP) was identified as another regulator for plant innate immunity and systemic acquired resistance (SAR). Although the biosynthetic pathway leading to NHP formation is already been identified, how NHP is further metabolized is unclear. Here, we present UGT76B1 as a uridine diphosphate-dependent glycosyltransferase (UGT) that modifies NHP by catalyzing the formation of 1-*O*-glucosyl-pipecolic acid in *Arabidopsis thaliana*. Analysis of T-DNA and clustered regularly interspaced short palindromic repeats (CRISPR) knock-out mutant lines of UGT76B1 by targeted and nontargeted ultra-high performance liquid chromatography coupled to high-resolution mass spectrometry (UHPLC-HRMS) underlined NHP and SA as endogenous substrates of this enzyme in response to *Pseudomonas* infection and UV treatment. *ugt76b1* mutant plants have a dwarf phenotype and constitutive defense response which can be suppressed by loss of function of the NHP biosynthetic enzyme FLAVIN-DEPENDENT MONOOXYGENASE 1 (FMO1). This suggests that elevated accumulation of NHP contributes to the enhanced disease resistance in *ugt76b1*. Externally applied NHP can move to distal tissue in *ugt76b1* mutant plants. Although glycosylation is not required for the long-distance movement of NHP during SAR, it is crucial to balance growth and defense.

## Introduction

Plants are constantly exposed to biotic and abiotic stress. To deal with external threats, plants have developed an impressive repertoire of chemical compounds. However, there is a trade-off between defense and growth as shown in autoimmune mutants such as *snrc2-1D*, *npr1-1*, and *s3h s5h*, which accumulate high levels of defense hormones and exhibit severe dwarf phenotypes (Zhang et al., 2010, 2017). To balance growth and defense responses, plants constantly monitor and adjust the homeostasis of these compounds. Dynamic changes of the levels of immune signaling molecules allow plants to react rapidly and appropriately to danger (Hartmann and Zeier, 2019; Huang et al., 2020). The biosynthesis, transport, and homeostasis of the signaling molecules are therefore strictly regulated to prevent unintended consequences.

Two signaling molecules, salicylic acid (SA) and *N*-hydroxy-pipecolic acid (NHP), are particularly important in plant defense against biotrophic pathogens. Together they orchestrate the immune response in the local tissue to prevent pathogen spread (Hartmann et al., 2018; Guerra et al., 2020). Locally produced defense signals are further translocated to distal parts of the plant, leading to massive transcriptional, and metabolic reprogramming in the naive tissues, which enables a quick and robust response to subsequent infections (Bernsdorff et al., 2016). This induced immunity in distal tissue is termed as systemic acquired resistance (SAR). Most of the signaling molecules participating in the induction of SAR can be found in the phloem upon infection (Fu and Dong, 2013). The effect of SA and NHP in the context of plant immunity has been well documented (Chen et al., 2018; Hartmann et al., 2018; Zhang and Li, 2019; Huang et al., 2020).

Biosynthesis of SA is divided into two major routes that result in SA formation in planta: The phenylpropanoid or PHENYLAMMONIA LYASE (PAL) pathway and the ISOCHORISMIC ACID SYNTHASE 1 (ICS1) pathway (Yalpani et al., 1993; Wildermuth et al., 2001). Nevertheless, in *Arabidopsis thaliana* ~90% of endogenous SA derives from chloroplast-derived isochorismic acid, which is exported to the cytosol via ENHANCED DISEASE SUSCEPTIBILITY 5 (EDS5) and conjugated to glutamate by AvrPphB SUSCEPTIBLE 3 (PBS3). The formed isochorismic acid-9-glutamic acid then spontaneously decomposes into SA and enolpyruvyl-*N*-glutamic acid (Rekhter et al., 2019b). Furthermore, ENHANCED PSEUDOMONAS SUSCEPTIBILITY 1 (EPS1) has been shown to enhance SA formation from isochorismic acid-9-glutamic acid (Torrens-Spence et al., 2019).

NHP was recently discovered as a signaling compound for plant defense against biotrophic pathogens (Chen et al., 2018; Hartmann et al., 2018). So far, research has focused on the biosynthesis of NHP from lysine. In the first step, the  $\alpha$ -aminotransferase AGD2-LIKE DEFENSE RESPONSE PROTEIN 1 (ALD1) catalyzes the transamination of lysine into  $\epsilon$ -amino- $\alpha$ -keto caproic acid (Song et al., 2004; Navarova et al., 2012; Vogel-Adghough et al., 2013) (Figure 1). This compound spontaneously cyclizes and thereby yields  $\Delta^1$ -

piperidine-2-carboxylic acid (P2C). In a second step, the ketimine reductase SAR-DEFICIENT 4 (SARD4) catalyzes the formation of pipecolic acid (Pip) from P2C (Ding et al., 2016; Hartmann et al., 2017). Pip requires *N*-hydroxylation to NHP in order to reach its full protective capacity. This activation is catalyzed by FLAVIN-DEPENDENT MONOOXYGENASE 1 (FMO1) (Chen et al., 2018; Hartmann et al., 2018) (Figure 1).

One important strategy to maintain a preferred concentration of an active metabolite is chemical modification, which can change the bioavailability and activity of the compound. Different modifications of SA such as hydroxylation and methylation have been described (Song et al., 2009; Zhang et al., 2017). SA itself as well as its catabolites can be further xylosylated (addition of the pentose xylose) and glycosylated (addition of a hexose) (Song et al., 2008; Bartsch et al., 2010; Huang et al., 2018). The transfer of an activated sugar moiety onto a target molecule is predominantly catalyzed by the widespread enzyme family of uridine diphosphate (UDP)-DEPENDENT GLYCOSYL TRANSFERASES (UGTs). The closely related UGT74F1 and UGT74F2 catalyze the formation SA-glycoside (SAG) and SA glucose ester (SGE), respectively (Dean and Delaney, 2008; George Thompson et al., 2017). Another enzyme UGT71C3 was recently shown to be responsible for the biosynthesis of methyl-SA glycoside (Chen et al., 2019). Despite the high abundance of these glycosides upon stress, the biological significance of the formation of these compounds is elusive. Blocking glycosylation of SA has been shown to result in enhanced disease resistance (Noutoshi et al., 2012). In tobacco (*Nicotiana tabacum*), SAG is transported from the cytosol into vacuoles, suggesting that the glucosides are a storage form of SA. On the other hand, the formation of SAG may be important for the vascular transport, as there is evidence that SAG can be hydrolyzed back into SA in the extracellular space (Hennig et al., 1993; Seo et al., 1995).

So far, only one metabolite of NHP was identified, namely NHP-*O*-glycoside (NHP-OGlc) (Chen et al., 2018; Hartmann et al., 2018). Intriguingly, externally supplied NHP can be found in distal tissues in uninfected *fmo1* mutant plants as NHP and NHP-OGlc, suggesting that at least one of these molecules is mobile *in planta* (Chen et al., 2018). Until now, neither the function of NHP-OGlc nor the enzyme that catalyzes the glycosylation of NHP has been identified. Here we report that UGT76B1, which was previously reported to glycosylate SA and 2-hydroxy-3-methyl-pentanoic acid (isoleucic acid, ILA), catalyzes the formation of NHP-OGlc (von Saint Paul et al., 2011; Noutoshi et al., 2012; Maksym et al., 2018). UGT76B1 has strong *in vitro* activity toward NHP and no detectable amount of NHP-OGlc is synthesized in *ugt76b1* mutant plants, which results in increased NHP accumulation, a dwarf phenotype, and enhanced disease resistance against biotrophic pathogens. Moreover, we show that externally applied NHP is mobile to distal tissue in the absence of UGT76B1 and that transport of NHP seems not to depend on further glycosylation.

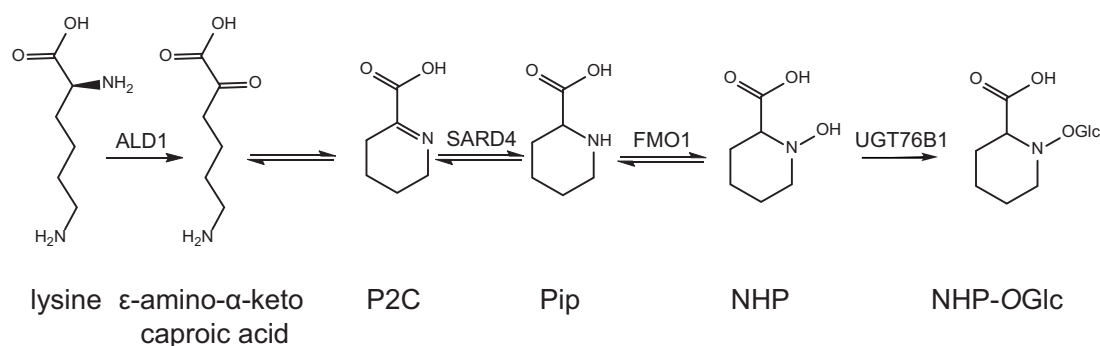


**Figure 1** Biosynthesis of NHP-OGlc. The biosynthesis of NHP-OGlc starts from L-lysine, which is converted by ALD1 to  $\epsilon$ -amino- $\alpha$ -keto caproic acid (Song et al., 2004; Navarova et al., 2012; Vogel-Adghough et al., 2013). The compound spontaneously cyclizes to P2C and is reduced by SARD4 to Pip (Ding et al., 2016; Hartmann et al., 2017). FMO1 hydroxylates Pip to form NHP, the biologically active pipercolate (Chen et al., 2018; Hartmann et al., 2018). In a last step, NHP is glucosylated at the hydroxyl functional group to form NHP-OGlc.

## Results

### Nontargeted metabolome analysis of infected leaf tissue revealed NHP as the *in vivo* substrate of UGT76B1

Searching for the protein that catalyzes the formation of NHP-OGlc, we identified *UGT76B1* as a recurring candidate gene from several studies (von Saint Paul et al., 2011; Noutoshi et al., 2012; Gruner et al., 2013; Hartmann et al., 2018). *UGT76B1* was classified as a SAR gene in these studies. In addition, by screening online co-expression databases, we established that *UGT76B1* is co-expressed with *FMO1*. This encouraged us to further investigate the role *UGT76B1* in plant immunity. The loss-of-function mutant *ugt76b1-1* showed enhanced resistance against *Pseudomonas* infections (von Saint Paul et al., 2011; Noutoshi et al., 2012; Maksym et al., 2018). Although *UGT76B1* has previously been shown to exhibit SA glycosyltransferase activity, the enzyme has a high level of substrate promiscuity *in vitro*. Additional substrates are ILA, leucic acid, 2-ethyl-2-hydroxybutyric acid, and valic acid (von Saint Paul et al., 2011; Noutoshi et al., 2012; Maksym et al., 2018). Since *UGT76B1* has been shown to influence SA metabolism, we wondered if *UGT76B1* has other substrates *in vivo*.

We conducted a nontargeted metabolome analysis on Col-0 and *ugt76b1-1* leaves after mock or *Pseudomonas* treatment. The dataset obtained by the nontargeted ultra-high performance liquid chromatography coupled to high-resolution mass spectrometry (UHPLC-HRMS) analysis showed relative intensity profiles of 448 metabolite features [false discovery rate {FDR} < 0.005], which were arranged into seven clusters by means of one-dimensional self-organizing maps (Figure 2). NHP-OGlc was not detectable in infected *ugt76b1-1* mutant plants and SAG was strongly reduced compared to the *Pseudomonas syringae* ES4326 (*P.s.m.*) infected wild-type plants (Col-0; Figure 2, Cluster 1). In contrast to that, NHP and SA showed a three- and two-fold accumulation, respectively, in infected *ugt76b1-1* plants compared to the respective wild-type plants (Cluster 3). Interestingly, the NHP precursor Pip, as well as 2HNG as a fragment of the SA-precursor isochorismic acid-9-glutamic

acid, showed comparable amounts in infected wild-type and *ugt76b1-1* mutant plants (Cluster 2). We could not find evidence for additional substrates or products of *UGT76B1* under our conditions with the nontargeted approach. However, we detected increased levels of the second SA-derived metabolite SGE in *ugt76b1-1* plants after infection (Cluster 3). Together, the experiment leads to the identification of NHP as an *in vivo* substrate of *UGT76B1*.

### *UGT76B1* loss-of-function mutant plants do not accumulate NHP-OGlc

In addition to nontargeted metabolome analysis, we quantitatively analyzed the amount of NHP, NHP-OGlc, SA, and SAG in wild-type (Col-0), *fmo1-1*, and *ugt76b1-1* plants after infection with *P.s.m.* (Figure 3A). Twenty-four hours post-infection (hpi), wild-type plants accumulated NHP and NHP-OGlc to levels of 68 and 89 nmol/g fresh weight (f.w.), as well as of SA and SAG to 7 and 166 nmol/g f.w., respectively. *ugt76b1-1* plants exhibited nearly a three-fold higher accumulation of NHP (184 nmol/g f.w.) compared to wild-type, whereas NHP-OGlc was not detected in the mutant after infection. As expected, *fmo1-1* plants, which cannot generate NHP from Pip, accumulated neither NHP nor NHP-OGlc. Additionally, we observed an about 2.5-fold higher accumulation of SA after infection in *ugt76b1-1* plants compared to the wild-type, whereas *fmo1-1* plants exhibited comparable SA levels to the wild-type, and moderately reduced SAG levels.

Similar results were obtained when we used UV-C to stimulate the production of NHP and SA independently of pathogen infection (Yalpani et al., 1994; Rekhter et al., 2019a). Twenty-four hour post-UV-C-treatment, we detected 56 and 131 nmol/g f.w. of NHP and NHP-OGlc as well as 1.74 and 73 nmol/g f.w. of SA and SAG in wild-type plants (Figure 3B). In *fmo1-1* plants, no detectable amounts of NHP and NHP-OGlc were found after UV-C treatment, while SA and SAG accumulated to wild-type levels. In *ugt76b1-1* plants, we observed a nearly three-fold increase in NHP compared to wild-type plants, but no formation of NHP-OGlc was detectable. There is also an increase in SA



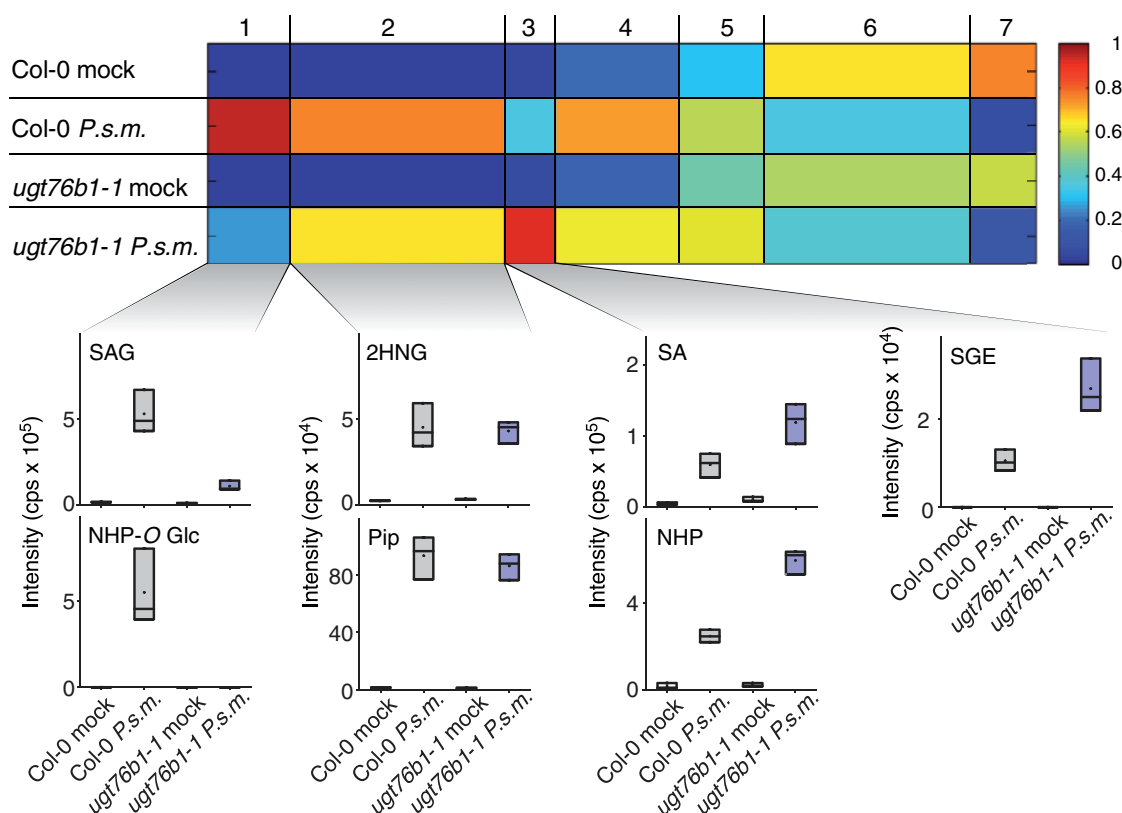


**Figure 2** Nontargeted metabolomics revealed NHP as a substrate of UGT76B1 in vivo. Col-0 and *ugt76b1-1* mutant plants were infiltrated with  $MgCl_2$  (mock) or *Pseudomonas syringae* ES4326 (*P.s.m.*) at  $OD_{600} = 0.05$ . Samples were collected 24 hpi. Metabolites of the polar extraction phase were analyzed by a metabolite fingerprinting approach based on UHPLC-HRMS. Intensity-based clustering by means of one-dimensional self-organizing maps of the relative intensities of 448 metabolite features ( $FDR < 0.005$ ) in seven clusters is shown. The heat map colors represent average intensity values according to the color map on the right-hand side. The width of each cluster is proportional to the number of features assigned to this cluster. Box plots for selected metabolites of the indicated clusters are shown. Borders represent the high and low value of the measurement and horizontal lines represent the median value. The identity of the metabolites was unequivocally confirmed by UHPLC-HRMSMS analyses. Data represent  $n = 3$  replicates. Each replicate represents an individual pool of 4–6 leaves of six plants per condition. The results were confirmed by a second independent experiment.

accumulation (2.87 nmol/g f.w.) and a decrease in SAG accumulation (27 nmol/g f.w.) in *ugt76b1-1*. Together, these data strengthen the hypothesis that NHP-OGlc formation is dependent on a functional UGT76B1 enzyme, as was additionally confirmed with two independent deletion mutant alleles of UGT76B1 (Supplemental Figure S1).

### UGT76B1 acts downstream of FMO1 thereby regulating plant immunity

We hypothesized that increased NHP accumulation in *ugt76b1-1* plants after infection is due to its impaired glycosylation and that the dwarfed and enhanced resistance phenotype requires NHP. Furthermore, we assumed that UGT76B1 acts downstream of FMO1. To test this hypothesis, we assessed the growth of *Hyaloperonospora arabidopsis* (*H.a.*) Noco 2 on Col-0, *fmo1-1*, *FMO1-3D* (a gain-of-function mutant for *FMO1*), three mutant alleles of UGT76B1 (*ugt76b1-1*, -3, and -4) and three *fmo1-1 ugt76b1* double knock-out mutant lines (*fmo1-1 ugt76b1-5*, *fmo1-1 ugt76b1-1-40*, and *fmo1-1 ugt76b1-1-104*; Figure 4). In comparison to Col-0, *FMO1-3D* showed high resistance against

*H. a.* Noco 2, while *fmo1-1* was more susceptible. *ugt76b1-1*, -3, and -4 exhibited strong resistance, but the double mutant lines showed similar susceptibility as *fmo1-1* (Figure 4A). Additionally, we found that basal *PR1* expression is enhanced in all three *ugt76b1* alleles compared to Col-0 (Figure 4B), consistent with findings from a previous report (von Saint Paul et al., 2011). In contrast, the expression level of *PR1* is similar in *fmo1-1 ugt76b1-5* and *fmo1-1*. In addition, the dwarf phenotype and dark green leaf color in the *ugt76b1* alleles are suppressed in the *fmo1-1 ugt76b1-5* double mutant (Figure 4C). The *fmo1-1 ugt76b1-1* double mutant plants accumulate neither NHP nor NHP-OGlc (Supplemental Figure S2). Altogether, the data indicate that UGT76B1 acts downstream of FMO1 and that NHP is required for both the enhanced resistance and dwarf phenotype of *ugt76b1* plants.

### Increased accumulation of NHP in *ugt76b1* plants underlines the importance of turnover via UGT76B1

Next, we wondered whether the enhanced accumulation of NHP and SA in the *ugt76b1* mutants after infection is due

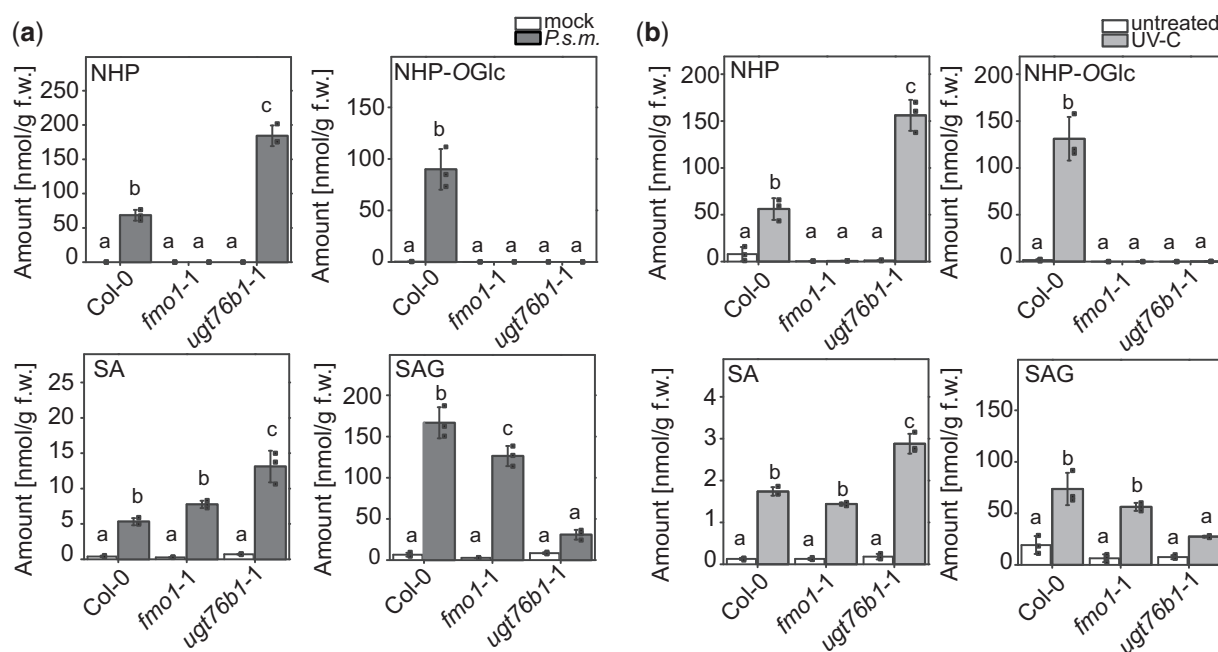


**Figure 3** UGT76B1 loss-of-function mutant plants are unable to synthesize NHP-OGlc. Absolute amounts of NHP, NHP-OGlc, SA, and SAG in wild-type (Col-0), *fmo1-1*, and *ugt76b1-1* plants after infection with *P.s.m.* (A) or UV treatment (B). Three leaves of 6-week-old plants, grown under short-day conditions (8-h light period), were infiltrated with *P.s.m.* at OD<sub>600</sub> = 0.05 in 10 mM MgCl<sub>2</sub> (*P.s.m.*) or with 10 mM MgCl<sub>2</sub> (mock). Twenty-four hpi, leaves were harvested and analyzed using UPLC-nanoESI-QTRAP-MS. Plants grown under long-day conditions (16-h light period) were treated for 20 min with UV-C. Twenty-four hours post-UV-C treatment, leaves were harvested and analyzed using quantitative UPLC-nanoESI-QTRAP-MS with authentic internal standards. Data represent the absolute amount of analyte in nmol/g fresh weight (f.w.). Error bars represent standard deviation. Letters indicate statistical differences ( $P < 0.05$ , one-way ANOVA;  $n = 3$ ). Replicates represent individual pools of 4–6 leaves from six plants per condition. The results were confirmed by a second independent experiment.

to impaired turnover or increased biosynthesis of NHP and SA. As an indirect measure, we analyzed the transcript levels of SA and NHP biosynthetic genes 24 hpi with *P.s.m.* by quantitative real time-polymerase chain reaction (RT-PCR). The transcript abundance of the SA biosynthetic genes *ICS1*, *EDS5*, and *PBS3* (Figure 5, A–C) was similar in the wild-type and *ugt76b1-1* mutant. Interestingly, transcripts of all three genes were upregulated in the mock-treated *ugt76b1-1*, suggesting that the basal expression levels of these SA biosynthetic genes are higher in the UGT76B1 knock-out background. This notion is supported by the transcript levels of *PR1* and *PR2* after mock treatment (Supplemental Figure S3). Despite the increased amount of NHP (Figure 3A), the transcript levels of NHP-biosynthetic genes *ALD1* and *FMO1* are significantly reduced in *ugt76b1-1* compared to the wild-type. As a control, we monitored the transcript level of *UGT74F2* in Col-0 and *ugt76b1-1*. The transcript abundance of *UGT74F2* did not change after infection in Col-0 and *ugt76b1-1* plants (Figure 5). Taken together, the increased SA and NHP levels in *ugt76b1* mutants upon pathogen infection are unlikely caused by increased biosynthesis as shown on the level of transcription of the biosynthetic genes, since the respective transcripts are not higher in *ugt76b1-1* than in the wild-type. These findings may support that UGT76B1 plays a central role in the turnover of NHP and influences the formation of SAG.

### UGT76B1 catalyzes the glycosylation of NHP in vitro

In addition, we checked whether UGT76B1 can glycosylate NHP in vitro. The His-tagged UGT76B1 was heterologously expressed in *Escherichia coli* and purified to homogeneity by affinity chromatography and size exclusion chromatography (Supplemental Figure S4). The enzymatic reaction of recombinant UGT76B1 with NHP and UDP-glucose as substrates was monitored by UHPLC-HRMS. As shown in Figure 6A, UGT76B1 catalyzes in vitro formation of NHP-OGlc ( $m/z$  308.1342, retention time [RT] 2.12 min). We also confirmed glycosylation of SA and ILA by UGT76B1 (von Saint Paul et al., 2011; Noutoshi et al., 2012). The formation of the respective glucosides SAG ( $m/z$  299.0793, RT 3.14 min) and ILA-glycoside (ILA-Glc) ( $m/z$  293.1240, RT 3.35 min) is shown in Figure 6, B and C. In addition, we determined the Michaelis–Menten constant ( $K_M$ ) for SA and NHP. We quantified the respective product signal area for NHP-OGlc and SAG via UPLC-nanoESI-QTRAP-MS, resulting in  $K_M(\text{NHP}) = 191 \pm 14 \mu\text{M}$  and  $K_M(\text{SA}) = 75 \pm 2 \mu\text{M}$  (Figure 6, D and E) and a catalytic efficiency ( $k_{\text{cat}}/K_M$ ) of  $k_{\text{cat}}/K_M(\text{NHP}) = 0.122 \text{ s}^{-1} \text{ mM}^{-1}$  as well as  $k_{\text{cat}}/K_M(\text{SA}) = 0.308 \text{ s}^{-1} \text{ mM}^{-1}$ . The data suggest that the glycosylation of SA by UGT76B1 is  $\sim 2.5$ -fold more efficient than the glycosylation of NHP. We further investigated the site of glycosylation by mass spectrometry (MS)-fragmentation studies on enzymatically produced (in vitro) and *in planta* NHP-OGlc (Figure 6, F and G), which have



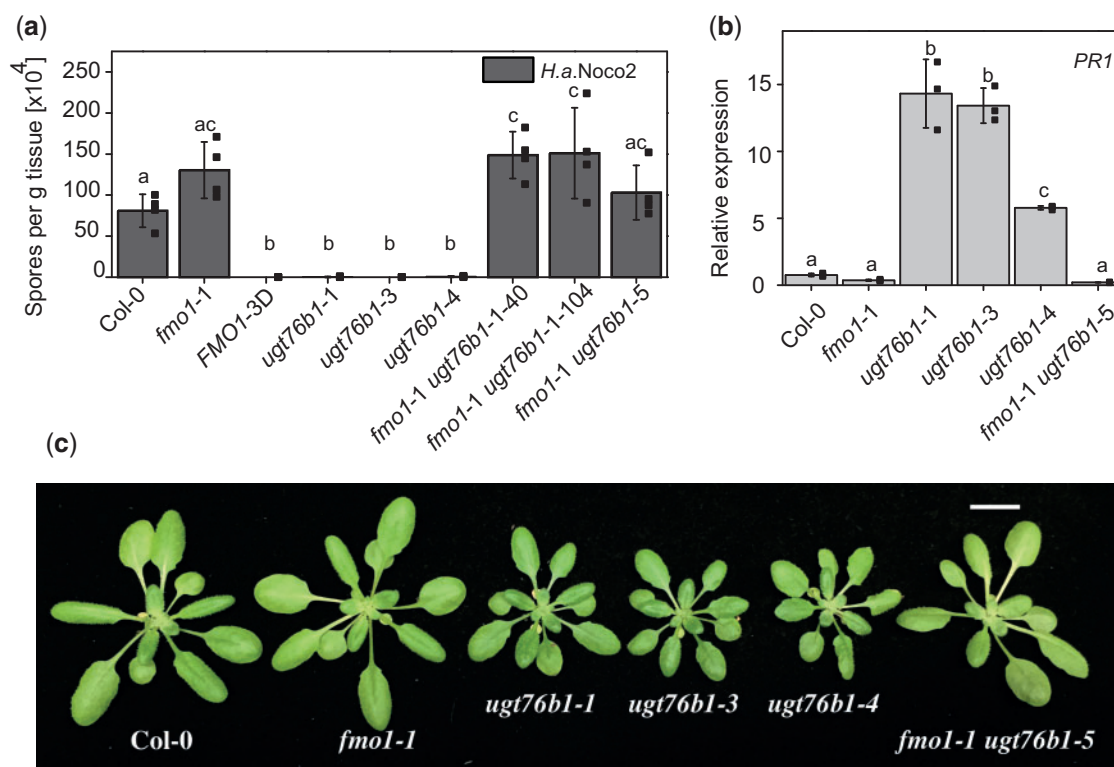


**Figure 4** Rescue of *ugt76b1* mutant phenotypes by introduction of the *fmo1-1* mutation. A, Growth of *H. a. Noco2* on wild-type (Col-0), *fmo1-1*, FMO1-3D, *ugt76b1-1*, *ugt76b1-3*, *ugt76b1-4*, *fmo1-1 ugt76b1-40*, *fmo1-1 ugt76b1-104*, and *fmo1-1 ugt76b1-5* plants. Two-week-old seedlings were sprayed with *H. a. Noco2* spore suspension ( $5 \times 10^4$  spores/mL). Infection was scored 7 days after infection. Error bars represent standard deviation. Letters indicate statistical differences ( $P < 0.05$ , one-way ANOVA;  $n = 4$ ). Each replicate represents the spore count on a single plant. B, Basal *PR1* gene expression in 4-week-old plants of the indicated genotypes determined via quantitative RT-PCR. Error bars represent standard deviation. Letters indicate statistical differences ( $P < 0.05$ , one-way ANOVA;  $n = 3$ ). Replicates represent a pool of 4–6 leaves per genotype. C, Growth phenotypes of Col-0, *fmo1-1*, *ugt76b1-1*, *ugt76b1-3*, *ugt76b1-4*, and *fmo1-1 ugt76b1-5*. Photographs are of 4-week-old plants grown under long-day conditions (16-h light/8-h dark cycle). Scale bar is 1 cm.

identical RTs in our chromatographic separations. The fragmentation analysis of both show dominant fragments for  $m/z$  146.081 [M-Glc + H<sub>2</sub>O + H]<sup>+</sup>,  $m/z$  128.070 [M-Glc + H]<sup>+</sup>, and  $m/z$  100.075 [M-Glc + H<sub>2</sub>O-CO<sub>2</sub> + H]<sup>+</sup> (Figure 6, F and G). The additional low abundant analytical fragment of  $m/z$  262.127 represents an NHP-OGlc fragment [M-CO<sub>2</sub> + H]<sup>+</sup> which has lost the carboxy group, however, it has the glucose moiety still attached via the ether-bond. This indicates that UGT76B1 catalyzes the *O*-glycosylation mechanism in vitro and in vivo. Together, our in vitro analysis shows that the purified recombinant UGT76B1 was active toward NHP, SA, and ILA. In addition, we show that UGT76B1 *O*-glycosylates NHP by producing NHP-OGlc.

We further analyzed active site residues in enzymes capable of glycosylating SA (UGT74F1 and UGT74F2) and compared them with the UGT76B1 protein sequence (Supplemental Figure S5a). In addition, we made an in silico structural prediction of UGT76B1 using the deposited structure of UGT74F2 (PDB accession 5V2J) (George Thompson et al., 2017) and modeled NHP in the electron density of the co-crystallized SA-analog 2-bromobenzoic acid (Supplemental Figure S5, b and c). Some residues such as

histidine at position 20 (His20) and aspartic acid at position 109 (Asp109) that have been shown to be important for the formation of SAG and SGE are conserved in all three UGTs (Supplemental Figure S5a) (George Thompson et al., 2017). However, two threonine residues involved in the glycosylation of SA in UGT74F2 are substituted by leucine at position 17 and glycine at position 363 (Supplemental Figure S5, a and c). Nevertheless, we identified a threonine at position 131 in a predicted loop region, which might compensate for the lack of Thr17 and Thr363 in the catalytic reaction (Supplemental Figure S5, a and c). These findings support our experimental data that the minimum subset of amino acids for fulfilling the glycosylation reactions on SA and NHP are present in UGT76B1's putative active site.

#### Deuterated NHP is translocated to distal tissue

NHP is the biological active metabolite of Pip in plant defense, especially in SAR (Chen et al., 2018; Hartmann et al., 2018). Nevertheless, it is still an open question whether NHP or NHP-OGlc might act as a mobile signal in SAR (Chen et al., 2018; Holmes et al., 2019). To address this question, we infiltrated uniformly deuterated NHP (D<sub>9</sub>-NHP) into leaves of Col-0, *fmo1-1*, and *ugt76b1-1* plants. Twenty-four

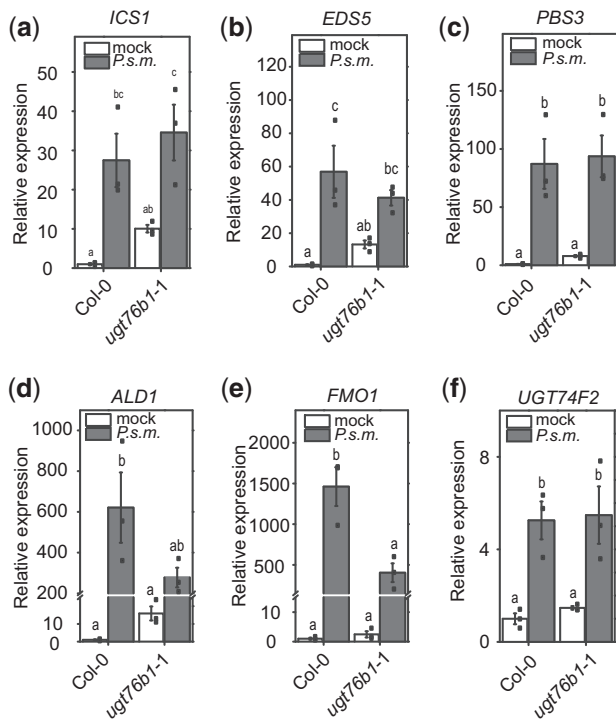


**Figure 5** Comparisons between transcript levels of *ICS1*, *EDS5*, *PBS3*, *ALD1*, *FMO1*, and *UGT74F2* in *ugt76b1*, and the wild-type. Transcript abundance of genes encoding SA and NHP biosynthetic enzymes was analyzed in wild-type and *ugt76b1-1* plants after infection with *P.s.m.*. Three leaves of 4–6-week-old plants were treated with *P.s.m.* ( $OD_{600} = 0.001$ ). Leaves were harvested 24 hpi and analyzed via RT-PCR using cDNA generated by reverse-transcriptase reaction as templates. Error bars represent standard deviation. Letters indicate statistical differences ( $P < 0.05$ , one-way ANOVA;  $n = 3$ ). Replicates represent pools of 4–6 leaves of six plants per condition. Graph d includes an axis break from 25 to 200. Graph e includes an axis brake from 15 to 150.

hours post-infiltration, local as well as systemic leaves were harvested. First, the formation of  $D_9$ -NHP-OGlc from the infiltrated  $D_9$ -NHP in the local leaves of Col-0, *fmo1-1*, and *ugt76b1-1* plants was monitored by qualitative UHPLC-HRMS. As expected, the applied  $D_9$ -NHP was converted to  $D_9$ -NHP-OGlc in the local leaves of wild-type and *fmo1-1* plants, but no  $D_9$ -NHP-OGlc was detected in *ugt76b1-1* plants (Figure 7). Accordingly, the relative signal area of  $D_9$ -NHP was two times higher in the local leaves of *ugt76b1-1* plants in comparison to Col-0. Further analysis showed that  $D_9$ -NHP was present in systemic tissue of the three genotypes Col-0, *fmo1-1*, and *ugt76b1-1*, whereas  $D_9$ -NHP-OGlc was only detected in Col-0 and *fmo1-1* plants. This indicates that  $D_9$ -NHP can move to distal tissues without glycosylation.

### *ugt76b1* plants exhibit enhanced resistance in systemic tissue

Next, we analyzed whether *ugt76b1-1* can still establish SAR without the accumulation of NHP-OGlc by conducting an *H.a. Noco 2* growth assay on plants pre-treated with *P.s.m.*

(Figure 8). Establishment of SAR strongly reduces the disease rate of distal leaves (indicated as disease categories from 0 to 5) during a second infection with *H.a. Noco 2*, as shown for Col-0 plants (Figure 8A). Plants mock treated on the primary leaf showed high infection rates, indicated by disease categories of four and five on the systemic leaves after plant *H.a. Noco 2* infection. For *ugt76b1-1* plants, infection on the systemic leaves was reduced to minimum (disease category 0) regardless of whether they were pre-induced with *P.s.m.* or not. These disease rates were as low as those known for the *FMO1-3D* mutant. In contrast, *fmo1-1* plants are not able to establish SAR and therefore show an increased susceptibility to *H.a. Noco2*, as known from the literature (Ding et al., 2016). This finding indicates that the distal parts of *ugt76b1-1*, regardless of a primary infection, exhibit enhanced resistance toward *H.a. Noco 2*. This is consistent with results from our local *H.a. Noco 2* infection assays for the *ugt76b1* lines (Figure 4A). In an independent approach, we analyzed the resistance of *ugt76b1-1* to a secondary infection by *P.s.m.*. As expected, Col-0 established SAR after primary infection, *fmo1-1* plants were not able to establish SAR, and *FMO1-3D* showed a constitutive SAR phenotype (Figure 8B). Nevertheless, *ugt76b1-1* exhibited reduced bacterial growth in distal leaves of both mock and *P.s.m.*-treated samples. Together, these data suggest that *ugt76b1-1* displays constitutive resistance toward pathogens.

## Discussion

The identification of *FMO1* as an NHP biosynthetic enzyme was a major breakthrough toward the understanding of Pip-mediated plant immunity and its involvement in the establishment of SAR (Chen et al., 2018; Hartmann et al., 2018; Holmes et al., 2019). In addition, NHP-OGlc was recently described as a metabolite of NHP (Chen et al., 2018). However, the enzyme catalyzing the formation of NHP-OGlc was unknown. In this study, we identified *UGT76B1* as the enzyme responsible for the glycosylation of NHP in vivo and in vitro—in addition to its previously identified substrates SA and ILA. Besides its glycosyltransferase activity toward NHP in vitro, we show that *UGT76B1* is required for the formation of NHP-OGlc in planta during pathogen infection. The absence of *UGT76B1* leads to a significantly increased accumulation of the plant immune regulator NHP, and the complete depletion of NHP-OGlc in *ugt76b1* mutant plants. Our data emphasize *UGT76B1* as the only enzyme that O-glycosylates NHP in planta.

*ugt76b1* mutants have been shown to exhibit enhanced disease resistance against biotrophic pathogens, which was suggested to be caused by increased accumulation of SA (Noutoshi et al., 2012). The substrate ILA was recently suggested to activate the immune response via SA by inactivating *UGT76B1* (Bauer et al., 2020). In *ugt76b1* mutants, however, NHP accumulates to considerably higher level than in the wild-type during pathogen infection, suggesting that the elevated NHP level, instead, may play a major role in enhancing disease resistance in the mutant plants. This is

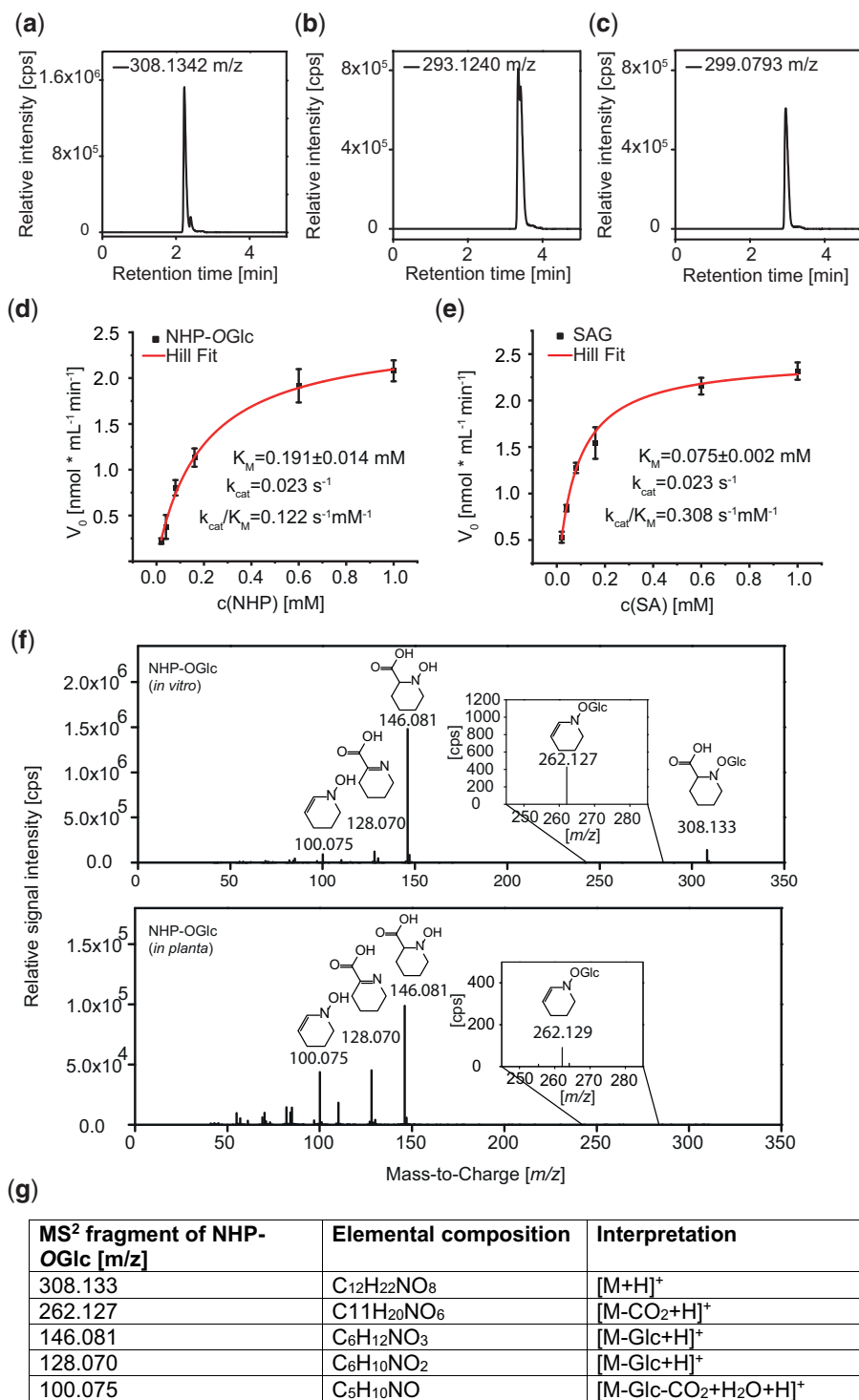


**Figure 6** Glycosylation of SA, ILA, and NHP by UGT76B1 *in vitro*. Activity assays were carried out using NHP, ILA, and SA as substrates for the recombinant UGT76B1. Extracted ion chromatograms of the reaction products (A) NHP-OGlc ( $m/z$  308.1342), (B) ILA-Glc ( $m/z$  293.1240), and (C) SAG ( $m/z$  299.0793) are shown. An aliquot of 10  $\mu\text{g}$  of recombinant UGT76B1 was incubated with 50  $\mu\text{M}$  substrate and 500  $\mu\text{M}$  UDP-Glc at 30°C for 30 min. The reaction was stopped by adding 25% ( $v/v$ ) acetonitrile. The kinetic constants ( $K_M$ ,  $k_{cat}$ , and  $k_{cat}/K_M$ ) of UGT76B1 were determined for the substrate NHP [coefficient of determination ( $R^2 = 0.996$ ) (D) and SA ( $R^2 = 0.997$ ) (E)], respectively. Mean signal area of the respective products (NHP-OGlc or SAG) after 5 min incubation at 25°C from three replicates at six different substrate concentrations. Non-linear Hill regression was performed with Origin Pro 2020 (OriginLab Corporation, Northampton, MA, USA). F, UHPLC-HRMS/MS-fragment spectra of enzymatically synthesized NHP-OGlc (*in vitro*) and of NHP-OGlc extracted from wild-type plants after infection with P.s.m. (*in planta*) is shown. The analytical fragment  $m/z$  262.127 represents the NHP-OGlc molecule without the carboxy group, being specific for an O-glycosylation. G, Interpretation of the NHP-OGlc fragments using the accurate mass information and the deduced elemental composition. All samples were measured via UHPLC-HRMS-analysis. The results were confirmed by a second independent experiment.

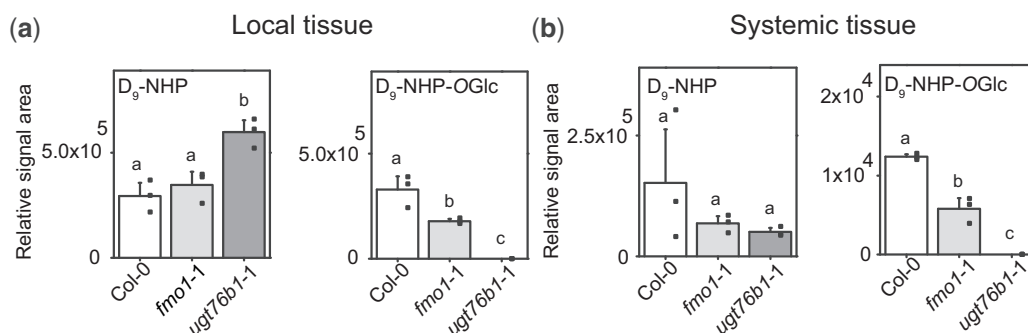


**Figure 7** Infiltrated D<sub>9</sub>-NHP moves systemically and is converted to D<sub>9</sub>-NHP-OGlc in wild-type and *fmo1-1* but not in *ugt76b1-1* plants. Relative signal areas of D<sub>9</sub>-NHP and its glucoside D<sub>9</sub>-NHP-OGlc was analyzed 24 h after infiltration of D<sub>9</sub>-NHP to local tissue. Local (A) and systemic (B) leaves were harvested and analyzed by UHPLC-HRMS. Error bars represent standard deviation. Letters indicate statistical differences ( $P < 0.05$ , one-way ANOVA;  $n = 3$ ). Replicates represent individual pools of 4–6 leaves out of six equally grown and treated plants. The results were confirmed by a second independent experiment.

supported by the complete suppression of the autoimmune phenotype of *ugt76b1* by loss of function of FMO1. The accumulation of NHP leads to dwarfism as reported for the FMO1-3D overexpression line. Furthermore, increased NHP levels lead to enhanced resistance of this mutant (Koch et al., 2006). In contrast, the plant size increases as the amount of NHP decreases and its susceptibility toward biotrophic pathogens increases (Figures 4 and 8) (Hartmann et al., 2018). The induction of UGT76B1 by *P.s.m.* infection therefore suggests that this gene plays a major role in regulating NHP homeostasis, which seems to be critical to balance growth and defense in plants.

Although the NHP level is higher in *ugt76b1* mutants, the increased accumulation of SA is most likely due to the reduced conversion of SA to SAG rather than the effect of NHP on the transcript levels of SA biosynthesis genes (Figure 5). In addition, the FMO1-3D mutant does not accumulate free SA to higher levels than the wild-type and a lack of NHP does not affect the accumulation of SA in *fmo1-1* plants (Koch et al., 2006; Bartsch et al., 2010). The increase of SA and NHP levels in *ugt76b1* mutants suggests that reduced turnover could be a critical mechanism for increasing the accumulation of SA as well as NHP (Supplemental Figure S6).

As there are three UGTs described to glycosylate SA, reduced accumulation of SAG could also hint at a deregulation mechanism in *ugt76b1-1* plants toward the previously described SA UGTs, especially SAG-forming enzyme UGT74F1 (Dean and Delaney, 2008; George Thompson et al., 2017). The increased basal SGE level in *ugt76b1-1* has already been addressed and connected to high basal PR1 expression (von Saint Paul et al., 2011). However, after infiltration with *P.s.m.*, transcript levels of PR1 are similar in Col-0 and *ugt76b1-1* (Supplemental Figure S3). Furthermore, the transcript levels of UGT74F2 encoding the SGE forming enzyme were similar in the wild-type and *ugt76b1-1* mutant.

We conclude that the reported increase of SGE after infection of *ugt76b1-1* is likely caused by the accumulation in UGT74F2's substrate SA (Figure 1).

ILA was previously identified as a substrate of UGT76B1 (von Saint Paul et al., 2011); however, it was not identified as a molecular marker of infection with *Pseudomonas* in our nontargeted metabolite fingerprinting approach by UHPLC-HRMS (Supplemental Dataset 1). We observed neither ILA accumulation in *ugt76b1-1*, nor the respective glucoside in wild-type plants after infection. Although there might be a chance that our workflow is not sufficient to detect these compounds in vivo, the intracellular concentration of ILA in the shoot was quantified to be approximately 2.5 ng/g dry weight and 7 ng/g dry weight for Col-0 and *ugt76b1-1*, respectively. Estimating a weight loss of at least 1:10 (*m/m*) between dry and fresh weight, the presented amounts of NHP are a multiple of ILA amounts in the shoot. Considering the determined  $K_M$  value of UGT76B1 for NHP in comparison with the one toward ILA presented earlier ( $472 \pm 97 \mu\text{M}$ ), we consider ILA of minor importance for the observed enhanced resistance phenotype (Maksym et al., 2018). Nevertheless, recent data suggest that ILA fulfills its role in controlling NHP and SA glycosylation reactions and therefore has the ability to fine-tune NHP and SA accumulation and their defense amplification loop (Bauer et al., 2020, 2021). This interplay between SA and NHP was additionally shown by Bauer and colleagues, identifying equally high susceptibility of the SA-deficient mutant NahG *sid2* and NahG *sid2 ugt76b1*. These observations suggest that NHP alone is not sufficient to fulfill a robust defense response. All things considered, it is most likely that the enhanced resistance phenotype of *ugt76b1-1* is due to increased accumulation of NHP and SA.

The catalytic efficiency of UGT76B1 toward SA has been determined to be 2.5-fold higher than for NHP. The determined catalytic efficiency for SA ( $k_{\text{cat}}/K_M = 0.308 \text{ s}^{-1} \text{ mM}^{-1}$ )



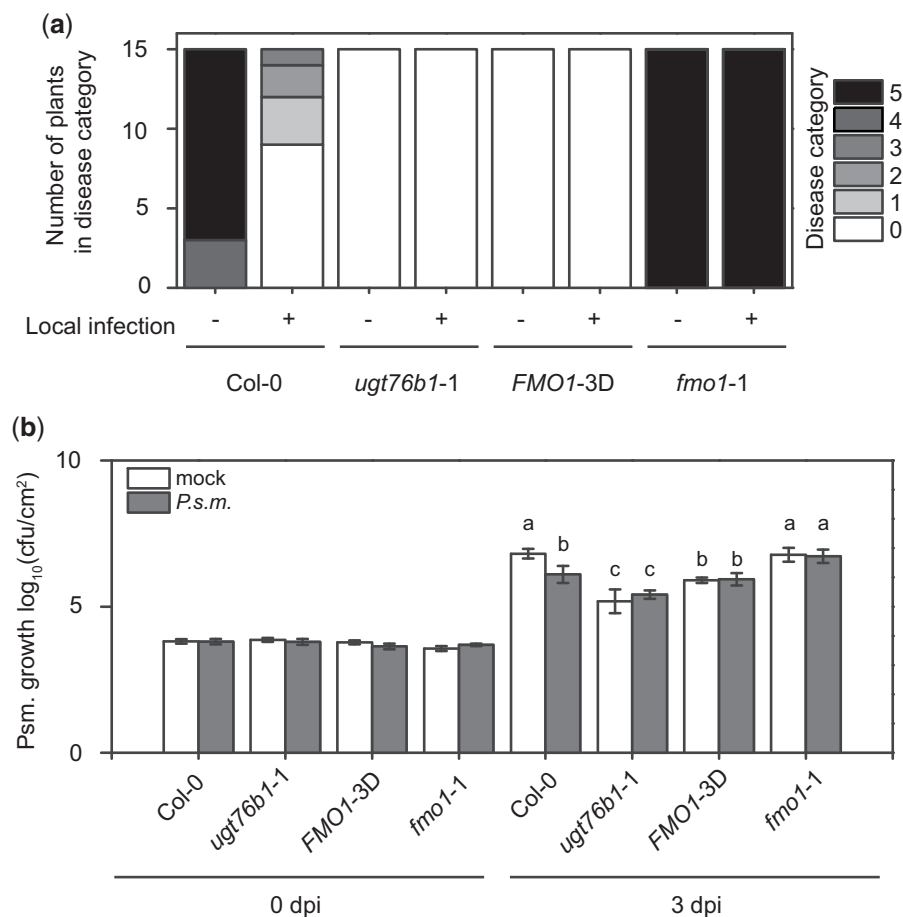


**Figure 8** Growth of *H.a. Noco2* and *P.s.m.* on the distal leaves of wild-type (Col-0), *ugt76b1-1*, *FMO1-3D*, and *fmo1-1* plants. A, Three-week-old plants were first infiltrated with *P.s.m.* ( $\text{OD}_{600} = 0.001$ ) or 10 mM  $\text{MgCl}_2$  (mock) on two primary leaves and sprayed with *H.a. Noco2* spores ( $5 \times 10^4$  spores/mL) 2 days later. Infections on systemic leaves were scored 7 days after inoculation as described previously (Zhang et al., 2010). A total of 15 plants were scored for each treatment. Disease rating scores are as follows: 0, no conidiophores on the plants; 1, one leaf was infected with no  $> 5$  conidiophores; 2, one leaf was infected with  $> 5$  conidiophores; 3, two leaves were infected but no  $> 5$  conidiophores on each infected leaf; 4, two leaves were infected with  $> 5$  conidiophores on each infected leaf; 5,  $> 2$  leaves were infected with  $> 5$  conidiophores. Similar results were obtained in three independent experiments. (B) Four-week-old plants were first infiltrated with *P.s.m.* ( $\text{OD}_{600} = 0.001$ ) or 10 mM  $\text{MgCl}_2$  (mock) on two primary leaves. Two days later, two upper leaves were challenged with *P.s.m.* ( $\text{OD}_{600} = 0.001$ ). Infections on systemic leaves were scored directly after (0 dpi) and 3 days post-inoculation (3 dpi). Error bars represent standard deviation. Letters indicate statistical differences ( $P < 0.05$ , one-way ANOVA;  $n = 7-8$  biological replicates each representing a single infected plant). The results were confirmed by a second independent experiment.

is twice as high as reported by Noutoshi et al. (2012) ( $k_{\text{cat}}/K_M = 0.15 \text{ s}^{-1} \text{ mM}^{-1}$ ) and  $\sim 7$  times less than reported by Maksym et al. (2018) ( $k_{\text{cat}}/K_M = 2.2 \text{ s}^{-1} \text{ mM}^{-1}$ ). Additionally, the  $K_M$ -value for SA determined in this work is two times lower ( $K_M = 0.075 \pm 0.002 \text{ mM}$ ) compared to earlier reports (Noutoshi et al., 2012; Maksym et al., 2018). Nevertheless, NHP and SA differ in their absolute amount in infected leaf material (Figure 3, A and B) by several orders of magnitude, suggesting that NHP is the more accessible and, therefore, the preferred substrate of UGT76B1. Although an amino acid sequence comparison of UGT74F1 and UGT74F2 with UGT76B1 revealed only 26.96% and 26.75% sequence identity, respectively, two critical residues for glycosylation (His20 and Asp109) in the putative active site are conserved among these UGTs (Supplemental Figure S5) (George

Thompson et al., 2017). Interestingly, we were not able to detect glycosylation of 4-hydroxy benzoic acid (4-OH-BA) by UGT76B1 either at the hydroxyl group or the carboxyl group. This suggests that a hydroxyl group in *ortho* or *meta* configuration adjacent to the carboxyl function is important for optimal binding of the ligand in the active site of UGT76B1.

The data presented in Figure 6, F and G indicate that UGT76B1 forms NHP-OGlc via an *O*-glycosylation reaction. The analytical fragment of  $m/z$  262.129 is specific for NHP-OGlc representing  $[\text{M}-\text{CO}_2 + \text{H}]^+$ . The nature of the glycosylation site of NHP at the *N*-hydroxy group by UGT76B1 was additionally confirmed via TMS-derivatization of NHP and transiently produced NHP-OGlc in a recent publication (Holmes et al., 2021). Furthermore, NHP derivatives were

methylated and analyzed by collision-induced dissociation. The fragments let the authors conclude that glycosylation by UGT76B1 results in NHP-OGlc rather than an NHP-OGlc-ester (Holmes et al., 2021).

From our transport experiments with D<sub>9</sub>-NHP, we suggest that native NHP rather than NHP-OGlc might be a mobile signal that can translocate from the apoplast to the cytosol and move to distal tissue during the establishment of SAR. This may be supported by an earlier study in which SAG was infiltrated into tobacco (*N. tabacum*) leaves (Hennig et al., 1993). Here, the authors showed that SAG was hydrolyzed in the apoplast to SA and that SA rather than SAG entered the cell. In addition, other studies support our notion that both NHP and SA are mobile between local and systemic tissue in Arabidopsis and tobacco (Yalpani et al., 1991; Chen et al., 2018; Lim et al., 2020). Nevertheless, this possibility remains a matter of debate, as evidence has also been presented that SA is not the mobile signal for SAR (Vernooij et al., 1994a, 1994b). However, the formation of SAG and NHP-OGlc probably have a central role in inactivating SA and NHP as biologically active molecules, as the dwarf phenotype of the corresponding mutant suggests (Figure 4c) (Noutoshi et al., 2012).

Together, our data extend the NHP metabolic pathway down to NHP-OGlc and illustrate the major importance of UGT76B1 in metabolic regulation and maintaining the balance between growth and defense responses.

## Materials and methods

### Plant materials and growth conditions

Plants used for this work are all in the *Arabidopsis thaliana* Col-0 ecotype background. The *fmo1-1* and *ugt76b1-1* (SAIL\_1171\_A11) T-DNA insertion lines were obtained from Nottingham Arabidopsis stock center (NASC; University of Nottingham) and were described previously (Bartsch et al., 2006; von Saint Paul et al., 2011). *ugt76b1-3* and *ugt76b1-4* are independent *ugt76b1-1* deletion lines generated by CRISPR-Cas9 in the Col-0 background, with original lab code of CRISPR UGT #5 and #17, respectively. Double mutant lines *fmo1-1 ugt76b1-40* and *fmo1-1 ugt76b1-104* were generated by crossing *ugt76b1-1* with *fmo1-1*. In addition, a CRISPR deletion line of *UGT76B1* was generated in the *fmo1-1* background and is referred to as *fmo1-1 ugt76b1-5*. The overexpression mutant *FMO1-3D* was described previously (Koch et al., 2006). Plants were grown for 4–6 weeks under short-day conditions (8-h light/18-h dark cycle) with 100–120  $\mu\text{mol}/\text{m}^2/\text{s}$  of light intensity at 80% relative humidity unless specified. The used bulb type was MASTER LEDtube HF 600 mm HO 8W840 T8 (PHILIPS AG, Amsterdam, Netherlands).

### Construction of plasmids for *UGT76b1* gene editing and generation of deletion mutants

Three deletion lines *ugt76b1-3*, *ugt76b1-4*, and *ugt76b1-5* *fmo1-1* (original lab code CRISPR UGT #5, CRISPR UGT #17, and CRISPR UGT in *fmo1* #1, respectively) were generated

by the CRISPR/Cas9 system as described (Xing et al., 2014). Two single guide RNAs were designed to target *UGT76B1* genomic DNA to generate a approximately 1,000-bp deletion. The PCR fragment containing the guide RNA sequences was amplified from the pCBC-DT1T2 vector with primers 3G11340-BsFF0 and 3G11340-BsRR0 and subsequently inserted into the pHEE401 vector using the BsaI site. The derived plasmid was transformed into *E. coli* and later *Agrobacterium* by electroporation. Col-0 and *fmo1-1* plants were transformed with the *Agrobacterium* carrying the plasmid by floral dipping (Clough and Bent, 1998). T<sub>1</sub> plants were screened for deletion mutants by PCR with primers listed in Supplemental Table S1. Homologous deletion mutants were obtained in the T<sub>2</sub> generation.

### Elicitation of defense response by UV-C and *P.s.m.*

Plants were treated for 20 min with UV-C radiation in a sterile bench (Telstar Bio-II-A, Azbil Telstar Technologies, Barcelona, Spain). The sterile bench was pretreated with UV-C for 20 min prior to radiating the plants. Untreated control plants and the UV-C-treated plants were harvested 24 h later. Infection of plants was conducted by infiltrating plant leaves with *P.s.m.* ES4326 at OD<sub>600</sub> = 0.05 in 10 mM MgCl<sub>2</sub>, if not stated otherwise, to induce defense. The bacteria were grown in LB medium with Rifampicin (50  $\mu\text{g}/\mu\text{L}$ ). In the D<sub>9</sub>-NHP tracking experiment, 82  $\mu\text{g}/\text{mL}$  of chemically synthesized D<sub>9</sub>-NHP was added to the infiltration solution.

### Metabolite extraction

Leaves were harvested 24 hpi and frozen in liquid nitrogen. The samples were ground under liquid nitrogen using Retsch 200 MM (Retsch, Haan, Germany). Ground material was weighed and extracted after a modified methyl-*tert*-butyl ether (MTBE) extraction (Feussner and Feussner, 2019). When metabolite quantification was desired, deuterium-labeled D<sub>9</sub>-NHP and D<sub>6</sub>-SA and isotopically labeled <sup>13</sup>C-SAG were added prior to extraction. The labeled compound served as a reference throughout the quantitative analysis.

### UPLC-nanoESI-QTRAP-MS-based metabolite quantification

Absolute quantification of NHP, NHP-OGlc, SA, and SAG was performed according to a method previously described with the following modifications (Herrfurth and Feussner, 2020). About 100 mg of flash-frozen leaf tissue was ground and subjected to MTBE extraction, including the addition of 50 ng D<sub>9</sub>-NHP (kindly provided by Prof. Ulf Diederichsen, Goettingen, Germany), 10 ng D<sub>4</sub>-SA (C/D/N Isotopes Inc., Pointe-Claire, Canada), and 50 ng <sup>13</sup>C<sub>6</sub>-SAG (kindly provided by Prof. Petr Karlovsky, Goettingen, Germany). For triple quadrupole linear ion trap (QTRAP)-MS detection, multiple reaction monitoring (MRM) transitions were analyzed as shown in Supplemental Table S2. For quantification, the signal area of each respective authentic standard was compared to the signal area of the analyte of the biological sample. Signals were analyzed in this study when the signal to noise ratio was >20. Furthermore, the determination

underlies the previously conducted calibration and technical optimization for each compound. Calibration was carried out using nine data points of varying concentrations for SA, SAG, and NHP-OGlc (Supplemental Figure S7, a, b and d). In the case of NHP, calibration was carried out using six data points, due to detection limitations in the low concentration range (Supplemental Figure S7c). Signals were used for calibration purposes when the minimal signal to noise ratio was  $>8$ . We determined the limit of detection as for SA (0.007 nmol), SAG (0.003 nmol), NHP (0.034 nmol), and NHP-OGlc (0.003 nmol). The limit of quantification was determined at a signal to noise ratio of eight in plant extract matrices for SA (0.013 nmol/100 mg), SAG (0.7 nmol/100 mg), NHP (1.03 nmol/100 mg), and NHP-OGlc (0.05 nmol/100 mg). D<sub>9</sub>-NHP was synthesized as described previously (Hartmann et al., 2018). Synthesized NHP was characterized via tandem MS (MS/MS) fragmentation (Rekhter et al., 2019a). The fragmentation behavior underlying the MRM transitions of NHP-OGlc were analyzed after thin-layer chromatographic purification of enzymatically produced NHP-OGlc using UGT76B1. As stationary phase, a TLC silica gel 60 (Merck KGaA, Darmstadt, Germany) was used in combination with butanol:water:acetic acid (4:1:1, v/v/v) as the solvent system (Song, 2006). Purified NHP-OGlc was extracted from the silica gel with MTBE corresponding to the extraction procedure as described (Herrfurth and Feussner, 2020). Successful purification of enzymatically produced NHP-OGlc was checked via nontargeted UHPLC-HRMS. The purified NHP-OGlc was quantified by direct infusion-MS with respect to SAG (kindly provided by Prof. Petr Karlovsky, Goettingen, Germany).

#### UHPLC-HRMS-based metabolite fingerprint analysis

Metabolites were extracted from 100 mg leaf material by two-phase extraction with MTBE, methanol, and water according to Feussner and Feussner (2019). Metabolite fingerprint analysis of the metabolites of the polar extraction phase was performed with the UHPLC1290 Infinity (Agilent Technologies, Santa Clara, CA, USA) coupled to an HRMS instrument (6540 UHD Accurate-Mass Q-TOF, Agilent Technologies, Santa Clara, CA, USA) with Agilent Dual Jet Stream Technology as electrospray ionization (ESI) source (Agilent Technologies, Santa Clara, CA, USA). For chromatographic separation, an ACQUITY HSS T3 column (2.1 × 100 mm, 1.8 μm particle size, Waters Corporation, Milford, MA, USA) was used with a flow rate of 500 μL/min at 40°C. The solvent systems A (water, 0.1% (v/v) formic acid) and B (acetonitrile, 0.1% (v/v) formic acid) were used for the following gradient elution: 0–3 min: 1–20% B; 3–8 min: 20–97% B; 8–12 min: 100% B; 12–15 min: 1% B. The quadrupole time of flight (QTOF) MS instrument was used in a range from *m/z* 50 to *m/z* 1700 with a detection frequency of 4 GHz, capillary voltage of 3000 V, and nozzle and fragmentor voltage of 200 and 100 V, respectively. The sheath gas was set to 300°C, and gas to 250°C. The gas flow of drying gas was set to 8 L/min and sheath gas to 8 L/min, respectively. Data were acquired with Mass Hunter

Acquisition B.03.01 (Agilent Technologies, Santa Clara, CA, USA) in positive as well as ESI mode. For data deconvolution, the software Profinder B.08.02 (Agilent Technologies, Santa Clara, CA, USA) was used. For further data processing, statistics, data mining, and visualization, the tools of the MarVis-Suite (Kaever et al. 2015, <http://marvis.gobics.de/>) were applied. Overall, 448 metabolite features (307 features from positive and 141 features from negative ESI mode) with an FDR  $< 0.005$  were selected and clustered by means of one-dimensional self-organizing maps. The accurate mass information of the metabolite features was used for metabolite annotation (Kyoto encyclopedia of genes and genomes [KEGG], <http://www.kegg.jp> and BioCyc, <http://biocyc.org>, in-house database). The chemical structure of the indicated metabolites was confirmed by LC-HRMS/MS analyses (NHP:  $[M + H]^+$  146.080, 128.070, 110.06, 100.076, 82.065, 70.065, and 55.055 (Rekhter et al., 2019b); NHP-OGlc:  $[M + H]^+$  308.132, 146.081, 128.0705, 110.06, 100.076, 82.062, 70.065, and 55.055 (Rekhter et al., 2019b); SA:  $[M-H]^-$  137.025 and 93.035 (METLIN, <https://metlin.scripps.edu/>), MID3263); SAG:  $[M-H]^-$  299.0719, 137.024, and 93.035; Pip:  $[M + H]^+$  130.086, 84.081, 70.065, and 56.050 (Ding et al., 2016); 2HNG:  $[M-H]^-$  216.051, 172.062, 128.072, and 86.025 (Rekhter et al., 2019b) and SGE:  $[M-H]^-$  299.078, 137.024, and 93.035). The results were confirmed by two independent experiments with three biological replicates each.

#### RNA extraction, reverse transcription, and qPCR

Plants for gene expression assays were grown on soil under long-day (16-h light) conditions. Three leaves of 4-week-old plants (~50 mg) were collected for RNA extraction using an EZ-10 Spin Column Plant RNA Miniprep Kit (Bio Basic Inc., Toronto, Canada). RNAs were then reverse transcribed into cDNAs by OneScript Reverse Transcriptase (Applied Biological Materials Inc., Richmond, Canada). qPCR was performed with cDNAs using SYBR Premix Ex Taq<sup>TM</sup> II (Takara, Shiga, Japan). For pathogen-induced gene expression assays, plants were grown under short-day (12 h light) conditions. Three leaves of 4–6-week-old plants were infiltrated with *P.s.m.* (OD<sub>600</sub> = 0.001). Leaves were harvested at 24 hpi and analyzed via the process described above. Primers for qPCR are listed in Supplemental Table S1.

#### Heterologous protein expression and purification

His-tagged UGT76B1 was purified via a combination of methods described recently (Maksym et al., 2018; Haroth et al., 2019). UGT76B1 (AT3G11340, GenBank Accession Number Q9C768.1) was amplified from total cDNA derived from infected leaf tissue and cloned into the pET28a vector (Merck, Darmstadt, Germany) using the BamHI and Sall restriction sites. The plasmid containing the UGT76B1 gene was transformed into BL21 Star (DE3) cells (Thermo Fisher Scientific, Waltham, MA, USA) by heat shock. Cell cultures were grown in auto-induction medium (Studier, 2005) at 16°C for 4 days. Cell pellets of a 1 L culture were resuspended in lysis buffer (50 mM Tris/HCl pH = 7.8, lysozyme, DNaseI, and 0.1 mM PMSF). After homogenization, cells



were disrupted by ultrasonication. Cleared lysate was obtained by centrifugation at  $25,000 \times g$  for 45 min at  $4^{\circ}\text{C}$ . The recombinant protein was purified from the cleared lysate using a combination of metal affinity chromatography using nickel-affinity (GE Healthcare, Chicago, IL, USA) and size exclusion chromatography using 16/600 Superdex 75 prep grade columns (GE Healthcare, Chicago, IL, USA).

### Liquid chromatography (LC)-MS-based activity assay and in vitro kinetics

UGT76B1 recombinant protein was incubated with substrates NHP, SA, and ILA for 30 min at  $30^{\circ}\text{C}$ . The reaction was stopped by the addition of 20% acetonitrile. Samples were analyzed using a 1290 Infinity UHPLC system coupled to a 6540 UHD Accurate-Mass Q-TOF (Agilent Technologies, Santa Clara, CA, USA) as previously described (Feussner and Feussner, 2019). Kinetic parameters of UGT76B1's substrates NHP, SA, and ILA were analyzed as described under UPLC-nanoESI-QTRAP-MS-based metabolite quantification. The reaction mixture contained 3.5- $\mu\text{g}$  UGT76B1, 2 mM UDP-Glc (Merck, Darmstadt, Germany), and 0–2.5 mM substrate. Before incubation with UGT76B1, the initial amount of substrate was determined for analysis of substrate reduction. The reaction was incubated for 15 min at  $30^{\circ}\text{C}$  and stopped by the addition of methanol. The difference in signal intensity of substrate was plotted for each substrate and concentration. The  $K_M$  was determined via Hill regression analysis using OriginPro version 8.5 (OriginLab Corporation, Northampton, MA, USA).

### Pathogen infection assay and SAR assay

Basal resistance against *H.a. Noco 2* was tested by spray-inoculating 2-week-old seedlings with spore solution (50,000 spores/mL). Inoculated seedlings were covered with a transparent lid and grown in a plant chamber with a relative humidity of  $\sim 80\%$ . Infection was scored at 7 dpi by counting conidia spores with a hemocytometer.

Induction of SAR against *H.a. Noco 2* was performed by infiltrating two full-grown leaves of 3-week-old plants with *P.s.m.* ES4326 ( $\text{OD}_{600} = 0.001$ ) or 10 mM  $\text{MgCl}_2$  (mock). Two days later, plants were sprayed with *H.a. Noco 2* spore solution (50,000 spores/mL). Infection on distal leaves was scored at 7 dpi as described previously (Ding et al., 2016).

Induction of SAR against *Pseudomonas* was tested by infiltrating *P.s.m.* ES4326 ( $\text{OD}_{600} = 0.001$ ) or 10 mM  $\text{MgCl}_2$  (mock) on two leaves of 4-week-old plants grown under short-day conditions. Two days later, two distal leaves were challenged with *P.s.m.* ES4326 ( $\text{OD}_{600} = 0.001$ ). Infection was scored at both 0 and 3 dpi by measuring the bacterial titer in the distal leaves.

### Structural prediction and ligand docking

The crystal structure of UGT74F2 (George Thompson et al., 2017), co-crystallized with SA-analog 2-bromobenzoic acid, UDP, 3-O- $\beta$ -D-glucopyranosyl- $\beta$ -D-glucopyranose, and  $\beta$ -D-glucose (PDB ID 5V2J) was used for structural prediction of UGT76B1. The structural prediction of UGT76B1 was done

using PHYR2Protein (Kelley et al., 2015). NHP was fit into the electron density of SA-analog 2-bromobenzoic acid using Coot (Emsley and Cowtan, 2004). Figures were created and distances were measured using PyMol (Schrödinger LLC, New York, NY, USA).

### Statistical analysis

Statistical analyses were performed using Origin Pro version 8.5 and Origin 2020 (OriginLab Corporation, Northampton, MA, USA). Results of the one-way-analysis of variance (ANOVA) calculations is provided in the [Supplemental Dataset 2](#).

### Accession numbers

Further deposited information can be found in The Arabidopsis Information Resource database under the accession numbers: AT3G11340 (UGT76B1) and AT1G19250 (FMO1). Mass spectrometric data of the underlying study have been deposited to Metabolights public repository (Haug et al., 2020) under the study MTBLS2334.

### Supplemental data

The following materials are available in the online version of this article.

**Supplemental Figure S1.** CRISPR deletion mutants of UGT76B1 are unable to synthesize NHP-OGlc after UV-treatment.

**Supplemental Figure S2.** *fmo1-1 ugt76b1-1* double loss-of-function mutant plants synthesize neither NHP nor NHP-OGlc after UV-treatment.

**Supplemental Figure S3.** Transcripts levels of PR1 and PR2 after infection with *P.s.m.* in *ugt76b1* and wild-type.

**Supplemental Figure S4.** Purification of UGT76B1 heterologously expressed in *E. coli*.

**Supplemental Figure S5.** Modeling of NHP into the SA-analog electron density in the predicted in silico UGT76B1 model.

**Supplemental Figure S6.** Transcripts of UGT76B1 were not present in the mutant.

**Supplemental Figure S7.** Calibration linearity as basis for quantification of SA, SAG, NHP, and NHP-OGlc.

**Supplemental Table S1.** List of primers used in this work

**Supplemental Table S2.** MRM parameters for absolute quantification of analytes.

**Supplemental Dataset 1.** Data matrix of 448 high-quality metabolite features ( $\text{FDR} < 0.005$ ) obtained by metabolite fingerprinting (UHPLC-HRMS analysis) of mock and *p.s.m.* infected Col-0 and *ugt76b1* plants.

**Supplemental Dataset 2.** ANOVA results underlying figure assignments.

### Acknowledgments

We would like to acknowledge Brigitte Worbs for the chemical synthesis of the NHP and  $\text{D}_3$ -labeled NHP standards. We thank Prof. Dr Petr Karlovsky for kindly providing the SAG



standard. We are very grateful to Ilka N Abreu for her support with depositing the data in a repository.

## Funding

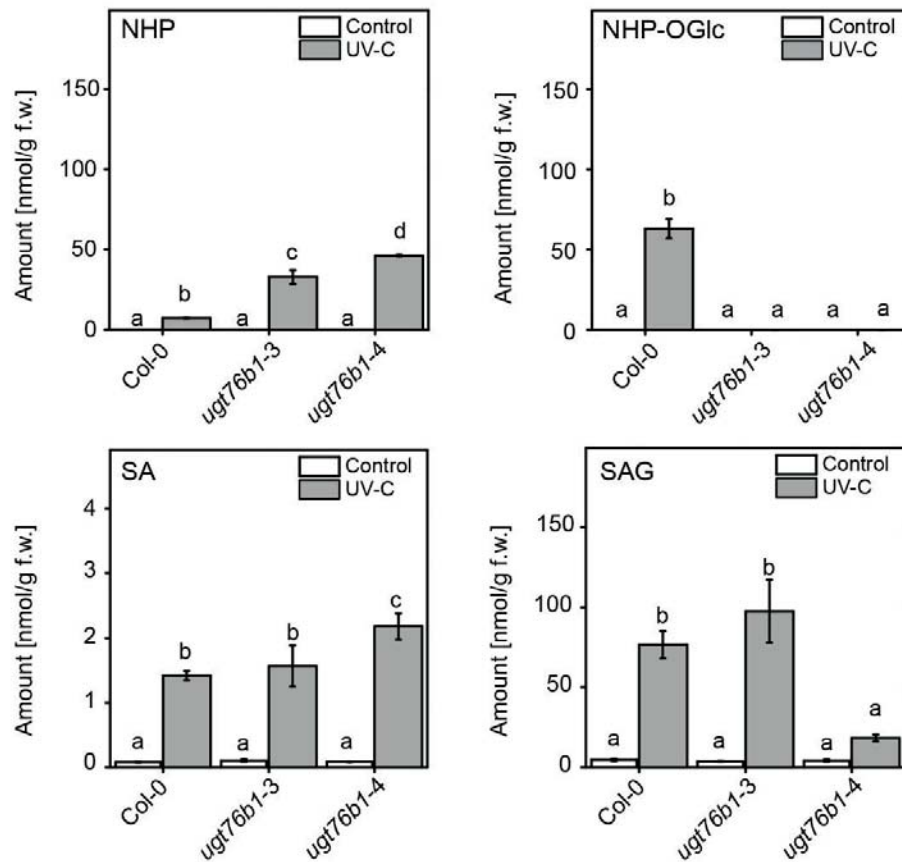
L.M. and D.R. were supported by the Goettingen Graduate School for Neurosciences, Biophysics, and Molecular Biosciences in frame of the PRoTECT program at the Georg August University Goettingen. I.F. acknowledges funding from the Deutsche Forschungsgemeinschaft (GRK 2172-PRoTECT, INST 186/822-1, and ZUK 45/2010). Y.Z. acknowledges funding from the Natural Sciences and Engineering Research Council (NSERC) Discovery Program. W.H. was supported by the China Scholarship Council and NSERC-CREATE (PRoTECT).

**Conflict of interest statement.** The authors have declared no conflict of interest.

## References

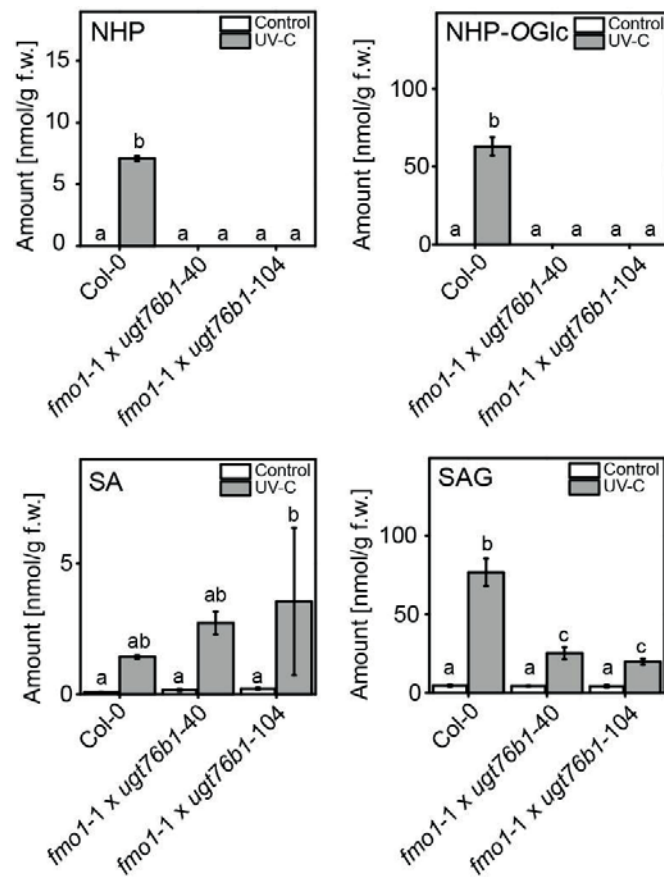
- Bauer S, Mekonnen DW, Geist B, Lange B, Ghirardo A, Zhang W, Schöffner AR (2020) The isoleucic acid triad: distinct impacts on plant defense, root growth, and formation of reactive oxygen species. *J Exp Bot* **71**: 4258–4270
- Bauer S, Mekonnen DW, Hartmann M, Janowski R, Lange B, Geist B, Zeier J, Schaeffner AR (2021) UGT76B1, a promiscuous hub of small molecule-based immune signaling, glucosylates N-hydroxypipicolinic acid and controls basal pathogen defense. *Plant Cell* **33**: 714–734
- Bernsdorff F, Döring AC, Gruner K, Schuck S, Bräutigam A, Zeier J (2016) Pipicolinic acid orchestrates plant systemic acquired resistance and defense priming via salicylic acid-dependent and -independent pathways. *Plant Cell* **28**: 102–129
- Chen L, Wang WS, Wang T, Meng XF, Chen TT, Huang XX, Li YJ, Hou BK (2019) Methyl salicylate glucosylation regulates plant defense signaling and systemic acquired resistance. *Plant Physiol* **180**: 2167–2181
- Chen YC, Holmes EC, Rajniak J, Kim JG, Tang S, Fischer CR, Mudgett MB, Sattely ES (2018) N-hydroxy-pipicolinic acid is a mobile metabolite that induces systemic disease resistance in *Arabidopsis*. *Proc Natl Acad Sci USA* **115**: E4920–E4929
- Clough SJ, Bent AF (1998) Floral dip: a simplified method for *Agrobacterium*-mediated transformation of *Arabidopsis thaliana*. *Plant J* **16**: 735–743
- Dean JV, Delaney SP (2008) Metabolism of salicylic acid in wild-type, *ugt74f1* and *ugt74f2* glucosyltransferase mutants of *Arabidopsis thaliana*. *Physiol Plant* **132**: 417–425
- Ding P, Rekhter D, Ding Y, Feussner K, Busta L, Haroth S, Xu S, Li X, Jetter R, Feussner I, et al. (2016) Characterization of a pipicolinic acid biosynthesis pathway required for systemic acquired resistance. *Plant Cell* **28**: 2603–2615
- Emsley P, Cowtan K (2004) Coot: model-building tools for molecular graphics. *Acta Crystallogr D Biol Crystallogr* **60**: 2126–2132
- Feussner K, Feussner I (2019) Comprehensive LC-MS-based metabolite fingerprinting approach for plant and fungal-derived samples. In A D'Alessandro, ed, *High-Throughput Metabolomics: Methods and Protocols*. Springer New York, New York, NY, pp 167–185
- Fu ZQ, Dong X (2013) Systemic acquired resistance: turning local infection into global defense. *Annu Rev Plant Biol* **64**: 839–863
- George Thompson AM, Iancu CV, Neet KE, Dean JV, Choe JY (2017) Differences in salicylic acid glucose conjugations by UGT74F1 and UGT74F2 from *Arabidopsis thaliana*. *Sci Rep* **7**: 46629
- Gruner K, Griebel T, Návarová H, Attaran E, Zeier J (2013) Reprogramming of plants during systemic acquired resistance. *Front Plant Sci* **4**: 252
- Guerra T, Schilling S, Hake K, Gorzalka K, Sylvester FP, Conrads B, Westermann B, Romeis T (2020) Calcium-dependent protein kinase 5 links calcium-signaling with N-Hydroxy-L-pipicolinic acid and SARD1-dependent immune memory in systemic acquired resistance. *New Phytol* **225**: 310–325
- Haroth S, Feussner K, Kelly AA, Zienkiewicz K, Shaikhqasem A, Herrfurth C, Feussner I (2019) The glucosyltransferase UGT76E1 significantly contributes to 12-O-glucopyranosyl-jasmonic acid formation in wounded *Arabidopsis thaliana* leaves. *J Biol Chem* **294**: 9858–9872
- Hartmann M, Kim D, Bernsdorff F, Ajami-Rashidi Z, Scholten N, Schreiber S, Zeier T, Schuck S, Reichel-Deland V, Zeier J (2017) Biochemical principles and functional aspects of pipicolinic acid biosynthesis in plant immunity. *Plant Physiol* **174**: 124–153
- Hartmann M, Zeier J (2019) N-Hydroxypipicolinic acid and salicylic acid: a metabolic duo for systemic acquired resistance. *Curr Opin Plant Biol* **50**: 44–57
- Hartmann M, Zeier T, Bernsdorff F, Reichel-Deland V, Kim D, Hohmann M, Scholten N, Schuck S, Bräutigam A, Hölzel T, et al. (2018) Flavin monooxygenase-generated N-hydroxypipicolinic acid is a critical element of plant systemic immunity. *Cell* **173**: 456–469
- Hennig J, Malamy J, Gryniewicz G, Indulski J, Klessing DF (1993) Interconversion of the salicylic acid signal and its glucoside in tobacco. *Plant J* **4**: 593–600
- Herrfurth C, Feussner I (2020) Quantitative jasmonate profiling using a high-throughput UPLC-NanoESI-MS/MS method. In A Champion, L Laplaze, eds. *Jasmonate in Plant Biology: Methods and Protocols*. Springer, New York, NY, pp 169–187
- Holmes E, Chen YC, Mudgett MB, Sattely E (2021) *Arabidopsis* UGT76B1 glucosylates N-hydroxy-pipicolinic acid and inactivates systemic acquired resistance in tomato. *Plant Cell* **33**: 750–765
- Holmes EC, Chen YC, Sattely ES, Mudgett MB (2019) An engineered pathway for N-hydroxy-pipicolinic acid synthesis enhances systemic acquired resistance in tomato. *Sci Signal* **12**: eaay3066
- Huang W, Wang Y, Li X, Zhang Y (2020) Biosynthesis and regulation of salicylic acid and N-hydroxypipicolinic acid in plant immunity. *Mol Plant* **13**: 31–41
- Huang X, Zhu GG, Liu Q, Chen L, Li YJ, Hou BK (2018) Modulation of plant salicylic acid-associated immune responses via glucosylation of dihydroxybenzoic acids. *Plant Physiol* **176**: 3103–3119
- Kelley LA, Mezulis S, Yates CM, Wass MN, Sternberg MJE (2015) The Phyre2 web portal for protein modeling, prediction and analysis. *Nat Protocol* **10**: 845–858
- Kaever A, Landesfeind M, Feussner K, Mosblech A, Heilmann I, Morgenstern B, Feussner I, Meinicke P (2015) MarVis-Pathway: integrative and exploratory pathway analysis of non-targeted metabolomics data. *Metabolomics* **11**: 764–777
- Koch M, Vorwerk S, Masur C, Sharifi-Sirchi G, Olivieri N, Schlaich NL (2006) A role for a flavin-containing mono-oxygenase in resistance against microbial pathogens in *Arabidopsis*. *Plant J* **47**: 629–639
- Lim GH, Liu H, Yu K, Liu R, Shine MB, Fernandez J, Burch-Smith T, Mobley JK, McLetchie N, Kachroo A, et al. (2020) The plant cuticle regulates apoplastic transport of salicylic acid during systemic acquired resistance. *Sci Adv* **6**: eaaz0478
- Maksym RP, Ghirardo A, Zhang W, von Saint Paul V, Lange B, Geist B, Hajirezaei MR, Schnitzler JP, Schöffner AR (2018) The defense-related isoleucic acid differentially accumulates in *Arabidopsis* among branched-chain amino acid-related 2-hydroxy carboxylic acids. *Front Plant Sci* **9**: 766
- Navarova H, Bernsdorff F, Döring AC, Zeier J (2012) Pipicolinic acid, an endogenous mediator of defense amplification and priming, is a critical regulator of inducible plant immunity. *Plant Cell* **24**: 5123–5141

- Noutoshi Y, Okazaki M, Kida T, Nishina Y, Morishita Y, Ogawa T, Suzuki H, Shibata D, Jikumaru Y, Hanada A, et al.** (2012) Novel plant immune-priming compounds identified via high-throughput chemical screening target salicylic acid glucosyltransferases in *Arabidopsis*. *Plant Cell* **24**: 3795–3804
- Rekhter D, Lüdke D, Ding Y, Feussner K, Zienkiewicz K, Lipka V, Wiermer M, Zhang Y, Feussner I** (2019b) Isochorismate-derived biosynthesis of the plant stress hormone salicylic acid. *Science* **365**: 498–502
- Rekhter D, Mohnike L, Feussner K, Zienkiewicz K, Zhang Y, Feussner I** (2019a) Enhanced disease susceptibility 5 (EDS5) is required for N-hydroxy pipecolic acid formation. *bioRxiv* **630723**
- Seo S, Ishizuka K, Ohashi Y** (1995) Induction of salicylic acid beta-glucosidase in tobacco leaves by exogenous salicylic acid. *Plant Cell Physiol* **36**: 447–453
- Song JT** (2006) Induction of a salicylic acid glucosyltransferase, AtSGT1, is an early disease response in *Arabidopsis thaliana*. *Mol Cell* **22**: 233–238
- Song JT, Koo YJ, Park JB, Cho YJ, Seo HS, Choi YD** (2009) The expression patterns of *AtBSMT1* and *AtSAGT1* encoding a salicylic acid (SA) methyltransferase and a SA glucosyltransferase, respectively, in *Arabidopsis* plants with altered defense responses. *Mol Cell* **28**: 105–109
- Song JT, Koo YJ, Seo HS, Kim MC, Choi YD, Kim JH** (2008) Overexpression of *AtSGT1*, an *Arabidopsis* salicylic acid glucosyltransferase, leads to increased susceptibility to *Pseudomonas syringae*. *Phytochemistry* **69**: 1128–1134
- Song JT, Lu H, McDowell JM, Greenberg JT** (2004) A key role for *ALD1* in activation of local and systemic defenses in *Arabidopsis*. *Plant J* **40**: 200–212
- Torrens-Spence MP, Bobokalonova A, Carballo V, Glinkerman CM, Pluskal T, Shen A, Weng JK** (2019) *PBS3* and *EPS1* complete salicylic acid biosynthesis from isochorismate in *Arabidopsis*. *Mol Plant* **12**: 1577–1586
- Vernooij B, Friedrich L, Morse A, Reist R, Kolditz-Jawhar R, Ward E, Uknes S, Kessmann H, Ryals J** (1994b) Salicylic acid is not the translocated signal responsible for inducing systemic acquired resistance but is required in signal transduction. *Plant Cell* **6**: 959–965
- Vernooij B, Uknes S, Ward E, Ryals J** (1994a) Salicylic acid as a signal molecule in plant-pathogen interactions. *Curr Opin Cell Biol* **6**: 275–279
- Vogel-Adghough D, Stahl E, Návárová H, Zeier J** (2013) Pipecolic acid enhances resistance to bacterial infection and primes salicylic acid and nicotine accumulation in tobacco. *Plant Signal Behav* **8**: e26366
- von Saint Paul V, Zhang W, Kanawati B, Geist B, Faus-Kessler T, Schmitt-Kopplin P, Schäffner AR** (2011) The *Arabidopsis* glucosyltransferase *UGT76B1* conjugates isoleucic acid and modulates plant defense and senescence. *Plant Cell* **23**: 4124–4145
- Wildermuth MC, Dewdney J, Wu G, Ausubel FM** (2001) Isochorismate synthase is required to synthesize salicylic acid for plant defence. *Nature* **414**: 562–565
- Xing HL, Dong L, Wang ZP, Zhang HY, Han CY, Liu B, Wang XC, Chen QJ** (2014) A CRISPR/Cas9 toolkit for multiplex genome editing in plants. *BMC Plant Biol* **14**: 327
- Yalpani N, Enyedi AJ, León J, Raskin I** (1994) Ultraviolet light and ozone stimulate accumulation of salicylic acid, pathogenesis-related proteins and virus resistance in tobacco. *Planta* **193**: 372–376
- Yalpani N, Leon J, Lawton MA, Raskin I** (1993) Pathway of salicylic acid biosynthesis in healthy and virus-inoculated tobacco. *Plant Physiol* **103**: 315–321
- Yalpani N, Silverman P, Wilson TM, Kleier DA, Raskin I** (1991) Salicylic acid is a systemic signal and an inducer of pathogenesis-related proteins in virus-infected tobacco. *Plant Cell* **3**: 809–818
- Zhang Y, Li X** (2019) Salicylic acid: biosynthesis, perception, and contributions to plant immunity. *Curr Opin Plant Biol* **50**: 29–36
- Zhang Y, Yang Y, Fang B, Gannon P, Ding P, Li X, Zhang Y** (2010) *Arabidopsis snc2-1D* activates receptor-like protein-mediated immunity transduced through *WRKY70*. *Plant Cell* **22**: 3153–3163
- Zhang Y, Zhao L, Zhao J, Li Y, Wang J, Guo R, Gan S, Liu CJ, Zhang K** (2017) *SSH/DMR6* encodes a salicylic acid 5-hydroxylase that fine-tunes salicylic acid homeostasis. *Plant Physiol* **175**: 1082–1093



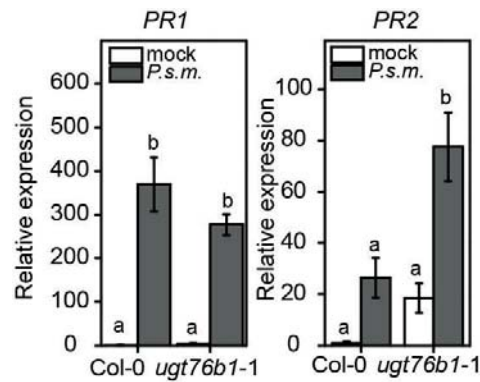
Supplemental Figure 1. **CRISPR deletion mutants of *UGT76B1* are unable to synthesize NHP-OGlc after UV-treatment.** Supports Figure 3. Absolute amounts of NHP, NHP-OGlc, SA and SAG were determined in wild type, *ugt76b1-3* and *ugt76b1-4* after UV-C treatment. Plants grown under long day conditions (16 hours light period), were treated for 20 min with UV-C or left untreated as control. Twenty-four hours post treatment, leaf material was harvested and analyzed using quantitative UPLC-nanoESI-QTRAP-MS. Error bars represent standard deviation. Letters indicate statistical differences ( $p < 0.05$ , one-way ANOVA;  $n=3$ ). Replicates represent a pool of 4–6 leaves of 6 plants per condition.

Supplemental Data. Mohnike and Rekhter et al. (2021). The glycosyltransferase UGT76B1 modulates *N*-hydroxy-pipecolic acid homeostasis and plant immunity. *Plant Cell*.



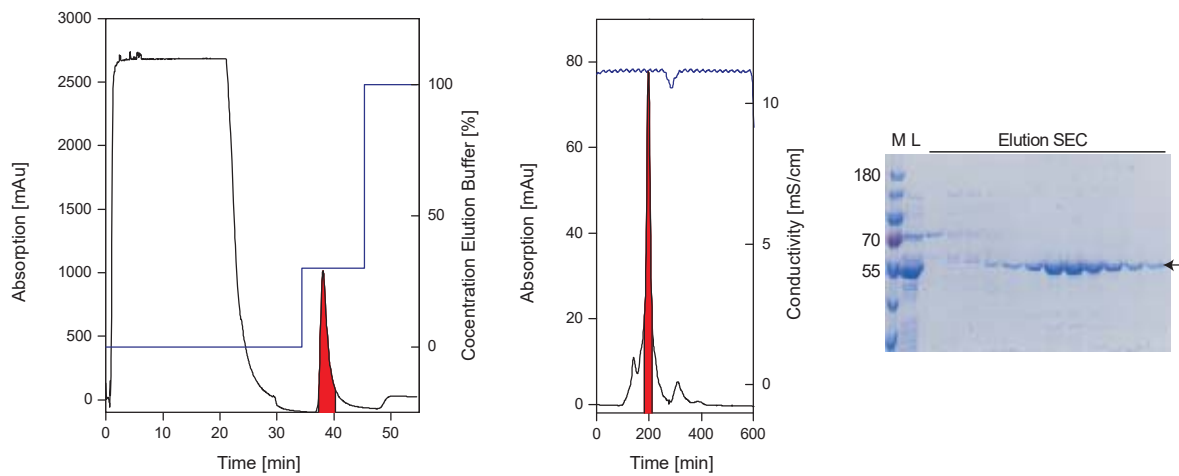
Supplemental Figure 2. *fmo1-1 ugt76b1-1* double loss-of-function mutant plants synthesize neither NHP nor NHP-OGlc after UV-treatment. Supports Figure 4. Absolute amounts of NHP, NHP-OGlc, SA and SAG were determined in wild type and two independent *fmo1-1 ugt76b1* lines after UV-C treatment. Plants grown under long day conditions (16 hour light period), were treated for 20 min with UV-C or left untreated as control. Twenty-four hours post treatment, leaf material was harvested and analyzed using quantitative UPLC-nanoESI-QTRAP-MS. Error bars represent standard deviation. Letters indicate statistical differences ( $p < 0.05$ , one-way ANOVA;  $n=3$ ). Replicates represent a pool of 4–6 leaves of 6 plants per condition.

Supplemental Data. Mohnike and Rekhter et al. (2021). The glycosyltransferase UGT76B1 modulates *N*-hydroxy-pipecolic acid homeostasis and plant immunity. *Plant Cell*.



Supplemental Figure 3. **Transcript levels of *PR1* and *PR2* after infection with *P.s.m.* in *ugt76b1* and wild type.** Supports Figure 5. Relative amount of transcripts of *PR1* and *PR1* was analyzed in wild type and *ugt76b1-1* plants after infection with *P.s.m.* ES4326. Three leaves of 4-6 week-old plants were treated with *P.s.m.* ES4326 ( $OD_{600}=0.001$ ). Leaves were harvested 24 hours post infiltration and analyzed for the level of transcripts via qPCR. Error bars represent standard deviation. Letters indicate statistical differences ( $p < 0.05$ , one-way ANOVA;  $n=3$ ). Replicates represent a pool of 4–6 leaves of 6 plants per condition.

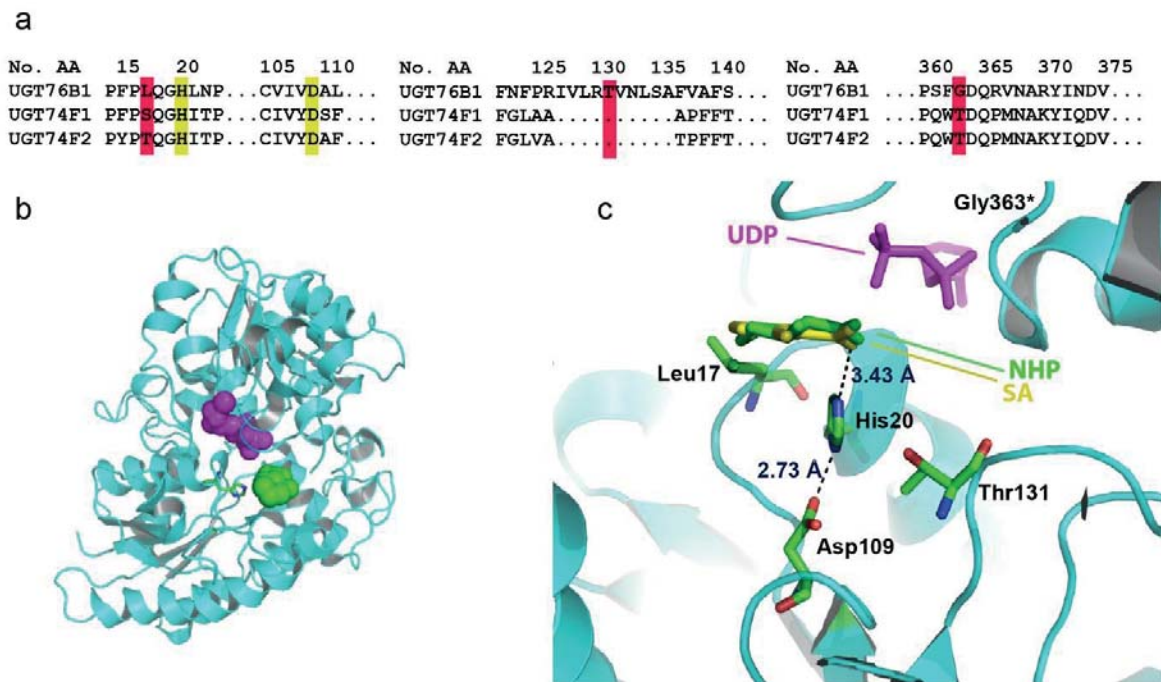
Supplemental Data. Mohnike and Rekhter et al. (2021). The glycosyltransferase UGT76B1 modulates *N*-hydroxy-pipecolic acid homeostasis and plant immunity. *Plant Cell*.



Supplemental Figure 4. **Purification of UGT76B1 heterologously expressed in *E. coli*.** Supports Figure 6. UGT76B1 fused with an N-terminal His-tag was heterologously expressed in *E. coli* BL21 Star (DE3) and purified via a combination of immobilized metal affinity chromatography (IMAC) and size exclusion chromatography (SEC). Chromatograms illustrate the absorption at 280 nm in milli absorption units (mAU) during protein elution. Secondary y-axes indicate the concentration of elution buffer in % for IMAC or the conductivity in mS/cm for SEC. Red areas represent corresponding signals to UGT76B1. The sodium dodecyl sulfate polyacrylamide gel electrophoresis (SDS-PAGE) gel shows the corresponding protein marker M, the load L (eluate IMAC) and the elution after SEC. The arrow indicates UGT76B1. The depicted purification is representative of at least three independent purifications.

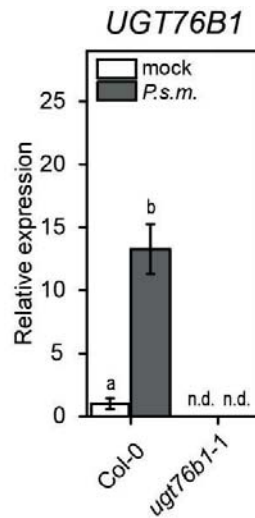


Supplemental Data. Mohnike and Rekhter et al. (2021). The glycosyltransferase UGT76B1 modulates *N*-hydroxy-pipecolic acid homeostasis and plant immunity. *Plant Cell*.



Supplemental Figure 5. **Modeling of NHP into the SA-analogues' electron density in the predicted *in silico* UGT76B1 model.** (supports Figure 6) **(a)** Protein sequence alignment comparing UGT76B1, UGT74F1 and UGT74F2 with the putative active site residues. Sequence identities are shown in yellow and miss matches in red. **(b)** Predicted model of UGT76B1 complexed with UDP and NHP using the deposited PDB structure 5V2J of UGT74F2 complexed with UDP and SA. UDP is shown as magenta balls and the modeled NHP is shown as green balls. His20 is shown as sticks. **(c)** Amino acids histidine (His<sup>20</sup>), aspartate (Asp<sup>109</sup>) and putatively threonine (Thr<sup>131</sup>), which may form the proposed catalytic triad by George Thompson et al., 2017, are predicted to the active center and in close proximity to the substrate and each other in the UGT76B1 model prediction. The structural prediction of UGT76B1 was done by PHYR2Protein (Kelley et al., 2015). NHP was fit into the electron density of SA-analogue 2-bromobenzoic acid using Coot (Emsley and Cowtan, 2004). Figures were created using PyMol (Schrödinger LLC, USA).

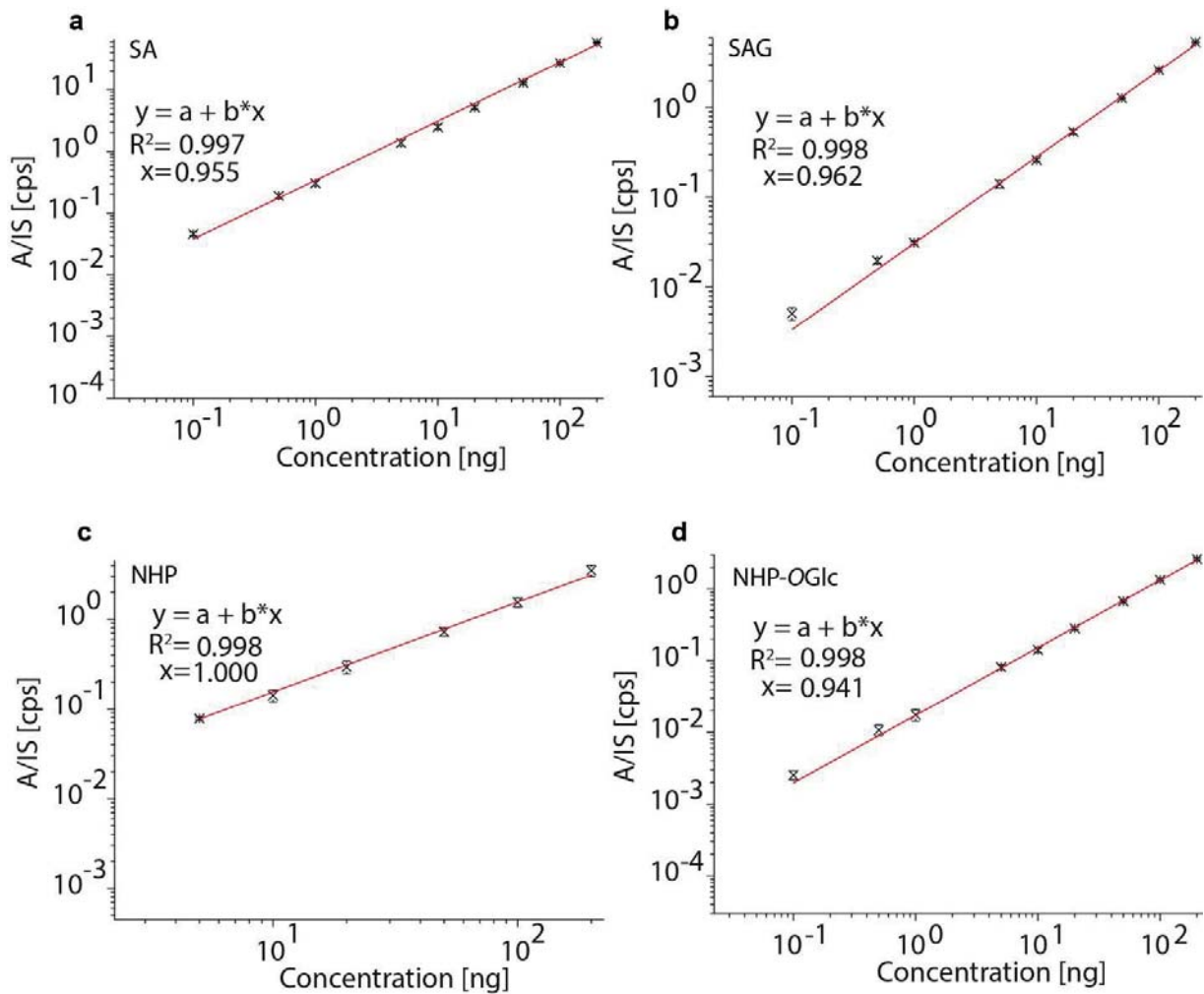
Supplemental Data. Mohnike and Rekhter et al. (2021). The glycosyltransferase UGT76B1 modulates *N*-hydroxy-pipecolic acid homeostasis and plant immunity. Plant Cell.



Supplemental Figure 6. **Transcripts of *UGT76B1* were not present in the mutant.** Supports Figures 1, 2, 3, 4, 5 and 7. Relative amounts of *UGT76B1* transcripts were analyzed in wild type and *ugt76b1-1* plants after infection with *P.s.m.* ES4326. Three leaves of 4–6 week-old plants were treated with *P.s.m.* ES4326 ( $OD_{600}=0.001$ ). Leaves were harvested 24 hours post infiltration and analyzed for the level of transcripts via qPCR. Error bars represent standard deviation. Letters indicate statistical differences ( $p < 0.05$ , one-way ANOVA;  $n=3$ ). Replicates represent a pool of 4-6 leaves of 6 plants per condition.



Supplemental Data. Mohnike and Rekhter et al. (2021). The glycosyltransferase UGT76B1 modulates *N*-hydroxy-pipecolic acid homeostasis and plant immunity. *Plant Cell*.



Supplemental Figure 7. **Calibration linearity as basis for quantification of SA, SAG, NHP, NHP-OGlc.** Supports Figure 3. Each substance was analyzed at different concentrations to determine the calibration linearity of the UPLC-nanoESI-QTRAP-MS-based method. Six to nine data points were collected for each compound. The data represent the counts per seconds (cps) of the analyte divided by the cps of the internal standard over the concentration dependency in ng of the substance. The data are shown in a log<sub>10</sub> scale on both axes. *n*=5 technical replicates of each data point.

Supplemental Data. Mohnike and Rekhter et al. (2021). The glycosyltransferase UGT76B1 modulates *N*-hydroxy-pipecolic acid homeostasis and plant immunity. *Plant Cell*.

Supplemental Table 1. **List of primers used in this work.** Information is divided by primer application for quantitative PCR analysis, genotyping, and cloning.

Real time PCR-primers

Gene ID	Forward primer	Reverse primer
AT2G37620	ACT1-F: cgatgaagctcaatccaaacga	ACT1-R: cagagtcgagcacaataccg
AT2G14610	PR1-RT-F2: AGGCAACTGCAGACTCATAC	PR1-RT-R2: TTGTTACACCTCACTTTGGC
AT4G39030	EDS5-F101-RT: GCCAAACAGGACAAGAAAGAAG	EDS5-R102-RT: GCCGAAACAATCTGTGAAGC
AT5G13320	PBS3-F101-RT: CTAAGTTCTGGAACCTTCTGG	PBS3-R102-RT: CATGACTGAAGCAAAGATGG
AT2G13810	ALD1-F101-RT: TTCCCAAGGCTAGTTTGGAC	ALD1-R102-RT: GCCTAAGAGTAGCTGAAGACG
AT1G19250	FMO1-F101-RT: GGAGATATTCAGTGGCATGC	FMO1-R102-RT: TTTGGTTAGGCCTATCATGG
AT1G73805	SARD1-RT-NF: TCAAGGCGTTGTGGTTTGTG	SARD1-RT-NR: CGTCAACGACGGATAGTTTC
AT3G11340	11340-RT-F: GGATTGTTCTCCGAACCGTTA	11340-RT-R: GTGAGTCTGCCTTAGTCTCTTG

Genotyping primers

Lines	Forward primer	Reverse primer
CRISPR ugt76b1 lines	11340-heter-F: GATCGAATCAGCATAATG	11340-heter-R: GTGTCTGATTATGGGAATGC
CRISPR ugt76b1 lines	11340-homo-F: GAATGAAGGATCTTCCATGG	11340-heter-R: GTGTCTGATTATGGGAATGC
SAIL_1171_A11	SAIL1171A11-tdna-F: TCAGGAATCATATTCAACGCC	SAIL1171A11-tdna-R: GCTGAAGACTAAGCGTCATGC

Cloning primers

Purpose	Primer	Sequence
CRISPR-deletion ( <i>UGT76B1</i> )	3G11340-BsFF0	ATATATGGTCTCGATTG TCTTCCCTTTCCCTTTA CAGTTTTAGAGCTAGAA ATAGC
CRISPR-deletion ( <i>UGT76B1</i> )	3G11340-BsRR0	ATTATTGGTCTCGAAAC CTTCCGAGCTCGTCATT AGCAATCTCTTAGTCGA CTCTAC
Heterologous expression ( <i>UGT76B1</i> )	UGT76B1 BamHI for	acgGGATCCATGGAGAC TAGAGAAACA

Supplemental Data. Mohnike and Rekhter et al. (2021). The glycosyltransferase UGT76B1 modulates *N*-hydroxy-pipecolic acid homeostasis and plant immunity. *Plant Cell*.

Heterologous expression ( <i>UGT76B1</i> )	UGT76B1 Sall reverse	acgGTCGACTTAGAAAG ACAATATATAAGCA
---	----------------------	-------------------------------------

Supplemental Table 2. **Multiple reaction monitoring parameters for absolute quantification of analytes.** For the presented quantitative plant hormone data we established a multiple reaction monitoring analysis of seven additional analytes to the ones published before (Herrfurth and Feussner, 2020). Q1 (precursor ion), Q3 (product ion) and the retention time (RT) of each analyte are shown, respectively. Furthermore, the declustering potential (DP), entrance potential (EP), collision energy (CE) and the cell exit potential (CXP) of each compound are provided.

Q1 ( <i>m/z</i> )	Q3 ( <i>m/z</i> )	RT (min)	Analyte	DP (eV)	EP (eV)	CE (eV)	CXP (eV)
137	93	2	SA	-25	-6	-20	-10
141	97	3	D <sub>4</sub> -SA	-25	-6	-22	-6
144	82	0.7	NHP	-60	-8	-15	-13
153	90	0.7	D <sub>9</sub> -NHP	-60	-8	-15	-13
299	137	1	SAG	-30	-4	-18	-2
305	137	1	<sup>13</sup> C <sub>6</sub> -SAG	-30	-4	-18	-2
306	89	0.9	NHP-OGlc	-65	-4	-18	-13

## 4. Chapter II. - *N*-hydroxy pipecolic acid methyl ester is involved in Arabidopsis immunity

The article was initially submitted in June 2022.

Additionally, it was published at bioRxiv and can be found online:

<https://doi.org/10.1101/2022.06.03.494702>.

### **Author contribution:**

Lennart Mohnike planned and performed the non-targeted metabolite analysis as well as the subsequent metabolite identification by UHPLC-ESI-HRMS. He expressed and established the purification of *At*NHPMT1. Moreover, he amplified, cloned, expressed and established the purification of *At*UGT74F2 and *At*UGT73D1. He conducted the analysis of *nhpmt1* mutant plants. He initiated the synthesis of MeNHP from methyl pipecolinate and performed the MeNHP infiltration studies as well as the metabolite analysis. Additionally, he conducted the infiltration of D<sub>9</sub>-NHP/NHP mixture and performed the data analysis. He analyzed, processed, displayed, interpreted and discussed the results, and wrote the first draft of the manuscript.

## ***N*-hydroxy pipecolic acid methyl ester is involved in *Arabidopsis* immunity**

**Lennart Mohnike<sup>1</sup>, Weijie Huang<sup>4</sup>, Brigitte Worbs<sup>5</sup>, Kirstin Feussner<sup>1,2</sup>, Yuelin Zhang<sup>4</sup> and Ivo Feussner<sup>1,3,\*</sup>**

<sup>1</sup>University of Goettingen, Albrecht-von-Haller-Institute for Plant Sciences, Department of Plant Biochemistry, D-37077 Goettingen, Germany.

<sup>2</sup>University of Goettingen, Goettingen Center for Molecular Biosciences (GZMB), Service Unit for Metabolomics and Lipidomics, D-37077 Goettingen, Germany.

<sup>3</sup>University of Goettingen, Goettingen Center for Molecular Biosciences (GZMB), Department of Plant Biochemistry, D-37077 Goettingen, Germany.

<sup>4</sup>University of British Columbia, Department of Botany, V6T 1Z4 Vancouver (BC), Canada.

<sup>5</sup>University of Goettingen, Institute for Organic and Biomolecular Chemistry, Department of Organic Chemistry, D-37077 Goettingen, Germany.

### **\* Correspondence:**

Ivo Feussner

ifeussn@uni-goettingen.de, ORCID iD: 0000-0002-9888-7003

Running title: *N*-hydroxy pipecolic acid metabolites in plant immunity

### **Highlight**

In this work, we identify *N*-hydroxy pipecolic acid (NHP) metabolites including methyl ester and complex glycosides. The application of methyl ester is able to rescue the disease phenotype of the biosynthesis deficient mutant of NHP.

### **Abstract**

The biosynthesis of *N*-hydroxy pipecolic acid (NHP) has been intensively studied, though knowledge on its metabolic turnover is still scarce. To close this gap, we discovered three novel metabolites via metabolite fingerprinting in *Arabidopsis thaliana* leaves. Exact mass information and fragmentation by mass spectrometry (MSMS) suggest a methylated derivative of NHP (MeNHP), a NHP-OGlc-hexosyl conjugate (NHP-OGlc-Hex) and an additional NHP-OGlc-derivative. All three compounds were formed in wildtype leaves but not present in the NHP deficient mutant *fmo1-1*. The identification of these novel NHP-based molecules was possible by a dual-infiltration experiment using a mixture of authentic NHP- and D<sub>9</sub>-NHP-standards for leaf infiltration followed by an UV-C treatment. Interestingly, the signal intensity

of MeNHP and other NHP-derived metabolites increased in *ugt76b1-1* mutant plants. This suggests a detour, for the inability to synthesize NHP-*O*-glucoside. For MeNHP, we unequivocally determined the site of methylation at the carboxylic acid function. MeNHP application by leaf infiltration leads to the detection of a MeNHP-*OGlc* as well as NHP, suggesting MeNHP-hydrolysis to NHP. This is in line with the observation that MeNHP-infiltration is able to rescue the *fmo1-1* susceptible phenotype against *Hyaloperonospora arabidopsidis* Noco 2. Together these data suggest MeNHP as additional storage or transport form of NHP.

**Keywords:** *Arabidopsis thaliana*, infection metabolism, *N*-hydroxy pipecolic acid methyl ester, non-targeted metabolomics, plant immunity, salicylic acid, UV-stress.

**Abbreviations:** 1D-SOM: one-dimensional-self organizing map, ALD1: AGD2-LIKE DEFENSE RESPONSE PROTEIN 1, BSMT1: BENZOIC ACID/SA METHYL-TRANSFERASE 1, CRISPR: Clustered Regularly Interspaced Short Palindromic Repeats, DHBA: di-hydroxy benzoic acid, EPS1: ENHANCED PSEUDOMONAS SUSCEPTIBILITY 1, ESI: electrospray ionization, hpUV: hours post ultra-violet light treatment, ICS1: ISOCHORISMIC ACID SYNTHASE 1, FMO1: FLAVINE-DEPENDENT MONOOXYGENASE 1, MeNHP: *N*-hydroxy pipecolic acid methyl ester, MeNHP-*OGlc*: MeNHP glycoside, MES: Methyl esterase, MeSA: Salicylic acid methyl ester, MeSAGlc: Salicylic acid methyl ester glycoside, MS: mass spectrometry, MTBE: Methyl-*tert*-butyl ether, NHP: *N*-hydroxy pipecolic acid, NHP-*OGlc*: NHP glucoside, NHP-*OGlc*-Hex: NHP glucoside hexose, NHP-GE: NHP glycosyl ester, NHPMT: NHP methyl transferase, PBS3: AvrPphB SUSCEPTIBLE 3, Pip: Pipecolic acid, *P.s.m.*: *Pseudomonas syringae* ES4326, RT: retention time, SA: Salicylic acid, S3H: SA-3-hydroxylase, S5H: SA-5-hydroxylase, SABP2: SA-binding protein 2, SAG: Salicylic acid glucoside, SARD4: SYSTEMIC ACQUIRED RESISTANCE DEFICIENT 4, SGE: Salicylic acid glucoside ester, UGT: UDP-dependent glycosyl transferase, UNK: unknown metabolite, UHPLC-HRMS: ultra-high-performance-liquid-chromatography high-resolution mass spectrometry.

## Introduction

Plants encounter reduced growth or induce early senescence, if they are unable to maintain a balance between growth and defense (von Saint Paul *et al.*, 2011; Zhang *et al.*, 2017). Their immune system depends on a tightly regulated and highly dynamic balance of activation and inactivation (Karasov *et al.*, 2017; Zeier, 2021). Salicylic acid (SA) and *N*-hydroxy pipecolic

acid (NHP) are two key molecules to concert the defense response against (hemi-)biotrophic pathogens (Fu and Dong, 2013; Hartmann and Zeier, 2019).

In the Brassicaceae model organism *Arabidopsis thaliana*, SA and NHP are synthesized upon pathogen infection. Roughly, 90 percent of SA derive from chorismic acid, which is converted via the ISOCHORISMIC ACID SYNTHASE 1 (ICS1) pathway. This pathway features the enzymes AvrPphB SUSCEPTIBLE 3 (PBS3) and ENHANCED PSEUDOMONAS SUSCEPTIBILITY 1 (EPS1) to synthesize SA (Rekhter *et al.*, 2019; Torrens-Spence *et al.*, 2019; Wildermuth *et al.*, 2001). NHP derives from L-lysine via the enzymatic route of AGD2-LIKE DEFENSE RESPONSE PROTEIN 1 (ALD1), SYSTEMIC ACQUIRED RESISTANCE DEFICIENT 4 (SARD4) and FLAVINE-DEPENDENT MONOOXYGENASE 1 (FMO1) (Fig. 1). Both molecules orchestrate defense signaling including the activation of protective measures, such as defense gene expression, and danger signal amplification (Chen *et al.*, 2018; Ding *et al.*, 2016; Hartmann *et al.*, 2018; Navarova *et al.*, 2012). In consequence, to prime distant leaf tissue for robust defense against secondary stressors, termed systemic acquired resistance (SAR) (Chen *et al.*, 2018; Hartmann *et al.*, 2018).

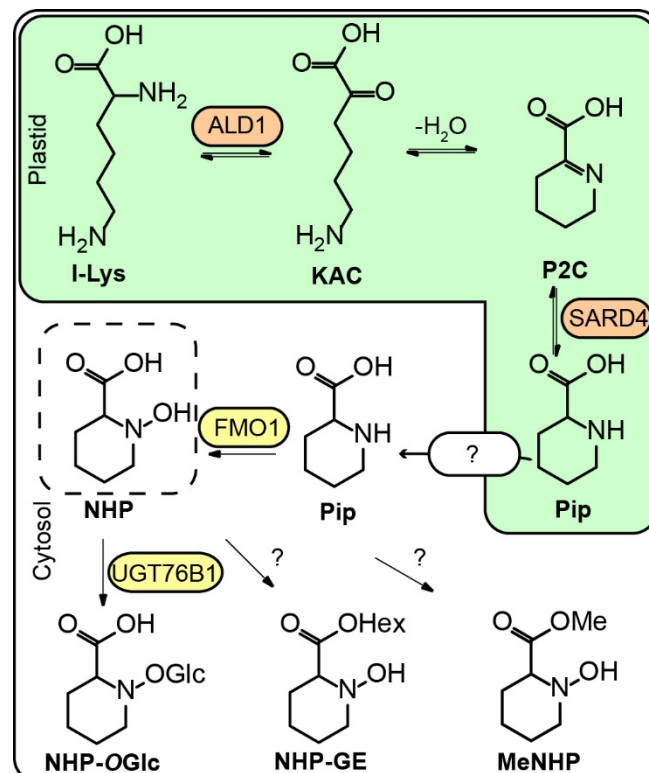


**Fig. 1.** Biosynthesis route of NHP-metabolites in *Arabidopsis*. In the plastid, l-lysine (l-Lys) is converted by AGD2-LIKE DEFENSE RESPONSE PROTEIN 1 (ALD1) to epsilon-amino-alpha-keto caproic acid (KAC). Via spontaneous cyclization under water loss of KAC, piperidein-2-carboxylic acid (P2C) is formed. A reductase capable to reduce P2C to pipercolic acid (Pip) is SYSTEMIC ACQUIRED RESISTANCE DEFICIENT 4 (SARD4). How

pipecolic acid is exported from the chloroplast is still elusive. The FLAVINE-DEPENDENT MONOOXYGENASE 1 (FMO1) catalyzes *N*-hydroxylation of Pip, resulting in *N*-hydroxy pipecolic acid (NHP) (Chen *et al.*, 2018; Ding *et al.*, 2016; Hartmann *et al.*, 2018; Navarova *et al.*, 2012). NHP was shown to be glycosylated by UGT76B1 to NHP-*O*-glycoside (NHP-*O*-Glc). Furthermore, NHP-glycoside-ester (NHP-GE) was described, but respective enzyme is not known (Bauer *et al.*, 2021; Hartmann and Zeier, 2018). Methylation of NHP to NHP-methyl-ester (MeNHP) was shown as an additional mechanism of NHP-turnover *in planta* in this study.

Abnormal accumulation of plant defense hormones can lead to phenotypes such as “dwarfism” or early senescence (Cai *et al.*, 2021; von Saint Paul *et al.*, 2011; Zhang *et al.*, 2017). One way to regulate the cellular concentrations of SA and NHP is by metabolic turnover. SA is glycosylated by a minimum of three UDP-dependent glycosyltransferases (UGTs): UGT74F1, UGT74F2 and UGT76B1, forming the SA-glycoside (SAG) (Dean and Delaney, 2008; George Thompson *et al.*, 2017; Maksym *et al.*, 2018; Noutoshi *et al.*, 2012). In addition, UGT74F2 was shown to produce SA-glycoside-ester (SGE) (Dean and Delaney, 2008; George Thompson *et al.*, 2017). Another mechanism of SA turnover is via the 3- and 5-hydroxylation via SA-3-hydroxylase (S3H) and SA-5-hydroxylase (S5H) (Zhang *et al.*, 2013; Zhang *et al.*, 2017). The metabolic products of the reactions are 2,3-di-hydroxy benzoic acid (2,3-DHBA) and 2,5-di-hydroxy benzoic acid (2,5-DHBA). These molecules themselves can be turned-over by UGT76D1 to 2,3- and 2,5-DHBA-glycosides (2,3- and 2,5-DHBA), respectively (Huang *et al.*, 2018). Arabidopsis plants harboring a mutation in *S5H* exhibit reduced growth and increased defense responses. The *s3h s5h* double mutant shows further increase in SA levels, reduced growth and enhanced resistance compared to wild type plants (Zhang *et al.*, 2017).

The identification of the *S*-adenosyl-dependent methyl transferase BENZOIC ACID/SA METHYL-TRANSFERASE 1 (BSMT1) and its volatile aromatic-ester product SA methyl ester (MeSA) opened novel aspects of defense priming and SAR (Chen *et al.*, 2003; Park *et al.*, 2007). MeSA has been shown to allow defense priming in systemic leaves and airborne plant-to-plant communication resulting in acquired immunity in receiver plants (Park *et al.*, 2007; Shulaev *et al.*, 1997). Nevertheless, the function of MeSA in Arabidopsis SAR is still under discussion. The Arabidopsis *bsmt1* mutant plants exhibit a wild type-like SAR response, without significant accumulation of MeSA in response to pathogen infection (Attaran *et al.*, 2009). Additionally, *bsmt1* mutants are not compromised in communicating airborne SAR induction (Wenig *et al.*, 2019). MeSA can be metabolized to MeSAGlc by UGT73C1 in Arabidopsis (Chen *et al.*, 2019).



In terms of the SAR mediator NHP, only two products of turnover were described. NHP glucosylation was identified in several independent studies resulting in the formation of NHP-OGlc (Bauer *et al.*, 2021; Cai *et al.*, 2021; Holmes *et al.*, 2021; Mohnike *et al.*, 2021). Bauer and colleagues have proposed a second glycoside form, NHP-Glc-ester (NHP-GE) (Bauer *et al.*, 2021). Nevertheless, the identification of NHP metabolites may so far be incomplete. Other modifications, such as, methylation or amino acid conjugation were not described for NHP yet.

Here we report infection and UV-C-dependent formation of methylated NHP (MeNHP) identified via ultra-high-performance-liquid-chromatography high-resolution mass spectrometry (UHPLC-HRMS) metabolome analysis. We confirmed NHP-methylation via D<sub>9</sub>-labeled NHP and determined carboxylic acid methylation via a comparison to a synthesized authentic MeNHP-standard. Furthermore, we showed that MeNHP is able to rescue the NHP-deficient phenotype of *fmo1-1* mutant plants and reduce oomycete spore growth in *Arabidopsis thaliana* interaction. In addition, we present a dual-infiltration experiment of a mixture of NHP and D<sub>9</sub>-NHP, to identify and to investigate novel metabolites of NHP in a non-targeted manner.

## Material and methods

### *Plant material and growth conditions*

*Arabidopsis thaliana* ecotype Col-0, *fmo1-1*, *ugt76b1-1*, *fmo1 ugt76b1* (CRISPR *ugt76b1-5* in *fmo1-1*) and *FMO1-3D* were used in this study accordingly (Mohnike *et al.*, 2021). Additionally, *FMO1-3D ald1* was used in this study. We obtained *nhpmt1-1* (SALK\_053006) and *nhpmt1-2* (SALKseq\_135601) mutant plants from SALK Nottingham. Plants were grown on steam sterilized soil under short day (8h light/16h dark) or long day (16h light/8h dark) for 4 and 6 weeks. The light intensity was 100-120  $\mu\text{mol}/\text{m}^2/\text{s}$  and the humidity was 80 % relative unless specified. The light source were MASTER LED tubes HF 600mm HO 8W840 T8 (PHILIPS AG, Amsterdam, Netherlands).

### *Pseudomonas infection and UV-treatment*

To induce defense metabolism, plants were treated with *Pseudomonas* bacteria or UV-C light. *Pseudomonas syringae* strain ES4326 (*P.s.m.*) were grown in LB-medium with 25 $\mu\text{g}$  Rifampecin overnight at 28 °C. The culture was pelleted, medium was decanted, and the bacteria were suspended in 10 mM MgCl<sub>2</sub>. Bacteria were diluted to OD<sub>600</sub>=0.05 and infiltrated to the abaxial side of the leaf. As mock treatment control 10 mM MgCl<sub>2</sub> were infiltrated to the leaf. Plants were incubated for 8, 24, or 48 hours, as stated accordingly in the results section and figure legends. UV-C treatment was performed for 20 min in a PrettleTelstar sterile bench

as described (Mohnike *et al.*, 2021). Plants were incubated for 24 hours post treatment if not stated otherwise.

#### *Chemical synthesis of MeNHP*

MeNHP was synthesized from methylpipercolinate hydrochloride after a modified procedure (de Sousa 2016, *Frontiers*). See supplemental material for a detailed description of the synthesis route, materials and techniques used to gain MeNHP. Additionally we deposited NMR-spectra and MS-spectra of the quality control measures.

#### *Dual infiltration of authentic NHP and D<sub>9</sub>-NHP standard*

Both 1 mM NHP and D<sub>9</sub>-NHP, respectively, in 10 mM MgCl<sub>2</sub> were co-infiltrated to 3 leaves of each individual plant of Col-0, *fmo1-1* and *ugt76b1-1*. As mock treatment 10 mM MgCl<sub>2</sub> was infiltrated accordingly. Both mock and NHPs infiltrated plants were either kept further untreated or were exposed to UV-C radiation for 20 minutes, as described above. Plants were incubated for 24 hours post treatment. Samples were harvested and stored in -80 °C until extraction with 80 % MeOH.

#### *MeNHP infiltration for metabolite tracking*

1 mM MeNHP were directly infiltrated to the apical side of the leaf. MeNHP was solved in 10 mM MgCl<sub>2</sub>. The infiltrated plants were incubated for 24 hours. Leaves were harvested and frozen in liquid nitrogen. The samples were stored at -80 °C.

#### *MeNHP induced resistance assay*

To investigate the MeNHP induced resistance, ddH<sub>2</sub>O (mock) or MeNHP at the indicated concentrations diluted in ddH<sub>2</sub>O were infiltrated with a needleless syringe on two full-grown leaves of 3-week-old *fmo1-1* and Col-0 plants. 24 hours post infiltration, plants were challenged with *Hyaloperonospora arabidopsidis* Noco 2 by spraying a conidiospore solution at a concentration of 50,000 spores/mL. The challenged plants were then grown in a plant chamber at 18°C with a relative humidity of 80% under short day cycle (8-h light/16-h dark). Infection was scored at 7 days post inoculation as described previously (Ding *et al.* 2016). In brief, infection was scored by the conidiospore growth on distal leaves with the following rating category: Category 5 = more than 5 conidiospores observed on more than 2 distal leaves, Category 4 = more than 5 conidiospores observed on 2 distal leaves, Category 3 = less than 5 conidiospores observed on 2 distal leaves, Category 2 = more than 5 conidiospores observed on

1 distal leaf, Category 1 = less than 5 conidiospores observed on 1 distal leaf, Category 0 = none conidiospore observed on all distal leaves.

#### *Extraction of plant metabolites*

Metabolite extracts were generated from frozen leaf material. Leaves were ground under liquid nitrogen and weight to 100 mg fresh weight (MTBE, only Fig. 2) or 50 mg (80 % MeOH). The MTBE extraction was performed as described earlier (Mohnike *et al.*, 2021). The 80 % MeOH extraction was slightly modified of an extraction protocol (kindly communicated by Prof. Dr. Armin Djamei). 50 mg ground leaf material were given into 2 mL Eppendorf cups and 800  $\mu$ L of 80% MeOH were added. The samples were vortexed to secure homogenization. Afterwards, ultrasonication was applied to the samples two times for each 15 min. The samples were centrifuged at 18.000  $\times$ g for 15 min. 700  $\mu$ L of debris free supernatant were transferred into new tubes and evaporated under streaming nitrogen. Metabolites were resolved in 20 % MeOH by vortex. The solutions were centrifuged at 18.000  $\times$ g for 10 min prior to LC-analysis to remove remaining debris. 80  $\mu$ L were transferred into the LC-MS vials.

#### *UHPLC-HRMS-based metabolite fingerprinting*

Metabolite fingerprinting was conducted according to Feussner and Feussner 2019, as described in Mohnike *et al.* 2021 (Feussner and Feussner, 2019; Mohnike *et al.*, 2021). In brief, extracted samples were analyzed with the UHPLC1290 (Agilent Technologies, Santa Clara, CA, USA) coupled to a HRMS instrument 6540 UHD Accurate Mass Q-TOF (Agilent Technologies) with Agilent Dual Jet Stream Technology as electrospray ionization (ESI) source (Agilent Technologies). The ACQUITY HSS T3 column (2.1 x 100 mm, 1.8  $\mu$ m particle size, Waters Corporation) was used for chromatographic separation at a flow rate of 500  $\mu$ L/min at 40 °C. The solvent system applied A (water, 0.1 % (v/v) formic acid) and B (acetonitrile, 0.1 % (v/v) formic acid) were used. The gradient applied was: 0 to 3 min 1 % to 20 % B; 3 to 8 min 20 % to 97 % B; 8 to 12 min: 100 % B; 12 to 15 min: 1 % B. For technical details were described recently (Mohnike *et al.* 2021). Data were acquired using Mass Hunter Acquisition B.03.01. Data deconvolution was performed using Profinder 10.0 (Agilent Technologies). Data were processed using MarVis-Suite (Kaeffer *et al.*, 2015; Kaeffer *et al.*, 2012; Kaeffer *et al.*, 2009) (<http://marvis.gobics.de>) or OriginPro2020 (OriginLab Corporation, Northampton, MA, USA).

## Results

### Identification of MeNHP via metabolite fingerprinting

Following the hypothesis that molecules of NHP-turnover are missing in *fmo1-1* plants, we compared Col-0 wild type against *fmo1-1* leaves that were infected with *P.s.m.* The leaf extracts were analyzed via UHPLC-HRMS and the obtained dataset was searched for hypothetical NHP-metabolites based on previously described modifications of SA and JA, for instance, hydroxylation, dehydrogenation, decarboxylation and methylation. As proof of concept, the dataset was analyzed for Pip, NHP and NHP-OGlc accumulation after *P.s.m.* treatment. As expected, NHP and NHP-OGlc were not detected in *fmo1-1* plants (Fig. 2). However, we detected exclusively in Col-0 a relative signal intensity with a mass-to-charge ratio ( $m/z$ ) of 160.097 in the positive ionization mode and a retention time of 2.63 minutes, which corresponds to the mass of methylated-NHP (put. MeNHP). The exact mass of this molecule has been calculated with 159.090 Da ( $C_7H_{13}NO_3$ ), showing a mass shift of 14.015 Da to NHP. This shift is equivalent to a methyl group deriving possibly from methylation of NHP.

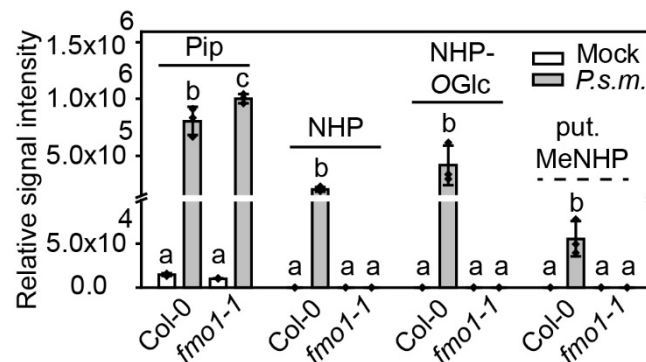


**Fig. 2.** Accumulation of selected *FMO1*-dependent and independent metabolites in Col-0 and *fmo1-1* leaves in response to *P.s.m.* infiltration. *A. thaliana* plants grown for 6 weeks under short-day conditions (8h light/16h dark) were infiltrated with 10 mM  $MgCl_2$  (Mock) or virulent *P. syringae* ES4326 strain at  $OD_{600} = 0.05$  in 10 mM  $MgCl_2$  (*P.s.m.*). Infiltrated leaves were harvested 24 hours post infiltration, extracted by MTBE-procedure and analyzed via UHPLC-HRMS. Data were processed using Profinder 8.0 (Agilent Technologies, Santa Clara, CA, USA) and OriginPro2020 (Origin, San Francisco, CA, USA). Relative signal intensities of Pip, NHP, NHP-OGlc and putative methyl-NHP (put. MeNHP) are shown. Y-axis has a brake between  $1 \times 10^5$  and  $1.5 \times 10^5$ . Bars represent mean values with standard deviation of  $n=3$  replicates. Letters indicate statistical differences, individually calculated for each metabolite ( $p < 0.05$ , one-way ANOVA post-hoc tukey-test). Each replicate represents an independent pool of nine infiltrated leaves from three plants.

*MeNHP is a metabolite of NHP and its identity was unequivocally confirmed by authentic NHP-methyl-ester-standard*

To confirm MeNHP as a metabolite of NHP, therefore, being dependent on functional *FMO1*, we infiltrated labeled D<sub>9</sub>-NHP into Col-0 and *fmo1-1* leaves and measured formation of D<sub>9</sub>-MeNHP. Indeed, we detected D<sub>9</sub>-MeNHP in both Col-0 and *fmo1-1* leaves. The labeled compound had a retention time shift towards a polar elution compared to MeNHP. Non-labeled native MeNHP was again only found in Col-0 leaves (Fig. 3A).

Next, we developed a strategy for the chemical synthesis of a NHP-methyl-ester standard to confirm the identity of MeNHP unequivocally. NHP-methyl-ester was synthesized from methyl piperidin (Supplementary File). Additionally, we tried to identify potential methyl transferase candidates with publicly available co-expression data files of the NHP-metabolizing enzyme UGT76B1 (ATTED II, version 11.0). One gene of interest was AT4G22530 (put. NHP-methyl transferase 1 (NHPMT1) which was annotated as *S*-adenosyl methionine-dependent methyl transferase and its expression is NHP-responsive (Yildiz *et al.*, 2021). The cDNA of the gene was cloned into a pET28a-expression vector, and the encoded protein was heterologously expressed in *E. coli*, purified to homogeneity, used for an *in vitro* activity assay with NHP as substrate. The reaction was followed by UHPLC-HRMS (Fig. S1). Indeed, the authentic MeNHP-standard coeluted with *in planta* and enzymatically generated MeNHP at a retention time of 2.57 min and is presented in the extracted ion chromatogram of *m/z* 160.097 (Fig. 3B).

In addition, the fragmentation pattern of the MS/MS-spectra of *m/z* 160.097 (MeNHP) exhibit identical fragments as the *in vivo* derived MeNHP and the authentic standard. The main fragments are *m/z* 142.08, *m/z* 127.063, *m/z* 110.060, *m/z* 100.076 and *m/z* 82.065 (mass accuracy of  $\pm 2$  mDa) (Fig. 3C). The fragment *m/z* 142.08 represents C<sub>7</sub>H<sub>12</sub>NO<sub>2</sub><sup>+</sup> after a loss of the *N*-hydroxy function, comparable to NHPs-fragment *m/z* 127.063 (Fig. S2). Moreover, identical fragmentation behavior of MeNHP (C<sub>7</sub>H<sub>13</sub>NO<sub>3</sub>) and NHP (C<sub>6</sub>H<sub>11</sub>NO<sub>3</sub>) is observed by fragment ions *m/z* 110.06, *m/z* 100.07 and *m/z* 82.06. First, *m/z* 110.06 represents C<sub>6</sub>H<sub>8</sub>NO<sup>+</sup> after loss of two hydroxy functions. Second, *m/z* 100.07 represents the fragment C<sub>5</sub>H<sub>10</sub>NO<sup>+</sup> obtained by the loss of the carboxylic acid function with NHP and methyl carboxylic acid function with MeNHP. Last, *m/z* 82.06 resembles the fragment of the N-containing hetero ring structure (C<sub>5</sub>H<sub>8</sub>N<sup>+</sup>, dihydropyridine) after loss of the hydroxyl function and carboxylic acid methyl-ester function. Together, the structure of the infection-dependent NHP-derived compound MeNHP as NHP-methyl-ester was confirmed.

To strengthen the hypothesis that MeNHP is a downstream metabolite of NHP, we investigated the influence of *ald1* loss-of-function mutation on the occurrence of MeNHP *in vivo* (Fig. 2d). We observed that MeNHP accumulated in Col-0 plants 24 hours post UV (hpUV) stress. Col-0 control plants and *ald1* control, as well as, *ald1* UV-treated plants did not show any signal for MeNHP 24 hpUV. Moreover, we tested *FMO1-3D* overexpression lines and *FMO1-3D ald1* double mutant plants on their basal MeNHP amount (Fig. 3D). We observed a constitutive accumulation of MeMHP in the *FMO1-3D* mutant background, whereas no MeNHP was detected in the *FMO1-3D ald1* background.

In conclusion, these data further support that MeNHP is NHP-methyl-ester produced *in planta* downstream of NHP. Mutations in the major biosynthetic genes *ald1* and *fmo1* lead to absence of MeNHP after stress induced biosynthesis. Additionally, we showed that NHPMT1 was able to catalyze the formation of MeNHP from NHP and SAM *in vitro* and therefore, provide additional data that confirm exact mass and retention time information from *in vivo* MeNHP and chemically synthesized authentic standard. Whether MeNHP has an influence on plant-immunity remains to be investigated. It remains to be determined whether additional molecules other than MeNHP, NHP-*O*-Glc and NHP-Glc-ester derive from NHP directly and are present in the Pip/NHP molecular network *in vivo*.

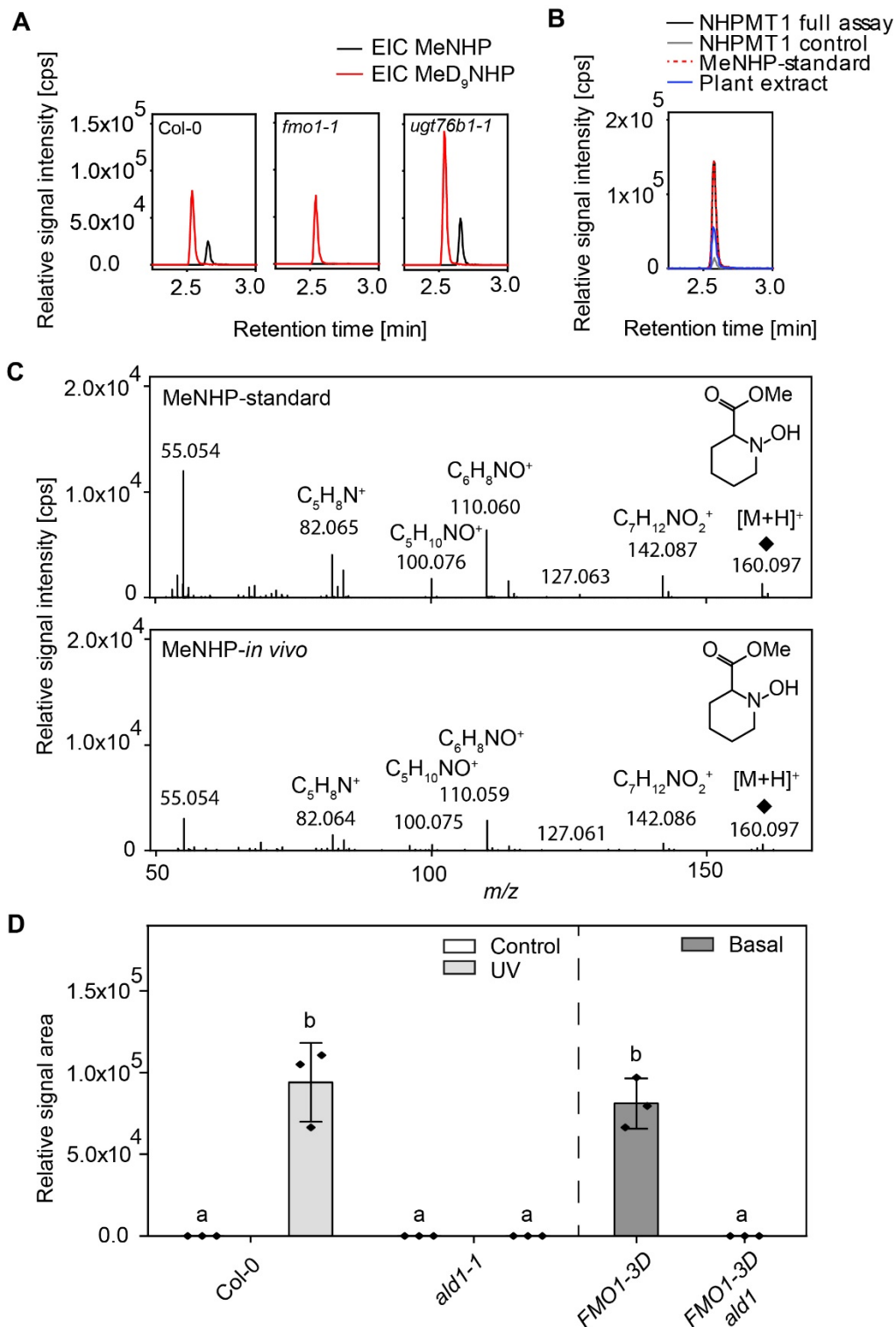


**Fig. 3.** Characterization of *N*-hydroxy pipecolic acid methyl ester (MeNHP). **A** Extracted ion chromatograms of MeNHP [M+H]<sup>+</sup> 160.097 and D<sub>9</sub>-MeNHP [M+H]<sup>+</sup> 169.153 in Col-0, *fmo1-1* and *ugt76b1-1* leaves. Col-0, *fmo1-1* and *ugt76b1-1* leaves were infiltrated with D<sub>9</sub>-NHP. After 24 hours, leaves were harvested, extracted and analyzed by UHPLC-HRMS. **B** Extracted ion chromatograms at [M+H]<sup>+</sup> 160.097 of *in vivo* metabolite extract, synthesized authentic NHP-methyl-ester standard, *in vitro* assay with NHPMT1 and *in vitro* assay with boiled NHPMT1 as control. **C** Comparison of MSMS-fragments of authentic MeNHP-



standard and *in planta* MeNHP. **D** Relative amount of MeNHP in Col-0, *ald1*, *FMO1-3D* and *FMO1-3D ald1* plants. Col-0 and *ald1* plants were kept untreated or treated with UV-C for 20 min. Plants were incubated for 24 hours before harvesting. *FMO1-3D* and *FMO1-3D ald1* plants were left untreated before harvesting. Data represents mean of three biological replicates for the MeNHP signal (relative signal area) via UHPLC-HRMS analysis. Error bars represent standard deviation. Letters indicate statistical differences, individually calculated for each experiment ( $p < 0.05$ , one-way ANOVA post-hoc tukey-test).

#### *Identification of NHP-derived metabolites via NHP and D<sub>9</sub>-NHP leaf infiltration, UV-treatment and non-targeted metabolomics*

To confirm the occurrence of the observed NHP-derivative after stress application and to screen for additional NHP-derivatives, a non-targeted metabolome experiment was performed as another independent line of evidence. We applied NHP and D<sub>9</sub>-NHP co-infiltration, as well as, mock infiltration with 10 mM MgCl<sub>2</sub> in leaves of WT, *fmo1-1* and *ugt76b1-1* plants, respectively, and treated the leaves with UV-C afterwards. The aim of this experimental setting was to identify all NHP-derived metabolites, by selecting pairwise features with a mass shift of 9.056 Da (exchange of all 9 hydrogens of the pyridine-moiety by deuterium in NHP) and a small retention time shift of  $< 0.13$  min that are enriched after NHP/D<sub>9</sub>-NHP infiltration, and ideally be synthesized *in vivo*, without external application. In addition, *ugt76b1-1* mutant plants were included as we hypothesized that other NHP-derived metabolites will accumulate as alternative routes for NHP-turnover, when NHP-OGlc cannot be synthesized.

The non-targeted metabolite fingerprinting identified 1152 metabolite features with a false discovery rate (FDR)  $< 10^{-5}$ . The representation of these features by pattern-based clustering via an one-dimensional-self organizing map (1D-SOM) shows two clusters (Fig. 4, cluster number 1 and 2), where metabolites accumulated as consequence of NHP/D<sub>9</sub>-NHP co-infiltration. Cluster 1 shows metabolites accumulating after NHPs infiltration in an *UGT76B1*, as well as, UV-C dependent manner. Here three feature pairs were detected with a mass shift of 9.056 Da. First, the pair NHP-OGlc/D<sub>9</sub>-NHP-OGlc was detected in cluster 1, as NHP-OGlc is known to be exclusively synthesized by UGT76B1 *in vivo*. This chemotype cannot be restored by external application of NHPs to the *ugt76b1-1* mutant plants. Furthermore, NHP-OGlc accumulated also in those Col-0 samples after UV-stress, where NHP/D<sub>9</sub>-NHP infiltration did not take place. As expected, D<sub>9</sub>-NHP-OGlc was present in Col-0 and *fmo1-1* plants after NHPs infiltration. The second pair of features with a mass shift of 9.056 Da has exact masses of  $[M+H]^+/[D_9M+H]^+$  470.185/479.241. The exact mass information and its UGT76B1-dependency let us tentatively assign the features as NHP-OGlc-Hex/D<sub>9</sub>-NHP-OGlc-Hex. Subtracting the exact mass of NHP-OGlc ( $[M+H]^+$  308.134) from the molecule of  $[M+H]^+$

470.185 results in a fragment of 162.051 Da, which corresponds to a hexose moiety. Since the feature pair is exclusively detected in the lines with functional UGT76B1, it strongly suggests that UGT76B1 is responsible for the *O*-glycosylation of NHP required for NHP-OGlc-Hex synthesis. In-source fragmentation analysis underlines the compound identity by the detection of NHP-OGlc as fragment ion of  $[M+H]^+$  308.134 (Fig. S3). In addition, NHP-OGlc-Hex is present in mock infiltrated UV-stressed Col-0 plants, which confirms NHP-OGlc-Hex as a native NHP-derivative. The third pair of features in cluster 1 fits to NHP-OGlc/D<sub>9</sub>-NHP-OGlc with an additional C<sub>3</sub>H<sub>3</sub>O<sub>3</sub>-moiety,  $[M+H]^+/[D_9M+H]^+$  394.132/403.188. It is *UGT76B1*-dependent, too, as the molecular features are not present in the *ugt76b1-1* background. A small amount of NHP-OGlc-C<sub>3</sub>H<sub>3</sub>O<sub>3</sub> in mock infiltrated, UV-stressed Col-0 plants confirmed that this metabolite is a native NHP-derivative. MS/MS-fragment analysis of the unknown molecule yielded a fragment of the NHP-backbone of  $[M+H]^+$  308.134, and suggests for an additional malonic acid residue of *m/z* 87.007 as the fragment ion (Fig. S4). Together the MS data led us to assign the third feature pair as NHP-OGlc-malonic acid.

Cluster 2 represents metabolites that enrich in all three genotypes after NHP/D<sub>9</sub>-NHP infiltration, with and without UV-C treatment. Via mass shift search, we detected Pip/D<sub>9</sub>-Pip and NHP/D<sub>9</sub>-NHP, MeNHP/D<sub>9</sub>-MeNHP and NHP-GE/D<sub>9</sub>-NHP-GE as NHP-derived metabolites. Pip, NHP and MeNHP accumulated in Col-0 and *ugt76b1-1* after UV-stress. In contrast, NHP-GE was detected only in *ugt76b1-1* after UV-stress in case the NHP/D<sub>9</sub>-NHP mixture was not additional infiltration. Interpretation of the MS/MS-fragment pattern confirmed the identity of NHP-GE (Fig. S5).

Together the experiment expands the number of novel NHP metabolites to MeNHP, NHP-OGlc-Hex, NHP-OGlc-malonic acid. Furthermore, the conversion of D<sub>9</sub>-NHP into D<sub>9</sub>-Pip led us to propose a so far unknown additional dehydration reaction.

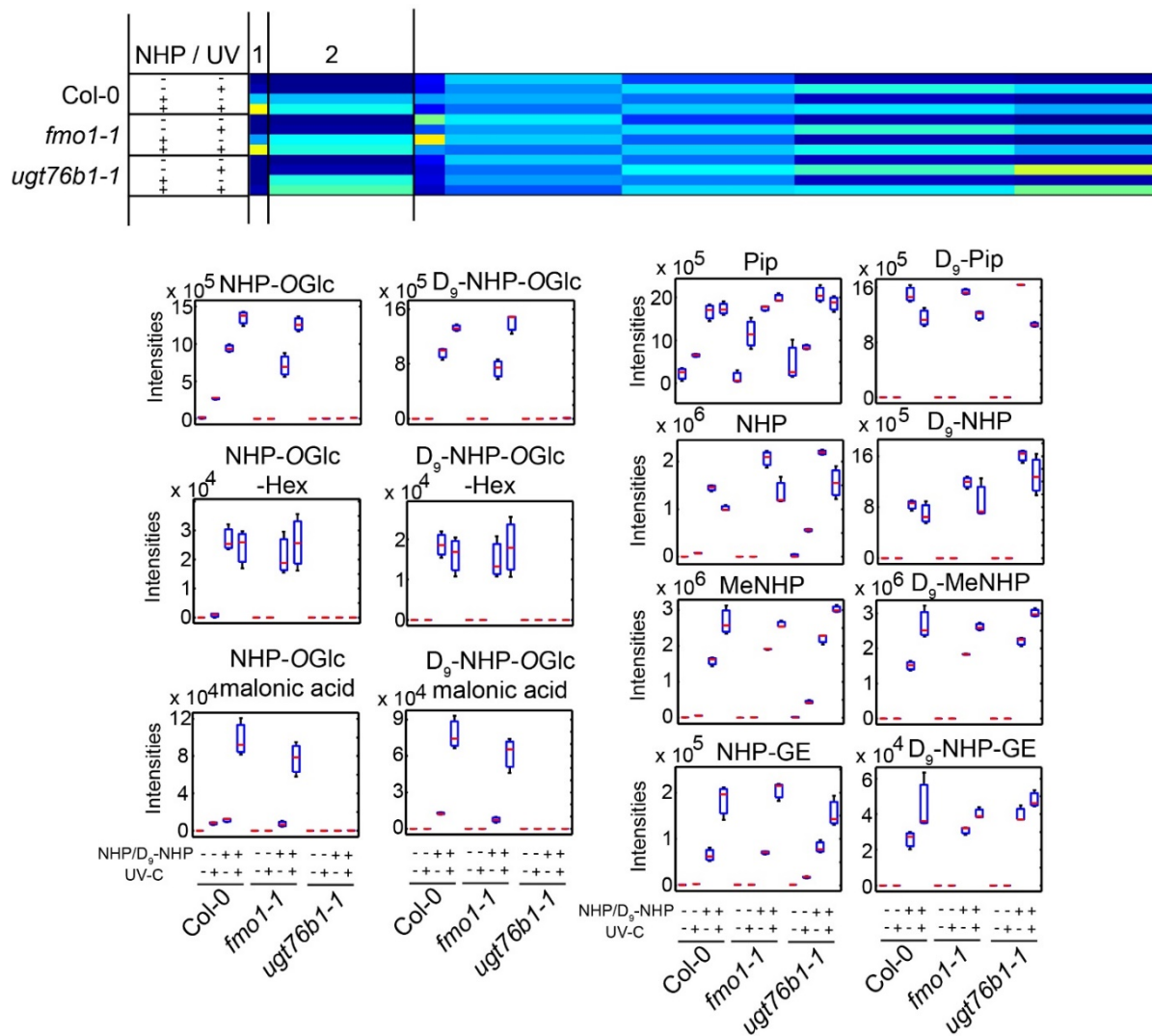


**Fig. 4.** Co-infiltration of NHP/D<sub>9</sub>-NHP into Col-0, *fmo1-1* and *ugt76b1-1* with a subsequent UV-C-trigger underlines additional *in planta* synthesis of NHP-derivates. Into unstressed leaves, either mock solution (10 mM MgCl<sub>2</sub>) or a mixture of 1 mM NHP and 1 mM D<sub>9</sub>-NHP were infiltrated. Plants were kept untreated as control or stressed afterwards for 20 min with UV-C light. The plants were incubated for 24 hours in short day conditions before infiltrated leaves were harvested. The extracted leaf material was analyzed with UHPLC-HRMS. Data was analyzed using Profinder 10.0 (Agilent Technologies, Santa Clara, CA, USA) and MarVis (Kaefer et al. 2015). Each sample represent an independent pool of 6 infiltrated leaves of two plants each. Data are shown in Box-Plots representing mean and standard deviation.

*MeNHP application rescues the susceptibility of fmo1-1 against Hyaloperonospora arabidopsidis Noco 2 infection*

To determine the metabolic fate of externally applied MeNHP and to assign its role in plant immunity, 0.1 mM MeNHP were infiltrated into leaves of Col-0, *fmo1-1* and *fmo1-1 ugt76b1* plants. Inspired by that SA-binding protein 2 (SABP2) and some of its Arabidopsis orthologous hydrolyze MeSA to SA, we wondered whether MeNHP is hydrolyzed to NHP in Arabidopsis as well (Forouhar *et al.*, 2005; Vlot *et al.*, 2008a). In addition, we aimed to figure out, which

other NHP-related metabolites accumulate upon infiltration of MeNHP and whether SA biosynthesis is induced by MeNHP or by MeNHP-derived metabolites. Furthermore, the mutant *fmo1 ugt76b1* was included to identify the origin of MeNHP-OGlc detected in our initial experiment described above (Fig. S6). After MeNHP-infiltration, MeNHP was detected in all three genotypes (Fig. 5), with a higher signal intensity in *fmo1 ugt76b1*. A comparable intensity pattern was observed for NHP, which was significantly enriched after MeNHP treatment in all three backgrounds and accumulated the most in *fmo1 ugt76b1*, which hints towards hydrolysis of the infiltrated MeNHP. Interestingly, the relative amount of Pip increased significantly in Col-0, *fmo1-1*, *fmo1 ugt76b1* plants after MeNHP infiltration in comparison to mock treated plants. NHP-OGlc was not detected in *fmo1 ugt76b1* plants, but significantly accumulates in Col-0 and *fmo1-1*. NHP-GE accumulates in all three backgrounds. Interestingly we identified a signal of m/z 322.149, which may represent MeNHP-OGlc. MeNHP-OGlc accumulated significantly after MeNHP infiltration independent of *UGT76B1*. To underline the identification, we conducted an enzymatic reaction using purified SAG forming enzyme UGT74F1 and were able to reproduce the MeNHP-OGlc signal *in vitro* (Fig. S6). Furthermore, MeNHP treatment resulted in neither a signal increase of SA nor the accumulation of SAG compared to mock treatment. Similar data were obtained after spraying MeNHP to Col-0 and *fmo1-1* plants (Fig. S7). From these results, we conclude that MeNHP can be metabolized in the plant after external application. We were able to detect accumulation of Pip, NHP, NHP-OGlc, NHP-GE and MeNHP-OGlc in Col-0 but more important in *fmo1-1* knock-out plants.

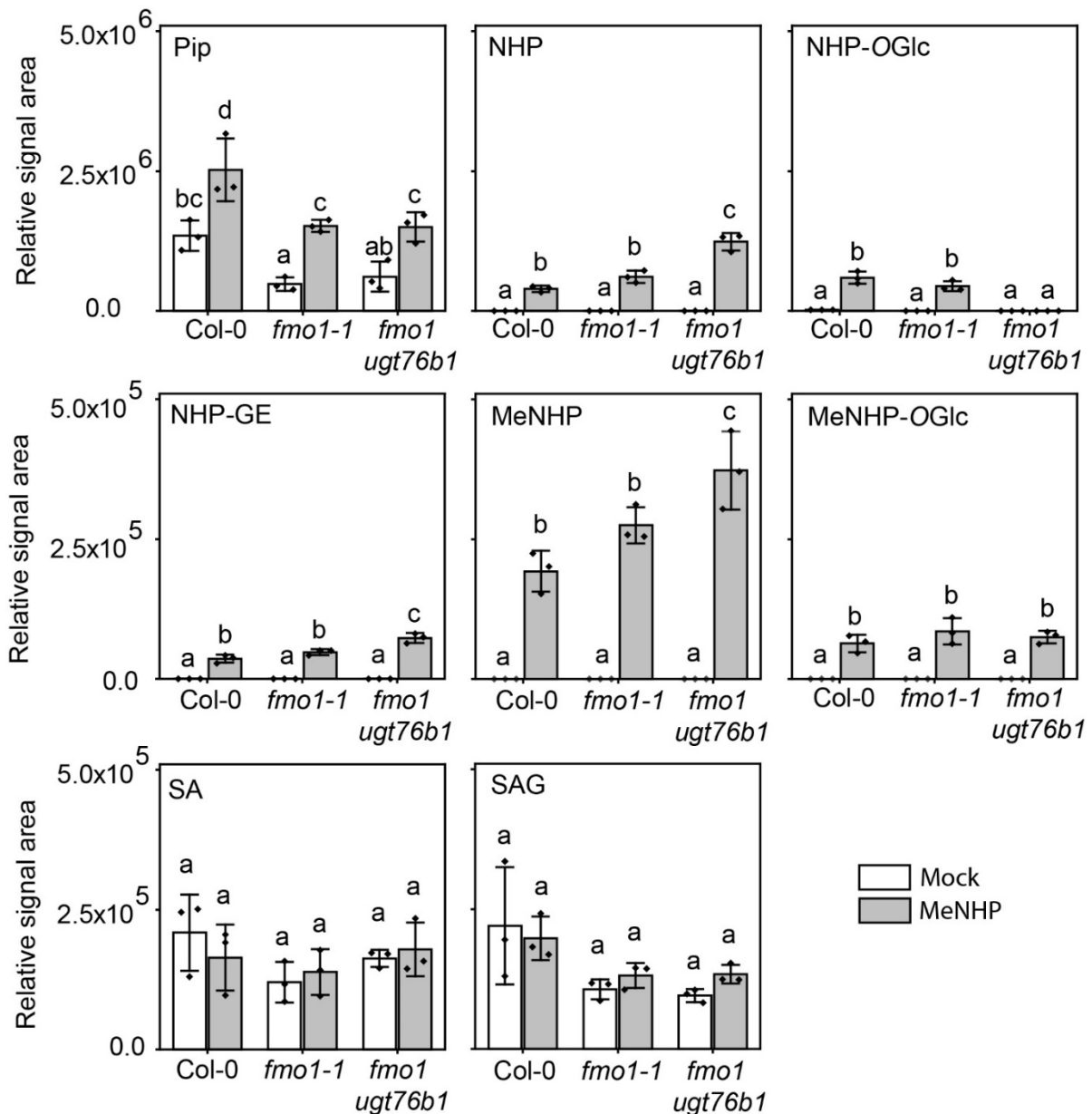


**Fig. 5.** MeNHP-infiltration leads to metabolite remodeling including NHP and Pip accumulation in *fmo1-1* mutant background. Col-0, *fmo1-1* and *fmo1ugt76b1* were grown in short day conditions for 5 weeks. Plants were infiltrated with 10 mM MgCl<sub>2</sub> (Mock) or 1 mM MeNHP in 10 mM MgCl<sub>2</sub> (MeNHP). The plants were incubated overnight and harvested 20 hours post infiltration. Samples were extracted with 80 % MeOH and measured with UHPLC-HRMS. Data were analyzed using Qualitative analysis (Agilent Technologies, Santa Clara, CA, USA) for relative signal area of the respective compound shown. Relative signal areas of MeNHP, SA, SAG, Pip, NHP, NHP-OGlc, NHP-GE and MeNHP-OGlc are shown in mock and MeNHP treated Col-0, *fmo1-1* and *fmo1ugt76b1*. Each replicate represents an independent pool of 6 infiltrated leaves from two plants. Data represent mean with standard deviation. Statistical analysis was done using Origin Pro 2020. Letters indicate statistical differences (p < 0.05, one-way ANOVA post-hoc tukey-test).

To test whether MeNHP is able to prime defense response in Arabidopsis and further to rescue the *fmo1-1* infection phenotype, we challenged MeNHP treated *fmo1-1* and Col-0 plants with a spore solution of *H. arabidopsidis* Noco 2 and analyzed spore growth on mock or MeNHP treated plants (Fig. 6A and B). A concentration gradient of 200  $\mu$ M, 125  $\mu$ M, 20  $\mu$ M and 1  $\mu$ M was applied to individual groups of *fmo1-1* mutant plants and spore growth was analyzed in comparison to mock treatments (Fig. 6A). We assayed two individual mock treatments against either 200  $\mu$ M and 125  $\mu$ M or 20  $\mu$ M and 1  $\mu$ M MeNHP. With treatment of 200  $\mu$ M MeNHP, 69 % of the pathogen growth was assigned to disease category zero (no spore growth), 8 % to category one and 23 % to category two. In the respective mock treatment, growth of the pathogen was grouped into disease category five at 100 %. The comparison shows reduced pathogen sporulation, therefore, lower disease categories with 200  $\mu$ M MeNHP treatment compared to mock. The 125  $\mu$ M MeNHP treatment resulted in a similar trend of reduced pathogen growth. Plants pretreated with 125  $\mu$ M MeNHP exhibited no spore growth at 15 % and disease categories one at 23 %, two at 38 %, three at 8 % and four at 15 %. A comparison between 20  $\mu$ M MeNHP and mock treatment showed a similar trend as above. Spore growth on mock treated plants was assigned to disease categories four 7 % and five 93 % of plants, whereas spore growth on plants treated with 20  $\mu$ M MeNHP was grouped into disease categories two 53 %, three 7 %, four 27% and five 13 %. At the lowest concentration of 1  $\mu$ M MeNHP 10 % of plants group into category three, 20 % in category four and 70 % of the challenged plants group into disease category five. We next applied 200  $\mu$ M and 125  $\mu$ M MeNHP to Col-0 and *fmo1-1* plants, respectively, to compare spore growth of *H.a.* Noco 2 (Fig. 6B). Mock treated Col-0 plants group into disease categories five and four. Treatment with 200  $\mu$ M MeNHP resulted in no spore growth on Col-0. Treatment with 125  $\mu$ M MeNHP resulted in disease categories zero and one. Mock treated *fmo1-1* mutant plants group into disease category five. Treatment with 200  $\mu$ M MeNHP resulted in categories zero, one and two. Application of 125  $\mu$ M MeNHP resulted in spore growth that was grouped into disease categories zero, two and three.

The experiments confirm that the applied MeNHP is metabolized to NHP in Arabidopsis and that MeNHP treatment is able to rescue the susceptible phenotype of NHP biosynthesis mutant *fmo1-1* and to induce resistance in Col-0. Furthermore, MeNHP treatment alone does not lead to an increase in signal intensity of SA and SAG, however, the amounts of Pip, NHP, NHP-OGlc, NHP-GE and MeNHP-OGlc increase significantly.

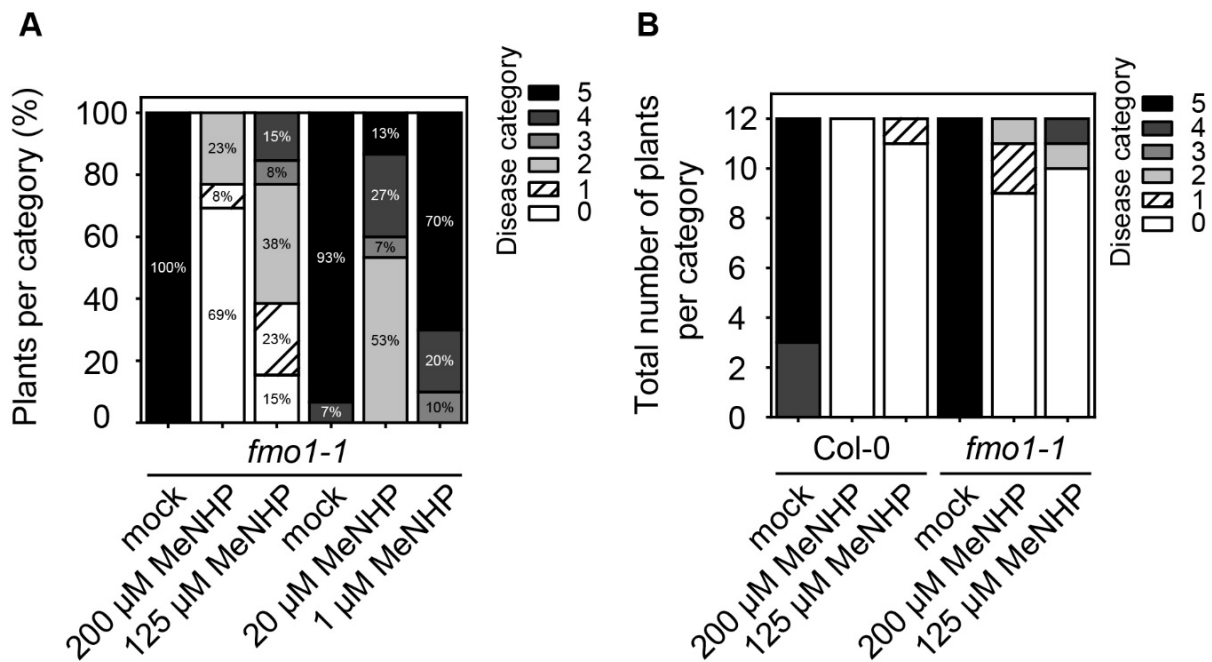


**Fig. 6.** MeNHP infiltration rescues the *fmo1-1* infection phenotype against *Hyaloperonospora arabidopsidis* Noco 2 compared to mock treatment. **A** Four different concentrations of MeNHP (200  $\mu$ M, 125  $\mu$ M, 20  $\mu$ M and 1  $\mu$ M) were applied to *fmo1-1* mutant plants and *H. arabidopsidis* Noco 2 spore growth was assayed compared to individual mock (water) treated plants. **B** Col-0 and *fmo1-1* mutant plants were treated with MeNHP at a concentration of 200  $\mu$ M or 125  $\mu$ M. *H. arabidopsidis* Noco 2 spore growth was assayed compared to individual mock (water) treated plants. Plants were grouped into disease categories from 5 (heavy spore growth) to 0 (no spore growth). Disease categories were assigned as following: Category 5 = more than two leaves harbor > 5 spores, 4 = two leaves harbor > 5 spores, 3 = two leaves < 5 spores, 2 = one leaf > 5 spores, 1 = one leaf < 5 spores, 0 = no spores at all. n= 10-15 plants per treatment.

## Discussion

Intact metabolite networks are key to hormonal balance in plants. In this work, we lay out the NHP-metabolome by non-targeted UHPLC-HRMS-based metabolomics. For the initial approach, a non-targeted dataset of Arabidopsis infection with *Pseudomonas* was recorded. The strategy was to identify NHP-metabolite features based on exact mass information of the sum formula. *In silico* modifications were performed, based on well-known metabolizing reactions, such as hydroxylation, methylation and amino acid conjugation. From the sum formula of the designed compound, its exact mass was identified and molecular identification was targeted. Via both, analysis of *P.s.m.* infiltrated Col-0 and *fmo1-1* mutant plants and dual infiltration of NHP/D<sub>9</sub>-NHP, three molecules of NHP-turnover were identified, namely, MeNHP, NHP-OGlc-Hex and NHP-OGlc-malonic acid (Fig. 2, 3 and 4). We detected all three metabolites in Col-0, however, not in the *fmo1-1* mutant background after *P.s.m.* infiltration or UV-C treatment. Moreover, we were able to show that MeNHP is metabolized to NHP and that

MeNHP treatment is able to rescue the susceptible phenotype of *fmo1-1* mutant plants against *H. arabidopsidis* Noco 2.

#### *Dual-infiltration as unbiased method to detect undescribed metabolites of NHP*

The dual-infiltration method was developed to overcome detection limitation of minor metabolites from native plant extracts and to enable unbiased molecular feature identification, independent of a targeted screen. Due to adding both authentic standard and D<sub>9</sub>-labeled authentic standard, the sensitivity to detect NHP metabolites was increased. Especially, the specificity to pin down a molecule to be of NHP origin was enhanced. By the distinctive mass shift fingerprint and retention time difference, we are able to assign metabolites to NHP-origin. Together with the possibility to identify the metabolites in the UV-stressed Col-0 plants, the analysis gives a broad picture of the NHP-metabolites. Most importantly, we are able to present molecules absent in the *fmo1-1* background underlining functional *FMO1*- and NHP-dependency. The data acquisition and analysis enclose both ionization modes positive ESI and negative ESI. To ensure high quality features, molecules with FDR < 10<sup>-5</sup> are included into the dataset underlying non-targeted analysis of D<sub>9</sub>-labeled and unlabeled molecular pairs. Yu and colleagues published a similar labeling approach to describe the ability of different species to metabolize nematode signaling molecules (Yu *et al.*, 2021). The researchers applied ascarosides and C<sup>13</sup>-labeled ascarosides to several organisms to identify their ability to metabolize the Nematode derived compounds by product and C<sup>13</sup>-labeled product analysis. Similarly, the group chose exact mass and retention time shift as quality measure for unbiased non-targeted analysis (Yu *et al.*, 2021). The successful application including metabolic turnover inspired us to investigate metabolite mass shifts with our NHP and D<sub>9</sub>-labeled NHP standard. NHP metabolites that have already been described are two glycoside forms NHP-OGlc and NHP-GE (Bauer *et al.*, 2021; Chen *et al.*, 2018; Hartmann *et al.*, 2018). Whereas the biosynthesis and infection dependency of NHP-OGlc have been characterized independently, the unambiguous identification of NHP-GE needs to be underlined and its route of biosynthesis remains unknown (Bauer *et al.*, 2021; Cai *et al.*, 2021; Holmes *et al.*, 2021; Mohnike *et al.*, 2021). We tested activity of heterologous expressed and purified UGT73D1 against NHP *in vitro*, however, no NHP-GE synthesizing activity was found (Fig S8.). In our analysis, NHP-GE is favorably detected in the *ugt76b1* background but of very low to no abundance in Col-0 plants after *P.s.m.* or UV treatment. As proof of the dual-infiltration concept, we showed the expected molecular feature pairs of NHP/D<sub>9</sub>-NHP and NHP-OGlc/D<sub>9</sub>-NHP-OGlc (Fig. 5). NHP and NHP-OGlc are missing in the *fmo1-1* mutant background without external application of NHP/D<sub>9</sub>NHP, but are



present when treated with the mixture. Similarly, the MeNHP signal was missing in the *fmo1-1* background and dual-infiltration restored the MeNHP/D<sub>9</sub>-MeNHP signal, respectively. Additionally, we were able to detect *UGT76B1*-dependent NHP-metabolites, namely, NHP-OGlc-Hex and NHP-OGlc-Mal. To collect evidence for their molecular structure, we analyzed mass spectra of the two compounds. Infiltrated plant metabolite extract was subject to spectra analysis. In source fragment ions, underline the identification of NHP-OGlc-Hex as the in-source fragment  $m/z$  308.134 represent NHP-OGlc (Fig. S3). Fragment spectrum analysis suggests malonic acid addition to NHP-OGlc represented by a fragment ion at  $m/z$  87.008 (Fig. S4). Malonic acid moieties at glucose residues are for example present at anthocyanin's (Bloor and Abrahams, 2002). Interestingly both molecules are synthesized *in vivo* after UV-stress without the need of additional infiltration.

#### *Structure elucidation and NHP-dependency of MeNHP synthesis*

The discovery of the molecular feature  $m/z$  160.097, which was underlined by the pairwise feature identification in dual-infiltration suggested NHP methylation. Nevertheless, we could only rely on the predicted exact mass information of the expected molecular formula that resembles MeNHP. NHP-dependency and the site of methylation remained unclear. To underline MeNHP detection and to identify its site of methylation, we chemically synthesized NHP-methyl-ester from pipercolic acid methyl ester. Due to the specificity of methylation at the carboxylic acid function within the MeNHP-standard, we were able to exclude hydroxyl methylation. We underline MeNHP as NHP-methyl-ester via retention time and MSMS-fragment comparison between authentic standard and the *in vivo* signal (Fig. 3c). Both the MeNHP-standard and the *in vivo* signal exhibit a retention time of 2.57 min, as well as similar fragmentation behavior. Their fragment ions  $m/z$  142.08,  $m/z$  127.063,  $m/z$  110.060,  $m/z$  100.076 and  $m/z$  82.065 are identical and derive from the mother mass  $m/z$  160.097. Especially the fragment ions  $m/z$  127.063,  $m/z$  100.076 and  $m/z$  82.065 are identical with NHP-fragments, underlining structural similarities and hint towards a NHP-derived molecule (Chen *et al.*, 2018; Hartmann *et al.*, 2018). To strengthen the hypothesis that MeNHP is a NHP-derived metabolite, we analyzed functional dependency on NHP-biosynthesis. Via analysis of UV-stressed Col-0 against *ald1* or the basal accumulation of MeNHP in *FMO1-3D* against *FMO1-3D ald1* mutant plants, the dependency of MeNHP on functional NHP biosynthesis was stressed further (Fig. 3d). To support exact mass accuracy and retention time data of MeNHP, we present an *in vitro* reaction of NHPMT1, which produced MeNHP by using NHP as substrate and SAM as co-substrate. Both *in vivo* and *in vitro* MeNHP compounds behave as authentic standard in

respect to RT and fragmentation pattern. Despite the *in vitro* activity of NHPMT1 with NHP, SALK\_053006 (*nhpmt1-1*), SALKseq\_135601 (*nhpmt1-2*) and *nhpmt1-1 ugt76b1-1* mutant plants did not show absence of MeNHP signal after UV-treatment. Surprisingly, the signal intensity of NHP and MeNHP was increased in the analyzed mutants (Fig. S9, Fig. S10). The analysis of *nhpmt1* mutant plants raises the question, if redundant MTases exist for MeNHP synthesis, or if NHPMT1 shows promiscuous MTase activity with NHP but has no influence on *in vivo* synthesis.

### *Physiological implications of NHP-metabolites*

By targeted and non-targeted metabolomics approaches, NHP metabolites were investigated and novel candidate molecules are presented. Additionally, we underline the discovery of NHP-GE by Bauer et al. and present three novel metabolites, which are most likely NHP derived and unambiguously *FMO1*-dependent after *P.s.m.* infiltration. Independently we present the NHP-metabolites in a dual infiltration study, tracking the metabolic fate via non-targeted UHPLC-HRMS metabolomics. However, their physiological implications remain elusive. In contrast to the data present by Bauer and colleagues, we detected accumulation of NHP-GE in *ugt76b1* background (Bauer *et al.*, 2021). Furthermore, we describe increased levels of MeNHP in *ugt76b1-1* mutant plants. Taken together we suggest the carboxy methylation and carboxy glycosylation of NHP as alternative route of NHP-turnover, when *O*-glycosylation is not available.

Nevertheless, the volatile nature of the methylated phytohormones MeJA and MeSA draw our attention on MeNHP's potential to enhance resistance. In analogy to MeSA's ability to induce systemic resistance in tobacco, we investigated the ability of MeNHP to rescue the *fmo1-1* susceptible phenotype towards oomycete pathogen (Hartmann *et al.*, 2018; Park *et al.*, 2007). MeSA is proposed to be cleaved by tobacco SABP2 resulting in SA and induced acquired resistance (Forouhar *et al.*, 2005; Park *et al.*, 2007). Several methylesterases (MES) are present in Arabidopsis that show sequence similarity to the tobacco SABP2, of which MES-1, -2, -4, -7 and -9 exhibit *in vitro* activity with MeSA in competition with SA (Vlot *et al.*, 2008b). The molecular structure of SA and NHP opens the question, if there is a shared MES capable to hydrolyze MeSA and MeNHP in Arabidopsis, similar to their shared mechanism for glucosylation by UGT76B1 (Mohnike *et al.*, 2021; Zeier, 2021). In Figure 5, we lay out NHP-related metabolites accumulated upon infiltration of MeNHP. The data suggest a hydrolysis of the externally applied MeNHP to NHP. The external application of MeNHP did not result in significant changes to the SA levels, neither in infiltration studies, nor after spray application

(Fig. 5, Fig. S7). Afterwards, we infiltrated MeNHP into *fmo1-1* mutant plants to investigate the potential to enhance disease resistance, especially aiming to rescue the susceptible phenotype of the *fmo1-1* mutants. We analyzed the spore count of *H.a. Noco 2* on Arabidopsis leaves pretreated with mock or various concentrations of MeNHP (Fig. 6A, B). The data suggests that MeNHP treatment is able to rescue the susceptible phenotype of *fmo1-1* mutant plants, resulting in reduced spore growth. The enhanced resistance after MeNHP treatment at different concentration might be due to the successful conversion of MeNHP to NHP in the *fmo1-1* background. Furthermore, restoring the NHP pool could be a crucial step to enhance disease resistance in the susceptible *fmo1-1* mutant background. In addition, MeNHP treatment increased Col-0 resistance against *H.a. Noco 2*, too. The applied concentrations ranging from 200  $\mu$ M to 1  $\mu$ M used for infiltration are within the range of similar studies that infiltrated NHP to induce defense from 1 mM to 1  $\mu$ M (Chen *et al.*, 2018; Hartmann *et al.*, 2018). Additionally, NHP induces SAR in Arabidopsis in low doses independent from the mode of application (Schnake *et al.*, 2020). Two independent studies underlined the potential of NHP to induce resistance beyond the scope of Arabidopsis (Holmes *et al.*, 2019; Schnake *et al.*, 2020). The successful induction of resistance after application of methylated compounds like MeSA and MeJA puts MeNHP in scope for future research in plant-to-plant communication. We suggest a sender receiver experiment applying stress to WT and *fmo1* mutant plants as sender and analyze the NHP chemotype of unstressed *fmo1* receiver plants. In the ideal case, the experiment would be conducted with a MeNHP synthesis mutant.

Interestingly we were able to identify another metabolite of MeNHP, when tracking its metabolic fate, namely, MeNHP-OHex. This compound is *UGT76B1* independent, suggesting an UGT able to use MeNHP as substrate, conjugating the glucosylation at the *N*-hydroxyl function. *In vitro* reaction using *UGT74F1* resulted in reproduction of the MeNHP-OGlc signal (Fig. 7, Fig. S3). *UGT74F1* might be another candidate protein for *in vivo* biosynthesis of the NHP-metabolite. Nevertheless, MeNHP-OGlc was not shown to be a native product in plant stress response without external application of MeNHP. Hypothetically, *UGT71C3* capable of synthesizing MeSA-OGlc may be another interesting candidate protein, due to the similarity in structure between MeNHP and MeSA (Chen *et al.*, 2019). We describe that Pip might also be a product of NHP-turnover, as not only Pip was accumulating after the dual infiltration of NHP and D<sub>9</sub>-NHP but also D<sub>9</sub>-Pip. It raises the question for a reaction to remove the *N*-hydroxylation from NHP via, for example, hydrolases or as FMO1-reverse reaction. The observation of NHP cleavage may also explain why Pip amounts are still increasing in time-course experiments,

when the NHP, NHP-OGlc are already decreasing in signal intensity (Hartmann and Zeier, 2019).

An additional mechanism to control hormonal activity is amino acid conjugation. On the one hand, conjugation can lead to activation as it is known in the case of JA and isoleucine by the enzyme JASMONATE RESPONSE LOCUS 1 (JAR1). The JA-modification by JAR1 results in the biological active form JA-Ile (Staswick and Tiryaki, 2004; Suza and Staswick, 2008). On the other hand, inactivation can be achieved. One example is the conjugation of aspartic acid (Asp) to SA in *A. thaliana* by GH3.5. The product SA-Asp is supposed to be biological inactive and a storage metabolite of SA (Chen 2013). Following the pairwise analysis of labeled and unlabeled metabolites, we can exclude the occurrence of NHP-amino acid conjugates in our experimental setting.

## **Conclusion**

Four novel metabolites were identified via UHPLC-HRMS: MeNHP, MeNHP-OGlc, NHP-OGlc-Hex and NHP-OGlc-Mal (Fig. 7). The potential of MeNHP to induce defense priming was investigated. Further research, however, is required to clarify the role of MeNHP in defense response, for example, in plant-to-plant communication. What is more is that metabolites of NHP accumulate in *ugt76b1* mutants, where an important mode of NHP turnover into NHP-OGlc is unavailable, suggesting the ability to shuttle NHP into other metabolic pathways to certain extent.

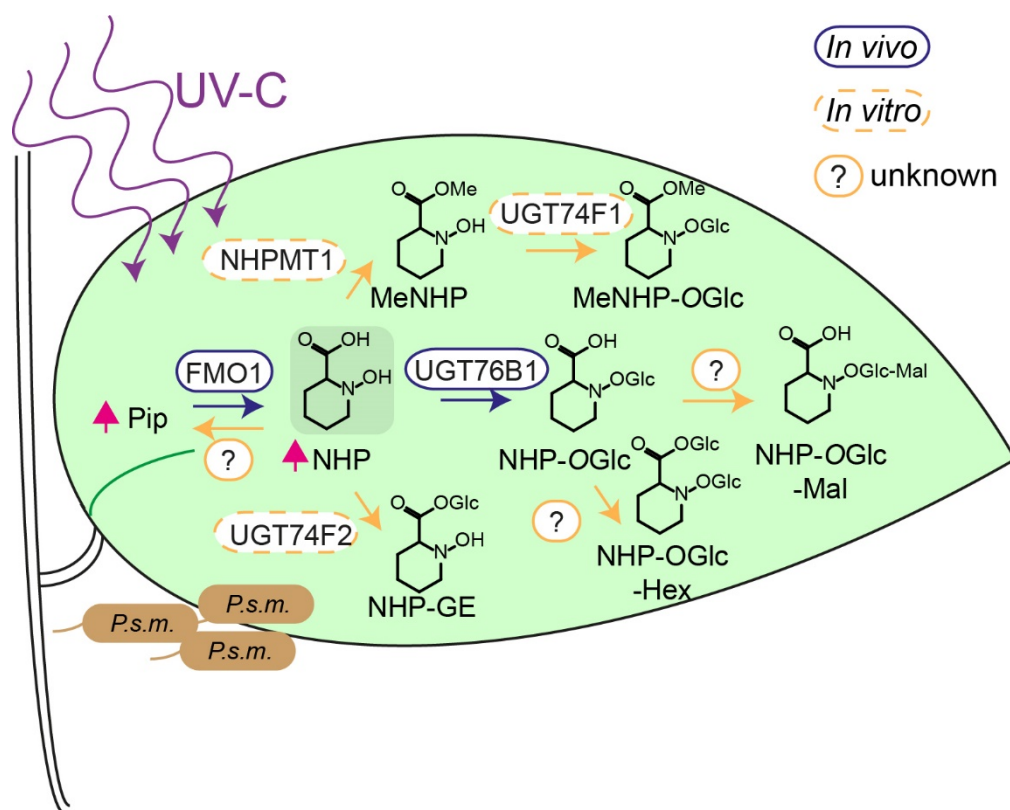


**Fig. 7.** NHP turnover in Arabidopsis induced by UV-C and *P.s.m.* infiltration. The scheme concludes the detected metabolic routes of NHP-turnover. In response to UV-C stress and *P.s.m.* infection, Arabidopsis synthesizes Pip and NHP. To reduce cellular NHP levels, it is hydrolyzed, glycosylated and methylated. Respective products were shown to be further metabolized to complex conjugates, NHP-OGlc-Hex and putatively to NHP-OGlc-malonic acid.

## Supplementary data

Fig. S1. SDS-PAGE from ion metal affinity chromatography purification of heterologously expressed AT4G22530 (NHPMT1).

Fig. S2. Collision induced dissociation fragments of MeNHP and NHP.

Fig. S3. Insource fragments of NHP-OGlc-Hex and D<sub>9</sub>-NHP-OGlc-Hex feature pair.

Fig. S4. Collision induced dissociation fragments of NHP-OGlc-malonic acid and D<sub>9</sub>-NHP-OGlc malonic acid feature pair.

Fig. S5. Collision induced dissociation fragments of NHP-GE.

Fig. S6. Infiltration of MeNHP leads to MeNHP-OGlc formation, which is underlined *in vitro*.

Fig. S7. Metabolite analysis after spray application of MeNHP.

Fig. S8. UGT73D1 is not active with NHP *in vitro*.

Fig. S9. Metabolite analysis of UV-treated Col-0 and *nhpmt1* mutant plants.

Fig. S10. MeNHP analysis of UV-stressed Col-0 vs. *ugt76b1-1 nhpmt1-1*.

Supplemental Protocol S11. Chemical synthesis of MeNHP.

Supplemental Dataset S12. UHPLC-HRMS-data of NHP/D9NHP dual-infiltration.

## **Acknowledgements**

We like to thank Prof. Dr. Christiane Gatz for fruitful discussion and Prof. Dr. Armin Djamei for proving the 80 % MeOH extraction protocol. We thank Dr. Ellen Hornung for cloning of NHPMT1 and crossing of *ugt76b1-1* with *nhpmt1-1* mutant plants to generate the double mutant. We acknowledge Moritz Klein and Sönke Beewen for laboratory support.

## **Author contributions**

L.M., W.H., B.W., K.F., Y.Z. and I.F. conceived and designed the experiments. L.M., W.H., B.W. and K.F. performed the experiments. L.M., W.H., B.W., K.F., Y.Z. and I.F. analysed and discussed the data, L.M., W.H., K.F., Y.Z. and I.F. wrote the article.

## **Conflict of interest**

The authors declare that the research was conducted in the absence of any commercial or financial relationships that could be construed as a potential conflict of interest.

## **Funding**

L.M. was supported by the Goettingen Graduate School for Neurosciences, Biophysics, and Molecular Biosciences in frame of the PRoTECT program at the University of Goettingen. I.F. acknowledges funding from the Deutsche Forschungsgemeinschaft (DFG; GRK 2172-PRoTECT, ZUK 45/2010 and INST 186/822-1). Y.Z. acknowledges funding from the Natural Sciences and Engineering Research Council (NSERC) Discovery Program. W.H. was supported by the China Scholarship Council and NSERC CREATE (PRoTECT).

## **Data availability**

All data generated or analyzed during this study are included in this published article and its supplementary information files.

## References

- Attaran E, Zeier TE, Griebel T, Zeier J.** 2009. Methyl salicylate production and jasmonate signaling are not essential for systemic acquired resistance in *Arabidopsis*. *The Plant Cell* **21**, 954-971.
- Bauer S, Mekonnen DW, Hartmann M, Yildiz I, Janowski R, Lange B, Geist B, Zeier J, Schäffner AR.** 2021. UGT76B1, a promiscuous hub of small molecule-based immune signaling, glucosylates N-hydroxypipicolinic acid and balances plant immunity. *The Plant Cell* **33**, 714–734.
- Bloor SJ, Abrahams S.** 2002. The structure of the major anthocyanin in *Arabidopsis thaliana*. *Phytochemistry* **59**, 343-346.
- Cai J, Jozwiak A, Holoidovsky L, Meijler MM, Meir S, Rogachev I, Aharoni A.** 2021. Glycosylation of N-hydroxy-pipicolinic acid equilibrates between systemic acquired resistance response and plant growth. *Molecular Plant* **14**, 440-455.
- Chen F, D'Auria JC, Tholl D, Ross JR, Gershenzon J, Noel JP, Pichersky E.** 2003. An *Arabidopsis thaliana* gene for methylsalicylate biosynthesis, identified by a biochemical genomics approach, has a role in defense. *The Plant Journal* **36**, 577-588.
- Chen L, Wang W-s, Wang T, Meng X-f, Chen T-t, Huang X-x, Li Y-J, Hou B-k.** 2019. Methyl salicylate glucosylation regulates plant defense signalling and systemic acquired resistance. *Plant Physiology* **180**, 2167–2181.
- Chen Y-C, Holmes EC, Rajniak J, Kim J-G, Tang S, Fischer CR, Mudgett MB, Sattely ES.** 2018. N-hydroxy-pipicolinic acid is a mobile metabolite that induces systemic disease resistance in *Arabidopsis*. *Proceedings of the National Academy of Sciences* **115**, E4920-E4929.
- Dean JV, Delaney SP.** 2008. Metabolism of salicylic acid in wild-type, *ugt74f1* and *ugt74f2* glucosyltransferase mutants of *Arabidopsis thaliana*. *Physiologia Plantarum* **132**, 417-425.
- Ding P, Rekhter D, Ding Y, Feussner K, Busta L, Haroth S, Xu S, Li X, Jetter R, Feussner I, Zhang Y.** 2016. Characterization of a pipicolinic acid biosynthesis pathway required for systemic acquired resistance. *The Plant Cell* **28**, 2603-2615.
- Feussner K, Feussner I.** 2019. Comprehensive LC-MS-based metabolite fingerprinting approach for plant and fungal-derived samples. In: D'Alessandro A, ed. *High-Throughput Metabolomics: Methods and Protocols*. New York, NY: Springer New York, 167-185.

- Forouhar F, Yang Y, Kumar D, Chen Y, Fridman E, Park SW, Chiang Y, Acton TB, Montelione GT, Pichersky E, Klessig DF, Tong L.** 2005. Structural and biochemical studies identify tobacco SABP2 as a methyl salicylate esterase and implicate it in plant innate immunity. *Proceedings of the National Academy of Sciences USA* **102**, 1773-1778.
- Fu ZQ, Dong X.** 2013. Systemic acquired resistance: Turning local infection into global defense. *Annual Review of Plant Biology* **64**, 839-863.
- George Thompson AM, Iancu CV, Neet KE, Dean JV, Choe JY.** 2017. Differences in salicylic acid glucose conjugations by UGT74F1 and UGT74F2 from *Arabidopsis thaliana*. *Scientific Reports* **7**, 46629.
- Greenberg JT, Guo A, Klessig DF, Ausubel FM.** 1994. Programmed cell death in plants: A pathogen-triggered response activated coordinately with multiple defense functions. *Cell* **77**, 551-563.
- Hartmann M, Zeier J.** 2018. L-lysine metabolism to *N*-hydroxypipecolic acid: an integral immune-activating pathway in plants. *The Plant Journal* **96**, 5-21.
- Hartmann M, Zeier J.** 2019. *N*-Hydroxypipecolic acid and salicylic acid: a metabolic duo for systemic acquired resistance. *Current Opinion in Plant Biology* **50**, 44-57.
- Hartmann M, Zeier T, Bernsdorff F, Reichel-Deland V, Kim D, Hohmann M, Scholten N, Schuck S, Bräutigam A, Hölzel T, Ganter C, Zeier J.** 2018. Flavin monooxygenase-generated *N*-hydroxypipecolic acid is a critical element of plant systemic immunity. *Cell* **173**, 456-469.
- Holmes EC, Chen Y-C, Sattely ES, Mudgett MB.** 2019. An engineered pathway for *N*-hydroxy-pipecolic acid synthesis enhances systemic acquired resistance in tomato. *Science Signaling* **12**, eaay3066.
- Holmes EC, Chen Y-C, Mudgett MB, Sattely ES.** 2021. Arabidopsis UGT76B1 glycosylates *N*-hydroxy-pipecolic acid and inactivates systemic acquired resistance in tomato. *The Plant Cell* **33**, 750–765.
- Huang X, Zhu G-q, Liu Q, Chen L, Li Y-J, Hou B-K.** 2018. Modulation of plant salicylic acid-associated immune responses via glycosylation of dihydroxybenzoic acids. *Plant Physiology* **176**, 3103-3119.
- Kaever A, Lingner T, Feussner K, Göbel C, Feussner I, Meinicke P.** 2009. MarVis: a tool for clustering and visualization of metabolic biomarkers. *BMC Bioinformatics* **10**, 92.



- Kaever A, Landesfeind M, Possienke M, Feussner K, Feussner I, Meinicke P.** 2012. MarVis-Filter: Ranking, filtering, adduct and isotope correction of mass spectrometry data. *Journal of Biomedicine and Biotechnology* **2012**, 263910.
- Kaever A, Landesfeind M, Feussner K, Mosblech A, Heilmann I, Morgenstern B, Feussner I, Meinicke P.** 2015. MarVis-Pathway: integrative and exploratory pathway analysis of non-targeted metabolomics data. *Metabolomics* **11**, 764-777.
- Karasov TL, Chae E, Herman JJ, Bergelson J.** 2017. Mechanisms to mitigate the trade-off between growth and defense. *The Plant Cell* **29**, 666-680.
- Maksym RP, Ghirardo A, Zhang W, von Saint Paul V, Lange B, Geist B, Hajirezaei M-R, Schnitzler J-P, Schäffner AR.** 2018. The defense-related isoleucic acid differentially accumulates in *Arabidopsis* among branched-chain amino acid-related 2-hydroxy carboxylic acids. *Frontiers in Plant Science* **9**, 766.
- Mohnike L, Rekhter D, Huang W, Feussner K, Tian H, Herrfurth C, Zhang Y, Feussner I.** 2021. The glycosyltransferase UGT76B1 modulates *N*-hydroxy-pipecolic acid homeostasis and plant immunity. *The Plant Cell* **33**, 735–749.
- Navarova H, Bernsdorff F, Döring A-C, Zeier J.** 2012. Pipecolic acid, an endogenous mediator of defense amplification and priming, is a critical regulator of inducible plant immunity. *The Plant Cell* **24**, 5123-5141.
- Noutoshi Y, Okazaki M, Kida T, Nishina Y, Morishita Y, Ogawa T, Suzuki H, Shibata D, Jikumaru Y, Hanada A, Kamiya Y, Shirasu K.** 2012. Novel plant immune-priming compounds identified via high-throughput chemical screening target salicylic acid glucosyltransferases in *Arabidopsis*. *The Plant Cell* **24**, 3795-3804.
- Park S-W, Kaimoyo E, Kumar D, Mosher S, Klessig DF.** 2007. Methyl Salicylate Is a Critical Mobile Signal for Plant Systemic Acquired Resistance. *Science* **318**, 113-116.
- Rekhter D, Lüdke D, Ding Y, Feussner K, Zienkiewicz K, Lipka V, Wiermer M, Zhang Y, Feussner I.** 2019. Isochorismate-derived biosynthesis of the plant stress hormone salicylic acid. *Science* **365**, 498-502.
- Schnake A, Hartmann M, Schreiber S, Malik J, Brahmman L, Yildiz I, von Dahlen J, Rose LE, Schaffrath U, Zeier J.** 2020. Inducible biosynthesis and immune function of the systemic acquired resistance inducer *N*-hydroxypipecolic acid in monocotyledonous and dicotyledonous plants. *Journal of Experimental Botany* **71**, 6444–6459.

**Shulaev V, Silverman P, Raskin I.** 1997. Airborne signalling by methyl salicylate in plant pathogen resistance. *Nature* **385**, 718-721.

**Staswick PE, Tiryaki I.** 2004. The oxylipin signal jasmonic acid is activated by an enzyme that conjugates it to isoleucine in Arabidopsis. *The Plant Cell* **16**, 2117-2127.

**Suza W, Staswick P.** 2008. The role of JAR1 in Jasmonoyl-l -isoleucine production during Arabidopsis wound response. *Planta* **227**, 1221-1232.

**Torrens-Spence MP, Bobokalonova A, Carballo V, Glinkerman CM, Pluskal T, Shen A, Weng J-K.** 2019. PBS3 and EPS1 complete salicylic acid biosynthesis from isochorismate in Arabidopsis. *Molecular Plant* **12**, 1577-1586.

**Vlot AC, Klessig DF, Park S-W.** 2008a. Systemic acquired resistance: the elusive signal(s). *Current Opinion in Plant Biology* **11**, 436-442.

**Vlot AC, Liu P-P, Cameron RK, Park S-W, Yang Y, Kumar D, Zhou F, Padukkavidana T, Gustafsson C, Pichersky E, Klessig DF.** 2008b. Identification of likely orthologs of tobacco salicylic acid-binding protein 2 and their role in systemic acquired resistance in Arabidopsis thaliana. *The Plant Journal* **56**, 445-456.

**von Saint Paul V, Zhang W, Kanawati B, Geist B, Faus-Kessler T, Schmitt-Kopplin P, Schäffner AR.** 2011. The Arabidopsis glucosyltransferase UGT76B1 conjugates isoleucic acid and modulates plant defense and senescence. *The Plant Cell* **23**, 4124-4145.

**Wenig M, Ghirardo A, Sales JH, Pabst ES, Breitenbach HH, Antritter F, Weber B, Lange B, Lenk M, Cameron RK, Schnitzler J-P, Vlot AC.** 2019. Systemic acquired resistance networks amplify airborne defense cues. *Nature Communications* **10**, 3813.

**Wildermuth MC, Dewdney J, Wu G, Ausubel FM.** 2001. Isochorismate synthase is required to synthesize salicylic acid for plant defence. *Nature* **414**, 562-565.

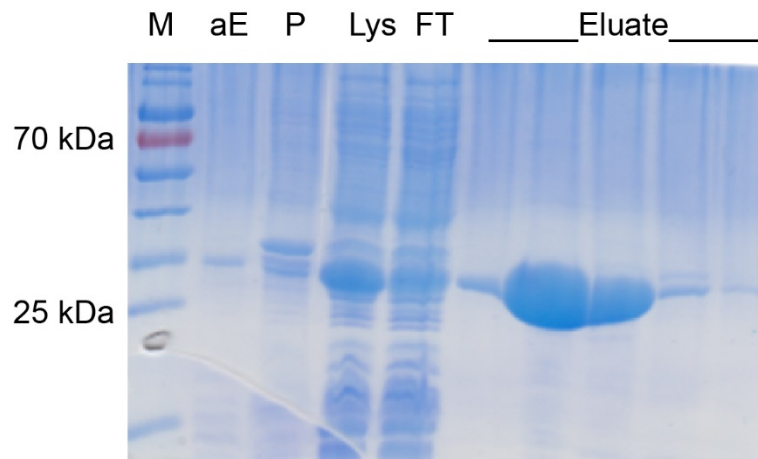
**Yildiz I, Mantz M, Hartmann M, Zeier T, Kessel J, Thurow C, Gatz C, Petzsch P, Köhrer K, Zeier J.** 2021. Mobile SAR signal N-hydroxyphenylacetic acid induces NPR1-dependent transcriptional reprogramming and immune priming. *Plant Physiology* **186**, 1679-1705.

**Yu Y, Zhang YK, Manohar M, Artyukhin AB, Kumari A, Tenjo-Castano FJ, Nguyen H, Routray P, Choe A, Klessig DF, Schroeder FC.** 2021. Nematode Signaling Molecules Are Extensively Metabolized by Animals, Plants, and Microorganisms. *ACS Chemical Biology* **16**, 1050-1058.

**Zeier J.** 2021. Metabolic regulation of systemic acquired resistance. *Current Opinion in Plant Biology* **62**, 102050.

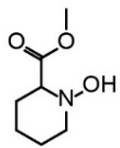
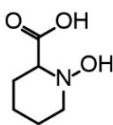
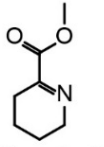
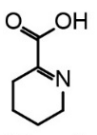
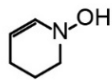
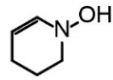
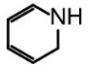
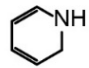
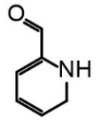
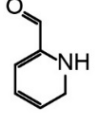
**Zhang K, Halitschke R, Yin C, Liu C-J, Gan S-S.** 2013. Salicylic acid 3-hydroxylase regulates Arabidopsis leaf longevity by mediating salicylic acid catabolism. *Proceedings of the National Academy of Sciences* **110**, 14807-14812.

**Zhang Y, Zhao L, Zhao J, Li Y, Wang J, Guo R, Gan S, Liu C-J, Zhang K.** 2017. *S5H/DMR6* encodes a salicylic acid 5-hydroxylase that fine-tunes salicylic acid homeostasis. *Plant Physiology* **175**, 1082-1093.



**Fig. S1.** SDS-PAGE from ion metal affinity chromatography purification of heterologous expressed AT4G22530 (NHPMT1).

From the left fractions represent marker (M), after expression (aE), pellet (P), lysate (Lys), flow through (FT) and combined eluate fractions according to the chromatographic signal of the purification at 280 nm absorption.

MeNHP	NHP
 <p>Chemical Formula: C<sub>7</sub>H<sub>13</sub>NO<sub>3</sub> Exact Mass: 159.090</p>	 <p>Chemical Formula: C<sub>6</sub>H<sub>11</sub>NO<sub>3</sub> Exact Mass: 145.074</p>
 <p>Chemical Formula: C<sub>7</sub>H<sub>11</sub>NO<sub>2</sub> Exact Mass: 141.079</p>	 <p>Chemical Formula: C<sub>6</sub>H<sub>9</sub>NO<sub>2</sub> Exact Mass: 127.063</p>
 <p>Chemical Formula: C<sub>5</sub>H<sub>9</sub>NO Exact Mass: 99.068</p>	 <p>Chemical Formula: C<sub>5</sub>H<sub>9</sub>NO Exact Mass: 99.068</p>
 <p>Chemical Formula: C<sub>5</sub>H<sub>7</sub>N Exact Mass: 81.058</p>	 <p>Chemical Formula: C<sub>5</sub>H<sub>7</sub>N Exact Mass: 81.058</p>
 <p>Chemical Formula: C<sub>6</sub>H<sub>7</sub>NO Exact Mass: 109.053</p>	 <p>Chemical Formula: C<sub>6</sub>H<sub>7</sub>NO Exact Mass: 109.053</p>

**Fig. S2.** Collision induced dissociation fragments of MeNHP and NHP.

Mass spectrometric signals according to MeNHP and NHP from *in vivo* metabolite extracts were subject to collision induced dissociation at 10 eV. Fragments were analyzed with high-resolution mass spectrometry. A unique fragment of MeNHP was C<sub>7</sub>H<sub>11</sub>NO<sub>2</sub> with a deduced neutral mass of 141.079 Da. This fragment is equivalent to the unique NHP fragment of C<sub>6</sub>H<sub>9</sub>NO<sub>2</sub> with a deduced neutral mass of 127.063 Da. The fragments represent loss of the *N*-hydroxy moiety. Identical fragments of both molecules show the formula C<sub>6</sub>H<sub>7</sub>NO. It arises by loss of two water and has been interpreted as loss of the *N*-hydroxy groups and loss of water derived from the carboxy function of NHP. Next, the fragment of C<sub>5</sub>H<sub>9</sub>NO occurs by loss of the carboxylic acid group. The fragment of C<sub>5</sub>H<sub>7</sub>N derived from loss of carboxylic acid and *N*-hydroxy group).

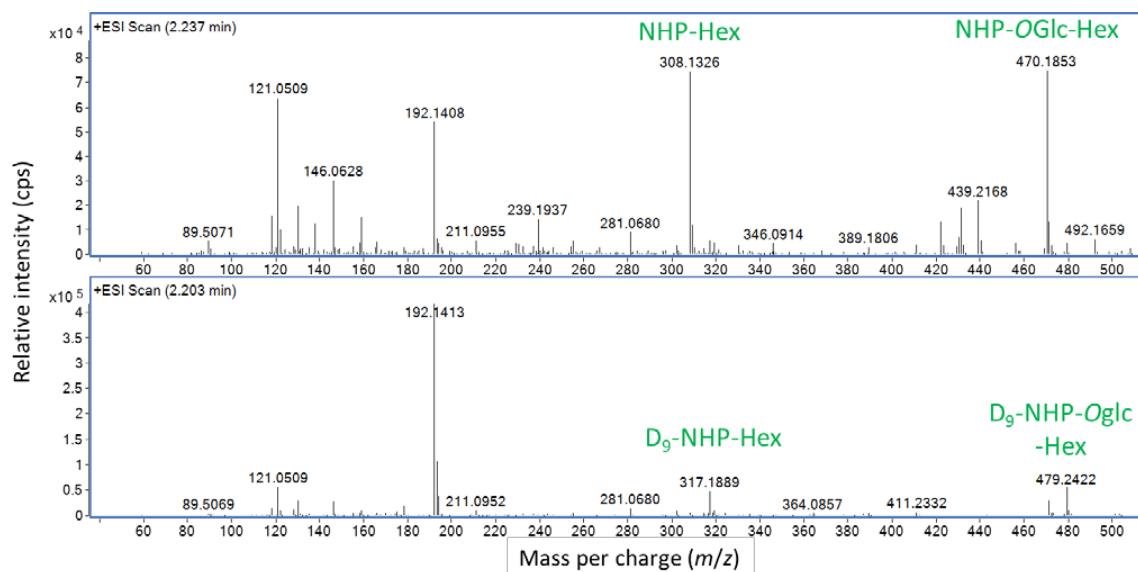


**Fig. S3.** Insource fragments of NHP-OGlc-Hex and D<sub>9</sub>-NHP-OGlc-Hex feature pair.

Mass spectrometric signals according to  $m/z$  470.185/479.242 from *in vivo* metabolite extracts were analyzed on in-source fragmentation. Fragments were analyzed with high-resolution mass spectrometry. NHP-Hex and D<sub>9</sub>-NHP-Hex fragments were identified as in-source fragments underlining the identification.

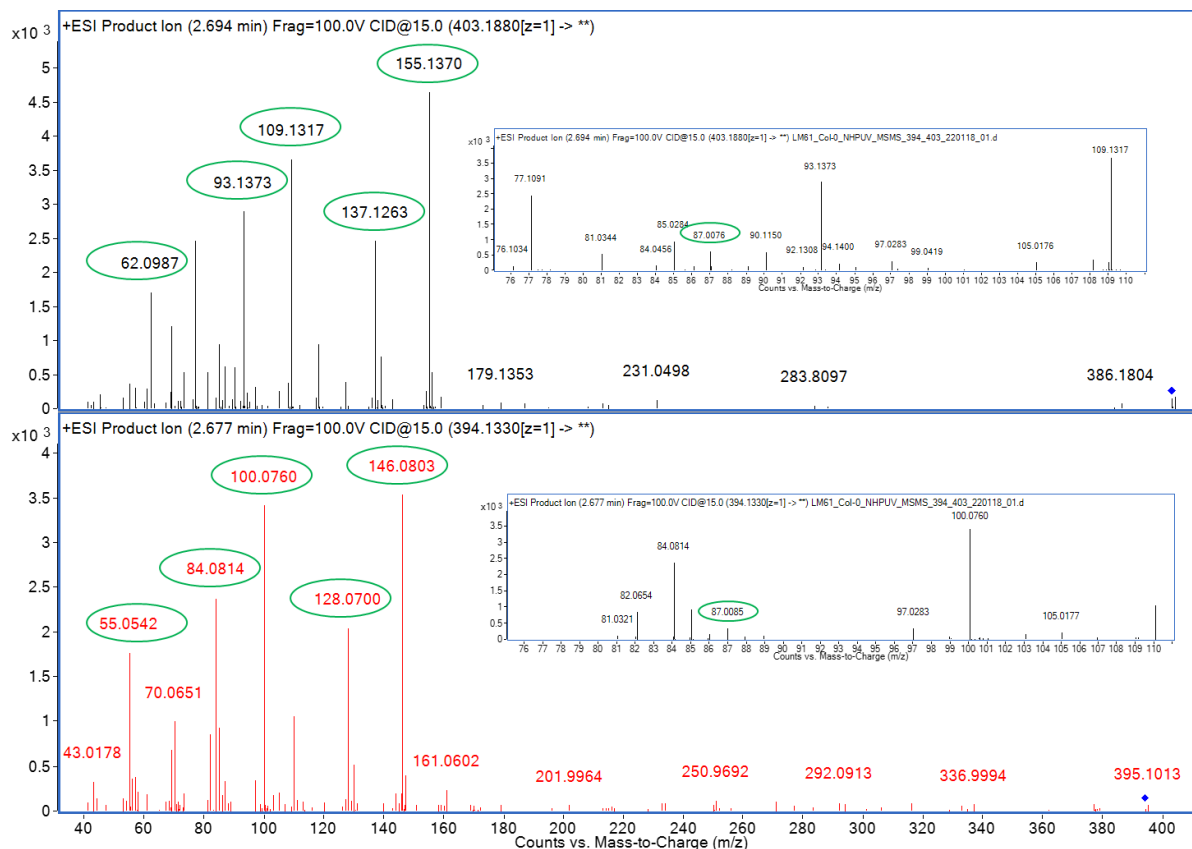


**Fig. S4.** Collision induced dissociation fragments of NHP-OGlc-malonic acid and D<sub>9</sub>-NHP-OGlc malonic acid feature pair.

Mass spectrometric signals according to  $m/z$  394.133/403.2188 from *in vivo* metabolite extracts were subject to collision induced dissociation at 15 eV. Fragments were analyzed with high-resolution mass spectrometry. NHP and D<sub>9</sub>-NHP fragments were identified. Additionally, a fragment of  $m/z$  87.007 was identified in both spectra, which could represent a malonic acid fragment (inserted spectra).

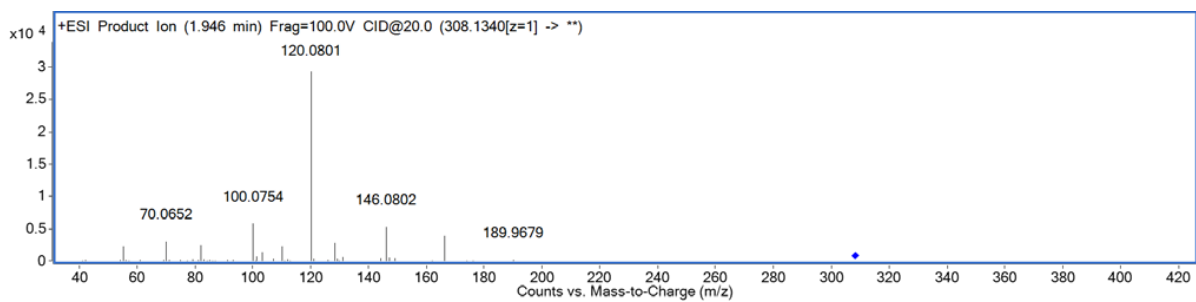


**Fig. S5.** Collision induced dissociation fragments of NHP-GE.

Mass spectrometric signals according to  $m/z$  308.134 from *in vivo* metabolite extract of *ugt76b1* plants that were soil drenched with 10 mM NHP. The NHP-GE signal was subject to collision induced dissociation at 20 eV. Fragments were analyzed with high-resolution mass spectrometry. NHP fragments were identified.



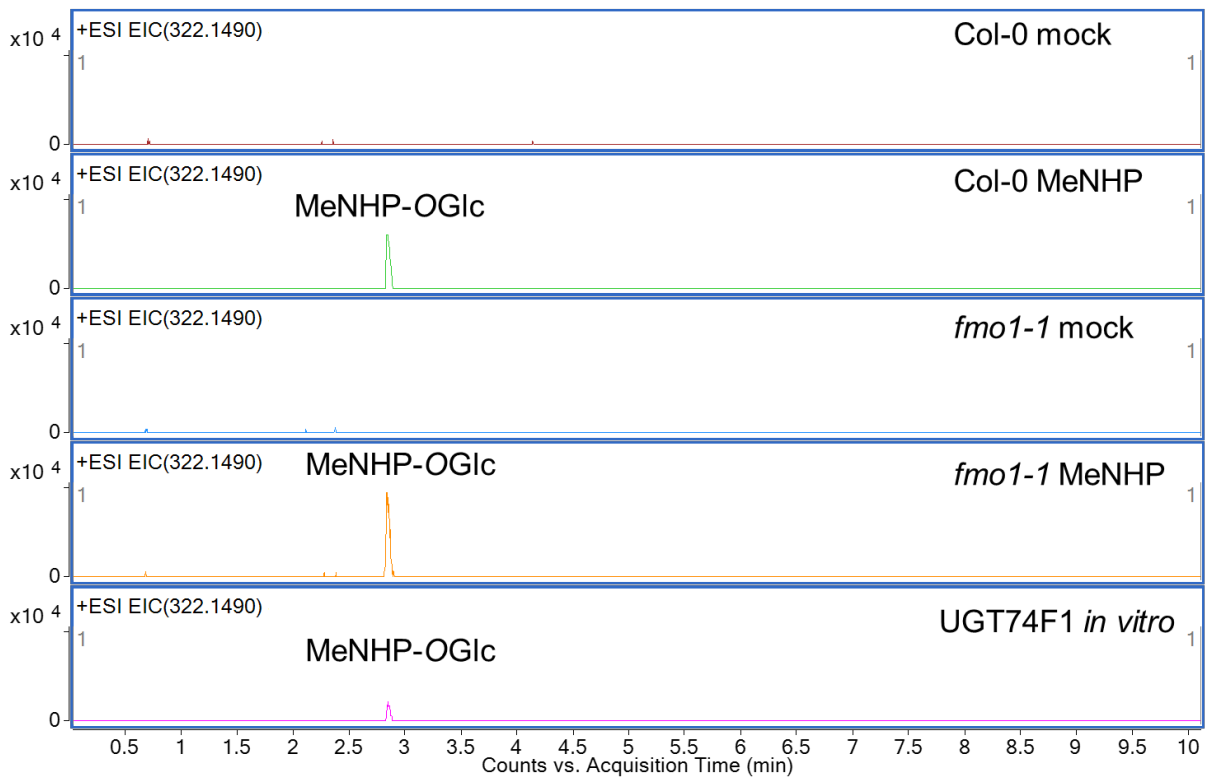


**Fig. S6.** Infiltration of MeNHP leads to MeNHP-OGlc formation, which is underlined *in vitro*.

10 mM MeNHP were infiltrated to WT and *fmo1-1* plants in 10 mM MgCl<sub>2</sub> solution. Plants were incubated for 24 hours at short day conditions. Leaves were harvested and frozen in liquid nitrogen. Metabolite extracts were analyzed by UHPLC-MS. The MeNHP-OGlc signal was reproduced *in vitro* with a reaction of UGT74F1, MeNHP and UDP-Glc.

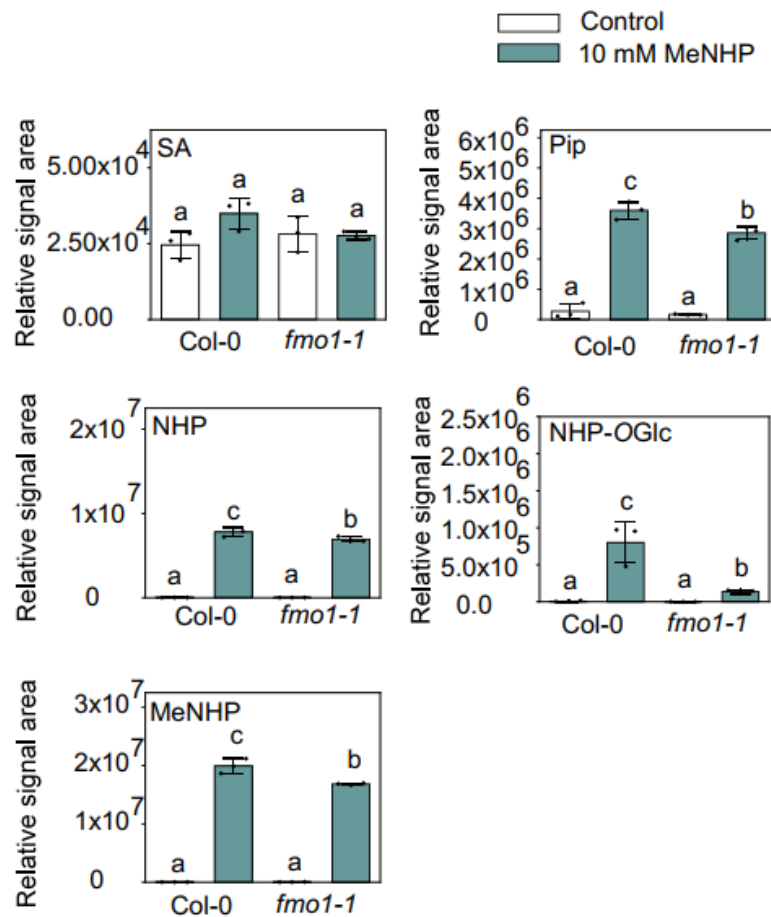


**Fig. S7.** Metabolite analysis after spray application of MeNHP.

10 mM MeNHP were sprayed to WT and *fmo1-1* plants in 10 mM MgCl<sub>2</sub> solution substituted with 0.1% Tween 20. Plants were let incubating for two hours in a closed environment. Afterwards, lids were removed to guarantee ideal growth conditions and the plants were incubated for another 22 hours, in long day conditions in the greenhouse. Leaves were harvested and frozen in liquid nitrogen. Metabolites were extracted using 80 % MeOH and samples were analyzed by UHPLC-MS. Mean relative signal area is shown for SA, Pip, NHP, NHP-OGlc and MeNHP. Error bars indicated standard deviation Letters indicate statistical differences ( $p < 0.05$ , one-way ANOVA post-hoc tukey-test,  $n=3$ ). Each replicate represents independent pools of 6-8 leaves from three plants.

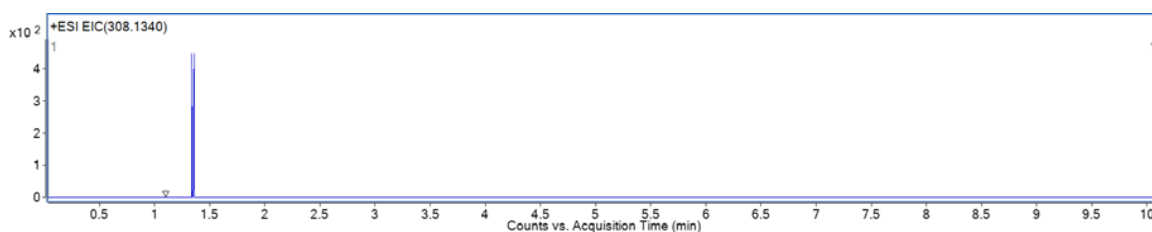


**Fig. S8.** UGT73D1 is not active with NHP *in vitro*.

UGT73D1 was cloned into pET28a expression vector and heterologous expressed in B121-expression cells. UGT73D1 was purified via ion metal affinity chromatography. Active UGT73D1 was mixed *in vitro* with 0.5 mM NHP and 0.5 mM UDP-Glc and incubated overnight. The reaction was stopped by the addition of 1/3 (v/v) MeOH and centrifuged prior to following UHPLC-MS analysis. The extracted ion chromatogram of  $[M+H]^+$  308.134 is shown at 0.005 mDa range.

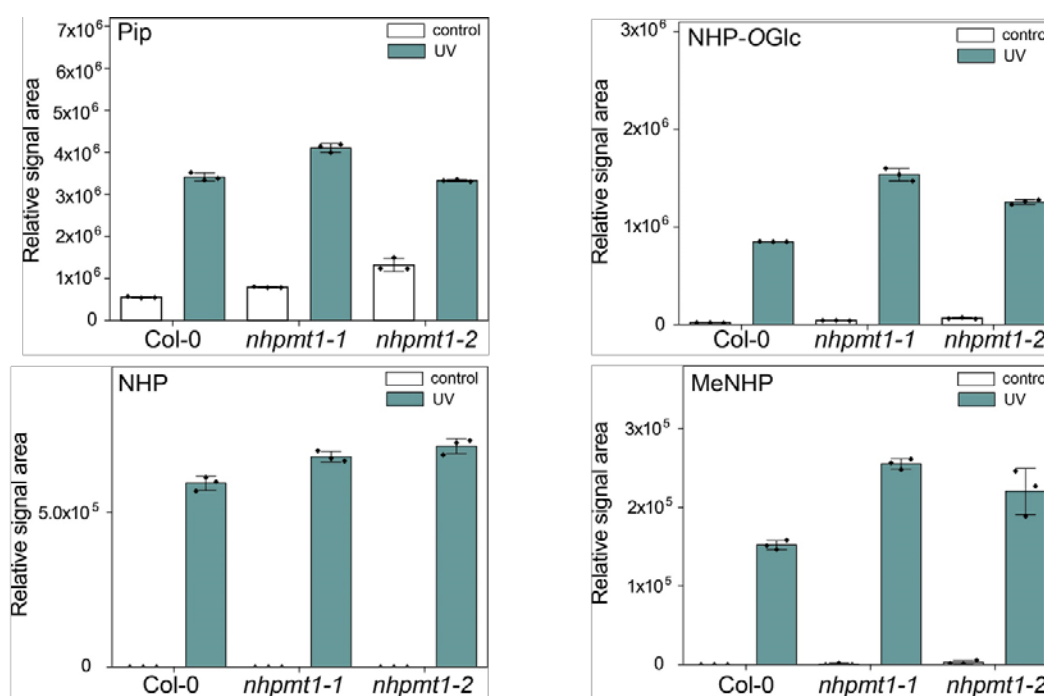


**Fig. S9.** Metabolite analysis of UV-treated Col-0 and *nhpmt1* mutant plants.

Col-0 and *nhpmt1-1* and *nhpmt1-2* mutant plants were analyzed on their relative signal intensities of pipecolic acid (Pip), *N*-hydroxy pipecolic acid (NHP), *N*-hydroxy pipecolic acid glucoside (NHP-OGlc) and methylated NHP (MeNHP), 12 hours post UV. Metabolites were extracted using 80 % MeOH and samples were analyzed using UHPLC-MS. Mean relative signal area is shown for Pip, NHP, NHP-OGlc and MeNHP. Error bars indicated standard deviation.  $n = 3$ . Each replicate represents independent pools of 6-8 leaves from three plants.

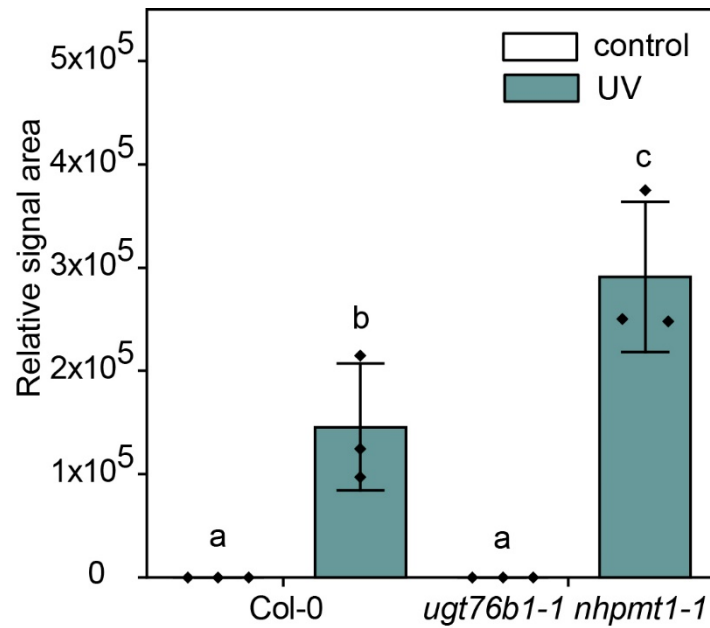


**Fig. S10** MeNHP analysis of UV-stressed Col-0 vs. *ugt76b1-1 nhpmt1-1*.

Plants were treated for 20 min with UV light or kept untreated as control. Plants were incubated for 24 hours post treatment. Individual samples were collect, frozen in liquid nitrogen and retched prior to extraction. Metabolites were extracted with 80 % MeOH solution and samples were anylzed using UHPLC-MS. Mean relative signal area is shown for MeNHP. Samples represent individual pools of a total of 6-8 leaves of three plants. n=3. Letters indicate statistical differences ( $p < 0.05$ , one-way ANOVA post-hoc tukey-test).

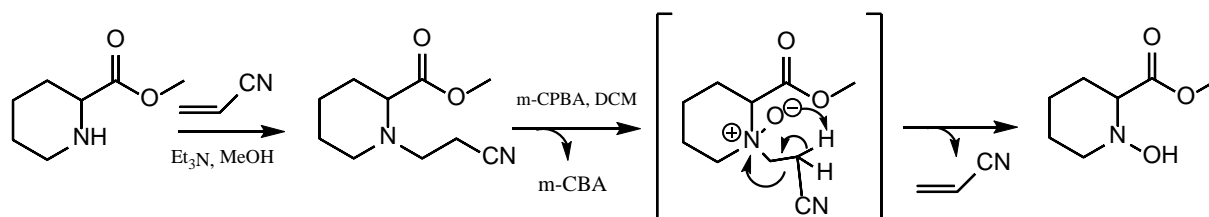
## S11. Supplemental Protocol - Chemical synthesis of MeNHP

### General notes

**Solvents and Reagents:** All technical grade solvents (EtOAc, hexane, Et<sub>2</sub>O, DCM) used for workup procedures and flash column chromatography were distilled prior to use. MeOH, Et<sub>3</sub>N and acrylonitrile, used in reactions, were p.a. grade and supplied from Fisher Scientific (Loughborough, UK) and Sigma Aldrich (Steinheim, Germany). Methylpipercolinate hydrochlorid and m-CPBA were from Sigma Aldrich (Steinheim, Germany) and used as supplied.

**Chromatography:** TLC was carried out on Merck silica gel 60 F<sub>254</sub> Aluminum plates (Darmstadt, Germany). Substances were detected under UV at 254 nm and dipping into a ninhydrin solution (3% in EtOH) followed by heating. Flash column chromatography on silica was performed using Machery-Nagel Silica Gel 60 with a particle size of 0.063-0.2 mm (Düren, Germany).

**Characterization:** The melting point was determined on a Stuart<sup>TM</sup> melting point apparatus SMP10 and is uncorrected. NMR spectra were recorded on a Bruker Advance Neo 400 spectrometer (Billerica, Massachusetts, USA). ESI-MS and HR-MS (ESI) spectra were obtained with BRUKER devices, maXis or MicrOTOF (Bremen, Germany).



### N-(2-cyanoethyl)-methylpipercolinate

To the stirred suspension of Methylpipercolinate hydrochloride (1.50 g, 8.35 mmol) in MeOH p.a. (8 ml) at 0°C under Argon was added Et<sub>3</sub>N (2.31 ml, 16.7 mmol) dropwise. The resulting solution was stirred for 15 min at 0°C. Then acrylonitrile (0.60 ml, 9.2 mmol) was added dropwise and after 15 min at 0°C the reaction mixture was allowed to come to room temperature. Stirring was continued for overnight. The solvent was removed by rotary evaporation. The residue was diluted with H<sub>2</sub>O (25 ml), extracted with Et<sub>2</sub>O (3 x 25 ml). The organic phase was washed with Brine (25 ml), dried over Na<sub>2</sub>SO<sub>4</sub>, filtered and concentrated. The oily residue was purified by flash column chromatography (eluent: Hex / EtOAc 3 : 1, R<sub>f</sub> : 0.65), affording a light yellow oil (1.02 g, 62 %).

<sup>1</sup>H NMR (600 MHz, Chloroform-*d*) δ 3.69 (s, 3H, CO<sub>2</sub>CH<sub>3</sub>), 3.26 (dd, *J* = 6.5, 4.8 Hz, 1H, H-2), 2.97 (ddd, *J* = 11.2, 7.0, 4.2 Hz, 1H, H-6), 2.91 – 2.83 (m, 1H, CH<sub>2</sub>CH<sub>2</sub>CN), 2.69 (ddd, *J* = 13.3, 7.5, 6.9 Hz, 1H, CH<sub>2</sub>CH<sub>2</sub>CN), 2.51 – 2.42 (m, 2H, CH<sub>2</sub>CH<sub>2</sub>CN), 2.38 (ddd, *J* = 11.2, 6.9, 4.3 Hz, 1H, H-6), 1.85 – 1.74 (m, 2H, H-3), 1.64 – 1.52 (m, 2H, H-5), 1.55 – 1.44 (m, 1H, H-4), 1.44 – 1.35 (m, 1H, H-4).

**<sup>13</sup>C NMR (151 MHz, Chloroform-*d*)**  $\delta$  173.58 ( CO<sub>2</sub>CH<sub>3</sub> ), 118.82 ( CN ), 63.68 ( C-2 ), 51.83( CH<sub>2</sub>CH<sub>2</sub>CN ). , 51.59 (CO<sub>2</sub>CH<sub>3</sub> ), 49.55( C-6 ), 29.24 ( C-3 ), 25.20 ( C-5 ), 21.79 ( C-4 ), 16.46 ( CH<sub>2</sub>CH<sub>2</sub>CN ).

**HRMS-ESI:** calculated for [C<sub>10</sub>H<sub>16</sub>N<sub>2</sub>O<sub>2</sub>]<sup>+</sup> (M + H<sup>+</sup>) 197.1285, found 197.1285  
[C<sub>10</sub>H<sub>16</sub>N<sub>2</sub>O<sub>2</sub>]<sup>+</sup> (M + Na<sup>+</sup>) 219.1104, found 219.1104

### ***N*-Hydroxy-methylpipercolinate**

To a stirred solution of the tert.- amine ( 4.45 g, 22.68 mmol ) in DCM p.a. ( 150 ml ) at 0°C under Argon was added m-CPBA 77% ( 5.08 g, 22.68 mmol ) portionwise. Afterwards the mixture was stirred for 1h at 0°C and then at room temperature until the reaction was complete ( ~ 2h, TLC controlled ). The solution was diluted with DCM ( 100 ml ) and washed with a sat. aq. NaHCO<sub>3</sub> solution ( 2 x 100 ml ) and brine ( 100 ml ). The organic extract was dried over Na<sub>2</sub>SO<sub>4</sub>, filtered and concentrated. The residue was purified by flash chromatography column ( eluent: Hex / EtOAc 1 : 1, R<sub>f</sub>: 0.23 ). The solid product was recrystallized from Hex / EtOAc 10 : 1, affording a colorless solid ( 3.05 g, 84 %). **m.p.** 80 – 82 °C

**<sup>1</sup>H NMR (400 MHz, DMSO-*d*<sub>6</sub>)**  $\delta$  8.15 (s, 1H, N-OH), 3.61 (s, 3H, CO<sub>2</sub>CH<sub>3</sub>), 3.16 – 3.07 (m, 1H, H-6), 3.00 (d, *J* = 11.4 Hz, 1H, H-2), 2.36 (t, *J* = 11.7 Hz, 1H, H-6), 1.83 – 1.70 (m, 1H, H-3), 1.69 – 1.41 (m, 4H, H-3, H-5, H-4), 1.17 (dt, *J* = 12.3, 4.3 Hz, 1H, H-4).

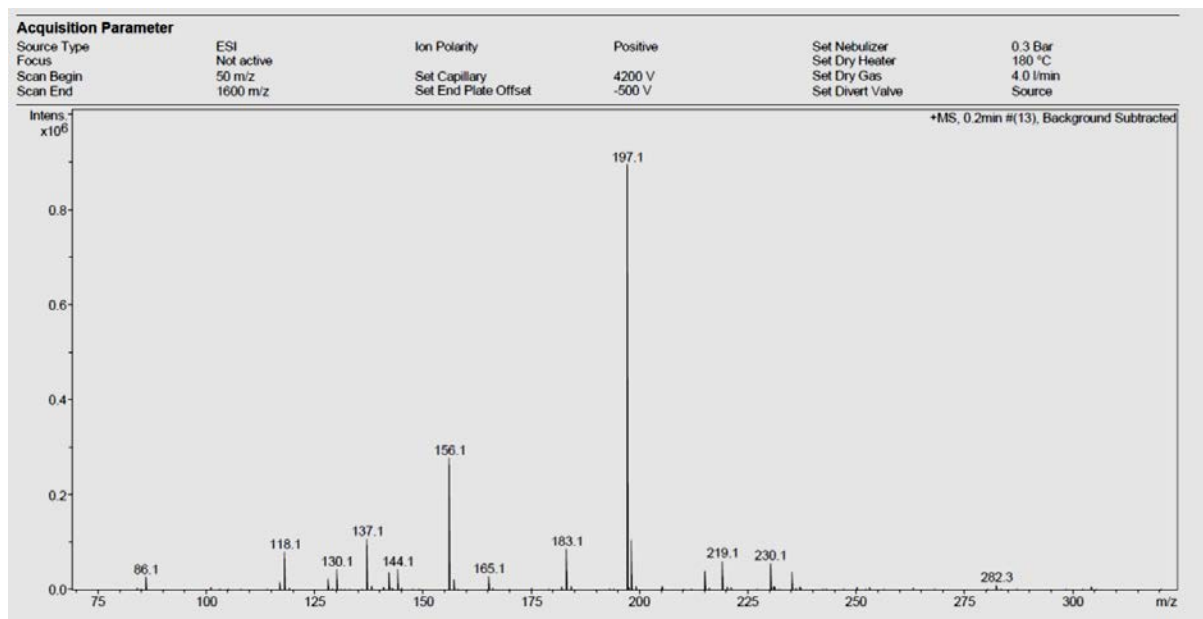
**<sup>1</sup>H NMR (400 MHz, Chloroform-*d*)**  $\delta$  6.46 (s, 1H, N-OH), 3.71 (s, 3H, CO<sub>2</sub>CH<sub>3</sub>), 3.45 – 3.28 (m, 1H, H-2), 3.14 (d, *J* = 11.9 Hz, 1H, H-6), 2.50 (s, 1H, H-6), 1.95 (d, *J* = 13.1 Hz, 1H, H-3), 1.83 – 1.42 (m, 4H, H-3, H-5, H-4), 1.26 – 1.10 (m, 1H, H-4).

**<sup>13</sup>C NMR (101 MHz, DMSO-*d*<sub>6</sub>)**  $\delta$  172.34 ( CO<sub>2</sub>CH<sub>3</sub> ), 70.68 ( C-2 ), 58.05 ( C-6 ), 51.06 ( CO<sub>2</sub>CH<sub>3</sub> ), 28.63 ( C-3 ), 24.54 ( C-5 ), 22.17 ( C-4 ).

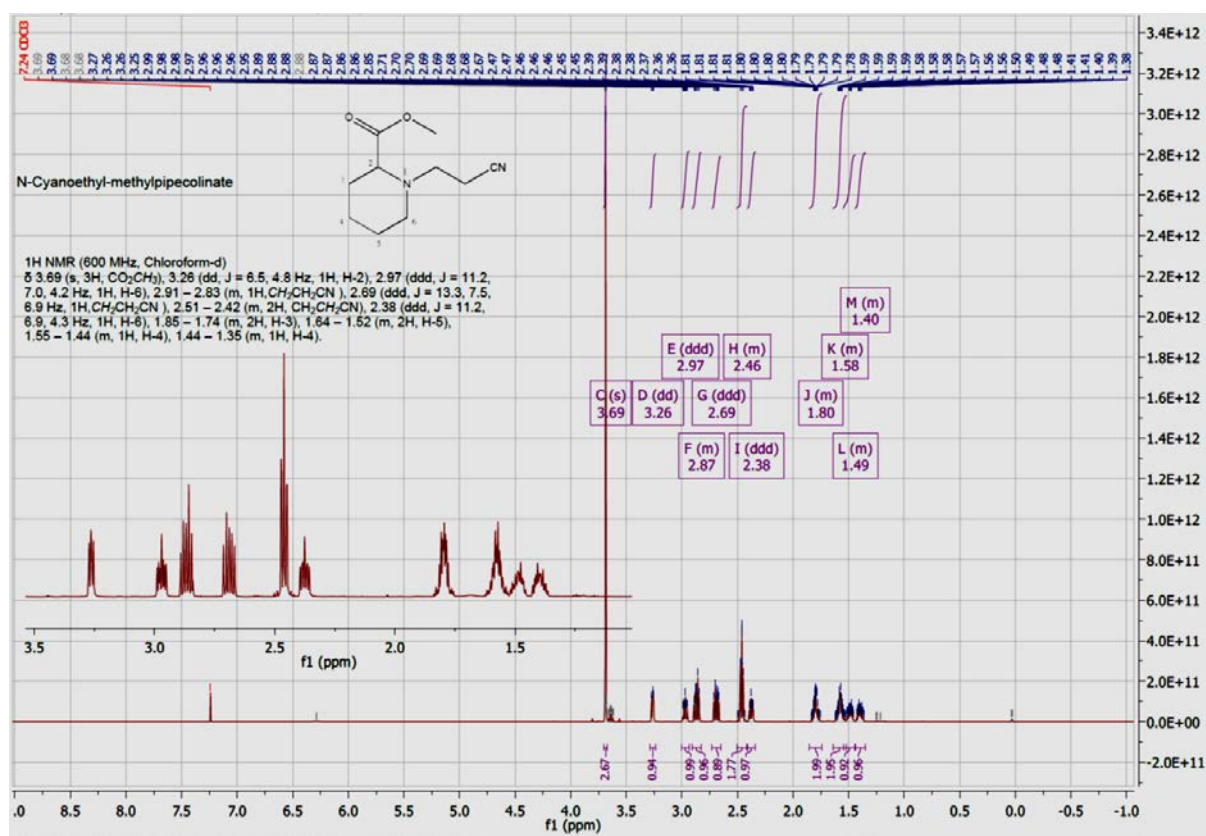
**<sup>13</sup>C NMR (101 MHz, Chloroform-*d*)**  $\delta$  173.13 ( CO<sub>2</sub>CH<sub>3</sub> ), 70.75 ( C-2 ), 57.67 ( C-6 ), 51.93 ( CO<sub>2</sub>CH<sub>3</sub> ), 29.42 ( C-3 ), 25.08 ( C-5 ), 22.91 ( C-4 ).

**HRMS-ESI:** calculated for [C<sub>7</sub>H<sub>13</sub>NO<sub>3</sub>]<sup>+</sup> (M + H<sup>+</sup>) 160.0968, found 160.0966  
[C<sub>7</sub>H<sub>13</sub>NO<sub>3</sub>]<sup>+</sup> (M + Na<sup>+</sup>) 182.0788, found 182.0792

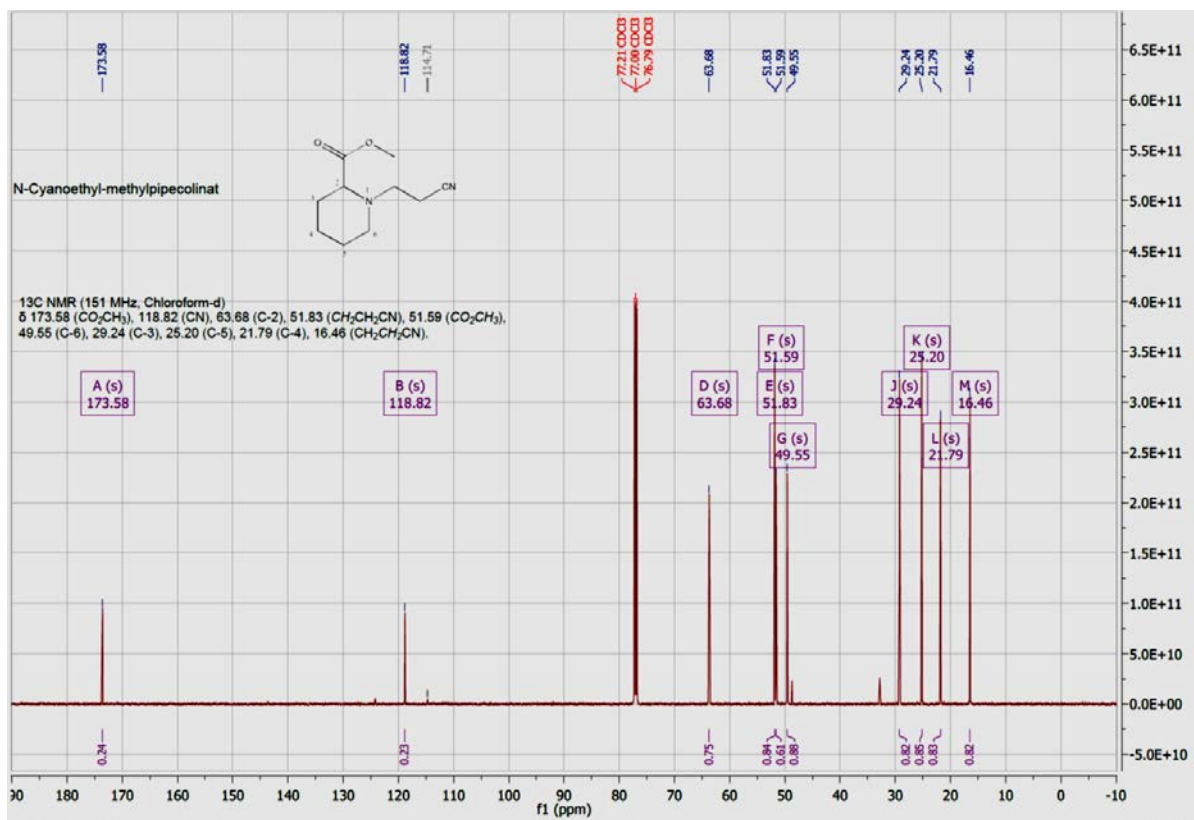
**Literature:** Organic Chemistry Frontiers, 2016, **3**, 1624 – 1634



**S11. Fig.1** Mass spectrum of *N*-(2-cyanoethyl)-methylpipercolinate

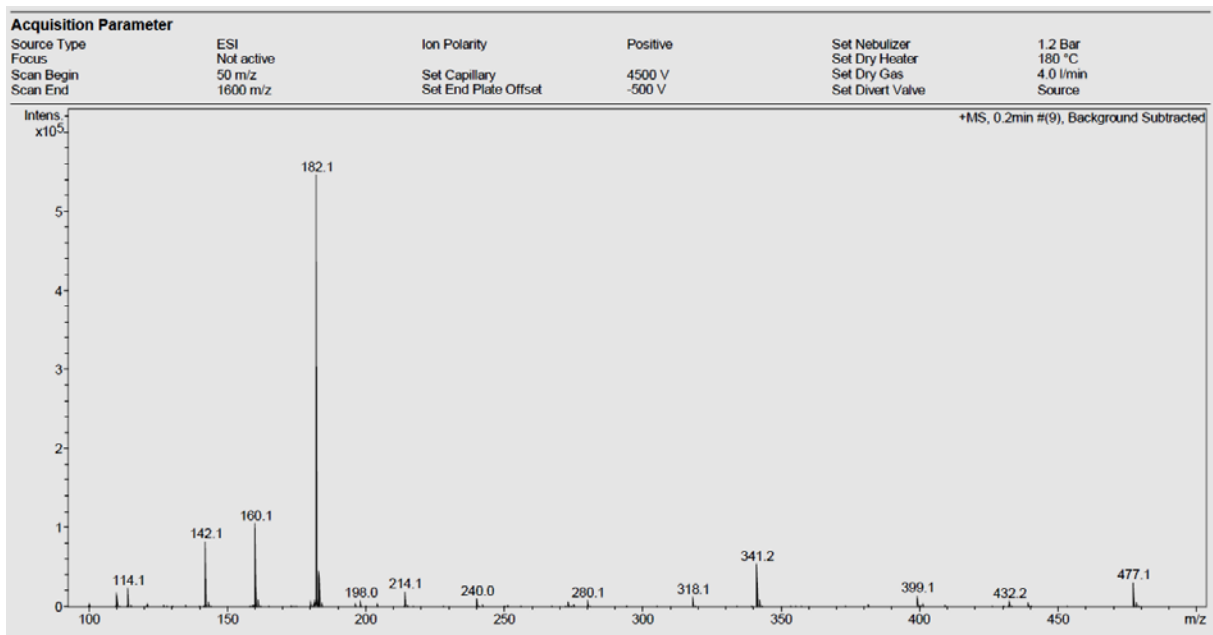


**S11. Fig.2** <sup>1</sup>H-NMR spectrum of *N*-(2-cyanoethyl)-methylpipercolinate

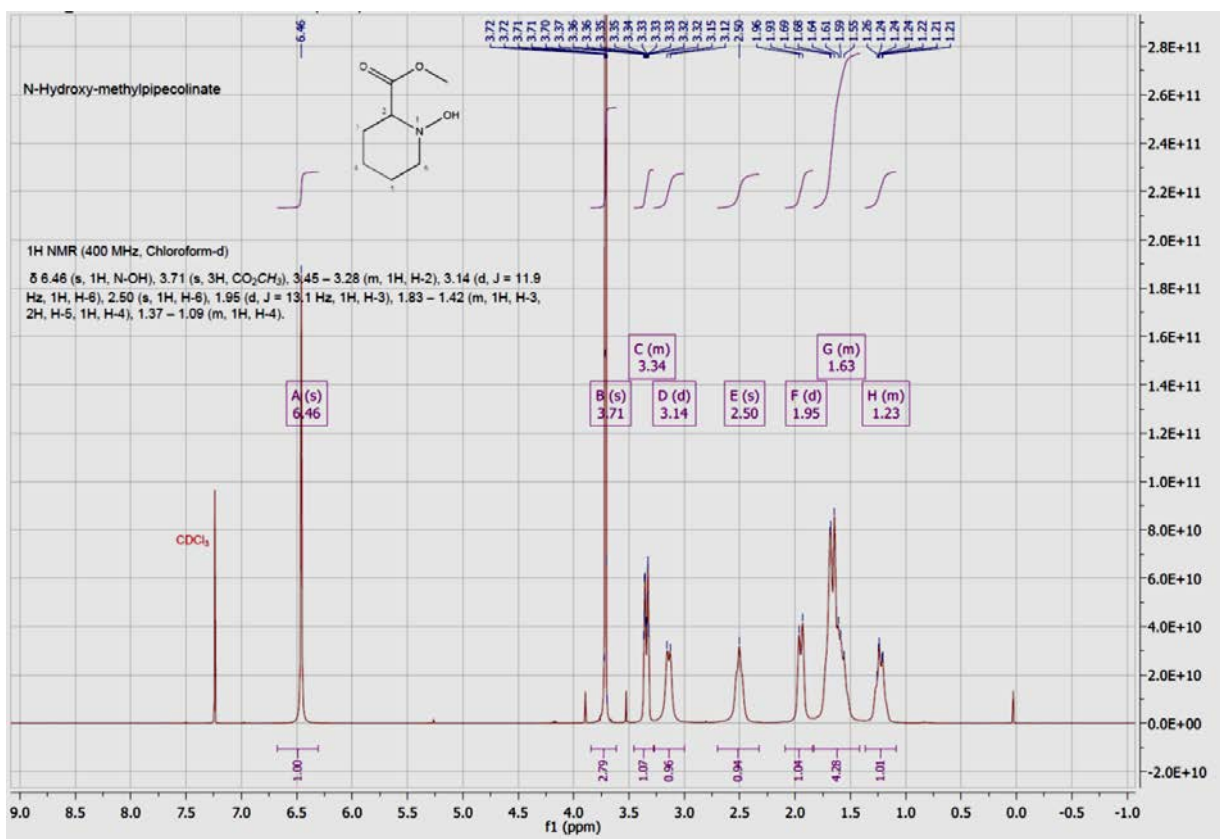


**S11. Fig.3** <sup>13</sup>C-NMR spectrum of *N*-(2-cyanoethyl)-methylpipercolinate

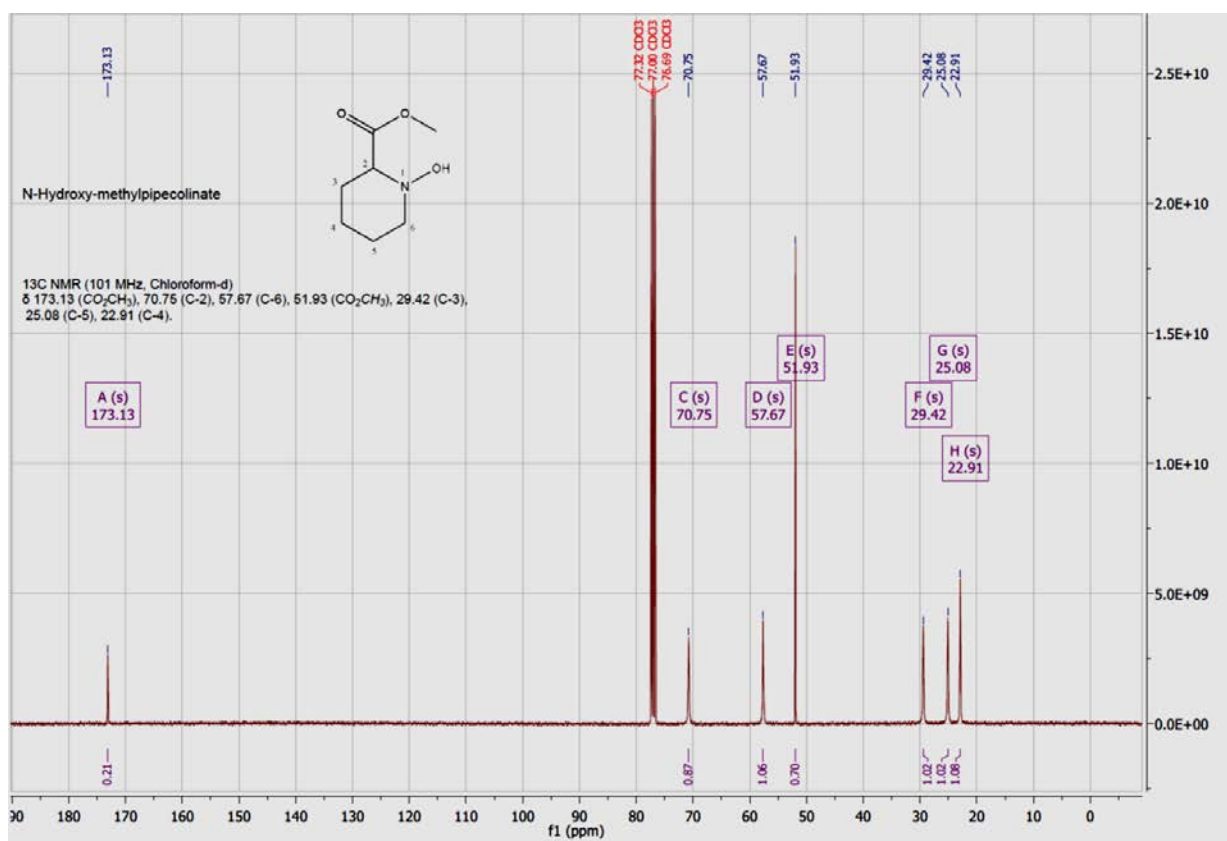




**S11. Fig.4** Mass spectrum of *N*-Hydroxy-methylpipercolinate



**S11. Fig.5** <sup>1</sup>H-NMR spectrum of *N*-Hydroxy-methylpipercolinate



**S11. Fig.6** <sup>13</sup>C-NMR spectrum of *N*-Hydroxy-methylpipercolinate

## 5. Chapter III. – Further analysis of missing links in SA- and NHP-biosynthesis and metabolism

In addition to the work on unraveling the role of UGT76B1 in SA- and NHP-mediated resistance and the identification of novel NHP-based metabolites, we investigated into missing links of NHP-metabolism, especially into the missing transporters. Besides the suggestion, that EDS5 might be the gatekeeper of both SA- and NHP-metabolism, no further study to underline this hypothesis was published (Rekhter et al., 2019a). Here, we show the results of our studies on an independent mutant allele of EDS5. We also checked whether other candidate transporters, which were described to be upregulated in response to *Pseudomonas* infection or with a contribution to SAR, like ABERRANT LATERAL ROOT FORMATION 5 (ALF5) or LYSINE/HISTIDINE 7 (LHT7) might be involved in NHP-biosynthesis (Yang and Ludewig, 2014; Bernsdorff et al., 2016). Additionally, we investigated into a specific aspect of the SA-biosynthesis. Here, EPS1 was published to be a factor in PBS3-dependent SA-biosynthesis by enhancing the degradation of the SA-precursor IC-9-Glu. Indeed, we were able to confirm the role of EPS1 in SA-biosynthesis contributing to IC-9-Glu degradation.

A landmark in the understanding of the SA-biosynthesis in Brassicaceae was the identification and description of the enzymatic activity of PBS3 by catalyzing the reaction from IC to IC-9-Glu published recently (Rekhter et al., 2019b). The latter one has the tendency to decompose spontaneously into SA and 2HNG. Torres-Spence and colleagues confirmed these results and described in addition the role of EPS1 in PBS3-dependent SA-biosynthesis by showing that EPS1 has IC-9-Glu lyase activity resulting in an enhanced SA- and 2HNG-accumulation (Torrens-Spence et al., 2019). One observation they made was that the PBS3-synthesized IC-9-Glu accumulated in plants harboring an *eps1* mutation (Torrens-Spence et al., 2019). To confirm their observation we decided to perform an analysis on IC-9-Glu-accumulation in UV-C stressed Col-0 and *eps1-2* mutant leaves, as well as, non-treated plants as controls (Figure 11). We characterized the *eps1-2* mutant plant line, which we obtained from the SALK stock center (SAIL\_734\_I07) to be homozygous and grew Col-0 and *eps1-2* mutant plants under long day conditions on soil for 4 weeks. To induce defense metabolism we treated the plants with UV-C radiation for 20 minutes as described earlier (Chapter I). 24 hours post UV (hpUV) treatment we harvested leaves of three plants per replicate. The leaf material was ground under liquid nitrogen and 100 mg fresh weight were extracted using methyl-*tert*-butyl ether (MTBE)-extraction as described in Chapter I. After solvent evaporation, the metabolite extract was solved in 100  $\mu$ L 20 % methanol. The samples were analyzed via UHPLC-ESI-HRMS. We generated extracted ion chromatograms of the mass spectrometric data for IC-9-Glu signal at  $m/z$  354.083 and compared relative signal area of IC-9-Glu in the different samples. IC-9-Glu

significantly accumulated in the *eps1-2* mutant background in response to UV-C treatment. Col-0 plants did not exhibit IC-9-Glu accumulation in response to UV-C. In Col-0 plants, the degradation of the PBS3-formed IC-9-Glu by EPS1 to SA is available and therefore, less IC-9-Glu enrichment might be detectable after treatment. All in all, we were thus able to confirm the observation by Torres-Spence and coworkers that IC-9-Glu is accumulating in the *eps1* mutant background, which supports the function of EPS1 to degrade IC-9-Glu into SA and 2HNG (Torrens-Spence et al., 2019).

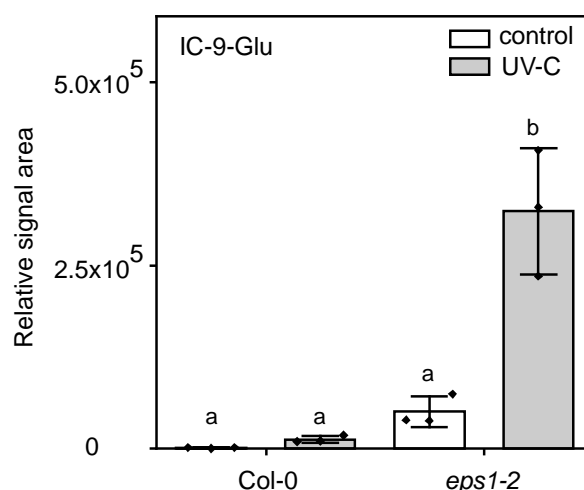


Figure 11: **Isochorismate-9-glutamic acid (IC-9-Glu) accumulates in UV stressed *eps1* mutant plants.** Relative signal intensities of *pbs3*-dependent SA-biosynthesis precursor isochorismate-9-glutamic acid are shown in response to UV-C treatment. Four-week-old Col-0 and *eps1-2* plants were challenged with UV-C treatment for 20 min to induce defense metabolism (grey) or left untreated as control (white). Samples were harvested 24 hours post UV treatment (hpUV). Leaf material was ground under liquid nitrogen and metabolites were extracted using methyl-*tert*-butyl ether, methanol and water extraction. The extracts were dried under streaming nitrogen and molecules were solved in 20 % methanol. The samples were analyzed using UHPLC-ESI-HRMS. Data represents mean relative signal area with standard deviation. n= 3 individual pools of leaves derived from three plants each. Letters indicate statistical differences,  $p < 0.05$ , one-way ANOVA with post-hoc Tukey-test.

We further aimed to identify transporters being involved in NHP-biosynthesis. EDS5 was the first candidate that was suggested to play a role in both SA- and Pip-biosynthesis (Rekhter et al., 2019a). EDS5 appears to be a suitable candidate transporter, because a shared signaling hub for both signaling molecules, SA and NHP, would allow coordinating both pathways simultaneously (Rekhter et al., 2019a). To analyze the role of EDS5 in the biosynthetic route of NHP as chloroplast exporter of Pip we investigated into a second independent mutant allele of the transporter (*eds5-2*, kindly provided by Prof. Dr. Christiane Nawrath). However, the role of EDS5 in NHP- and SA-biosynthesis could not be confirmed in *eds5-2* mutant plants (Figure 12). We challenged again Col-0 and *eds5-2* mutant plants with UV-C light and harvested samples 24 hpUV. We analyzed the levels of NHP via UHPLC-ESI-HRMS in the respective metabolite extracts. NHP-levels increased after UV-C treatment in both Col-0 and *eds5-2* mutant plants, strongly suggesting that EDS5 is either not the only transporter for NHP biosynthesis or may not be required as transporter for NHP-biosynthesis.

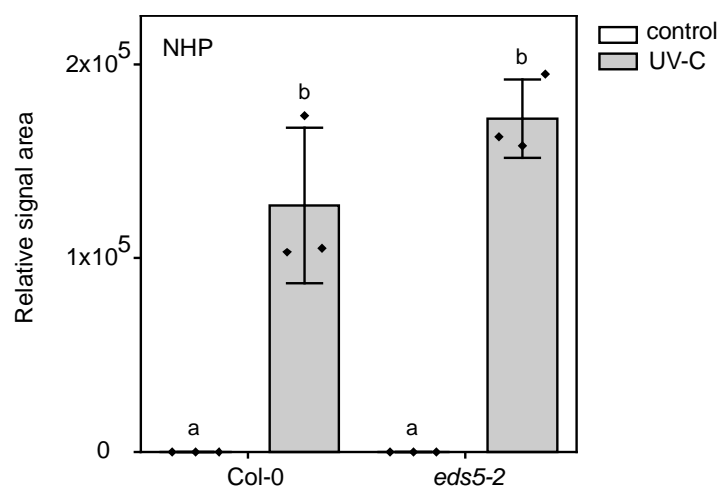


Figure 12: **Detection of NHP accumulation in eds5-2 mutant plants.** Relative signal area of the NHP-signal corresponding to  $m/z$  146.082 were analyzed. Col-0 and eds5-2 mutant plants were treated for 20 min with UV-C (grey), control plants were left untreated (white). The plants were incubated and leaves were harvested 24 hpUV and immediately frozen in liquid nitrogen. Plant material was ground and 100 mg were extracted using MTBE extraction. Samples were analyzed using UHPLC-ESI-HRMS. Data represents mean relative signal area with standard deviation.  $n=3$  individual pool of leaves derived from three plants each. Letters indicate statistical differences,  $p < 0.05$ , one-way ANOVA with post-hoc Tukey-test.

The second candidate we analyzed was the EDS5-homolog (EDS5H). Similar to EDS5 it belongs to the family of MATE exporters. It is 72 % similar and 59 % identical in sequence to EDS5, however it has been shown to be not involved in ICS1-dependent SA-biosynthesis (Parinthawong et al., 2015). We conducted a UV-C stress experiment with Col-0 and eds5h mutant plants (SALK\_043653). After 24 hours, leaves were harvested and metabolites were extracted using MTBE-extraction.

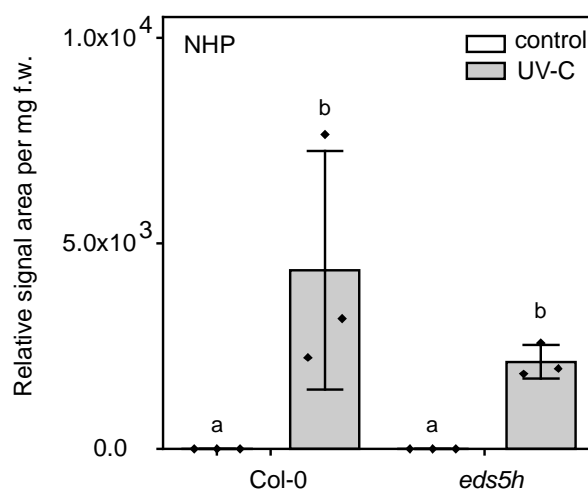


Figure 13: **Analysis of NHP-levels in Col-0 and eds5h mutant plants.** Relative signal area of the NHP-signal corresponding to  $m/z$  146.082 were analyzed. Col-0 and eds5h mutant plants were treated for 20 min with UV-C (grey), control plants were left untreated (white). The plants were incubated and leaves were harvested 24 hpUV and immediately frozen in liquid nitrogen. Plant material was ground and extracted using methyl-*tert*-butylether extraction. Samples were analyzed using UHPLC-ESI-HRMS. Signal area was normalized against the amount of plant material extracted. Data represents mean relative signal area with standard deviation.  $n=3$  individual pools of leaves derived from three plants each. Letters indicate statistical differences,  $p < 0.05$ , one-way ANOVA with post-hoc Tukey-test.

The samples were analyzed for their NHP-levels using UHPLC-ESI-HRMS (Figure 13). In both Col-0 and *eds5h* plants, NHP accumulated after UV-C stress without a significant difference.

We investigated into another candidate transporter from the MATE-family that was described to play a role in SAR, namely, ALF5 (Bernsdorff et al., 2016). We obtained the homozygous T-DNA insertion line (SALK\_047842C) from the SALK stock center. We conducted a *Pseudomonas syringae* pv. *maculicola* ES4326 (*P.s.m.*) infection experiment and analyzed the metabolite extracts with UHPLC-ESI-HRMS (Figure 14). In brief, *P.s.m.* bacteria were suspended in 10 mM MgCl<sub>2</sub> and were infiltrated to leaves with an OD<sub>600</sub>=0.05. As control 10 mM MgCl<sub>2</sub> was infiltrated to the leaves. The treated leaf material was harvested 48 hours post infiltration. Both Col-0 and the *alf5* mutant accumulated NHP in response to *P.s.m.* infection. Surprisingly, the accumulation of NHP in the *alf5* mutant plants was even higher than in the Col-0 plants. This might indicate that *alf5* mutant plants could exhibit enhanced disease resistance. We conclude that ALF5 seems not to play a role in NHP-biosynthesis. It may be speculated that increased NHP-levels derive from a disrupted cellular export or degradation. However, we cannot provide data that support this speculation.

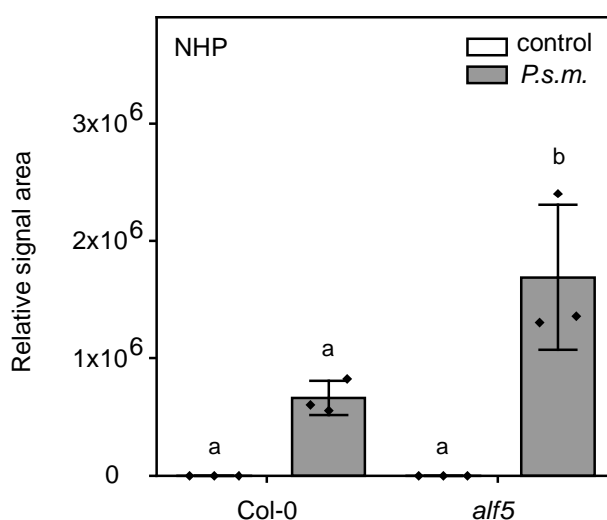


Figure 14: **Analysis of NHP levels in Col-0 and *alf5* mutant plants in response to *P.s.m.*** Relative signal area of the NHP signal corresponding to *m/z* 146.082 were analyzed. Col-0 and *alf5* mutant plants were infiltrated with 10 mM MgCl<sub>2</sub> (white) or *P.s.m.* at OD<sub>600</sub>=0.05 in 10 mM MgCl<sub>2</sub> (dark grey). Treated leaves were harvested 48 hours post treatment and immediately frozen in liquid nitrogen. Plant material was ground and extracted using 80 % methanol extraction. Samples were analyzed using UHPLC-ESI-HRMS. Signal area was normalized against the amount of plant material extracted. Data represents mean relative signal area with standard deviation. n= 3 individual pool of leaves. Letters indicate statistical differences, p < 0.05, one-way ANOVA with post-hoc Tukey-test.

In addition, we decided to analyze the amino acid transporter LHT7. The transporter was shown to be transcriptionally upregulated upon *P.s.m.* and Flagellin22 treatment (Yang and Ludwig, 2014). Similar to ALF5, LHT7 was classified to play a role in SAR (Bernsdorff et al., 2016). Additionally, it appeared in a co-expression network analysis with *ALD1* (Obayashi et al., 2022). Therefore, the *lht7* mutant (SALK\_027033) was obtained from the SALK stock

center and determined to be homozygous. The ability of *lht7* mutant plants to synthesize NHP in response to *P.s.m.* infection was investigated (Figure 15). We performed the *P.s.m.* infection experiment as described above and harvested leaf samples 48 hours post treatment. The samples were analyzed using UHPLC-ESI-HRMS. Both, Col-0 and *lht7* plants accumulated NHP in response to *P.s.m.* infection with comparable signal areas. Therefore, we concluded that LHT7 alone is not required for NHP-biosynthesis.

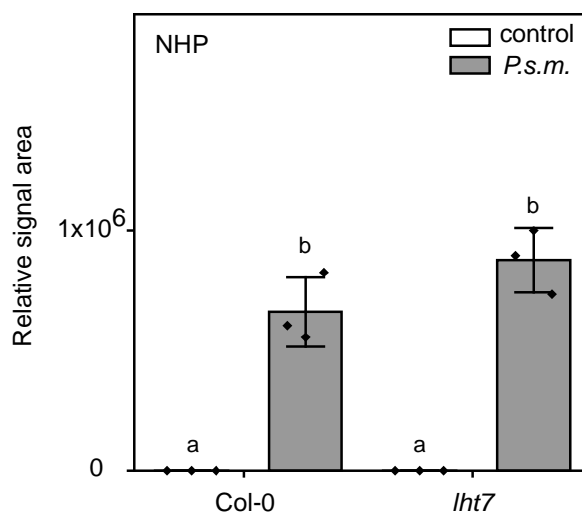


Figure 15: **Analysis of NHP in Col-0 and *lht7* plants in response to UV-C.** Relative signal area of the NHP signal corresponding to  $m/z$  146.082 were analyzed. Col-0 and *lht7* mutant plants were infiltrated with 10 mM  $MgCl_2$  (white) or *P.s.m.* at  $OD_{600}=0.05$  in 10 mM  $MgCl_2$  (dark grey). Treated leaves were harvested 48 hours post treatment and immediately frozen in liquid nitrogen. Plant material was ground and extracted using 80 % methanol extraction. Samples were analyzed using UHPLC-ESI-HRMS. Signal area was normalized against the amount of plant material extracted. Data represents mean relative signal area with standard deviation.  $n=3$  individual pool of leaves. Letters indicate statistical differences,  $p < 0.05$ , one-way ANOVA with post-hoc Tukey-test.

In summary, the experimental data obtained with the investigated transporter candidates, did not reveal any hint that they were involved in NHP-biosynthesis. Most importantly, we were not able to confirm the role of EDS5 in the biosynthesis of NHP. It might be the case that the transporter candidates did show differences in NHP accumulation in infected leaves because of genetic redundancy.

## 6. Discussion

Barriers, signaling and metabolite networks are a key for plant fitness. Sensing of external threats and signal proliferation lead to transcriptional and in consequence metabolic remodeling of the harmed tissue (Feussner and Polle, 2015; Bernsdorff et al., 2016). These signals can be distributed through the organism (Chen et al., 2018). Several mechanisms were described to be present in plant organisms ranging from fast responding calcium fluxes, over the accumulation of ROS, to long lasting metabolic responses at the onset of SAR and defense priming (Torres et al., 2006; Ma et al., 2013; Guerra et al., 2020). Two molecules that concert plant immunity are SA and NHP. SAs ability to enhance disease resistance is known since the 1990<sup>th</sup> and has been shown in numerous plant species. Its biosynthesis and working modes via the proposed receptors NPR1 and NPR3/4 have been described in Arabidopsis (Cao et al., 1997; Ding et al., 2018). The biosynthesis of NHP and its ability to induce disease resistance was described during the recent years (Chen et al., 2018; Hartmann et al., 2018). NHP synthesis was shown to be significantly induced upon *P. syringae* treatment in tobacco, tomato, Arabidopsis and mustard (Holmes et al., 2019). Furthermore, transient expression of *FMO1*-homologs from these species, in *N. benthamiana* resulted in successful synthesis and detection of NHP (Holmes et al., 2019). The same outcome has been observed using soybean or corn *FMO1*-homologs (Holmes et al., 2019). Similarly, NHP was applied to several plant species with the outcome that it enhanced disease resistance in, for instance, tomato, tobacco, soybean and barley (Holmes et al., 2019; Schnake et al., 2020). There is growing evidence that NHP is a phloem mobile signal during the establishment of SAR (Chen et al., 2018; Schnake et al., 2020).

In this work, we were able to show induction of metabolite remodeling in infection studies with *P.s.m.* bacteria and UV-C treatment. Applying both stresses, we investigated the role of UGT76B1 in plant immunity. We describe its central function in glycosylation of NHP, as well as, of SA and therefore regulating the amount of these active compounds and balancing plant immunity (Chapter I) (Figure 16). The *in vivo* metabolite analyses were accompanied via *in vitro* analysis using purified UGT76B1. Furthermore, we investigated the influence of functional *FMO1* on the *ugt76b1-1* phenotype. Therefore, also investigating the role of NHP in *ugt76b1-1*. In addition, we were able to describe novel NHP-based metabolites in response to UV-C and *P.s.m.* infection (Chapter II). We discuss molecular identities of MeNHP, NHPGE, NHP-OGlcHex, NHP-OGlcMal and possible synthesis routes. We strengthen their identification by authentic standards via chemical synthesis, *in vitro* enzymatic synthesis and MSMS-fragmentation experiments. Moreover, with the chemically synthesized MeNHP standard in hand, we performed plant infiltration experiments to investigate its metabolic fate and its potential to rescue the *fmo1-1* susceptibility phenotype.



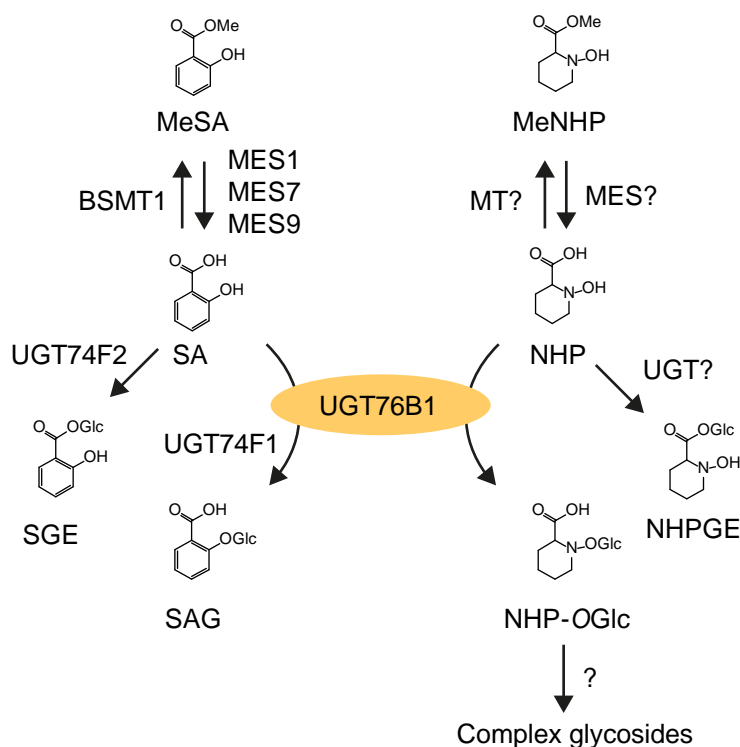


Figure 16: **Metabolic modifications of SA and NHP by glucosylation and methylation in Arabidopsis.** Enzymes for glucosylation and methylation of NHP and SA that have been shown to play a role in Arabidopsis *in planta* and its enzymatic products, respectively. UGT76B1 is the central enzyme to glucosylate both NHP and SA. UGT74F1 is able to form SAG, and UGT74F2 was shown to form SGE, respectively, via glucosylation. BSMT1 was shown to form MeSA. MeSA can be converted back to SA by MES1, 7 and 9. NHP-metabolites MeNHP, NHPGE and the complex glycosides were described without enzymes fulfilling their formation *in vivo*. So far, not identified enzymes for a suggested enzymatic activity were labeled with a question mark. Unclear routes were labeled with a question mark only.

The basis for our studies of SA- and NHP-metabolism were UHPLC-ESI-HRMS-based non-targeted metabolome analysis, and quantitative metabolomics analyses. The methods enable investigation into metabolite changes between wild type and mutant plants, deficient in the activity of individual enzymes. Further, the combination of enzyme purification and *in vitro* analysis combined with the mass spectrometry platform allowed the determination of enzymatic activities and product discovery. In combination with infection studies with *P.s.m.* and *H.a Noco 2*, we were able to investigate the *in planta* role of UGT76B1 and to describe novel NHP-metabolites, such as MeNHP in the onset of plant-microbe interactions. Furthermore, we were able to confirm the role of EPS1 in SA biosynthesis by the detection of IC-9-Glu accumulation as proposed by Torres-Spence and coworkers (Torrens-Spence et al., 2019). Besides, we provide insights into the role of the potential transporters EDS5, EDS5H, ALF5 and LHT7 to be, at least not alone responsible for Pip export from the chloroplast to the cytosol for NHP biosynthesis (Chapter III).

## 6.1 UGT76B1 is the central hub of NHP and SA inactivation

During the metabolic response of plant immunity, UGTs are able to catalyze the conjugation of glucose to the defense concerting molecules SA and NHP (Song et al., 2008; Chen et al., 2018; Cai et al., 2021). UGT76B1 has been shown to regulate the concentration of SA, by forming SAG (von Saint Paul et al., 2011; Noutoshi et al., 2012; Maksym et al., 2018). Additionally, UGT76B1 is responsible for the metabolic turnover of branched chain amino acid-like compound ILA (von Saint Paul et al., 2011; Noutoshi et al., 2012; Maksym et al., 2018). *UGT76B1* is transcriptionally upregulated upon various abiotic and biotic stresses like osmotic stress, UV-B, *Pseudomonas* bacteria or *Phytophthora infestans* (von Saint Paul et al., 2011). Furthermore, application of the defense related compounds SA, Pip or NHP triggers transcriptional upregulation of *UGT76B1* (Blanco et al., 2009; Bernsdorff et al., 2016; Hartmann et al., 2018). This is in line with the co-expression of *UGT76B1* with defense responsive Pip biosynthesis genes *ALD1* and *FMO1*, which themselves exhibit co-expression with SA biosynthetic genes *PBS3* and *ICS1* (ATTED-II, ver.11, accessed 220607) (Obayashi et al., 2022). Von Saint Paul and colleagues already identified an enhanced resistance phenotype of *ugt76b1-1* mutant plants and *vice versa* enhanced susceptibility of the *UGT76B1-OE-7* overexpression line against (hemi-) biotrophic *P. syringae* (von Saint Paul et al., 2011). In line with this observation, infection with the necrotrophic pathogen *Alternaria brassicicola* resulted in susceptibility of *ugt76b1-1* and enhanced resistance of the *UGT76B1-OE-7* overexpression line (von Saint Paul et al., 2011). The infection data is in line with the marker gene expression, as upregulation of basal *PR1*-transcripts associated with SA was described. What is more, downregulation of *VSP2*-transcripts, associated with JA, in *ugt76b1-1* mutant lines compared to wild type was observed (von Saint Paul et al., 2011). The basal *PR1*-gene expression presented earlier matches the expression profile presented by von Saint Paul and colleagues and was further underlined in the independent CRISPR *ugt76b1-3* and *ugt76b1-4* mutant plants (Chapter I). Furthermore, SA levels were significantly higher in five-week-old seedlings of *ugt76b1-1* mutants compared to Col-0 and *UGT76B1-OE-7* (von Saint Paul et al., 2011). Similarly, SA levels were significantly increased in *ugt76b1* mutants six hours post infection with *P. syringae* avrRpm1 in comparison to wild type (Noutoshi et al., 2012). SAG amounts were significantly reduced in *ugt76b1* mutants compared to wild type after infection (Noutoshi et al., 2012). It is interesting to mention that basal SAG levels in five-week-old seedlings were significantly increased likewise in *ugt76b1-1* and *UGT76B1-OE-7* compared to Col-0 (von Saint Paul et al., 2011). This could be explained by the already high stress levels in the basal state of the *ugt76b1-1* mutant, that are represented by high SA levels, which can be turned over by the other known UGTs UGT74F1 and UGT74F2. The explanation would be

---

in line with the additional report about significantly increased levels of SGE in the *ugt76b1-1* mutant seedlings (von Saint Paul et al., 2011).

### 6.1.1 *In vivo* annotation of UGT76B1 to NHP-OGlc synthesis

We performed a *P.s.m.* infection experiment with *ugt76b1-1* mutants and wild type plants to identify *ugt76b1* mutation dependent differences at the basis of the metabolome (Chapter I). The metabolome is the characteristic read out of transcriptional reprogramming (Feussner and Polle, 2015). The dataset was recorded with UHPLC-ESI-HRMS and analyzed using Agilent MassHunter Profinder and the MarVis-software package (Agilent Technologies, Santa Clara, CA, USA) (Kaefer et al., 2012; Kaefer et al., 2013; Kaefer et al., 2015; Feussner and Feussner, 2019). By non-targeted metabolome analysis, we reproduced the described SAG chemotype of *ugt76b1-1* and strikingly did not observe any NHP-OGlc in the mutant plants. In addition, signal intensities corresponding to SA and NHP were increased in the *ugt76b1-1* mutant background. The data suggests NHP as additional substrate of UGT76B1 *in vivo*. To this point, only one NHP-glycoside was described from two independent studies, without the functional annotation of an enzyme able to synthesize NHP-OGlc (Chen et al., 2018; Hartmann and Zeier, 2018). Later it turned out that at this point already both NHP-OGlc and NHPGE had been detected (Chen et al., 2018; Hartmann and Zeier, 2018; Bauer et al., 2021). A later study by Bauer and colleagues described both NHP-glycosides in *P.s.m.* infiltrated wild type plants of which only the NHP-OGlc was missing in *ugt76b1* background (Bauer et al., 2021). The second NHP-glycoside resembled NHPGE. To underline the molecular identity of NHP-OGlc and to exclude the signal from NHPGE in our UHPLC-ESI-HRMS analysis, we performed MSMS-fragmentation experiments. The detection of the analytical fragment  $m/z$  262.127 from the *in vivo* and *in vitro* analyte strengthens the identification that UGT76B1 synthesizes NHP-OGlc. Holmes and colleagues supply additional evidence by MSMS-fragmentation combined with trimethylsilyldiazomethane derivatization that selectively methylates carboxylic acids also underlining NHP-OGlc as product of UGT76B1 (Holmes et al., 2021). Additionally, the NHP-glycoside signal annotated to be UGT76B1-dependent was not used by esterase treatment, suggesting NHP-OGlc, in the studies conducted by Bauer and colleagues (Bauer et al., 2021). Several approaches underlined the functional characterization of UGT76B1 to synthesized NHP-OGlc from NHP. Nevertheless, an authentic standard would still be required to unambiguously assign the NHP-OGlc mass spectrometric signal (Holmes et al., 2021).

### 6.1.2 Heterologous expression and *in vitro* data support UGT76B1 function

To gain further insight into the ability of UGT76B1 to glycosylate NHP several *in vitro* strategies were addressed by different working groups. On the one hand, heterologous expression, enzyme purification and *in vitro* enzyme reactions were conducted. In the reaction assays with purified UGT76B1 enzyme, NHP substrate and UDP-Glc resulted in successful detection of NHP-OGlc compared to their respective no enzyme controls (Bauer et al., 2021; Cai et al., 2021; Holmes et al., 2021; Mohnike et al., 2021). On the other hand, heterologous expression of gene products, responsible for NHP and NHP-OGlc biosynthesis were conducted in different plant systems. Cai and colleagues performed NHP supplementation studies to yeast cells expressing *UGT76B1* or an empty vector control, leading to NHP-OGlc formation in the sample combining *UGT76B1* expression and NHP supplementation (Cai et al., 2021). In addition, heterologous expression of NHP or NHP-OGlc synthesis genes *ALD1*, *SARD4*, *FMO1* and *ALD1*, *SARD4*, *FMO1*, *UGT76B1*, respectively, resulting in their enzyme products, were conducted in *Nicotiana benthamiana*. NHP and NHP-OGlc synthesis was observed in the respective trials, which was increased by lysine supplementation (Cai et al., 2021). Strikingly they were able to detect NHP-OGlc from the *N. benthamiana* samples expressing the set NHP-biosynthesis genes supplemented with lysine only (Cai et al., 2021). This suggests the presence of a native UGT from *N. benthamiana* to use NHP as substrate. Holmes and colleagues chose a similar approach of heterologous expression of NHP and NHP-OGlc pathway genes in *Solanum lycopersicum*. Via successful heterologous expression of *ALD1* and *FMO1*, producing their respective gene products, the group was able to detect Pip and NHP, respectively. Similarly, they successfully detected NHP-OGlc when heterologous expression of *ALD1*, *FMO1* and *UGT76B1* was performed (Holmes et al., 2021). What is more is that they describe SA-accumulation from tomato leaves expressing genes of the NHP-biosynthesis pathway without *UGT76B1*. However, when combining the genes of NHP-biosynthesis with *UGT76B1*, SA-signal intensities are reduced again and SAG-signal intensities increased significantly (Holmes et al., 2021). Together with the metabolite analysis of *ugt76b1* mutant plants, purified UGT76B1 and heterologous expression systems, the role of UGT76B1 in glycoside formation of NHP, in addition to SA was identified.

### 6.1.3 Functional *FMO1* is required for *ugt76b1* phenotypic characteristics

The *ugt76b1* mutant of *A. thaliana* was described to exhibit reduced growth, enhanced resistance to *P. synrigae* and enhanced susceptibility to *A. brassicicola* (von Saint Paul et al., 2011). Additionally, it was reported to exhibit early senescence (von Saint Paul et al., 2011).

To connect the novel insight about NHP-glycosylation by UGT76B1 to the phenotypic characteristics of *ugt76b1-1* mutant plants, NHP deficient *fmo1 ugt76b1* double mutants were investigated. Neither in our study nor Bauer and colleagues were able to detect NHP-accumulation in *fmo1 ugt76b1* double mutants (Bauer et al., 2021; Mohnike et al., 2021). Similarly, the enhanced resistance phenotype of *ugt76b1* was not observed in the double mutants, which exhibit *fmo1*-like susceptibility towards two different *Pseudomonas* strains pv. tomato DC3000 and *P.s.m.* (Bauer et al., 2021; Mohnike et al., 2021). These data show the influence of *FMO1* and NHP on enhanced resistance. An enhanced resistance phenotype is often connected to reduced growth, which was already described for *ugt76b1-1* (von Saint Paul et al., 2011). In this study, we underline reduced growth of *ugt76b1* with different mutant alleles. Similarly, the growth phenotype was reproduced analyzing the diameter of the rosette leaves and fresh weight in comparison between wild type, *ugt76b1* and *UGT76B1-OE1* (overexpression) plants, resulting in significantly smaller plants having a reduced weight when *ugt76b1* was mutated (Cai et al., 2021). To investigate the role of *FMO1* and NHP on the reduced growth phenotype of *ugt76b1* mutants we compared them with *fmo1 ugt76b1* double mutants. In comparison to the reduced growth of three independent *ugt76b1* lines, *fmo1 ugt76b1* double mutant plants grow bigger than the single mutant does. Indicating an influence of *FMO1* and NHP on the balance between immunity and growth. In terms of the early senescence phenotype described by von St. Paul and coworkers the cell death phenotype of *N. benthamiana* leaves, expressing NHP-biosynthesis genes suggests an influence of NHP on the regulation of cell death. In comparison to the expression of NHP-OGlc biosynthetic genes, the expression of *UGT76B1* abolishes cell death. In conclusion, *UGT76B1* and NHP have an influence on senescence exhibited as cell death (von Saint Paul et al., 2011; Cai et al., 2021). However, a direct connection of NHP-OGlc to delayed senescence is not supported by experimental data. Similarly, the direct effects of NHP-OGlc on growth promotion remain unclear.

#### 6.1.4 Outlook to NHP, UGT76B1 and NHP-glucosides influences on plant health

In terms of a mobile signal to induce SAR, evidence for NHP-mobility has been collected over the last couple of years. NHP was shown to move systemically and to induce SAR in several experimental setups (Chen et al., 2018; Schnake et al., 2020; Mohnike et al., 2021). Whether NHP-OGlc fulfills a function in immune signal distribution and if a hydrolysis to NHP is happening *in vivo*, remains to be investigated. The tracking experiment we performed with D<sub>9</sub>-NHP and NHP suggests for NHP mobility without further need of O-glycosylation, as D<sub>9</sub>-NHP was successfully detected in systemic tissue of locally infiltrated *ugt76b1-1* mutants.

Nevertheless, glycosides are proposed to exhibit enhanced solubility, which may be beneficial for transport through the vasculature. Additionally, the external application of NHP may not resemble the physiological state since the signal is not generated endogenously at the correct time point and location. Therefore, no information about the requirements of NHP-OGlc for cellular export, for example, can be drawn. Furthermore, the role of NHPGE in NHP-distribution remains elusive and if it could carry out the function of a mobile signal in *ugt76b1-1* background. Unfortunately, we were not able to follow NHP-OGlc or NHPGE by external application, due to the lack of authentic standards. However, we were able to show *in vitro* activity of UGT74F2 that exhibited glycoside-ester forming activity with NHP to result in formation of NHPGE. The enzymatic reaction was used to confirm the retention time difference between NHPGE and NHP-OGlc (Supplemental Figure 1). Interestingly, UGT74F2 has also been reported to glycosylate NAM, the product of TIR-domain mediated NAD-cleavage (Li et al., 2015). However, for future research it would be interesting to see, if NHP-glycosides are systemically mobile, and if they can be hydrolyzed into the active NHP-signal. After the identification of the NHP-GE forming UGT *in vivo*, a double mutant may answer the question of NHP-mobility excluding any kind of NHP-glycoside.

Additionally, NHP-OGlc may be a candidate for external application to induce defense response in crop plants. For SAG, it has been shown to be a mild alternative to SA, to induce plant protection. SAG-application shows in comparison to SA a lower rate of induction of PR-gene expression and ROS-levels, but it is nevertheless able to enhance defense resistance against *Pseudomonas* (Swayambhu et al., 2021). Whether NHP-OGlc has similar traits, will have to be investigated.

Another interesting aspect is the fact that *UGT76B1*-expression was high in roots and that it showed expressional changes upon abiotic stresses as mentioned above (von Saint Paul et al., 2011). It would be interesting to investigate the role of UGT76B1 for the root metabolome and to further identify whether these molecular changes have an influence on stress responses. The observation that *UGT76B1*-expression was induced when *Arabidopsis* plants were transferred from iron deficient to iron sufficient medium suggests for a possible role in iron homeostasis (Schuler et al., 2011; Koen et al., 2014). We tested UGT76B1 activity with scopoletin *in vitro* and were able to detect the glycoside scopolin (Supplemental Figure 2). It can be speculated that UGT76B1 may be involved in the biosynthesis of scopolin in roots. Its aglycon scopoletin was shown to chelate iron (Nakano et al., 2014). The coumarin scopolin was additionally shown to influence the root microbiome, which would open a vast new field for UGT76B1 influence on plant fitness (Stringlis et al., 2018). The root microbiome was shown to play a significant role in plant fitness and protection in plant-pathogen interactions (Haney

et al., 2015). Moreover, it will be interesting to analyze whether UGT76B1 plays a role in root to shoot signaling.

Remaining questions are the subcellular localization about the activation of Pip by FMO1 and inactivation of NHP by UGT76B1 (Zeier, 2021). Additionally, the translation of the NHP-signal into gene expression and metabolite remodeling remains unknown, as no receptor protein has been described in the literature so far. The shared modus of inactivation of SA and NHP by UGT76B1 suggests a tight interplay between the two active compounds. However, it can only be speculated, if the SA-receptor NPR1 plays a role in NHP-recognition. So far, attempts to study binding kinetics between NHP and NPR1 did not suggest that SA and NHP share this signaling hub (Nair et al., 2021). Furthermore, the ability to sense NHP-concentration by the transcriptional corepressors NPR3/4 has not been investigated. It remains therefore unclear how NHP is perceived in local and systemic tissue. Another interesting question to answer in the future will be, if the NHP- and SA-glycosides may resemble a molecular “immune memory”. In a long-term SAR experiment, it would be interesting to see, if the glycosides are stored and whether, they are hydrolyzed back into SA or NHP, respectively, upon secondary infection. This may be a fast way to enhance the cellular concentration of SA and NHP compared to *de novo* synthesis (Jones and Vogt, 2001).

Concluding our studies about UGT76B1 and the formation of NHP-OGlc, we decided to investigate and uncover other molecules involved in NHP-turnover.

## 6.2 Novel NHP-metabolites as candidates for plant priming, storage or degradation?

With an established workflow to induce immune metabolism and the NHP-deficient mutant *fmo1-1* in hand, we began to investigate comparisons between stressed wild type plants against *fmo1-1* (Chapter II). We aimed to detect molecular differences in non-targeted metabolome datasets. To this point, no other NHP-metabolite than NHP-OGlc was described by other research groups (Chen et al., 2018). Throughout the ongoing of this thesis, an additional metabolite namely NHP-GE was shown to be synthesized in Arabidopsis in response to *P. syringae* treatment (Bauer et al., 2021). Its molecular identity as glucoside ester was demonstrated using esterase treatment (Bauer et al., 2021). The treatment did only reduce one of the two NHP-glycosides associated signals, leading to annotation of the respective site of glycosylation (Bauer et al., 2021).

Initially, we investigated into NHP-modifications with a focus on described modifications of other well-studied plant hormones, like SA and JA in a targeted manner (Wasternack and Hause, 2013; Zeier, 2021). Those modifications were methylation, hydroxylation or amino acid conjugation. Following that strategy we were able to identify a signal in wild-type, but not *fmo1-1* plants, with an accurate ion mass of  $[M+H]^+$  160.097 that matched our exact mass prediction for methylated NHP. To that point, we were not able to discriminate between the carboxy and the hydroxy function of NHP as sites of methylation by MSMS-fragmentation. An approach to methylate NHP resulted in more than one signal in the chromatogram, which did not contribute to a successful identification of the site of methylation. Similarly, selective chemical methylation of NHP did not appear to be trivial, as there is no available synthesis route and guarding of either hydroxyl or carboxy group was not easily feasible. Chen and coworkers described a chemical hydroxylation mechanism using Pip resulting in NHP (Chen et al., 2018). This led us to follow the idea to pass on from chemical methylation of NHP and to perform hydroxylation on a commercially available methyl pipecolate. A new scheme for the respective chemical synthesis of NHP-methyl ester was developed via *N*-(2-cyanoethyl)-methylpipecolate. Indeed NMR confirmed the chemical structure of the pure MeNHP-standard. Comparing retention time and the MSMS-spectra of the *in vivo* substance to the authentic MeNHP-standard, we were able to confirm the presence of MeNHP, which is a NHP-methyl ester in Arabidopsis. *In planta*, MeNHP is synthesized in response to *P.s.m.* infection and UV-C treatment.

In order to search for NHP-derived metabolites in a non-targeted manner we designed a co-infiltration experiment of NHP and D<sub>9</sub>-NHP. The idea for that experiment was given by an approach described by Yu and coworkers (Yu et al., 2021b). The researchers applied a mixture of stably labeled nematode pheromone together with their unlabeled native substance to track metabolite turnover of the pheromone in different organisms (Yu et al., 2021b). In our approach, we searched in the MS dataset for compound pairs, which show a characteristic mass shift of 9.056 Da resulting from D<sub>9</sub>. To tackle the question, if the NHP-derived molecules are also present in native, non-NHP/D<sub>9</sub>-NHP-infiltrated plants, we included an UV-C treatment. We were able to describe several additional NHP-derived metabolites that were lacking in the *fmo1-1* and *ugt76b1-1* mutants but were present after stress in wild type plants. The molecules besides MeNHP were the complex glucosides, NHP-OGlc-Hex and NHP-OGlcMal. We were not only able to describe the metabolites in the infiltrated tissue, but in the UV-C treated plants without of NHP-infiltration. This again confirms their synthesis *in vivo*. The control conditions of the experiment excluded that the discovered metabolites are artefacts due to the external application of NHP and D<sub>9</sub>-NHP. The detection of NHP-OGlc-Hex was supported by exact mass information exhibiting the in source fragment *m/z* 308.134 corresponding to NHP-OGlc and UGT76B1-dependancy. However, we were not able to confirm the identification via an



enzymatic synthesis of the compound or authentic standard validation. Nevertheless, diglycosides were already described as for example the flavonol-3,7-*O*-glycosides (Ablajan et al., 2006). Plant-derived compounds containing an acylated glucose have also already been described as for example medicarpin-3-*O*-glucosides-6''-*O*-malonate and the flavonoid genistein-7-*O*-glucoside being malonylated (Kessmann et al., 1990; Kachlicki et al., 2008). Another example is the major anthocyanin purified from *Arabidopsis* that exhibited a glucose residue acylated with malonic acid (Bloor and Abrahams, 2002). Possienke described in her doctoral thesis the MSMS-fragmentation behavior of the malonic acid acylated compound 1-(6-*O*-malonyl- $\beta$ -D-glucopyranosyl)-2-mercapto-1*H*-indole-3-carboxylic acid and detected a similar fragment of *m/z* 87 describing malonic acid [C<sub>3</sub>H<sub>3</sub>O<sub>3</sub>]<sup>+</sup>, as earlier described for NHP-OGlcMal (Chapter II) (Possienke, 2012). With respect to the biosynthesis of malonyl acylated compounds a malonyl transferase for the anthocyanidin-5-*O*-glucoside was described in *Arabidopsis* (D'Auria et al., 2007). Matern and coworkers were able to show that flavonoids uptake into parsley vacuoles was dependent on acylation of glycosides (Matern et al., 1986). By comparing labeled [2-<sup>14</sup>C] apigenin-7-*O*-glucoside uptake with [2-<sup>14</sup>C] apigenin-7-*O*-(6-*O*-malonylglucoside) into isolated vacuoles they were able to show rapid accumulation by the acylated substance (Matern et al., 1986). Hopp and Seitz made a similar observation showing that [<sup>3</sup>H] deacylated anthocyanin was taken up at lower rates than [<sup>3</sup>H] anthocyanin into isolated vacuoles from *Daucus carota* (Hopp and Seitz, 1987). Maybe the newly described NHP-OGlcMal compound plays a role in NHP degradation or storage in the vacuole.

To get further ideas about the physiological relevance of these newly described compounds we investigated the appearance of NHP and its metabolites over a time-course after UV-C treatment (Supplemental Figure 3). Similarly, we recorded data for SA and SAG to investigate SA and SAG occurrence over time (Supplemental Figure 4). The time-course of UV treatment reveals that MeNHP has a similar pattern of accumulation as NHP-OGlc, beginning at 8 hpUV (Supplemental Figure 3A). The accumulation of NHP-OGlc and MeNHP follows the initial enrichment of NHP 6 hours post UV treatment. The time course of UV-C induced metabolism may indicate that MeNHP-synthesis goes in line with NHP-OGlc synthesis, suggesting to be an additional or even alternative mechanism of metabolic turnover to control the NHP concentration. NHP-methylation as mode of inactivation may be seen in analogy to the methylation of SA by BSMT1 (Chen et al., 2003). The overexpression of *OsBSMT1* from rice in transgenic *Arabidopsis* lead to a decrease in SA mediated resistance to the biotrophic pathogen *Globinomyces orontii* (Koo et al., 2007). The two UGT76B1-dependent, therefore NHP-OGlc-derived metabolites, NHP-OGlc-Hex and NHP-OGlcMal, began to accumulate 10 hpUV (Supplemental Figure 3B). Their levels were clearly increased up to 24 hpUV treatment. This trend may hint towards their role in degradation or storage. To investigate even

later time points like 48 hpUV or 72 hpUV may give an idea, if these metabolites will be degraded or are constantly accumulating after stress, which would suggest for storage. In parallel, we also monitored SA and SAG-accumulation over the first 24 hpUV treatment. SA levels increase already 2 hpUV until 6 hpUV (Supplemental Figure 4). Interestingly, SA signal intensity again decreased 8 hours and 10 hours post UV. At 24 hpUV, the signal intensities were equal to the ones from 6 hpUV again. SAG levels began to increase from 8 hpUV and continuously increased 24 hpUV. It can be speculated that the circadian rhythm could have an influence on SA concentration (Zhang et al., 2019). Griebel and Zeier have also reported a daytime dependency to plant immunity in response to infection (Griebel and Zeier, 2008).

An obvious question in respect to the newly identified compound MeNHP was, if MeNHP plays an active role in the NHP-mediated processes of plant immunity. For MeJA it was reported that it successfully recovered fertility in JA-insufficient plants (Park et al., 2002). Furthermore, MeSA application can induce SA-mediated resistance (Shulaev et al., 1997; Park et al., 2007). To test the influence of MeNHP on Arabidopsis disease resistance phenotype, we applied MeNHP to wild type and *fmo1-1* mutant plants. Our experimental setup aimed to identify whether MeNHP-application, arguably due to hydrolysis to NHP, is able to rescue the *fmo1-1* susceptibility phenotype to *H.a. Noco 2* and whether it is able to induce defense responses in wild type. The observation that both wild type and *fmo1-1* mutant plants exhibited reduced spore growth of the oomycete pathogen underlined a role of MeNHP in plant immunity. Whether it may play a role in transport or storage of the NHP-signal remains to be uncovered. Furthermore, if MeNHP has the potential to induce systemic resistance as volatile is unknown too. This would harbor unknown modes of action for the novel metabolite. MeJA for example was found as volatile emitted by sagebrush and connected to interplant communication (Baldwin et al., 2006). What we could clearly show is that MeNHP can be hydrolyzed to NHP in Arabidopsis, as we were able to rescue NHP-levels in the biosynthesis deficient mutant *fmo1-1* by MeNHP-application. Tamogami and colleagues made a similar observation with MeJA when tracking D<sub>2</sub>-labeled MeJA. They observed labeled D<sub>2</sub>-JA, as well as, the labeled JA amino acid conjugates D<sub>2</sub>-JA-Ile and D<sub>2</sub>-JA-Leu from plant extracts after treatment with D<sub>2</sub>-labeled MeJA (Tamogami et al., 2008). The external application of MeJA enhanced plant resistance against herbivores (Wu et al., 2008). In addition, it resulted in changes of the phenolic acid content in poplar leaves (An et al., 2006). In analogy to MeSAGlc, which biosynthesis is dependent on UGT71C3 we were able to describe MeNHP-OGlc after external application of MeNHP to Arabidopsis (Chen et al., 2019). We hypothesize that MeNHP-OGlc is a result of reducing the artificially high cellular MeNHP-concentration after infiltration. In accordance therewith, we were not able to detect MeNHP-OGlc upon infection or UV-stress in our experiments. However, we could confirm the identity of MeNHP-OGlc from the MeNHP-infiltration experiment with an *in vitro* reaction assay of MeNHP with UGT74F1. By

---

UHPLC-ESI-HRMS-analyses it was shown, that the reaction product co-eluted showing the same exact mass information as the MeNHP-OGlc signal obtained from the infection or UV-stress experiments.

Nevertheless, many questions remain unanswered concerning the biosynthesis, function and metabolite network of MeNHP. We were not able to present *in vivo* data about the biosynthesis of MeNHP in Arabidopsis. A promising candidate for MeNHP-biosynthesis was NHPMT1. It was identified by co-expression network analysis with *UGT76B1* and was determined to be Pip and NHP-responsive (Bernsdorff et al., 2016; Yildiz et al., 2021). Additionally, *NHPMT1* expression was induced in response to H<sub>2</sub>O<sub>2</sub> (Inzé et al., 2012). Furthermore, the fact that the *nhpmt1* mutant plants were less sensitive to UV-stress let the gene to appear as a suitable candidate (Piofczyk et al., 2015). The investigated recombinant enzyme NHPMT1 showed indeed *in vitro* activity with NHP as substrate and gave us an additional layer of evidence for MeNHP-identification. However, the analysis of *nhpmt1-1* and *nhpmt1-2* mutants, as well as, *nhpmt1-1 ugt76b1* double mutant lines led us to decline the hypothesis that NHPMT1 is solely responsible for the biosynthesis of MeNHP *in vivo*. However, it could be hypothesized, that redundancies in MeNHP-synthesizing MTs are present and that several NHPMTs including NHPMT1 are involved in MeNHP biosynthesis. Nevertheless, the closest homologue of *NHPMT1*, NHPMT1-like (*At5G10830*), did not show *in vitro* activity with NHP. Similarly, we were not able to detect *in vitro* activity with heterologously expressed and purified BSMT1 that is responsible for the biosynthesis of MeSA. Activity with NHP was even not detected after the addition of divalent cations, which reportedly are required for several MT enzymes (Chen et al., 2003; Chatterjee et al., 2015). Nevertheless, after another search for candidate MTs in a transcriptomics data set of Pip and NHP treated leaves by Bernsdorff and Yildiz, respectively, we found another candidate gene *At1G6670*. The gene is annotated as *Paraxanthin methyltransferase 1 (PXMT1)*, however its transcripts were responsive to NHP-treatment (Bernsdorff et al., 2016; Yildiz et al., 2021). We cloned the coding sequence of full length *PXMT1* into pET28a expression vector and heterologously expressed the enzyme in *E. coli*. After successful purification, we tested its activity with NHP *in vitro* and detected MeNHP in the enzymatic assay (Supplemental Figure 5). Therefore, redundancies in the biosynthesis of the novel described NHP metabolite MeNHP increase the challenges to unravel its biosynthesis in plants. However, at this point I would like to mention that to establish an *in vivo* relationship between an enzyme and a product molecule depends on several additional parameters, like compartmentalization, or local substrate availability and is not always as straight forward as the detection of an *in vitro* activity successfully converting the added substrate. It will be interesting to investigate the MeNHP chemotype of *pxmt1* mutant plants to challenge, if it might play a role in the *in vivo* synthesis in Arabidopsis. In addition, the

---

*nhpmt1-1 pxmt1* double mutant should be generated to confirm if redundancy in MeNHP-synthesizing MTs are of relevance *in planta*.

Another open question are target proteins and enzyme(s) responsible for MeNHP-signaling and hydrolysis to NHP. In 2005, Forouhar and coworkers described the MES for MeSA in tobacco, namely, SABP2 (Forouhar et al., 2005). Several MES-candidate genes were described in Arabidopsis, which are similar to the described SABP2 (Vlot et al., 2008). In addition, the MeJA-esterase belongs to the MES family (Koo et al., 2013). The enzyme family appears to be a likely target to investigate functional MeNHP-hydrolysis, possibly able to reactivate the NHP-signal without the need of *de novo* synthesis. Especially, because MES exhibit a broad substrate range (Koo et al., 2013). The discovery of MeNHP-biosynthesis now is a prerequisite to investigate its role in defense responses and SAR.

In conclusion, we were able to describe novel molecules of NHP-turnover. Applying a targeted search for NHP-modifications and an unbiased NHP/D<sub>9</sub>-NHP-co-infiltration experiment, we were able to detect so far unknown NHP-derived metabolites. Via authentic standard, MSMS-analyses and *in vitro* synthesis using enzymes with described ability to form O-glycosides or glycoside-esters we were able to strengthen compound identification. We demonstrated that MeNHP has the potential to induce resistance upon external application and that it can be converted into MeNHP-OGlc. However, if MeNHP plays a role in NHP-inactivation, its storage and/or transport needs to be investigated. Similarly, the role of complex glycosides, like NHP-OGlcHex and NHP-OGlcMal, as well as, their unambiguous structural characterization remains to be uncovered.

### 6.3 The exporter of Pip from the chloroplast remains unknown

After the annotation of FMO1 to be responsible for NHP biosynthesis by Chen and coworkers and Hartmann and coworkers in 2018, the open question about the chloroplast-localized exporter required for NHP synthesis remained open. It was suggested that both SA and NHP biosynthesis might be dependent on functional EDS5. To share an export hub like EDS5 would allow the plant to control both biosynthetic pathways simultaneously. As EDS5 was proposed to be relevant for the chloroplastial export during NHP biosynthesis in Arabidopsis, we investigated into its potential analyzing *eds5-2* mutant plants in response to UV-C treatment. However, we were not able to confirm the observation, when we investigated the *eds5-2* allele (Chapter III). We therefore decided to investigate into the EDS5H, which had been reported to not play a role in chloroplast export of isochorismate during SA-biosynthesis (Parinthawong et al., 2015). Nevertheless, the metabolite analysis of UV-C treated Col-0 and *eds5h* mutant

plants let us conclude that also EDS5H does not solely contribute to NHP-biosynthesis. We detected a similar behavior for the other transporters investigated like ALF5 and LHT7, which were shown to be responsive to *P.s.m.* infection. LHT7 in addition was an interesting candidate as it is annotated as lysine and histidine transporter, and Pip/NHP are lysine-derived metabolites that resemble a ring like structure, however not identical, as histidine. Neither the analysis of *alf5*, nor *lht7* mutant plants after UV-C treatment, let suggest to be responsible for Pip export. Therefore, we can concluded that either the Pip exporter, which might alone be responsible, has not been discovered, or that several transporters share functional redundancies. To that point, we cannot answer this question. Maybe in the future, a transporter candidate will arise from a forward genetic screen that can be functionally connected to NHP biosynthesis.

## 6.4 Future perspectives in plant immunity

The constant strive for knowledge coupled with technical innovation of laboratory instruments is a driving force in molecular research. The upcoming field of machine learning will allow in-depth metabolite analysis and identification in the future, to challenge complex metabolic networks in the context of an individual organism. Moreover, it will be a challenge to implement the information about a single organism into a more global community-based context, as for example the interplay between a plant and its associated microbial community (Haney et al., 2015; Shalev et al., 2022). The resulting metabolic networks can answer questions about symbiotic relations beneficial for both plant and microbes. Furthermore, it will be in scope to describe protein-protein interactions mechanistically to gain insight in signaling cascades and enzymatic activity (Martin et al., 2020; Bi et al., 2021; Kumar et al., 2022). To implement the gathered knowledge, to develop resilient crop plants for future generations will be the major challenge in a quickly changing environment.

Under controlled laboratory conditions, it may be feasible to pin down a single gene's functions to a distinct thread. This may lead to unravel signaling pathways and immune responses. However, in a field with a changing environment and multiple influences at a time the analysis of a plants immune response will be challenging. The fact that several stressors may threat a plant simultaneously requires strictly regulated pathways that depend on a tight interplay. The complexity of different influences on the plant fitness suggests that general defense mechanisms for activation and inactivation maybe useful, as for example *UGT76B1* transcription is upregulated upon diverse abiotic and biotic stresses (von Saint Paul et al., 2011). However, to explain response mechanisms of plants may not be as straight forward as the model that SA/NHP confer the response to biotrophic pathogens and JA/ET the response

to necrotrophic pathogen suggests (Thomma et al., 1998; Glazebrook, 2005). For example insect eggs of *Pieris brassicae* trigger systemic resistance against both necrotrophic *Botrytis cinerea* and (hemi-)biotrophic *P. syringae* and oomycete *H.a. Noco 2* (Alfonso et al., 2021). Oviposition of *P. brassicae* triggers SA and Pip accumulation in Arabidopsis (Bruessow et al., 2010; Hilfiker et al., 2014). Furthermore, oviposition triggers SAR against different *P. syringae* strains on the host and on neighboring plants (Hilfiker et al., 2014; Orlovskis and Reymond, 2020). Alfonso and colleagues connected the activation of defense responses to oviposition and egg-extract treatment with SA and NHP dependency (Alfonso et al., 2021). This observation matches the model that SAR depends on both NHP and SA. Nevertheless, it is surprising that a necrotrophic pathogen like *Botrytis* is challenged by this immune response. The authors suggest involvement of tryptophan-derived molecules, like camalexin, showing that the biosynthesis deficient mutant *phytoalexin deficient 3 (pad3)* is unable to establish successful defense (Alfonso et al., 2021). This example, however illustrates the diversity and complexity of responses contributing to successful defense. Liu and coworkers investigated into a similar direction to understand SA and JA-crosstalk in the response to biotrophic pathogens (Liu et al., 2016). They were able to show that the SA-receptor molecules NPR3 and NPR4 are able to interact with JAZ-proteins promoting JAZ-degradation, therefore activating a JA-mediated defense response (Liu et al., 2016). Which, appears to be counter intuitive, taking SA and JA-antagonism into account. Nevertheless, the authors argue that activation of both pathways enables PCD against the invading biotrophic pathogen, without increased vulnerability against necrotrophic pathogens (Liu et al., 2016). This model would also allow to explain the observations by Alfonso and colleagues of successful resistance against both biotrophes and necrotrophes, who identified *npr1-1*, SA- and NHP-signaling to be required for the successful immune response against *Botrytis*. SA and Pip treatment alone however, was insufficient to induce resistance against *Botrytis* (Alfonso et al., 2021). In conclusion, it will be a future goal to further understand these mechanisms in response to complex stresses and to be clear about individual specificities when comparing one and other organisms.

State-of-the-art structural biochemistry methods like cryo-electron microscopy in combination with x-ray crystallography allow investigating protein complexes in ligand-bound states and protein-protein interactions. Recent insight into the structural basis of NPR1 in TGA-mediated transcriptional reprogramming suggests a tandem-like dimer conformation to bind two proximate *activation sequence-1* promoter elements (Kumar et al., 2022). The dimeric NPR1 bridging two fatty-acid-bound TGA3 dimers forming an “enhanceosome” adds a novel aspect to understanding NPR1-mediated immunity (Kumar et al., 2022). Furthermore, it is another example of multi protein complexes that contribute to plant immunity. In the plant immunity field, it comes into focus to understand protein-protein interactions that lead to novel functions

including but also beyond enzymatic activity in the context of resistosomes. As already mentioned during the introduction, CNL-resistosomes are multi protein complexes able to form pores in the plasma membrane to enable calcium fluxes (Bi et al., 2021). Similarly, TNL-resistosomes were shown to gain novel enzymatic functions when oligomerized (Horsefield et al., 2019; Wan et al., 2019b). Due to this recent research progress there are still novel defense related compounds discovered. The AMP-based molecules, which production is catalyzed by TIR-containing proteins, 2'-(5''-phosphoribosyl)-5'-adenosine mono-/di-phosphate (pRib-AMP/ADP), are proposed to interact directly with the central protein complex EDS1-PAD4 (Huang et al., 2022). The interaction results in conformational changes in the complex and enables enhanced protein-protein interaction with the helper NLR ACTIVATED DISEASE RESISTANCE 1-LIKE 1 (ADR1-L1) (Huang et al., 2022). Jet two other molecules, ADP-ribosylated-ATP and di-ADP-ribose, specifically bind to EDS1-SAG101 to promote N REQUIREMENT GENE 1A (NRG1A)-interaction (Jia et al., 2022). The phenomenon to make use of cADPR to overcome infection appears to be conserved in different kingdoms. Bacterial organisms share a common defense mechanism against virus infection (Leavitt et al., 2022).

To detect and describe the plethora of metabolites within an organism responding to stress, will be a major task for the future in metabolomics. So far, some metabolites as for example complex phosphorylated molecules are still hard to detect. In addition, compound identification is still a major challenge in non-targeted mass spectrometry. Novel approaches combining LC-MS with nuclear magnetic resonance spectroscopy may allow broad-spectrum compound identification and annotation in the future (Letertre et al., 2020). Until now, it was not possible to describe a whole metabolome for any organism (Viant et al., 2017). However, continues progress in the development of mass spectrometry based analytics including standardized data deposition in repositories will enhance data interpretation in the future (Haug et al., 2017; Alseekh et al., 2021). Furthermore, multi omics approaches combining transcriptome with metabolome analysis already enable system interpretation at several layers of information, and will be helpful to understand complex relationships, especially analyzing plants in the field (Kasper et al., 2022). Designing experimental setups to detect novel metabolites, by providing a pair of native and the respective labelled compound, like the co-infiltration studies performed in this work are an additional way to identify novel metabolites and to tackle identification.

## 6.5 Concluding remarks

All things considered, research on plant immunity is still a fast growing and developing field, trying to focus on linear mechanisms in response to distinct stresses. Still not everything is clear, understanding the linear routes of signal transduction, however great progress has been achieved since the discovery that SA is a central molecule in immune responses against biotrophic pathogens. The discovery and annotation of Pip and NHP to fulfill a role in the immune network marks another achievement. Today we have a general understanding of pathogen recognition and cellular response mechanisms. In addition, we mostly understand biosynthetic routes of pathogen resistance mediating hormones SA, Pip/NHP and JA-Ile. In terms of SA or JA-Ile, we understand routes of signal proliferation via NPR1 and NPR3/4 or the SCF/COI1 protein complexes, respectively. So far, no receptor complex for Pip or NHP was described. Similarly, the downstream metabolic networks of SA and JA were intensively described, including most of the responsible enzymes for turnover. Recent identification of UGT76B1 as the enzyme synthesizing NHP-OGlc marks the first enzyme to metabolize NHP to NHP-OGlc. By mutant analyses, it could be shown that UGT76B1 has a great impact on plant immunity. By the identification of NHP-GE, MeNHP and NHP complex glycosides, the field is now open to investigate the enzymatic routes and function of downstream molecules.



---

## 7. References

- Ablajan, K., Abliz, Z., Shang, X.Y., He, J.M., Zhang, R.P., and Shi, J.G.** (2006). Structural characterization of flavonol 3,7-di-O-glycosides and determination of the glycosylation position by using negative ion electrospray ionization tandem mass spectrometry. *J Mass Spectrom* **41**, 352-360.
- Albesa-Jové, D., and Guerin, M.E.** (2016). The conformational plasticity of glycosyltransferases. *Curr. Opin. Struc. Biol.* **40**, 23-32.
- Alfonso, E., Stahl, E., Glauser, G., Bellani, E., Raaymakers, T.M., Van den Ackerveken, G., Zeier, J., and Reymond, P.** (2021). Insect eggs trigger systemic acquired resistance against a fungal and an oomycete pathogen. *New Phytol.* **232**, 2491-2505.
- Alseikh, S., and Fernie, A.R.** (2018). Metabolomics 20 years on: what have we learned and what hurdles remain? *Plant J.* **94**, 933-942.
- Alseikh, S., Aharoni, A., Brotman, Y., Contrepois, K., D'Auria, J., Ewald, J., C. Ewald, J., Fraser, P.D., Giavalisco, P., Hall, R.D., Heinemann, M., Link, H., Luo, J., Neumann, S., Nielsen, J., Perez de Souza, L., Saito, K., Sauer, U., Schroeder, F.C., Schuster, S., Siuzdak, G., Skirycz, A., Sumner, L.W., Snyder, M.P., Tang, H., Tohge, T., Wang, Y., Wen, W., Wu, S., Xu, G., Zamboni, N., and Fernie, A.R.** (2021). Mass spectrometry-based metabolomics: a guide for annotation, quantification and best reporting practices. *Nat. Meth.* **18**, 747-756.
- An, Y., Shen, Y.-b., Wu, L.-j., and Zhang, Z.-x.** (2006). A change of phenolic acids content in poplar leaves induced by methyl salicylate and methyl jasmonate. *Journal of Forestry Research* **17**, 107-110.
- Atkinson, N.J., and Urwin, P.E.** (2012). The interaction of plant biotic and abiotic stresses: from genes to the field. *J. Exp. Bot.* **63**, 3523-3543.
- Aziz, A., Heyraud, A., and Lambert, B.** (2004). Oligogalacturonide signal transduction, induction of defense-related responses and protection of grapevine against *Botrytis cinerea*. *Planta* **218**, 767-774.
- Baldwin, I.T., Halitschke, R., Paschold, A., von Dahl, C.C., and Preston, C.A.** (2006). Volatile Signaling in Plant-Plant Interactions: "Talking Trees" in the Genomics Era. *Science* **311**, 812-815.
- Banerjee, S., and Mazumdar, S.** (2012). Electrospray ionization mass spectrometry: a technique to access the information beyond the molecular weight of the analyte. *International Journal of Analytical Chemistry* **2012**.
- Banerjee, S.P., and Snyder, S.H.** (1973). Methyltetrahydrofolic acid mediates *N*- and *O*-methylation of biogenic amines. *Science* **182**, 74-75.
- Bauer, S., Mekonnen, D.W., Hartmann, M., Yildiz, I., Janowski, R., Lange, B., Geist, B., Zeier, J., and Schäffner, A.R.** (2021). UGT76B1, a promiscuous hub of small molecule-based immune signaling, glucosylates *N*-hydroxypipicolinic acid and balances plant immunity. *Plant Cell* **33**, 714-734.
- Bennett, R.N., and Wallsgrove, R.M.** (1994). Secondary metabolites in plant defence mechanisms. *New Phytol.* **127**, 617-633.
- Bernsdorff, F., Döring, A.-C., Gruner, K., Schuck, S., Bräutigam, A., and Zeier, J.** (2016). Pipicolinic acid orchestrates plant systemic acquired resistance and defense priming via salicylic acid-dependent and -independent pathways. *Plant Cell* **28**, 102-129.

- Bi, G., Su, M., Li, N., Liang, Y., Dang, S., Xu, J., Hu, M., Wang, J., Zou, M., and Deng, Y.** (2021). The ZAR1 resistosome is a calcium-permeable channel triggering plant immune signaling. *Cell* **184**, 3528-3541.
- Blanco, F., Salinas, P., Cecchini, N., Jordana, X., Van Hummelen, P., Alvarez, M., and Holuigue, L.** (2009). Early genomic responses to salicylic acid in *Arabidopsis*. *Plant Mol. Biol.* **70**, 79-102.
- Bloor, S.J., and Abrahams, S.** (2002). The structure of the major anthocyanin in *Arabidopsis thaliana*. *Phytochemistry* **59**, 343-346.
- Boller, T., and Felix, G.** (2009). A renaissance of elicitors: perception of microbe-associated molecular patterns and danger signals by pattern-recognition receptors. *Annu. Rev. Plant Biol.* **60**, 379-406.
- Bowles, D., Lim, E.-K., Poppenberger, B., and Vaistij, F.E.** (2006). Glycosyltransferases of lipophilic small molecules. *Annu. Rev. Plant Biol.* **57**, 567-597.
- Breton, C., Fournel-Gigleux, S., and Palcic, M.M.** (2012). Recent structures, evolution and mechanisms of glycosyltransferases. *Curr. Opin. Struc. Biol.* **22**, 540-549.
- Bruessow, F., Gouhier-Darimont, C., Buchala, A., Metraux, J.P., and Reymond, P.** (2010). Insect eggs suppress plant defence against chewing herbivores. *Plant J.* **62**, 876-885.
- Burdon, J.J., and Thrall, P.H.** (2009). Coevolution of plants and their pathogens in natural habitats. *Science* **324**, 755-756.
- Cai, J., Jozwiak, A., Holoidovsky, L., Meijler, M.M., Meir, S., Rogachev, I., and Aharoni, A.** (2021). Glycosylation of *N*-hydroxy-pipecolic acid equilibrates between systemic acquired resistance response and plant growth. *Mol. Plant* **14**, 440-455.
- Cao, H., Bowling, S.A., Gordon, A.S., and Dong, X.N.** (1994). Characterization of an *Arabidopsis* mutant that is nonresponsive to inducers of systemic acquired resistance. *Plant Cell* **6**, 1583-1592.
- Cao, H., Glazebrook, J., Clarke, J.D., Volko, S., and Dong, X.** (1997). The *Arabidopsis NPR1* Gene That Controls Systemic Acquired Resistance Encodes a Novel Protein Containing Ankyrin Repeats. *Cell* **88**, 57-63.
- Casanova-Sáez, R., Mateo-Bonmatí, E., Šimura, J., Pěňčík, A., Novák, O., Staswick, P., and Ljung, K.** (2022). Inactivation of the entire *Arabidopsis* group II GH3s confers tolerance to salinity and water deficit. *New Phytol.* **235**, 263-275.
- Chanda, B., Xia, Y., Mandal, M.K., Yu, K., Sekine, K., Gao, Q.-m., Selote, D., Hu, Y., Stromberg, A., Navarre, D., Kachroo, A., and Kachroo, P.** (2011). Glycerol-3-phosphate is a critical mobile inducer of systemic immunity in plants. *Nature genetics* **43**, 421-427.
- Chatterjee, D., Kudlinzki, D., Linhard, V., Saxena, K., Schieberr, U., Gande, S.L., Wurm, J.P., Wöhnert, J., Abele, R., and Rogov, V.V.** (2015). Structure and biophysical characterization of the *S*-adenosylmethionine-dependent *O*-methyltransferase PaMTH1, a putative enzyme accumulating during senescence of *Podospora anserina*. *J. Biol. Chem.* **290**, 16415-16430.
- Chen, F., D'Auria, J.C., Tholl, D., Ross, J.R., Gershenzon, J., Noel, J.P., and Pichersky, E.** (2003). An *Arabidopsis thaliana* gene for methylsalicylate biosynthesis, identified by a biochemical genomics approach, has a role in defense. *Plant J.* **36**, 577-588.
- Chen, H., Chen, J., Li, M., Chang, M., Xu, K., Shang, Z., Zhao, Y., Palmer, I., Zhang, Y., and McGill, J.** (2017). A bacterial type III effector targets the master regulator of salicylic acid signaling, NPR1, to subvert plant immunity. *Cell Host & Microbe* **22**, 777-788.

- Chen, L., Wang, W.-s., Wang, T., Meng, X.-f., Chen, T.-t., Huang, X.-x., Li, Y.-J., and Hou, B.-k. (2019). Methyl salicylate glucosylation regulates plant defense signalling and systemic acquired resistance. *Plant Physiol.* **180**, 2167–2181.
- Chen, Y.-C., Holmes, E.C., Rajniak, J., Kim, J.-G., Tang, S., Fischer, C.R., Mudgett, M.B., and Sattely, E.S. (2018). *N*-hydroxy-pipecolic acid is a mobile metabolite that induces systemic disease resistance in *Arabidopsis*. *Proc. Natl. Acad. Sci. USA* **115**, E4920-E4929.
- Chen, Y., Shen, H., Wang, M., Li, Q., and He, Z. (2013). Salicyloyl-aspartate synthesized by the acetyl-amido synthetase GH3.5 is a potential activator of plant immunity in *Arabidopsis*. *Acta Biochimica et Biophysica Sinica* **45**, 827-836.
- Chong, J., Wishart, D.S., and Xia, J. (2019). Using MetaboAnalyst 4.0 for Comprehensive and Integrative Metabolomics Data Analysis. *Current Protocols in Bioinformatics* **68**, e86.
- Claverie, J., Balacey, S., Lemaître-Guillier, C., Brulé, D., Chiltz, A., Granet, L., Noirot, E., Daire, X., Darblade, B., and Héloir, M.-C. (2018). The cell wall-derived xyloglucan is a new DAMP triggering plant immunity in *Vitis vinifera* and *Arabidopsis thaliana*. *Front. Plant Sci.* **9**, 1725.
- D'Auria, J.C., Chen, F., and Pichersky, E. (2003). Chapter eleven: The SABATH family of MTS in *Arabidopsis thaliana* and other plant species. In *Recent Advances in Phytochemistry* (Elsevier), pp. 253-283.
- D'Auria, J.C., Pichersky, E., Schaub, A., Hansel, A., and Gershenzon, J. (2007). Characterization of a BAHD acyltransferase responsible for producing the green leaf volatile (*Z*)-3-hexen-1-yl acetate in *Arabidopsis thaliana*. *Plant J.* **49**, 194-207.
- Dai, A. (2013). Increasing drought under global warming in observations and models. *Nature Climate Change* **3**, 52-58.
- de Vries, J., and Archibald, J.M. (2018). Plant evolution: landmarks on the path to terrestrial life. *New Phytol.* **217**, 1428-1434.
- Dean, J.V., and Delaney, S.P. (2008). Metabolism of salicylic acid in wild-type, *ugt74f1* and *ugt74f2* glucosyltransferase mutants of *Arabidopsis thaliana*. *Physiologia Plantarum* **132**, 417-425.
- Delaney, T.P., Uknes, S., Vernooij, B., Friedrich, L., Weymann, K., Negrotto, D., Gaffney, T., Gut-Rella, M., Kessmann, H., Ward, E., and Ryals, J. (1994). A central role of salicylic acid in plant disease resistance. *Science* **266**, 1247-1250.
- Delfin, J.C., Kanno, Y., Seo, M., Kitaoka, N., Matsuura, H., Tohge, T., and Shimizu, T. (2022). AtGH3.10 is another jasmonic acid-amido synthetase in *Arabidopsis thaliana*. *Plant J.* **110**, 1082-1096.
- Dempsey, D.M.A., and Klessig, D.F. (2012). SOS - too many signals for systemic acquired resistance? *Trends Plant Sci.* **17**, 538-545.
- Devoto, A., and Turner, J.G. (2005). Jasmonate-regulated *Arabidopsis* stress signalling network. *Physiol Plant* **123**, 161-172.
- Ding, P., Rekhter, D., Ding, Y., Feussner, K., Busta, L., Haroth, S., Xu, S., Li, X., Jetter, R., Feussner, I., and Zhang, Y. (2016). Characterization of a pipecolic acid biosynthesis pathway required for systemic acquired resistance. *Plant Cell* **28**, 2603-2615.
- Ding, Y., Sun, T., Ao, K., Peng, Y., Zhang, Y., Li, X., and Zhang, Y. (2018). Opposite roles of salicylic acid receptors NPR1 and NPR3/NPR4 in transcriptional regulation of plant immunity. *Cell* **173**, 1454-1467.e1415.

- Djordjevic, S., and Stock, A.M.** (1997). Crystal structure of the chemotaxis receptor methyltransferase CheR suggests a conserved structural motif for binding S-adenosylmethionine. *Structure* **5**, 545-558.
- Dresselhaus, T., and Hückelhoven, R.** (2018). Biotic and abiotic stress responses in crop plants. *Agronomy* **8**, 267.
- Fan, W., and Dong, X.** (2002). *In vivo* interaction between NPR1 and transcription factor TGA2 leads to salicylic acid-mediated gene activation in Arabidopsis. *Plant Cell* **14**, 1377-1389.
- Farmer, E.E., Alméras, E., and Krishnamurthy, V.** (2003). Jasmonates and related oxylipins in plant responses to pathogenesis and herbivory. *Curr. Opin. Plant Biol.* **6**, 372-378.
- Felton, G.W., and Korth, K.L.** (2000). Trade-offs between pathogen and herbivore resistance. *Curr. Opin. Plant Biol.* **3**, 309-314.
- Ferrari, S., Galletti, R., Denoux, C., De Lorenzo, G., Ausubel, F.M., and Dewdney, J.** (2007). Resistance to *Botrytis cinerea* Induced in Arabidopsis by Elicitors Is Independent of Salicylic Acid, Ethylene, or Jasmonate Signaling But Requires *PHYTOALEXIN DEFICIENT3*. *Plant Physiol.* **144**, 367-379.
- Ferrari, S., Savatin, D.V., Sicilia, F., Gramegna, G., Cervone, F., and De Lorenzo, G.** (2013). Oligogalacturonides: plant damage-associated molecular patterns and regulators of growth and development. *Front. Plant Sci.* **4**, 49.
- Feussner, I., and Polle, A.** (2015). What the transcriptome does not tell — proteomics and metabolomics are closer to the plants' patho-phenotype. *Curr. Opin. Plant Biol.* **26**, 26-31.
- Feussner, K., and Feussner, I.** (2019). Comprehensive LC-MS-based metabolite fingerprinting approach for plant and fungal-derived samples. In *High-Throughput Metabolomics: Methods and Protocols*, A. D'Alessandro, ed (New York, NY: Springer New York), pp. 167-185.
- Feys, B.J., and Parker, J.E.** (2000). Interplay of signaling pathways in plant disease resistance. *Trends in Genetics* **16**, 449-455.
- Fonseca, S., Chini, A., Hamberg, M., Adie, B., Porzel, A., Kramell, R., Miersch, O., Wasternack, C., and Solano, R.** (2009). (+)-7-iso-Jasmonoyl-L-isoleucine is the endogenous bioactive jasmonate. *Nat. Chem. Biol.* **5**, 344-350.
- Forouhar, F., Yang, Y., Kumar, D., Chen, Y., Fridman, E., Park, S.W., Chiang, Y., Acton, T.B., Montelione, G.T., Pichersky, E., Klessig, D.F., and Tong, L.** (2005). Structural and biochemical studies identify tobacco SABP2 as a methyl salicylate esterase and implicate it in plant innate immunity. *Proc. Natl. Acad. Sci. USA* **102**, 1773-1778.
- Fu, Z.Q., and Dong, X.** (2013). Systemic acquired resistance: Turning local infection into global defense. *Annu. Rev. Plant Biol.* **64**, 839-863.
- Fu, Z.Q., Yan, S., Saleh, A., Wang, W., Ruble, J., Oka, N., Mohan, R., Spoel, S.H., Tada, Y., Zheng, N., and Dong, X.** (2012). NPR3 and NPR4 are receptors for the immune signal salicylic acid in plants. *Nature* **486**, 228-232.
- Gaffney, T., Friedrich, L., Vernooij, B., Negrotto, D., Nye, G., Uknes, S., Ward, E., Kessmann, H., and Ryals, J.** (1993). Requirement of salicylic acid for the induction of systemic acquired resistance. *Science* **261**, 754-756.
- Gao, H., Zhou, Q., Yang, L., Zhang, K., Ma, Y., and Xu, Z.-Q.** (2020). Metabolomics analysis identifies metabolites associated with systemic acquired resistance in Arabidopsis. *PeerJ* **8**, e10047.

- Geng, X., Cheng, J., Gangadharan, A., and Mackey, D.** (2012). The coronatine toxin of *Pseudomonas syringae* is a multifunctional suppressor of Arabidopsis defense. *Plant Cell* **24**, 4763-4774.
- George Thompson, A.M., Iancu, C.V., Neet, K.E., Dean, J.V., and Choe, J.Y.** (2017). Differences in salicylic acid glucose conjugations by UGT74F1 and UGT74F2 from *Arabidopsis thaliana*. *Sci. Rep.* **7**, 46629.
- Glazebrook, J.** (2005). Contrasting Mechanisms of Defense Against Biotrophic and Necrotrophic Pathogens. *Annu. Rev. Phytopathol.* **43**, 205-227.
- Griebel, T., and Zeier, J.** (2008). Light regulation and daytime dependency of inducible plant defenses in Arabidopsis: phytochrome signaling controls systemic acquired resistance rather than local defense. *Plant Physiol.* **147**, 790-801.
- Griffiths, A.** (1889). The existence of salicylic acid in certain genera of the Liliaceae. *Chemical News* **60**, 59.
- Grimaldi, S.** (1905). Occurrence of salicylic acid in plants. *Staz. Sper. Agr. Ital* **38**, 618.
- Gruner, K., Griebel, T., Návarová, H., Attaran, E., and Zeier, J.** (2013). Reprogramming of plants during systemic acquired resistance. *Front. Plant Sci.* **4**, 252.
- Guerra, T., Schilling, S., Hake, K., Gorzolka, K., Sylvester, F.-P., Conrads, B., Westermann, B., and Romeis, T.** (2020). Calcium-dependent protein kinase 5 links calcium-signaling with *N*-Hydroxy-L-pipecolic acid- and *SARD1*-dependent immune memory in systemic acquired resistance. *New Phytol.* **225**, 310-325.
- Ha, Y., Shang, Y., and Nam, K.H.** (2016). Brassinosteroids modulate ABA-induced stomatal closure in Arabidopsis. *J. Exp. Bot.* **67**, 6297-6308.
- Haas, B.J., Kamoun, S., Zody, M.C., Jiang, R.H.Y., Handsaker, R.E., Cano, L.M., Grabherr, M., Kodira, C.D., Raffaele, S., Torto-Alalibo, T., Bozkurt, T.O., Ah-Fong, A.M.V., Alvarado, L., Anderson, V.L., Armstrong, M.R., Avrova, A., Baxter, L., Beynon, J., Boevink, P.C., Bollmann, S.R., Bos, J.I.B., Bulone, V., Cai, G., Cakir, C., Carrington, J.C., Chawner, M., Conti, L., Costanzo, S., Ewan, R., Fahlgren, N., Fischbach, M.A., Fugelstad, J., Gilroy, E.M., Gnerre, S., Green, P.J., Grenville-Briggs, L.J., Griffith, J., Grünwald, N.J., Horn, K., Horner, N.R., Hu, C.-H., Huitema, E., Jeong, D.-H., Jones, A.M.E., Jones, J.D.G., Jones, R.W., Karlsson, E.K., Kunjeti, S.G., Lamour, K., Liu, Z., Ma, L., MacLean, D., Chibucos, M.C., McDonald, H., McWalters, J., Meijer, H.J.G., Morgan, W., Morris, P.F., Munro, C.A., O'Neill, K., Ospina-Giraldo, M., Pinzón, A., Pritchard, L., Ramsahoye, B., Ren, Q., Restrepo, S., Roy, S., Sadanandom, A., Savidor, A., Schornack, S., Schwartz, D.C., Schumann, U.D., Schwessinger, B., Seyer, L., Sharpe, T., Silvar, C., Song, J., Studholme, D.J., Sykes, S., Thines, M., van de Vondervoort, P.J.I., Phuntumart, V., Wawra, S., Weide, R., Win, J., Young, C., Zhou, S., Fry, W., Meyers, B.C., van West, P., Ristaino, J., Govers, F., Birch, P.R.J., Whisson, S.C., Judelson, H.S., and Nusbaum, C.** (2009). Genome sequence and analysis of the Irish potato famine pathogen *Phytophthora infestans*. *Nature* **461**, 393-398.
- Haney, C.H., Samuel, B.S., Bush, J., and Ausubel, F.M.** (2015). Associations with rhizosphere bacteria can confer an adaptive advantage to plants. *Nat. Plants* **1**, 15051.
- Haro, S., Feussner, K., Kelly, A.A., Zienkiewicz, K., Shaikhqasem, A., Herrfurth, C., and Feussner, I.** (2019). The glycosyltransferase UGT76E1 significantly contributes to 12-O-glucopyranosyl-jasmonic acid formation in wounded *Arabidopsis thaliana* leaves. *J. Biol. Chem.* **294**, 9858-9872.
- Hartmann, M., and Zeier, J.** (2018). L-lysine metabolism to *N*-hydroxypipecolic acid: an integral immune-activating pathway in plants. *Plant J.* **96**, 5-21.
- Hartmann, M., Zeier, T., Bernsdorff, F., Reichel-Deland, V., Kim, D., Hohmann, M., Scholten, N., Schuck, S., Bräutigam, A., Hölzel, T., Ganter, C., and Zeier, J.** (2018).

- Flavin monooxygenase-generated *N*-hydroxypipelicolic acid is a critical element of plant systemic immunity. *Cell* **173**, 456-469.
- Haug, K., Salek, R.M., and Steinbeck, C.** (2017). Global open data management in metabolomics. *Curr. Opin. Chem. Biol.* **36**, 58-63.
- Haug, K., Cochrane, K., Nainala, V.C., Williams, M., Chang, J., Jayaseelan, K.V., and O'Donovan, C.** (2020). MetaboLights: a resource evolving in response to the needs of its scientific community. *Nucleic Acids Res.* **48**, D440-D444.
- Herrfurth, C., and Feussner, I.** (2020). Quantitative jasmonate profiling using a high-throughput UPLC-NanoESI-MS/MS method. In *Jasmonate in Plant Biology: Methods and Protocols*, A. Champion and L. Laplaze, eds (New York, NY: Springer US), pp. 169-187.
- Hilfiker, O., Groux, R., Bruessow, F., Kiefer, K., Zeier, J., and Reymond, P.** (2014). Insect eggs induce a systemic acquired resistance in Arabidopsis. *Plant J.* **80**, 1085-1094.
- Holmes, E.C., Chen, Y.-C., Sattely, E.S., and Mudgett, M.B.** (2019). An engineered pathway for *N*-hydroxy-pipelicolic acid synthesis enhances systemic acquired resistance in tomato. *Science Signaling* **12**, eaay3066.
- Holmes, E.C., Chen, Y.-C., Mudgett, M.B., and Sattely, E.S.** (2021). Arabidopsis UGT76B1 glycosylates *N*-hydroxy-pipelicolic acid and inactivates systemic acquired resistance in tomato. *Plant Cell* **33**, 750-765.
- Holmes, F.O.** (1938). Inheritance of resistance to tobacco-mosaic disease in tobacco. *Phytopath.* **28**.
- Hopp, W., and Seitz, H.U.** (1987). The uptake of acylated anthocyanin into isolated vacuoles from a cell suspension culture of *Daucus carota*. *Planta* **170**, 74-85.
- Horsefield, S., Burdett, H., Zhang, X., Manik, M.K., Shi, Y., Chen, J., Qi, T., Gilley, J., Lai, J.-S., Rank, M.X., Casey, L.W., Gu, W., Ericsson, D.J., Foley, G., Hughes, R.O., Bosanac, T., Itzstein, M.v., Rathjen, J.P., Nanson, J.D., Boden, M., Dry, I.B., Williams, S.J., Staskawicz, B.J., Coleman, M.P., Ve, T., Dodds, P.N., and Kobe, B.** (2019). NAD<sup>+</sup> cleavage activity by animal and plant TIR domains in cell death pathways. *Science* **365**, 793-799.
- Huang, s., Jia, A., Song, W., Hessler, G., Meng, Y., Sun, Y., Xu, L., Laessle, H., Jirschitzka, J., Ma, S., Xiao, Y., Yu, D., Hou, J., Liu, R., Sun, H., Liu, X., Han, Z., Chang, J., Parker, J.E., and Chai, J.** (2022). Identification and receptor mechanism of TIR-catalyzed small molecules in plant immunity. *bioRxiv*, 2022.2004.2001.486681.
- Huang, X., Zhu, G.-q., Liu, Q., Chen, L., Li, Y.-J., and Hou, B.-K.** (2018). Modulation of plant salicylic acid-associated immune responses via glycosylation of dihydroxybenzoic acids. *Plant Physiol.* **176**, 3103-3119.
- Inzé, A., Vanderauwera, S., Hoerberichts, F.A., Vidorpe, M., van Gaever, T., and van Breusegem, F.** (2012). A subcellular localization compendium of hydrogen peroxide-induced proteins. *Plant, Cell & Environment* **35**, 308-320.
- Jia, A., Huang, S., Song, W., Wang, J., Meng, Y., Sun, Y., Xu, L., Laessle, H., Jirschitzka, J., Hou, J., Zhang, T., Yu, W., Hessler, G., Li, E., Ma, S., Yu, D., Gebauer, J., Baumann, U., Liu, X., Han, Z., Chang, J., Parker, J.E., and Chai, J.** (2022). TIR-catalyzed ADP-ribosylation reactions produce signaling molecules for plant immunity. *bioRxiv*.
- Jones, J.D., and Dangl, J.L.** (2006). The plant immune system. *Nature* **444**, 323-329.
- Jones, P., and Vogt, T.** (2001). Glycosyltransferases in secondary plant metabolism: tranquilizers and stimulant controllers. *Planta* **213**, 164-174.

- Jung, H.W., Tschaplinski, T.J., Wang, L., Glazebrook, J., and Greenberg, J.T. (2009). Priming in systemic plant immunity. *Science* **324**, 89-91.
- Kachlicki, P., Einhorn, J., Muth, D., Kerhoas, L., and Stobiecki, M. (2008). Evaluation of glycosylation and malonylation patterns in flavonoid glycosides during LC/MS/MS metabolite profiling. *J Mass Spectrom* **43**, 572-586.
- Kaever, A., Landesfeind, M., Feussner, K., Feussner, I., and Meinicke, P. (2013). Metabolite clustering and visualization of mass spectrometry data using one-dimensional self-organizing maps. In *The Handbook of Plant Metabolomics*, W. Weckwerth and G. Kahl, eds (Weinheim: Wiley-VCH), pp. 273-287.
- Kaever, A., Lingner, T., Feussner, K., Göbel, C., Feussner, I., and Meinicke, P. (2009). MarVis: a tool for clustering and visualization of metabolic biomarkers. *BMC Bioinformatics* **10**, 92.
- Kaever, A., Landesfeind, M., Possienke, M., Feussner, K., Feussner, I., and Meinicke, P. (2012). MarVis-Filter: Ranking, filtering, adduct and isotope correction of mass spectrometry data. *J Biomed Biotechnol* **2012**, 263910.
- Kaever, A., Landesfeind, M., Feussner, K., Mosblech, A., Heilmann, I., Morgenstern, B., Feussner, I., and Meinicke, P. (2015). MarVis-Pathway: integrative and exploratory pathway analysis of non-targeted metabolomics data. *Metabolomics* **11**, 764-777.
- Kasper, K., Abreu, I.N., Feussner, K., Zienkiewicz, K., Herrfurth, C., Ischebeck, T., Janz, D., Majcherczyk, A., Schmitt, K., Valerius, O., Braus, G.H., Feussner, I., and Polle, A. (2022). Multi-omics analysis of xylem sap uncovers dynamic modulation of poplar defenses by ammonium and nitrate. *Plant J.* **111**, 282-303.
- Kessmann, H., Edwards, R., Geno, P.W., and Dixon, R.A. (1990). Stress responses in Alfalfa (*Medicago sativa* L.). *Plant Physiol.* **94**, 227-232.
- Kinkema, M., Fan, W., and Dong, X. (2000). Nuclear localization of NPR1 is required for activation of *PR* gene expression. *Plant Cell* **12**, 2339-2350.
- Klessig, D.F., Choi, H.W., and Dempsey, D.M.A. (2018). Systemic acquired resistance and salicylic acid: past, present and future. *Molecular Plant-Microbe Interactions* **31**, 871-888.
- Koen, E., Trapet, P., Brulé, D., Kulik, A., Klinguer, A., Atauri-Miranda, L., Meunier-Prest, R., Boni, G., Glauser, G., and Mauch-Mani, B. (2014).  $\beta$ -Aminobutyric acid (BABA)-induced resistance in *Arabidopsis thaliana*: link with iron homeostasis. *Molecular Plant-Microbe Interactions* **27**, 1226-1240.
- Kohl, F. (1999). Ein „Jahrhundertpharmakon“ wird hundert. *Der Schmerz* **13**, 341-346.
- Kolbe, H. (1860). Ueber Synthese der Salicylsäure. *Justus Liebigs Annalen der Chemie* **113**, 125-127.
- König, S., Feussner, K., Kaever, A., Landesfeind, M., Thurow, C., Karlovsky, P., Gatz, C., Polle, A., and Feussner, I. (2014). Soluble phenylpropanoids are involved in the defense response of *Arabidopsis* against *Verticillium longisporum*. *New Phytol.* **202**, 823-837.
- Koo, A.J.K., and Howe, G.A. (2009). The wound hormone jasmonate. *Phytochemistry* **70**, 1571-1580.
- Koo, Y.J., Yoon, E.S., Seo, J.S., Kim, J.-K., and Choi, Y.D. (2013). Characterization of a methyl jasmonate specific esterase in *Arabidopsis*. *Journal of the Korean Society for Applied Biological Chemistry* **56**, 27-33.
- Koo, Y.J., Kim, M., Kim, E.H., Song, J.T., Jung, C., Moon, J.-K., Kim, J.-H., Seo, H.S., Song, S.I., and Kim, J.-K. (2007). Overexpression of salicylic acid carboxyl

- methyltransferase reduces salicylic acid-mediated pathogen resistance in *Arabidopsis thaliana*. *Plant Mol. Biol.* **64**, 1-15.
- Kumar, S., Zavaliev, R., Wu, Q., Zhou, Y., Cheng, J., Dillard, L., Powers, J., Withers, J., Zhao, J., and Guan, Z.** (2022). Structural basis of NPR1 in activating plant immunity. *Nature* **605**, 561-566.
- Laduron, P.** (1972). *N*-methylation of dopamine to epinine in brain tissue using *N*-methyltetrahydrofolic acid as the methyl donor. *Nature New Biology* **238**, 212-213.
- Lairson, L.L., Henrissat, B., Davies, G.J., and Withers, S.G.** (2008). Glycosyltransferases: structures, functions, and mechanisms. *Annu Rev Biochem* **77**, 521-555.
- Lapin, D., Johandrees, O., Wu, Z., Li, X., and Parker, J.E.** (2022). Molecular innovations in plant TIR-based immunity signaling. *Plant Cell* **34**, 1479-1496.
- Lapin, D., Kovacova, V., Sun, X., Dongus, J.A., Bhandari, D., von Born, P., Bautor, J., Guarneri, N., Rzemieniewski, J., Stuttmann, J., Beyer, A., and Parker, J.E.** (2019). A coevolved EDS1-SAG101-NRG1 module mediates cell death signaling by TIR-domain immune receptors. *Plant Cell* **31**, 2430-2455.
- Leavitt, A., Yirmiya, E., Amitai, G., Lu, A., Garb, J., Morehouse, B.R., Hobbs, S.J., Kranzusch, P.J., and Sorek, R.** (2022). Viruses inhibit TIR gcADPR signaling to overcome bacterial defense. *bioRxiv*.
- Lee, S., Fu, F., Xu, S., Lee, S.Y., Yun, D.-J., and Mengiste, T.** (2016). Global regulation of plant immunity by histone lysine methyl transferases. *Plant Cell* **28**, 1640-1661.
- Letertre, M.P.M., Dervilly, G., and Giraudeau, P.** (2020). Combined nuclear magnetic resonance spectroscopy and mass spectrometry approaches for metabolomics. *Anal. Chem.* **93**, 500-518.
- Lewandowska, M., Keyl, A., and Feussner, I.** (2020). Wax biosynthesis upon danger: its regulation upon abiotic and biotic stress. *New Phytol.* **227**, 698-713.
- Li, W., Zhang, F., Chang, Y., Zhao, T., Schranz, M.E., and Wang, G.** (2015). Nicotinate *O*-glucosylation is an evolutionarily metabolic trait important for seed germination under stress conditions in *Arabidopsis thaliana*. *Plant Cell* **27**, 1907-1924.
- Li, X., Svedin, E., Mo, H., Atwell, S., Dilkes, B.P., and Chapple, C.** (2014). Exploiting natural variation of secondary metabolism identifies a gene controlling the glycosylation diversity of dihydroxybenzoic acids in *Arabidopsis thaliana*. *Genetics* **198**, 1267-1276.
- Li, Y., Baldauf, S., Lim, E.-K., and Bowles, D.J.** (2001). Phylogenetic analysis of the UDP-glycosyltransferase multigene family of *Arabidopsis thaliana*. *J. Biol. Chem.* **276**, 4338-4343.
- Lim, C.W., Baek, W., Jung, J., Kim, J.-H., and Lee, S.C.** (2015). Function of ABA in stomatal defense against biotic and drought stresses. *International Journal of Molecular Sciences* **16**, 15251-15270.
- Lim, E.-K., Baldauf, S., Li, Y., Elias, L., Worrall, D., Spencer, S.P., Jackson, R.G., Taguchi, G., Ross, J., and Bowles, D.J.** (2003). Evolution of substrate recognition across a multigene family of glycosyltransferases in *Arabidopsis*. *Glycobiology* **13**, 139-145.
- Liu, L., Sonbol, F.M., Huot, B., Gu, Y., Withers, J., Mwimba, M., Yao, J., He, S.Y., and Dong, X.** (2016). Salicylic acid receptors activate jasmonic acid signalling through a non-canonical pathway to promote effector-triggered immunity. *Nat. Commun.* **7**, 13099.
- Ma, Y., Zhao, Y., Walker, R.K., and Berkowitz, G.A.** (2013). Molecular steps in the immune signaling pathway evoked by plant elicitor peptides:  $Ca^{2+}$ -dependent protein kinases, nitric oxide, and reactive oxygen species are downstream from the early  $Ca^{2+}$  signal. *Plant Physiol.* **163**, 1459-1471.



- Mackelprang, R., Okrent, R.A., and Wildermuth, M.C.** (2017). Preference of *Arabidopsis thaliana* GH3.5 acyl amido synthetase for growth versus defense hormone acyl substrates is dictated by concentration of amino acid substrate aspartate. *Phytochemistry* **143**, 19-28.
- Mackenzie, P.I., Owens, I.S., Burchell, B., Bock, K.W., Bairoch, A., Belanger, A., Fournel-Gigleux, S., Green, M., Hum, D.W., and Iyanagi, T.** (1997). The UDP glycosyltransferase gene superfamily: recommended nomenclature update based on evolutionary divergence. *Pharmacogenetics* **7**, 255-269.
- Maksym, R.P., Ghirardo, A., Zhang, W., von Saint Paul, V., Lange, B., Geist, B., Hajirezaei, M.-R., Schnitzler, J.-P., and Schäffner, A.R.** (2018). The defense-related isoleucic acid differentially accumulates in *Arabidopsis* among branched-chain amino acid-related 2-hydroxy carboxylic acids. *Front. Plant Sci.* **9**, 766.
- Malamy, J., and Klessig, D.F.** (1992). Salicylic acid and plant disease resistance. *Plant J.* **2**, 643-654.
- Malamy, J., Carr, J.P., Klessig, D.F., and Raskin, I.** (1990). Salicylic acid: a likely endogenous signal in the resistance response of tobacco to viral infection. *Science* **250**, 1002-1004.
- Manosalva, P.M., Park, S.-W., Forouhar, F., Tong, L., Fry, W.E., and Klessig, D.F.** (2010). *Methyl esterase 1 (StMES1)* is required for systemic acquired resistance in potato. *Molecular Plant-Microbe Interactions* **23**, 1151-1163.
- Markham, G.D., Hafner, E.W., Tabor, C.W., and Tabor, H.** (1980). *S*-Adenosylmethionine synthetase from *Escherichia coli*. *J. Biol. Chem.* **255**, 9082-9092.
- Martin, R., Qi, T., Zhang, H., Liu, F., King, M., Toth, C., Nogales, E., and Staskawicz, B.J.** (2020). Structure of the activated ROQ1 resistosome directly recognizing the pathogen effector XopQ. *Science* **370**, eabd9993.
- Matern, U., Reichenbach, C., and Heller, W.** (1986). Efficient uptake of flavonoids into parsley (*Petroselinum hortense*) vacuoles requires acylated glycosides. *Planta* **167**, 183-189.
- Mendgen, K., and Hahn, M.** (2002). Plant infection and the establishment of fungal biotrophy. *Trends Plant Sci.* **7**, 352-356.
- Metraux, J.P., Signer, H., Ryals, J., Ward, E., Wyss-Benz, M., Gaudin, J., Raschdorf, K., Schmid, E., Blum, W., and Inverardi, B.** (1990). Increase in salicylic acid at the onset of systemic acquired resistance in cucumber. *Science* **250**, 1004-1006.
- Mishina, T.E., and Zeier, J.** (2006). The *Arabidopsis* flavin-dependent monooxygenase FMO1 is an essential component of biologically induced systemic acquired resistance. *Plant Physiol.* **141**, 1666-1675.
- Mohnike, L., Rehkter, D., Huang, W., Feussner, K., Tian, H., Herrfurth, C., Zhang, Y., and Feussner, I.** (2021). The glycosyltransferase UGT76B1 modulates *N*-hydroxypipicolinic acid homeostasis and plant immunity. *Plant Cell* **33**, 735-749.
- Mou, Z., Fan, W., and Dong, X.** (2003). Inducers of plant systemic acquired resistance regulate NPR1 function through redox changes. *Cell* **113**, 935-944.
- Nair, A., Goyal, I., Voß, E., Mrozek, P., Prajapati, S., Thurow, C., Tietze, L., Tittmann, K., and Gatz, C.** (2021). *N*-hydroxypipicolinic acid-induced transcription requires the salicylic acid signaling pathway at basal SA levels. *Plant Physiol.* **187**, 2803-2819.
- Nakano, R., Yamada, K., Bednarek, P., Nishimura, M., and Hara-Nishimura, I.** (2014). ER bodies in plants of the *Brassicales* order: biogenesis and association with innate immunity. *Front. Plant Sci.* **5**, 73.

- Nakashima, K., and Yamaguchi-Shinozaki, K.** (2013). ABA signaling in stress-response and seed development. *Plant Cell Rep.* **32**, 959-970.
- Navarova, H., Bernsdorff, F., Döring, A.-C., and Zeier, J.** (2012). Pipecolic acid, an endogenous mediator of defense amplification and priming, is a critical regulator of inducible plant immunity. *Plant Cell* **24**, 5123-5141.
- Nawrath, C., Heck, S., Parinthewong, N., and Métraux, J.-P.** (2002). EDS5, an essential component of salicylic acid-dependent signaling for disease resistance in *Arabidopsis*, is a member of the MATE transporter family. *Plant Cell* **14**, 275-286.
- Ngou, B.P.M., Ding, P., and Jones, J.D.G.** (2022). Thirty years of resistance: Zig-zag through the plant immune system. *Plant Cell* **34**, 1447-1478.
- Ngou, B.P.M., Ahn, H.-K., Ding, P., and Jones, J.D.** (2021). Mutual potentiation of plant immunity by cell-surface and intracellular receptors. *Nature* **592**, 110-115.
- Nomoto, M., Skelly, M.J., Itaya, T., Mori, T., Suzuki, T., Matsushita, T., Tokizawa, M., Kuwata, K., Mori, H., Yamamoto, Y.Y., Higashiyama, T., Tsukagoshi, H., Spoel, S.H., and Tada, Y.** (2021). Suppression of MYC transcription activators by the immune cofactor NPR1 fine-tunes plant immune responses. *Cell Reports* **37**.
- Noutoshi, Y., Okazaki, M., Kida, T., Nishina, Y., Morishita, Y., Ogawa, T., Suzuki, H., Shibata, D., Jikumaru, Y., Hanada, A., Kamiya, Y., and Shirasu, K.** (2012). Novel plant immune-priming compounds identified via high-throughput chemical screening target salicylic acid glucosyltransferases in *Arabidopsis*. *Plant Cell* **24**, 3795-3804.
- Obayashi, T., Hibara, H., Kagaya, Y., Aoki, Y., and Kinoshita, K.** (2022). ATTED-II v11: A Plant Gene Coexpression Database Using a Sample Balancing Technique by Subagging of Principal Components. *Plant Cell Physiol.* **63**, 869-881.
- Orlovskis, Z., and Reymond, P.** (2020). *Pieris brassicae* eggs trigger inter-plant systemic acquired resistance against a foliar pathogen in *Arabidopsis*. *New Phytol.* **228**, 1652-1661.
- Pang, H., Jia, W., and Hu, Z.** (2019). Emerging applications of metabolomics in clinical pharmacology. *Clinical Pharmacology & Therapeutics* **106**, 544-556.
- Parinthewong, N., Cottier, S., Buchala, A., Nawrath, C., and Metraux, J.P.** (2015). Localization and expression of EDS5H a homologue of the SA transporter EDS5. *BMC Plant Biol.* **15**, 135.
- Park, J.-H., Halitschke, R., Kim, H.B., Baldwin, I.T., Feldmann, K.A., and Feyereisen, R.** (2002). A knock-out mutation in allene oxide synthase results in male sterility and defective wound signal transduction in *Arabidopsis* due to a block in jasmonic acid biosynthesis. *Plant J.* **31**, 1-12.
- Park, S.-W., Kaimoyo, E., Kumar, D., Mosher, S., and Klessig, D.F.** (2007). Methyl salicylate is a critical mobile signal for plant systemic acquired resistance. *Science* **318**, 113-116.
- Parker, J.E., Hessler, G., and Cui, H.** (2022). A new biochemistry connecting pathogen detection to induced defense in plants. *New Phytol.* **234**, 819-826.
- Patti, G.J., Yanes, O., and Siuzdak, G.** (2012). Innovation: Metabolomics: the apogee of the omics trilogy. *Nature Reviews Molecular Cell Biology* **13**, 263-269.
- Piofczyk, T., Jeena, G., and Pecinka, A.** (2015). *Arabidopsis thaliana* natural variation reveals connections between UV radiation stress and plant pathogen-like defense responses. *Plant Physiology and Biochemistry* **93**, 34-43.
- Pirrello, C., Malacarne, G., Moretto, M., Lenzi, L., Perazzolli, M., Zeilmaker, T., Van den Ackerveken, G., Pilati, S., Moser, C., and Giacomelli, L.** (2022). Grapevine DMR6-1 is a candidate gene for susceptibility to downy mildew. *Biomolecules* **12**, 182.

- Possienke, M.** (2012). Signals and metabolic consequences during the interaction of Brassicaceae and *Verticillium longisporum* (Goettingen).
- Pruitt, R.N., Locci, F., Wanke, F., Zhang, L., Saile, S.C., Joe, A., Karelina, D., Hua, C., Fröhlich, K., Wan, W.-L., Hu, M., Rao, S., Stolze, S.C., Harzen, A., Gust, A.A., Harter, K., Joosten, M.H.A.J., Thomma, B.P.H.J., Zhou, J.-M., Dangl, J.L., Weigel, D., Nakagami, H., Oecking, C., Kasmi, F.E., Parker, J.E., and Nürnberger, T.** (2021). The EDS1–PAD4–ADR1 node mediates Arabidopsis pattern-triggered immunity. *Nature* **598**, 495-499.
- Rasmussen, J.B., Hammerschmidt, R., and Zook, M.N.** (1991). Systemic induction of salicylic acid accumulation in cucumber after inoculation with *Pseudomonas-syringae* pv *syringae*. *Plant Physiol.* **97**, 1342-1347.
- Rekhter, D., Mohnike, L., Feussner, K., Zienkiewicz, K., Zhang, Y., and Feussner, I.** (2019a). Enhanced Disease Susceptibility 5 (EDS5) is required for *N*-hydroxy pipelicolic acid formation. *bioRxiv*, 630723.
- Rekhter, D., Lüdke, D., Ding, Y., Feussner, K., Zienkiewicz, K., Lipka, V., Wiermer, M., Zhang, Y., and Feussner, I.** (2019b). Isochorismate-derived biosynthesis of the plant stress hormone salicylic acid. *Science* **365**, 498-502.
- Resemann, H.C., Herrfurth, C., Feussner, K., Hornung, E., Ostendorf, A.K., Gömann, J., Mittag, J., van Gessel, N., de Vries, J., Ludwig-Müller, J., Markham, J., Reski, R., and Feussner, I.** (2021). Convergence of sphingolipid desaturation across over 500 million years of plant evolution. *Nat. Plants* **7**, 219–232.
- Ross, A.F.** (1961). Systemic acquired resistance induced by localized virus infections in plants. *Virology* **14**, 340-358.
- Ross, J., Li, Y., Lim, E.-K., and Bowles, D.J.** (2001). Higher plant glycosyltransferases. *Genome Biol.* **2**, reviews3004.3001.
- Saado, I., Chia, K.-S., Betz, R., Alcântara, A., Pettkó-Szandtner, A., Navarrete, F., D'Auria, J.C., Kolomiets, M.V., Melzer, M., Feussner, I., and Djamei, A.** (2022). Effector-mediated relocalization of a maize lipoxygenase protein triggers susceptibility to *Ustilago maydis*. *Plant Cell* **34**, 2785–2805.
- Samaniego, L., Thober, S., Kumar, R., Wanders, N., Rakovec, O., Pan, M., Zink, M., Sheffield, J., Wood, E.F., and Marx, A.** (2018). Anthropogenic warming exacerbates european soil moisture droughts. *Nature Climate Change* **8**, 421-426.
- Schnake, A., Hartmann, M., Schreiber, S., Malik, J., Brahmman, L., Yildiz, I., von Dahlen, J., Rose, L.E., Schaffrath, U., and Zeier, J.** (2020). Inducible biosynthesis and immune function of the systemic acquired resistance inducer *N*-hydroxypipelicolic acid in monocotyledonous and dicotyledonous plants. *J. Exp. Bot.* **71**, 6444–6459.
- Schuler, M., Keller, A., Backes, C., Philippar, K., Lenhof, H.-P., and Bauer, P.** (2011). Transcriptome analysis by GeneTrail revealed regulation of functional categories in response to alterations of iron homeostasis in *Arabidopsis thaliana*. *BMC Plant Biol.* **11**, 1-10.
- Schütte, H.R., and Seelig, G.** (1967). Zur Biosynthese der Pipelicolinsäure in *Phaseolus vulgaris*. *Zeitschrift für Naturforschung B* **22**, 824-826.
- Seo, H.S., Song, J.T., Cheong, J.J., Lee, Y.H., Lee, Y.W., Hwang, I., Lee, J.S., and Choi, Y.D.** (2001). Jasmonic acid carboxyl methyltransferase: a key enzyme for jasmonate-regulated plant responses. *Proceedings of the National Academy of Sciences USA* **98**, 4788-4793.
- Serrano, M., Wang, B., Aryal, B., Garcion, C., Abou-Mansour, E., Heck, S., Geisler, M., Mauch, F., Nawrath, C., and Metraux, J.P.** (2013). Export of salicylic acid from the

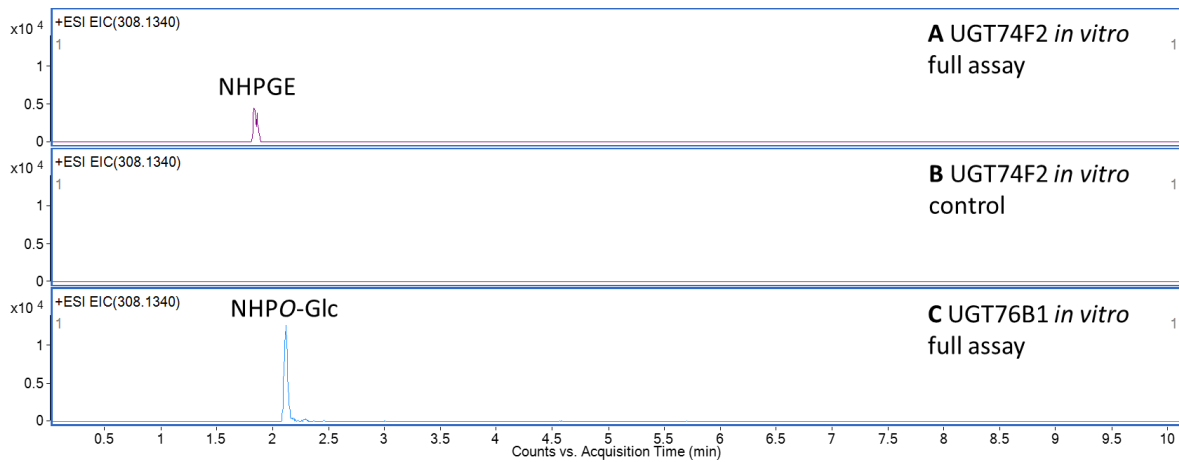
- chloroplast requires the multidrug and toxin extrusion-like transporter EDS5. *Plant Physiol.* **162**, 1815-1821.
- Shah, J., and Zeier, J.** (2013). Long-distance communication and signal amplification in systemic acquired resistance. *Front. Plant Sci.* **4**, 30.
- Shalev, O., Ashkenazy, H., Neumann, M., and Weigel, D.** (2022). Commensal *Pseudomonas* protect *Arabidopsis thaliana* from a coexisting pathogen via multiple lineage-dependent mechanisms. *ISME J.* **16**, 1235-1244.
- Shulaev, V., Silverman, P., and Raskin, I.** (1997). Airborne signalling by methyl salicylate in plant pathogen resistance. *Nature* **385**, 718-721.
- Song, J.T.** (2006). Induction of a salicylic acid glucosyltransferase, AtSGT1, is an early disease response in *Arabidopsis thaliana*. *Molecules and Cells* **22**, 233-238.
- Song, J.T., Koo, Y.J., Seo, H.S., Kim, M.C., Choi, Y.D., and Kim, J.H.** (2008). Overexpression of AtSGT1, an *Arabidopsis* salicylic acid glucosyltransferase, leads to increased susceptibility to *Pseudomonas syringae*. *Phytochemistry* **69**, 1128–1134.
- Staswick, P.E., and Tiryaki, I.** (2004). The oxylipin signal jasmonic acid is activated by an enzyme that conjugates it to isoleucine in *Arabidopsis*. *Plant Cell* **16**, 2117-2127.
- Stringlis, I.A., Yu, K., Feussner, K., de Jonge, R., Van Bentum, S., Van Verk, M.C., Berendsen, R.L., Bakker, P.A.H.M., Feussner, I., and Pieterse, C.M.J.** (2018). MYB72-dependent coumarin exudation shapes root microbiome assembly to promote plant health. *Proc. Natl. Acad. Sci. USA* **115**, E5213-E5222.
- Struck, A.W., Thompson, M.L., Wong, L.S., and Micklefield, J.** (2012). S-adenosyl-methionine-dependent methyltransferases: highly versatile enzymes in biocatalysis, biosynthesis and other biotechnological applications. *ChemBioChem* **13**, 2642-2655.
- Sun, T., Zhang, Y., Li, Y., Zhang, Q., Ding, Y., and Zhang, Y.** (2015). ChIP-seq reveals broad roles of SARD1 and CBP60g in regulating plant immunity. *Nat. Commun.* **6**, 10159.
- Sun, T., Busta, L., Zhang, Q., Ding, P., Jetter, R., and Zhang, Y.** (2018). TGACG-BINDING FACTOR 1 (TGA1) and TGA4 regulate salicylic acid and pipelicolic acid biosynthesis by modulating the expression of *SYSTEMIC ACQUIRED RESISTANCE DEFICIENT 1* (SARD1) and *CALMODULIN-BINDING PROTEIN 60g* (CBP60g). *New Phytol.* **217**, 344-354.
- Suza, W., and Staswick, P.** (2008). The role of JAR1 in Jasmonoyl-I -isoleucine production during *Arabidopsis* wound response. *Planta* **227**, 1221-1232.
- Suzuki, N., Rivero, R.M., Shulaev, V., Blumwald, E., and Mittler, R.** (2014). Abiotic and biotic stress combinations. *New Phytol.* **203**, 32-43.
- Swayambhu, G., Raghavan, I., Ravi, B.G., Pfeifer, B.A., and Wang, Z.Q.** (2021). Salicylate glucoside as a nontoxic plant protectant alternative to salicylic acid. *ACS Agricultural Science & Technology* **1**, 515-521.
- Tada, Y., Spoel, S.H., Pajerowska-Mukhtar, K., Mou, Z., Song, J., Wang, C., Zuo, J., and Dong, X.** (2008). Plant immunity requires conformational changes of NPR1 via S-nitrosylation and thioredoxins. *Science* **321**, 952-956.
- Tamogami, S., Rakwal, R., and Agrawal, G.K.** (2008). Interplant communication: Airborne methyl jasmonate is essentially converted into JA and JA-Ile activating jasmonate signaling pathway and VOCs emission. *Biochem. Biophys. Res. Commun.* **376**, 723-727.
- Thomma, B.P.H.J., Eggermont, K., Penninckx, I.A.M.A., Mauch-Mani, B., Vogelsang, R., Cammue, B.P.A., and Broekaert, W.F.** (1998). Separate jasmonate-dependent and salicylate-dependent defense-response pathways in *Arabidopsis* are essential for

- resistance to distinct microbial pathogens. *Proc. Natl. Acad. Sci. USA* **95**, 15107-15111.
- Tian, H., Wu, Z., Chen, S., Ao, K., Huang, W., Yaghmaiean, H., Sun, T., Xu, F., Zhang, Y., and Wang, S.** (2021). Activation of TIR signalling boosts pattern-triggered immunity. *Nature* **598**, 500-503.
- Torrens-Spence, M.P., Bobokalonova, A., Carballo, V., Glinkerman, C.M., Pluskal, T., Shen, A., and Weng, J.-K.** (2019). PBS3 and EPS1 complete salicylic acid biosynthesis from isochorismate in *Arabidopsis*. *Mol. Plant* **12**, 1577-1586.
- Torres, M.A., Jones, J.D.G., and Dangl, J.L.** (2006). Reactive oxygen species signaling in response to pathogens. *Plant Physiol.* **141**, 373-378.
- Traphagen, F., and Burke, E.** (1903). Occurrence of salicylic acid in fruits. *J. Am. Chem. Soc.* **25**, 242-244.
- Truman, W., Bennett, M.H., Kubigsteltig, I., Turnbull, C., and Grant, M.** (2007). *Arabidopsis* systemic immunity uses conserved defense signaling pathways and is mediated by jasmonates. *PNAS* **104**, 1075-1080.
- Vanholme, R., Demedts, B., Morreel, K., Ralph, J., and Boerjan, W.** (2010). Lignin Biosynthesis and Structure. *Plant Physiol.* **153**, 895-905.
- Vernooij, B., Uknes, S., Ward, E., and Ryals, J.** (1994). Salicylic acid as a signal molecule in plant-pathogen interactions. *Current Opinion in Cell Biology* **6**, 275-279.
- Viant, M.R., Kurland, I.J., Jones, M.R., and Dunn, W.B.** (2017). How close are we to complete annotation of metabolomes? *Curr. Opin. Chem. Biol.* **36**, 64-69.
- Vlot, A.C., Liu, P.-P., Cameron, R.K., Park, S.-W., Yang, Y., Kumar, D., Zhou, F., Padukkavidana, T., Gustafsson, C., Pichersky, E., and Klessig, D.F.** (2008). Identification of likely orthologs of tobacco salicylic acid-binding protein 2 and their role in systemic acquired resistance in *Arabidopsis thaliana*. *Plant J.* **56**, 445-456.
- von Saint Paul, V., Zhang, W., Kanawati, B., Geist, B., Faus-Kessler, T., Schmitt-Kopplin, P., and Schäffner, A.R.** (2011). The *Arabidopsis* glucosyltransferase UGT76B1 conjugates isoleucic acid and modulates plant defense and senescence. *Plant Cell* **23**, 4124-4145.
- Waadt, R., Seller, C.A., Hsu, P.-K., Takahashi, Y., Munemasa, S., and Schroeder, J.I.** (2022). Plant hormone regulation of abiotic stress responses. *Nature Reviews Molecular Cell Biology* **n**, n.
- Wan, L., Essuman, K., Anderson, R.G., Sasaki, Y., Monteiro, F., Chung, E.-H., Nishimura, E.O., DiAntonio, A., Milbrandt, J., Dangl, J.L., and Nishimura, M.T.** (2019a). TIR domains of plant immune receptors are NAD<sup>+</sup>-cleaving enzymes that promote cell death. *Science* **365**, 799-803.
- Wan, W.-L., Fröhlich, K., Pruitt, R.N., Nürnberger, T., and Zhang, L.** (2019b). Plant cell surface immune receptor complex signaling. *Curr. Opin. Plant Biol.* **50**, 18-28.
- Ward, L.C., McCue, H.V., and Carnell, A.J.** (2021). Carboxyl methyltransferases: natural functions and potential applications in industrial biotechnology. *ChemCatChem* **13**, 121-128.
- Wasternack, C., and Hause, B.** (2013). Jasmonates: biosynthesis, perception, signal transduction and action in plant stress response, growth and development. An update to the 2007 review in *Annals of Botany*. *Ann. Bot.* **111**, 1021-1058.
- Westfall, C.S., Herrmann, J., Chen, Q., Wang, S., and Jez, J.M.** (2010). Modulating plant hormones by enzyme action: the GH3 family of acyl acid amido synthetases. *Plant Signaling & Behavior* **5**, 1607-1612.

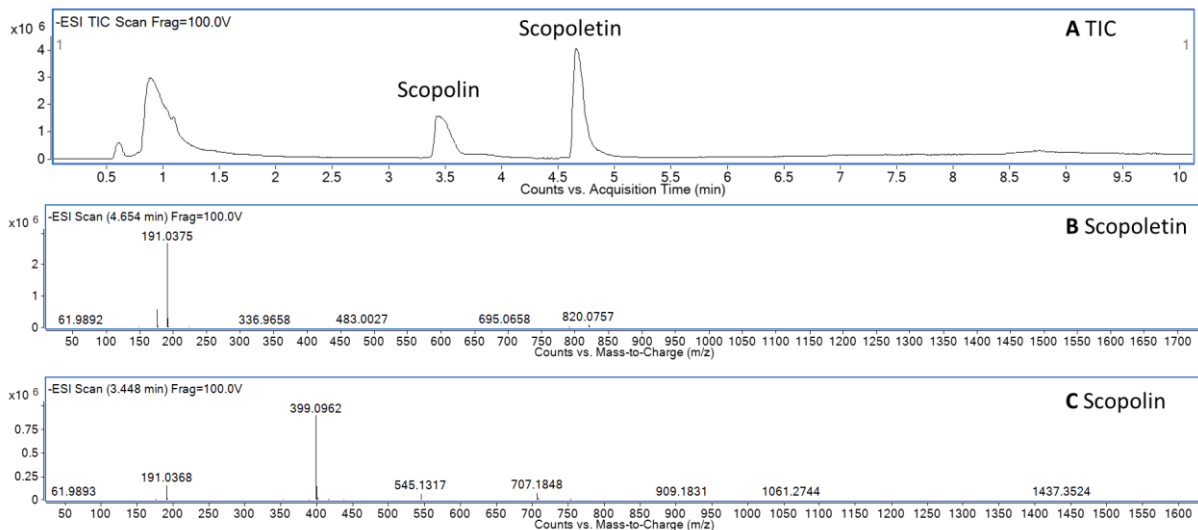
- Westfall, C.S., Sherp, A.M., Zubieta, C., Alvarez, S., Schraft, E., Marcellin, R., Ramirez, L., and Jez, J.M. (2016). *Arabidopsis thaliana* GH3.5 acyl acid amido synthetase mediates metabolic crosstalk in auxin and salicylic acid homeostasis. *Proc. Natl. Acad. Sci. USA* **113**, 13917-13922.
- Weyrich, L.S., Duchene, S., Soubrier, J., Arriola, L., Llamas, B., Breen, J., Morris, A.G., Alt, K.W., Caramelli, D., Dresely, V., Farrell, M., Farrer, A.G., Francken, M., Gully, N., Haak, W., Hardy, K., Harvati, K., Held, P., Holmes, E.C., Kaidonis, J., Lalueza-Fox, C., de la Rasilla, M., Rosas, A., Semal, P., Soltysiak, A., Townsend, G., Usai, D., Wahl, J., Huson, D.H., Dobney, K., and Cooper, A. (2017). Neanderthal behaviour, diet, and disease inferred from ancient DNA in dental calculus. *Nature* **544**, 357-361.
- Wildermuth, M.C., Dewdney, J., Wu, G., and Ausubel, F.M. (2001). Isochorismate synthase is required to synthesize salicylic acid for plant defence. *Nature* **414**, 562-565.
- Wu, J., Wang, L., and Baldwin, I. (2008). Methyl jasmonate-elicited herbivore resistance: does MeJA function as a signal without being hydrolyzed to JA? *Planta* **227**, 1161-1168.
- Wu, Y., Zhang, D., Chu, J.Y., Boyle, P., Wang, Y., Brindle, I.D., De Luca, V., and Després, C. (2012). The *Arabidopsis* NPR1 protein is a receptor for the plant defense hormone salicylic acid. *Cell Reports* **1**, 639-647.
- Yalpani, N., Leon, J., Lawton, M.A., and Raskin, I. (1993). Pathway of salicylic acid biosynthesis in healthy and virus-inoculated Tobacco. *Plant Physiol.* **103**, 315-321.
- Yang, H., and Ludewig, U. (2014). Lysine catabolism, amino acid transport, and systemic acquired resistance. *Plant Signaling & Behavior* **9**, e28933.
- Yildiz, I., Mantz, M., Hartmann, M., Zeier, T., Kessel, J., Thurow, C., Gatz, C., Petzsch, P., Köhrer, K., and Zeier, J. (2021). Mobile SAR signal N-hydroxypipicolic acid induces NPR1-dependent transcriptional reprogramming and immune priming. *Plant Physiol.* **186**, 1679-1705.
- Yu, D., Song, W., Tan, E.Y.J., Liu, L., Cao, Y., Jirschitzka, J., Li, E., Logemann, E., Xu, C., Huang, S., Jia, A., Chang, X., Han, Z., Wu, B., Schulze-Lefert, P., and Chai, J. (2021a). TIR domains of plant immune receptors are 2',3'-cAMP/cGMP synthetases mediating cell death. *bioRxiv*, 2021.2011.2009.467869.
- Yu, Y., Zhang, Y.K., Manohar, M., Artyukhin, A.B., Kumari, A., Tenjo-Castano, F.J., Nguyen, H., Routray, P., Choe, A., Klessig, D.F., and Schroeder, F.C. (2021b). Nematode signaling molecules are extensively metabolized by animals, plants, and microorganisms. *ACS Chem. Biol.* **16**, 1050-1058.
- Yuan, M., Jiang, Z., Bi, G., Nomura, K., Liu, M., Wang, Y., Cai, B., Zhou, J.-M., He, S.Y., and Xin, X.-F. (2021). Pattern-recognition receptors are required for NLR-mediated plant immunity. *Nature* **592**, 105-109.
- Zeier, J. (2021). Metabolic regulation of systemic acquired resistance. *Curr. Opin. Plant Biol.* **62**, 102050.
- Zhang, H., Lang, Z., and Zhu, J.-K. (2018). Dynamics and function of DNA methylation in plants. *Nature Reviews Molecular cell biology* **19**, 489-506.
- Zhang, H., Zhu, J., Gong, Z., and Zhu, J.-K. (2022). Abiotic stress responses in plants. *Nature Reviews Genetics* **23**, 104-119.
- Zhang, J., Ren, Z., Zhou, Y., Ma, Z., Ma, Y., Hou, D., Xu, Z., and Huang, X. (2019). NPR1 and redox rhythm: connections, between circadian clock and plant Immunity. *Int. J. Mol. Sci.* **20**, 1211.

- Zhang, K., Halitschke, R., Yin, C., Liu, C.-J., and Gan, S.-S.** (2013). Salicylic acid 3-hydroxylase regulates Arabidopsis leaf longevity by mediating salicylic acid catabolism. *Proc. Natl. Acad. Sci. USA* **110**, 14807-14812.
- Zhang, Y., Fan, W., Kinkema, M., Li, X., and Dong, X.** (1999). Interaction of NPR1 with basic leucine zipper protein transcription factors that bind sequences required for salicylic acid induction of the *PR-1* gene. *Proc. Natl. Acad. Sci. USA* **96**, 6523-6528.
- Zhang, Y., Yang, Y., Fang, B., Gannon, P., Ding, P., Li, X., and Zhang, Y.** (2010). *Arabidopsis snc2-1D* activates receptor-like protein-mediated immunity transduced through WRKY70. *Plant Cell* **22**, 3153-3163.
- Zhang, Y., Zhao, L., Zhao, J., Li, Y., Wang, J., Guo, R., Gan, S., Liu, C.-J., and Zhang, K.** (2017). *S5H/DMR6* encodes a salicylic acid 5-hydroxylase that fine-tunes salicylic acid homeostasis. *Plant Physiol.* **175**, 1082-1093.
- Zhang, Z., Li, Q., Li, Z., Staswick, P.E., Wang, M., Zhu, Y., and He, Z.** (2007). Dual regulation role of GH3.5 in salicylic acid and auxin signaling during Arabidopsis-*Pseudomonas syringae* interaction. *Plant Physiol.* **145**, 450-464.
- Zhu, Z.-J., Schultz, A.W., Wang, J., Johnson, C.H., Yannone, S.M., Patti, G.J., and Siuzdak, G.** (2013). Liquid chromatography quadrupole time-of-flight mass spectrometry characterization of metabolites guided by the METLIN database. *Nat. Protoc.* **8**, 451-460.
- Zipfel, C., Robatzek, S., Navarro, L., Oakeley, E.J., Jones, J.D.G., Felix, G., and Boller, T.** (2004). Bacterial disease resistance in Arabidopsis through flagellin perception. *Nature* **428**, 764-767.
- Zubieta, C., He, X.-Z., Dixon, R.A., and Noel, J.P.** (2001). Structures of two natural product methyltransferases reveal the basis for substrate specificity in plant O-methyltransferases. *Nat. Struct. Biol.* **8**, 271-279.
- Zubieta, C., Ross, J.R., Koscheski, P., Yang, Y., Pichersky, E., and Noel, J.P.** (2003). Structural basis for substrate recognition in the salicylic acid carboxyl methyltransferase family. *Plant Cell* **15**, 1704-1716.

## 8. Supplemental materials

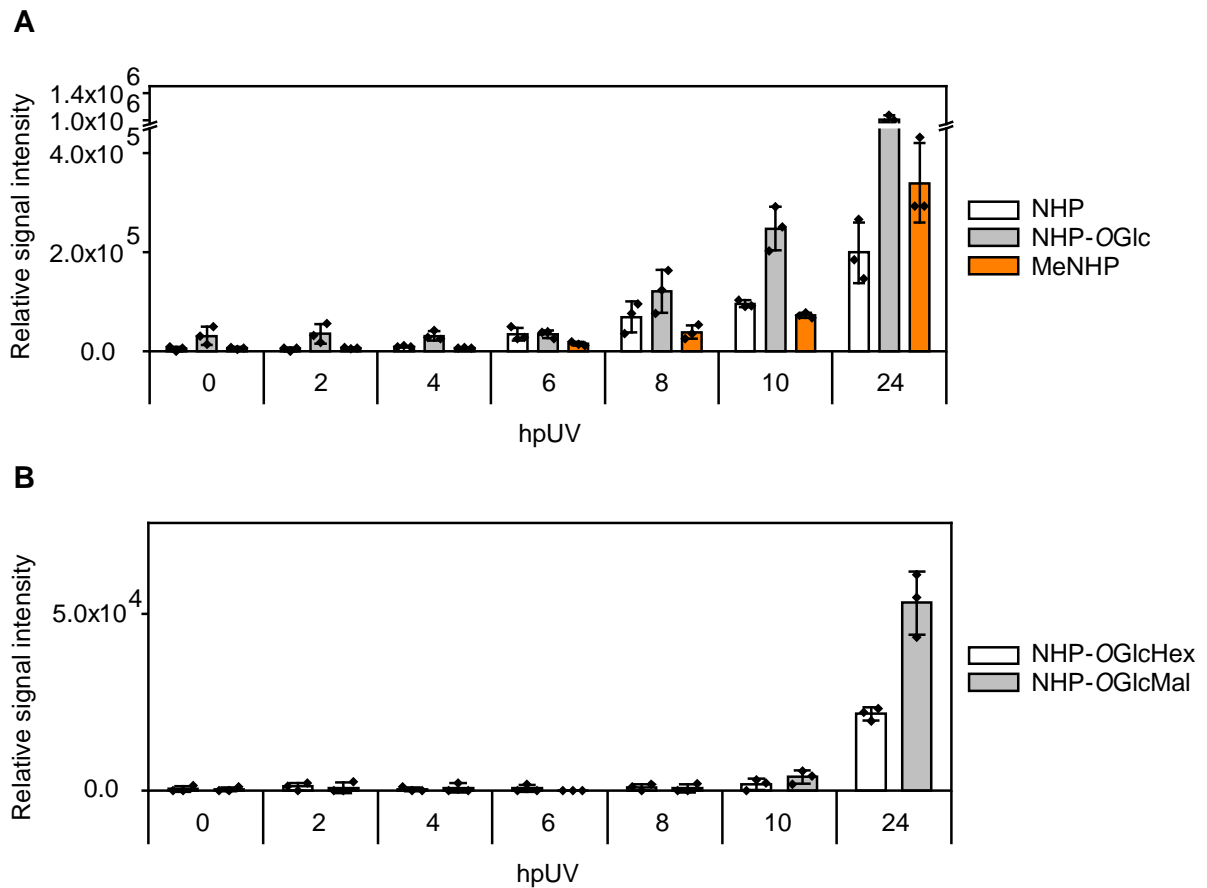


Supplemental figure 1: **Comparison between *in vitro* activity assay with UGT74F2 and UGT76B1 with NHP.** To test the ability of UGT74F2 to glycosylate NHP to NHPGE, to be able to compare retention time differences between NHPGE and NHP-O-Glc, we set-up an *in vitro* reaction in 100 mM Tris/HCl pH=7.8 with 0.5 mM NHP 0.5 mM UDP-Glc and 100  $\mu$ g purified UGT74F2. The reaction was incubated for overnight at 30 °C. The reaction was stopped by adding 50  $\mu$ L methanol. The sample was centrifuged and the supernatant was given to an LC-MS vial. The sample was analyzed using UHPLC-ESI-HRMS. (A) shows the extracted ion chromatogram (EIC) of  $m/z$  308.134 in the UGT74F2 full *in vitro* reaction, RT= 1.87 min. The signal retention time corresponds to NHPGE. (B) shows the EIC of  $m/z$  308.134 in the UGT74F2 *in vitro* control reaction with boiled enzyme for inactivation. (C) shows the EIC of  $m/z$  308.134 in the UGT76B1 full *in vitro* reaction. The signal retention time corresponds to NHP-O-Glc, RT= 2.12 min.

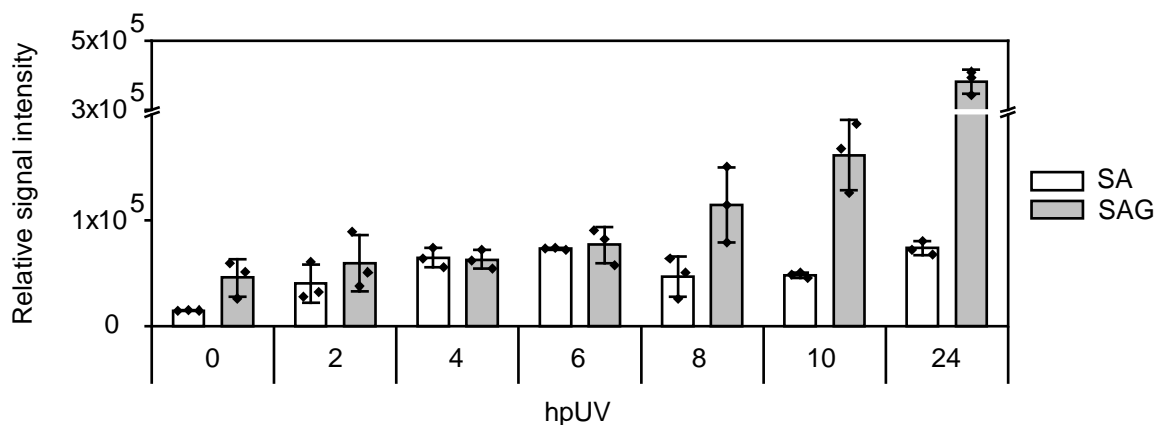


Supplemental figure 2: ***In vitro* activity assay with UGT76B1 and scopoletin.** To test the ability of UGT76B1 to glycosylate scopoletin to scopolin we set-up an *in vitro* reaction in 100 mM Tris/HCl pH=7.8 with 0.5 mM scopoletin 0.5 mM UDP-Glc and 20  $\mu$ g purified UGT76B1. The reaction was incubated for 30 min at 30 °C. The reaction was stopped by adding 25  $\mu$ L acetonitrile. The reaction was centrifuged and the supernatant was given to an LC-MS vial. The sample was analyzed using UHPLC-ESI-HRMS. (A) shows the total ion chromatogram of the reaction sample. The corresponding signals to scopoletin and scopolin are labeled. (B) shows the ion spectrum at retention time 4.654 min, according to scopoletin  $[M-H]^-$  191.037. (C) shows the ion spectrum at retention time 3.448 min, according to scopolin  $[M+COOH]^-$  399.096 and the in source fragment  $m/z$  191.036 (scopoletin).

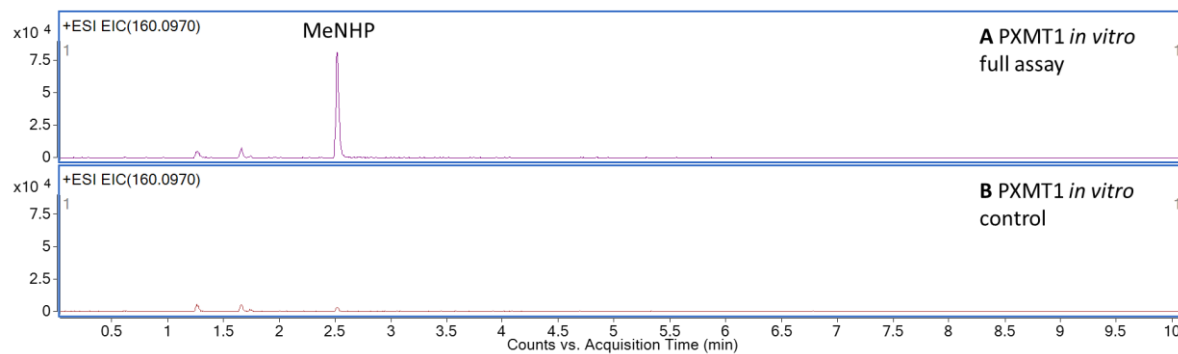




Supplemental figure 3: **Time course of NHP metabolites after UV-C treatment.** Col-0 plants were treated with UV-C for 20 min and incubated at long day conditions. Samples were harvested after 0, 2, 4, 6, 8, 10 and 24 hours post UV treatment (hpUV). **(A)** Relative signal intensities of NHP (white), NHP-OGlc (grey) and MeNHP (orange) are shown over the time course. Y-axis brake from  $4.5 \times 10^5$  cps to  $9.5 \times 10^5$  cps. **(B)** Relative signal intensities of NHP-OGlcHex (white) and NHP-OGlcMal (grey) are shown over the time course. Data represent mean signal intensity plus standard deviation,  $n = 3$  individual pool of leaves.



Supplemental figure 4: **Time course of SA and SAG after UV-C treatment.** Col-0 plants were treated with UV-C for 20 min and incubated at long day conditions. Samples were harvested after 0, 2, 4, 6, 8, 10 and 24 hpUV. Relative signal intensities of NHP (white), NHP-OGlc (grey) and MeNHP (orange) are shown over the time course. Data represent mean signal intensity plus standard deviation,  $n = 3$  individual pool of leaves. Y-axis brake from  $2 \times 10^5$  cps to  $3 \times 10^5$  cps.



Supplemental figure 5: ***In vitro* activity assay with PXMT1 and NHP.** To test the ability of PXMT1 to methylate NHP to MeNHP we set-up an *in vitro* reaction in 20 mM Tris/HCl pH=7.8 with 0.5 mM NHP 0.5 mM SAM and 100  $\mu$ g purified PXMT1. The reaction was incubated overnight at 30 °C. The reaction was stopped by adding 50  $\mu$ L methanol. The reaction was centrifuged and the supernatant was given to an LC-MS vial. The sample was analyzed using UHPLC-ESI-HRMS. **(A)** EIC of  $m/z$  160.097 corresponding to MeNHP from the PXMT1 *in vitro* assay with function enzyme. **(B)** EIC of  $m/z$  160.097 corresponding to MeNHP from the control reaction with boiled PXMT1.

---

## 9. Acknowledgments

To begin with, I would like to thank Prof. Dr. Ivo Feussner for his academic supervision and for giving me the opportunity to work on this fascinating project conducting hands-on metabolomics. I would like to thank Prof. Dr. Christiane Gatz and Prof. Dr. Yuelin Zhang for their guidance, fruitful discussions and being part of my thesis advisory committee. In addition, I would like to thank Yuelin for hosting me in his lab during my research stay at UBC Vancouver.

A big thank you goes to Dr. Kirstin Feussner, who supported me and raised my interest for metabolomics. I am very grateful for your support, be it critical reading of manuscripts/thesis, or scientific and non-scientific discussions. I want to thank Dr. Cornelia Herrfurth and Dr. Ellen Hornung for personal communications in and outside the lab and especially for the experimental support with cloning, crossing and metabolite quantification. In that regard, I would like to thank Brigitte Worbs for chemical synthesis of NHP- and MeNHP-standards.

Another big thank you goes to Weijie Huang, who was a great tandem partner within IRTG PRoTECT on and off the bench, in Vancouver and Göttingen, and who played a big part in this successful collaboration. Mentioning Vancouver, I would like to thank Anja Pelizaeus for the great time with her as my flat mate. In general, I would like to say thank you to all the members of IRTG PRoTECT for creating a great atmosphere. Thank you Steven Dreischoff and Alisa Keyl for taking care of us. I am looking back to challenging hikes, ice skating, ice hockey, football matches and numerous dinners, yum.

I would like to thank Dr. Sven Haroth and Dr. Dmitrij Rekhter for sharing their knowledge and skills with me in the department and for very good times at the barbecue. In that regard, I would also like to thank Sabine Freitag for all the great support and conversations we had over the last years. A big thank you goes to Moritz Klein for being the greatest student assistant. Thanks to all the past and current members of the Department for Plant Biochemistry for creating a great working atmosphere and for the beautiful free time activities we had.

Thank you so much Isabel Maurus, for everything you did to support me over the last years, but the hardest must have been the last weeks. I will do my best to return you the favor and am looking very much forward to our next adventure.

Finally yet importantly, special thanks go to my family, who supported me over the last 9 years from undergrad to a doctoral student. This path would not have been possible without you and I am very much looking forward to see you all this summer.

In Erinnerung an Edel Düweke und Herbert Mohnike.